

UNCLASSIFIED

AD 402 779

*Reproduced
by the*

DEFENSE DOCUMENTATION CENTER

FOR

SCIENTIFIC AND TECHNICAL INFORMATION

CAMERON STATION, ALEXANDRIA, VIRGINIA



UNCLASSIFIED

NOTICE: When government or other drawings, specifications or other data are used for any purpose other than in connection with a definitely related government procurement operation, the U. S. Government thereby incurs no responsibility, nor any obligation whatsoever; and the fact that the Government may have formulated, furnished, or in any way supplied the said drawings, specifications, or other data is not to be regarded by implication or otherwise as in any manner licensing the holder or any other person or corporation, or conveying any rights or permission to manufacture, use or sell any patented invention that may in any way be related thereto.

AFSWC-TDR-62-91

6323
SWC
TDR
62-91

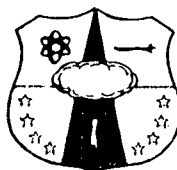
402779

THE ENERGY ABSORPTION CAPACITY OF GRANULAR
MATERIALS IN ONE-DIMENSIONAL COMPRESSION

TECHNICAL DOCUMENTARY REPORT NUMBER AFSWC-TDR-62-91

Final Report

January 1963



Research Directorate
AIR FORCE SPECIAL WEAPONS CENTER
Air Force Systems Command
Kirtland Air Force Base
New Mexico

This research has been funded by the
Defense Atomic Support Agency under WEB No. 13.146

Project No. 1080, Task No. 108001

(Prepared under Contract AF 29(601)-4302
by Alfred J. Hendron, Jr., Robert E.
Fulton, and Bijan Mohraz, The Department
of Civil Engineering, University of Illinois,
Urbana, Illinois)

ASTIA

MAY 1 1963

HEADQUARTERS
AIR FORCE SPECIAL WEAPONS CENTER
Air Force Systems Command
Kirtland Air Force Base
New Mexico

When Government drawings, specifications, or other data are used for any purpose other than in connection with a definitely related Government procurement operation, the United States Government thereby incurs no responsibility nor any obligation whatsoever; and the fact that the Government may have formulated, furnished, or in any way supplied the said drawings, specifications, or other data, is not to be regarded by implication or otherwise as in any manner licensing the holder or any other person or corporation, or conveying any rights or permission to manufacture, use, or sell any patented invention that may in any way be related thereto.

This report is made available for study upon the understanding that the Government's proprietary interests in and relating thereto shall not be impaired. In case of apparent conflict between the Government's proprietary interests and those of others, notify the Staff Judge Advocate, Air Force Systems Command, Andrews AF Base, Washington 25, DC.

This report is published for the exchange and stimulation of ideas; it does not necessarily express the intent or policy of any higher headquarters.


Qualified requesters may obtain copies of this report from ASTIA. Orders will be expedited if placed through the librarian or other staff member designated to request and receive documents from ASTIA.

A B S T R A C T

Energy absorbing mechanisms in sand subjected to one-dimensional compression are reported. For pressures below crushing of the grains, a granular medium of equal radii elastic spheres in a face-centered cubic array is analyzed. Expressions are obtained for the axial stress-strain curve, constrained modulus, coefficient of earth pressure at rest, and relationship between absorbed energy and input energy for one cycle of loading. The energy absorbed as a result of crushing is considered by analyzing statistical relationships between changes in grain size distribution curves and the new surface areas created. An apparatus is described which has the capability of maintaining conditions at zero radial strain under increasing axial stress. The lateral stresses developed under these conditions are measured. Preliminary experimental results are presented for one sand which show the variation of the coefficient of earth pressure at rest and the stress-strain relationships with initial void ratio, overconsolidation ratio, and strain rate. A correlation of theory and test results is presented.

PUBLICATION REVIEW

This report has been reviewed and is approved.


DONALD I. PRICKETT
Colonel USAF
Director, Research Directorate



JOHN J. DISHUCK
Colonel USAF
DCS/Plans & Operations

TABLE OF CONTENTS

	<u>Page</u>
1. INTRODUCTION	1
1.1 Object and Scope.	1
1.2 Acknowledgement	5
Figures.	7
2. SELECTED SUMMARY OF PREVIOUS WORK.	9
2.1 Theories of Granular Media.	9
2.2 Experimental Results.	12
References	14
Figure	17
3. THEORETICAL APPROACH FOR PREDICTING THE STRESS-STRAIN BEHAVIOR OF DENSE SANDS PRIOR TO PARTICLE CRUSHING.	18
3.1 The Mindlin-Duffy Theory of Granular Media.	19
3.1.1 Basic Theory	19
3.1.2 Application to a Hydrostatic State of Stress	26
3.2 One Dimensional Theory of Granular Media.	28
3.2.1 Monotonically Increasing Load.	28
3.2.2 Unloading Cycle.	39
3.2.3 Energy Absorption.	41
3.3 Equivalent Discrete Mass Model for One Dimensional Static and Dynamic Behavior.	42
3.3.1 Horizontal Model	43
3.3.2 Vertical Model	44
References	45
Tables	46
Figures.	48
4. EFFECT OF GRAIN CRUSHING ON THE BEHAVIOR OF SANDS.	64
4.1 Introduction.	64
4.2 Energy Absorbed Due to Crushing	64
4.2.1 Statistical Evaluation of Grain Size Distribution Curve.	64
4.2.2 Graphical Determination of the Geometric Mean Diameter and Standard Deviation.	70
4.2.3 Particle Size Measurements Using Sieves.	70
4.2.4 Energy - New Surface Area Relationship	72
4.2.5 Analysis of a Grain Size Distribution Curve for Sand	74
4.3 Stress-Strain Behavior of Sand After Crushing Commences	76
4.3.1 Experimental Results	76
4.3.2 Theoretical Stress-Strain Curve in the Crushing Region	78
4.4 Determination of the Stresses at Which Grain Crushing Occurs.	80
References	82
Table.	84
Figures.	85

TABLE OF CONTENTS (Cont'd.)

	<u>Page</u>
5. EXPERIMENTAL PROGRAM	103
5.1 Introduction.	103
5.2 Experimental Apparatus.	105
5.2.1 Description of the Apparatus	105
5.2.2 Fabrication and Calibration of the Strain Gages on the Steel Ring	106
5.2.3 Description of the Testing Head.	108
5.2.4 Proportions of Test Specimen	109
5.3 Description of Tests.	111
5.3.1 General.	111
5.3.2 Preparation of Test Specimens.	112
5.4 Test Results.	112
5.4.1 Axial Stress-Strain Relationships.	112
5.4.2 The Coefficient of Earth Pressure at Rest.	116
5.4.3 Energy Absorption.	118
References	121
Tables	122
Figures.	124
APPENDIX A - APPLICATION OF THE HERTZ THEORY TO THE BEHAVIOR OF A GRANULAR MEDIUM.	172
APPENDIX B - NUMERICAL SOLUTION TO THE EQUATIONS GOVERNING THE BEHAVIOR OF A GRANULAR MEDIUM HAVING RESTRICTED LATERAL STRAINS. .	185
DISTRIBUTION	195

CHAPTER 1

INTRODUCTION

1.1 Object and Scope

The object of this study is to define the mechanisms by which granular materials such as dry sands and gravels absorb energy when subjected to an applied state of stress. The study therefore is an investigation of the stress-strain behavior and hysteresis effects in cohesionless granular materials subjected to increments of stress extending into the higher pressure ranges.

The usual concept of a stress-strain relationship for elastic solids does not apply to granular materials. The ideal group of materials classified as elastic solids exhibit a linear stress-strain relation. In such a material the stress-strain properties may be described by elastic constants. A granular medium such as soil is entirely different however, in that constants cannot be used to describe the stress-strain properties of the medium even if the material properties of the particles and the packing arrangement are known. The stiffness of a granular medium is not only dependent upon the material composition of the particles and the packing arrangement (relative density), but the stiffness is also a non-linear function of the stress tensor. The dependence of the stress-strain relation can be illustrated by considering various states of stress on the cylindrical sample of soil shown in Fig. 1.1. Curve 1 shows an axial stress-strain curve for a sample of soil which was compressed hydrostatically with $\sigma_a = \sigma_r$. The concave upward stress-strain relationship is a typical relationship because as the soil becomes denser the resistance to volume change increases. Curve 3 illustrates an axial stress-strain curve for a sample under constant radial

stress which is deformed by increasing the axial stress. The resulting stress-strain curve is concave downward indicating that the resistance to deformation increases at a decreasing rate. This behavior is typical where the primary resistance to deformation is a shearing resistance rather than a resistance to volume change. Curve 2 is a one dimensional compression curve where the axial stress is increased under the conditions of zero radial strain. In this situation the lateral stresses are not controlled and are statically indeterminate. The concave upward stress-strain curve shows that the resistance to deformation in one dimensional compression is primarily a resistance to a change in volume. These examples illustrate the various types of behavior manifested by soil and demonstrates the dependence of the stress-strain relation on the applied state of stress. The general stress-strain relations in a granular material are therefore very complicated, especially when the shearing stresses predominate as in curve 3 and particles rotate, slide, and a rearrangement of particles is constantly taking place.

In order to eliminate the variables introduced by gross rearrangement and other uncertainties which occur under large shearing stresses, this study was limited to those cases where the shearing stresses are small with respect to the normal stresses. The behavior in one dimensional compression has been emphasized because this case is of practical importance to the Air Force. The one dimensional case is a reasonable representation for an important group of protective construction problems; those where the air blast induced ground shock is of primary importance. In this condition of loading the radial extent of the loaded area is large in comparison to the thickness of highly compressible surface soil and near surface unconsolidated rock strata. Under this condition of loading, the strata are laterally confined such that the

only displacement that can occur is in the direction of stress wave propagation.

A typical stress-strain curve for a granular material such as sand subjected to static loads in one dimensional compression is shown qualitatively in Fig. 1.2. This curve shows that the stress-strain behavior and consequently the energy absorption mechanisms are dependent to a large extent on the magnitude of pressure.

The behavior in the very low stress ranges, (Region 1, Fig. 1.2), reflects a rearrangement of the grains and the stress-strain curve is concave downward. The energy absorbed in the compaction process is of course non-recoverable; however, if the pressure subsequently becomes quite large this energy loss is quite small compared to losses caused by other phenomena.

As the load is increased the particles begin to lock together and become a stable matrix of elastic particles (Region 2). In this higher stress region the strains that take place in the material are due primarily to the deformation of the particles at the points of contact. There is of course some rearrangement continuing in this region but studies indicate that the rearrangement is not significant at this pressure level. The behavior in this region is essentially a non-linear elastic behavior in that there is little permanent set resulting from an increment of stress applied and removed within Region 2. This behavior can be analytically studied by means of the Hertz-Mindlin contact theory which is discussed in detail in Chapter 3. A study of this type was made on a face centered array of equal radii spheres. A theoretical stress-strain curve was derived for the array of spheres in hydrostatic compression and the concepts were extended to obtain a

stress-strain relationship for the array subjected to the boundary conditions concomitant with one dimensional compression. It was found that in one dimensional compression it is possible to have energy absorbed due to friction at the contacts when no permanent strain results from a cycle of loading. The question arises as to whether such a theory based on the theories of contact stresses is applicable to soils because of the magnitude of the stresses and the small radii of the grains. Appendix A treats this topic and shows that for the stress ranges of interest, namely those in Region 2 prior to particle crushing, the contact theory is applicable. For certain cases other than complete confinement with various amounts of lateral deformation permitted, it was necessary to obtain numerical solutions to the theory of granular media since a closed form solution was not possible. Appendix B outlines the work carried out and the program coded for a digital computer.

As the stress continues to increase to the neighborhood of one to five thousand psi the contact forces become so large that the particles begin to crush. The crushing is accompanied by a certain amount of rearrangement which is reflected in the concave downward stress-strain curve shown in Region 3. Energy is absorbed in this range by the creation of new surface area during crushing and energy is dissipated as heat due to rearrangement of the new particles into a denser configuration. Both of these mechanisms absorb energy which is no longer in the form of recoverable strain energy.

As the pressure continues to increase, the particles lock again and the curve again becomes concave upward as shown in Region 4, Fig. 1.2. In general the stress-strain curve in Region 4 tends to follow the same general pattern which took place in Region 2 before crushing except that

the particles are smaller and more angular than before. There is evidence however, which indicates that particles are continuing to crush throughout Region 4. Chapter 4 considers the energy required to create new surfaces. It is found that after crushing begins the energy absorbed due to particle crushing seems to be linearly related to the stress level.

Unfortunately, there are no data available in the literature which can be used to fully corroborate the analytical conclusions summarized above and presented in detail in Chapters 3 and 4. In order to fill this gap in our experimental knowledge a series of exploratory tests on smooth uniform sand in one dimensional compression were conducted to provide a better understanding of the mechanisms by which sand absorbs energy. The design and construction of a new testing apparatus was required to obtain the necessary data in the higher pressure ranges. The design of the apparatus and the test results are described in Chapter 5.

The data presented in Chapter 5 show that energy can be absorbed by sand in stress ranges below crushing with only very small permanent strains resulting. This behavior is substantially the same as predicted from the analysis of the medium composed of equi-radii spheres.

1.2 Acknowledgment

This study was performed as part of an investigation conducted in the Civil Engineering Department of the University of Illinois under Contract AF 29(601)-4302 with the Air Force Special Weapons Center, Albuquerque, New Mexico. This report was prepared under the general direction of Dr. N. M. Newmark, Head of the Department of Civil Engineering and the general supervision of Dr. J. L. Merritt, Associate Professor of Civil

Engineering. The immediate supervision of this phase of the research program is the responsibility of Mr. A. J. Hendron, Research Associate in Civil Engineering. Project personnel included Dr. Robert E. Fulton, formerly responsible for immediate supervision and Mr. Bijan Mohraz, Research Assistant in Civil Engineering.

The writers would like to express appreciation to Dr. R. B. Peck, Professor of Foundation Engineering, and Dr. Don U. Deere, Professor of Civil Engineering and of Geology for their encouragement and suggestions in this study. Appreciation is also expressed to the United States Air Force for the support which has made this study possible, particularly to the project monitor, Capt. H. E. Auld for his cooperation and interest toward the successful completion of the study.

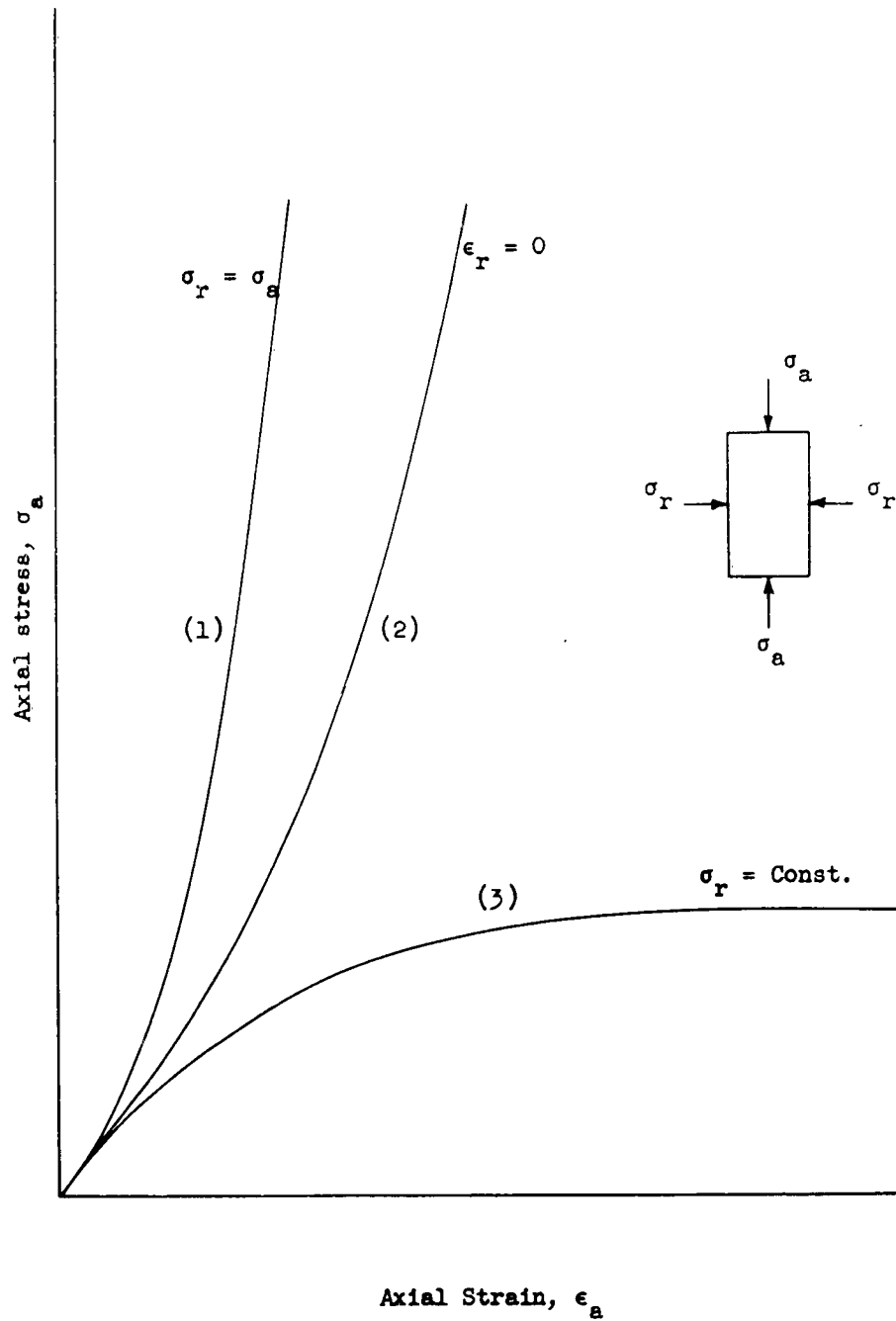


Fig. 1.1 AXIAL STRESS-STRAIN CURVES FOR SOIL SUBJECTED TO VARIOUS STATES OF STRESS

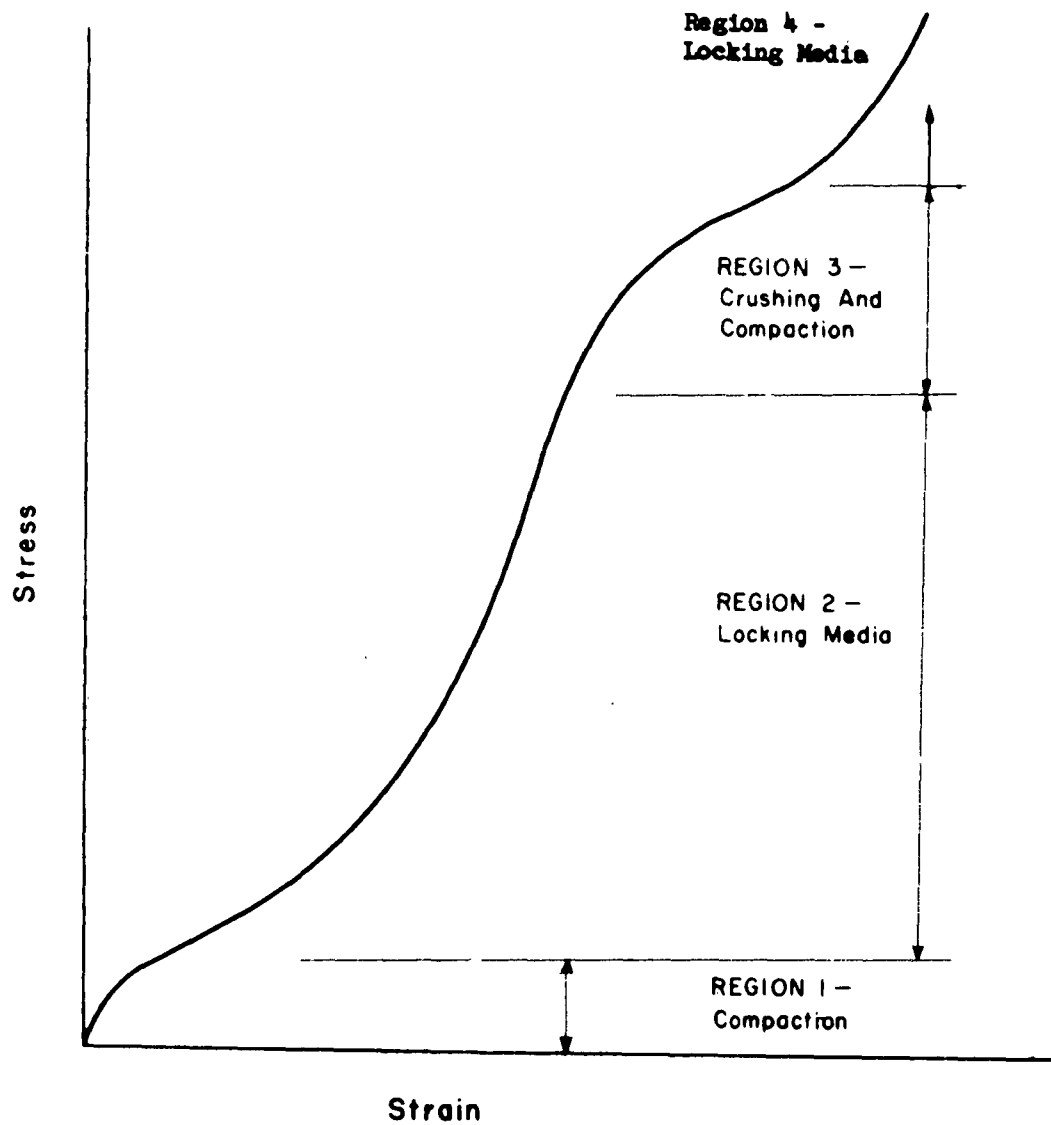


Fig. 1.2 QUALITATIVE ONE DIMENSIONAL STRESS-STRAIN CURVE FOR GRANULAR MATERIAL

CHAPTER 2

SELECTED SUMMARY OF PREVIOUS WORK

It is not the purpose herein to make a thorough survey of all of the important results reported in the literature which have contributed to an understanding of the behavior of granular materials and soils. Such an effort would be quite voluminous and an extensive report in itself. It is the writers' understanding that Professor R. V. Whitman at MIT is currently preparing such a report, [2.37]. Furthermore, a very excellent comprehensive summary of the state of knowledge, on the behavior of granular materials, up to 1957 has been made by Deresiewicz [2.1]. The reader is referred to these works for a comprehensive survey of the literature on the behavior of soils.

The purpose of this chapter is to call attention to some of the more recent findings which are important in understanding soil behavior and also to point out some other works which, while not new, have been somewhat overlooked in the literature. It is hoped that the few comments made here will be useful to the reader as supplements to the two above noted works.

2.1 Theories of Granular Media

There are many theories which have been developed in the past to attempt to predict or rationalize the behavior of granular materials. Some of these have been based on the concepts of the theory of plasticity. Others have been founded on a study of spherical arrays such as that summarized by Deresiewicz [2.1].

A recent publication worthy of note is a summary of Russian contributions in soil mechanics by Klein [2.2]. This is primarily a historical account of the development of the theory of granular media in

Russia from 1917 to 1957 and includes little actual theory. Its major contribution is that it provides an excellent bibliography of only Russian work (some 175 listings) in this area up to the early part of 1957. Another survey of recent Russian work in soil mechanics was also conducted by Drashevskaya [2.34] in 1958.

One of the most recent theories of soil mechanics developed in Russia is that presented by Grigoryan [2.3]. He formulates a theory which is presumed to be applicable for soils subjected to extremely large pressures (in terms of thousands of psi). His theory suggests that the behavior of a soil is dependent on two functions, one characterizing the volume deformation of the medium and the other the properties of the medium during shear deformation. It should be noted that the most important difference between the Grigoryan model and the usual plasticity theory is that here the volume deformation relationships between the mean pressure $p = -1/3 (\sigma_x + \sigma_y + \sigma_z)$ and the density is not assumed to be elastic (reversible). They are, however, connected by a well defined relationship which is different for increasing and decreasing pressure. This theory gives a loading and unloading stress-strain curve similar in shape to Fig. 2.1. Grigoryan's theory is discussed in greater detail in a later publication [2.4] and some inaccuracies in the original work are corrected.

Some experimental work is presented by Alekseenko, Grigoryan, et al [2.4] in support of the theory proposed by Grigoryan for granular media. A series of TNT explosions was set off, and the soil behavior was measured radially outward away from the blasts. The results seemed to show a definite linear relationship between the mean compressive stress and the square root of the second stress invariant. For average stresses

less than 15 kg/cm^2 it was found that the second stress invariant could be related to the average stress.

Another recent theory of soil mechanics has been presented in a monograph by Geniev [2.5]. Here a theory for the plane motion of a granular medium is formulated which is an extension of the work of Sokolovsky. The equations of motion consist of (1) two equations of equilibrium (2) conditions for Coulomb boundary equilibrium (3) incompressibility conditions and (4) conditions of convergence of the directions of maximum velocities of shear deformation with the direction of lines of slip. The application of Geniev's theory to the dynamic soil-structure interaction problem is currently under study at the University of Illinois [2.35].

One theoretical treatment which is not too well known is that developed by Oshima [2.6] wherein an attempt is made to specify in tensor notation all of the contributing effects which should be included in a theory of granular media. The approach has some merit in that an attempt is made to present a consistent theory which encompasses the entire geometry of the medium. Unfortunately, while the abstractness presents a convenient compact form for the theory, there is difficulty in obtaining all of the terms in the significant tensors.

Katz and others [2.7 and 2.8] have studied the propagation of plane stress-waves in sand with a two-parameter exponential stress-strain law, including hysteresis. Along a similar line Parkin has treated the one dimensional wave propagation in sand in an attempt to explain the behavior measured by Whitman [2.15] in some experiments carried out in the early 1950's. The subsequent discussions of the latter paper by Fulton and Hendron [2.11], Selig and Vey [2.12], Whitman [2.13] and Parkin [2.14]

are particularly interesting in summarizing the current state of knowledge and problems associated with predicting the behavior of sand. An investigation of the dynamic soil-structure interaction problem using a discrete mass-spring model to represent the soil is currently under way at the University of Illinois [2.36].

Some of the more recent papers in English on the application of the theory of plasticity to the behavior of soils include [2.16 - 2.20]. Theoretical studies of the stress conditions existing in tri-axial compression have been formulated by Balla [2.21] and Haythornthwaite [2.22].

2.2 Experimental Results

One result which is of importance to this study is given in a paper by Allen, et al [2.23], which contains the results of a series of tests on sand (Fig. 2.2). The particular significance of these tests is that the pressures were extremely high (approximately 90,000 psi). The sample was placed inside a steel cylinder to approximate conditions of one dimensional compression. Unfortunately, the sample size was of the wrong proportion for a one dimensional test (2.31 inches in diameter and 7.88 inches high) and the stress-strain behavior may very well be significantly affected by the deformations of the container and side friction effects. These results are of significance, however, in indicating the general shape of the stress-strain curve in the high pressure regions. Grigoryan used this general shape to support his theory of granular media.

J. M Roberts [2.24] has investigated the hysteresis characteristics of an Ottawa sand with lateral confinement closely approximating one dimensional conditions. Some 200 loading cycles were carried out in

a stress region below 50 psi. It was found from the hysteresis loops that sand can absorb energy without having any permanent displacements. The reason for this phenomenon noted by Roberts and more conclusive experimental results, are given by the authors in the present report.

Studies on the one dimensional stress-strain behavior of sand and quartz in the higher pressure regions were carried out by J. E. Roberts and others at MIT [2.25, 2.26]. Some of these data are analyzed in Chapter 4 of this report in an effort to shed some light on the mechanism by which sand absorbs energy in pressure regions of 5,000 - 20,000 psi.

Tests on the static and dynamic stress-strain characteristics of sands in the low pressure regions have been conducted by Thompson at the Ballistics Research Laboratory and the results have been published in a series of short reports [2.27, 2.28, 2.29].

Kjellman and Jakobson [2.30] investigated the influence of grain shape and grain size on the behavior of granular materials incased in a series of steel rings in an attempt to eliminate the side friction effects. A triaxial compression apparatus was modified by Weissman and Hart [2.31] to study the damping capacity of granular soils as reflected by the hysteresis loop. Wolfskill and Buchanan [2.32] discuss some of the aspects of dynamic foundation loads supported by a granular soil. Other recent work on dynamic triaxial tests includes that by Shannon, et al [2.33].

REFERENCES

- 2.1 Deresiewicz, H., "Mechanics of Granular Matter," Advances in Applied Mechanics, Vol. 5, Academic Press, Inc., New York, New York, 1958, p. 233.
- 2.2 Klein, G. K., "Pressure and Resistance of Granular (Cohesionless) Media, Analysis of Retaining Walls and Subterranean Structures," Ch. 9 of Structural Mechanics in the U.S.S.R. 1917-1957 ed. by I. M. Rabinovich, Pergamon Press, pp. 396-426.
- 2.3 Grigoryan, S. S., "The General Equation of Soil Mechanics," Soviet Physics Doklady, Vol. 4, No. 1, Aug./Dec. 1959.
- 2.4 Grigoryan, S. S., "On Basic Concepts in Soil Dynamics," PMM Jour. Appl. Math. and Mech., Vol. 24, No. 6, 1960, pp. 1604-1627.
- 2.5 Genieve, G. A., "Questions of the Dynamics of a Granular Medium" (in Russian), Nauch. Soobsheh. Tsentr. Nauk-i. In-ta Stroit. Konstruktsii Akad. Str-va i Arkhitekt. SSSR No. 2, 1958.
- 2.6 Oshima, N., "Dynamics of Granular Media" Ch. D-6 Memoirs of the Unifying Study of the Basic Problems in Engineering Sciences by Means of Geometry, Vol. I, ed. by K. Kondo, Gakujuts Bunken Fukya-Kai, Tokyo, 1955.
- 2.7 Katz, S., and Ahrens, T. J., "Propagation of Plane Waves in Granular Materials, Part I," Tech. Report No. 1, Ballistics Research Laboratory, Contract No. DA-115-509-ORD-1009, Dec. 1959.
- 2.8 Katz, S., and Woeber, A. F., "Propagation of Plane Waves in Granular Materials, Part II" Tech. Report No. 2, Ballistics Research Laboratory, Contract No. DA-115-509-ORD-1009, Sept. 1960.
- 2.9 Parkin, B. R., "Impact Wave Propagation in Columns of Sand," Report No. RM-2486, The RAND Corporation, Nov. 1959.
- 2.10 Parkin, B. R., "Impact Waves in Sand: Theory Compared with Experiments on Sand Columns," Proc. ASCE, Vol. 87, SM3, June 1961, pp. 1-32.
- 2.11 Fulton, R. E., and Hendron, A. J., Jr., "Discussion: Impact Waves in Sand: Theory Compared with Experiments on Sand Columns," Proc. ASCE, Vol. 87, No. SM6, Dec. 1961, pp. 69-73.
- 2.12 Selig, E. T., and Vey, E., "Discussion: Impact Waves in Sand: Theory Compared with Experiments on Sand Columns," Proc. ASCE, Vol. 87, No. SM6, Dec. 1961, pp. 73-76.
- 2.13 Whitman, R. V., "Discussion: Impact Waves in Sand: Theory Compared with Experiments on Sand Columns," Proc. ASCE, Vol. 88, No. SM1, Feb. 1962, pp. 49-58.
- 2.14 Parkin, B. R., "Discussion: Impact Waves in Sand: Theory Compared with Experiments on Sand Columns," Proc. ASCE, Vol. 88, No. SM3, June 1962, pp. 205-207.

- 2.15 Whitman, R. V., et al, "The Behavior of Soils Under Dynamic Loading: 3. Final Report of Laboratory Studies," Dept. of Civ. and San. Engrg., M.I.T., Aug. 1954.
- 2.16 Drucker, D. C., Gibson, R. E., and Henkel, D. J., "Soil Mechanics and Work Hardening Theories of Plasticity" Trans. ASCE. Vol. 122, 1957, pp. 338-346.
- 2.17 Drucker, D. C., "Coulomb Friction, Plasticity, and Limit Loads, Jour. Appl. Mech., Vol. 21, 1954, pp. 71-74.
- 2.18 Jenike, A. W., and Shield, R. T., "On the Plastic Flow of Coulomb Solids Beyond Original Failure," Jour. Appl. Mech., Vol. 26, 1959, pp. 599-602.
- 2.19 Kirkpatrick, W. M., "The Condition of Failure for Sands," Proc. 4th Intl. Conf. Soil Mech., 1957, pp. 172-178.
- 2.20 Takagi, S., Plane Plastic Deformation of Soils, Proc. ASCE, Vol. 88, No. EM3, June 1962.
- 2.21 Balla, A., "Stress Conditions in Triaxial Compression," Proc. ASCE, Vol. 86, No. SM6, Dec. 1960, pp. 57-84.
- 2.22 Haythornthwaite, R. M., "Mechanics of the Triaxial Test for Soils," Proc. ASCE, Vol. 86, No. SM5, Oct. 1960.
- 2.23 Allen, W. M., Mayfield, E. B., and Morrison, H. L., "Dynamics of a Projectile Penetrating Sand," Journal Appl. Physics, Vol. 28, No. 3, March 1957, pp. 370-376.
- 2.24 Roberts, J. M., "A Study of Hysteresis in Granular Soils," M.S. Thesis, Massachusetts Institute of Technology, June 1961.
- 2.25 "Study of Soils Consolidated Under High Pressure," Report for the Creole Petroleum Corp., Maracaiba, Venezuela, Massachusetts Institute of Technology, Oct. 1959.
- 2.26 Roberts, J. E. and de Souza, J. M., "The Compressibility of Sands," Proceedings ASTM, Vol. 58, 1958, p. 1269.
- 2.27 Thompson, A. A., "The Relation of Seismic Energy Attenuation to the Area Under the Stress-Strain Curve," Memorandum Report 1261, Ballistics Research Laboratory, Apr. 1960.
- 2.28 Thompson, A. A., "A Comparison of the Dynamic and Static Stress-Strain Curve in Sand Under Confined and Unconfined Conditions," Memorandum Report 1262, Ballistics Research Laboratory, Apr. 1960.
- 2.29 Thompson, A. A., "The Comparison of Strain and Kinetic Energy in a Plastic Wave Moving Through Sand," Memorandum Report 1263, Ballistics Research Laboratory, Apr. 1960.

- 2.30 Kjellman, W., and Jakobson, B., "Some Relations Between Stress and Strain in Coarse-Grained Cohesionless Materials," Bulletin No. 9, Proc. Royal Swedish Geotechnical Institute, Stockholm 1955.
- 2.31 Weissman, G. F. and Hart, R. R., "The Damping Capacity of Some Granular Soils," ASTM Spec, Tech. Pub. No. 305, 45-54, 1961.
- 2.32 Wolfskill, L. A., and Buchanan, S. J., "Dynamic Stress-Strain Characteristics of Granular Materials," Presented at National Convention ASCE, Houston, Texas, Feb. 1962.
- 2.33 Shannon, W. L., Yamane, G., and Dietrich, R. J., "Dynamic Triaxial Tests on Sand," Proc. First Panamerican Conf. on Soil Mech. and Found. Engrg., Mexico City, Sept. 1959.
- 2.34 Drashevskaya, L., "Review of Recent U.S.S.R. Publications in Selected Fields of Engineering Soil Science," M.A. Thesis, Columbia University, 1958.
- 2.35 Bedesem, W. B., Jennings, R. L., Das, Y. C., and Robinson, A. R., "Soil Structure Interaction and Dynamics of Shells," Interim Technical Report for Air Force Special Weapons Center, Contract AF29(601)-4508, University of Illinois, Aug. 1962.
- 2.36 Ang, A., and Newmark, N. M., "Computation of Underground Structural Response," Technical Supplement Report for Defense Atomic Support Agency, Contract DA-49-146-XZ-104, University of Illinois, March 1962.
- 2.37 Whitman, R. V., Nuclear Geoplosics, Part Two - Mechanical Properties of Earth Materials. 3203 (11) Draft (Unpublished) Prepared for the Defense Atomic Support Agency, Washington 25, D. D., under Contract Nos. DA-22-079-eng-224 and DA-49-146-xz-030.

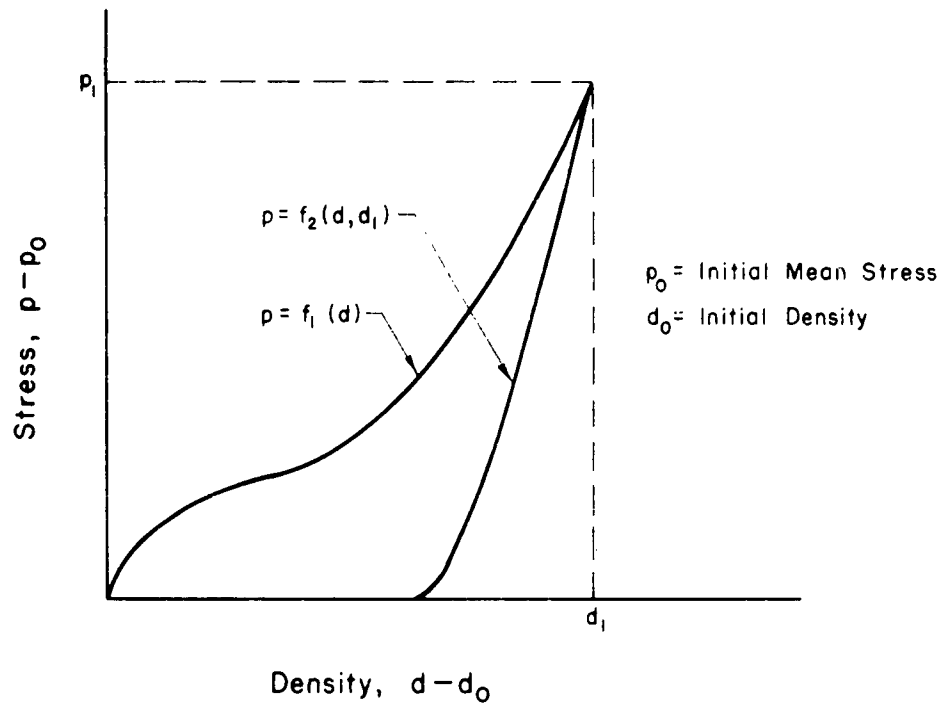


Fig. 2.1 ASSUMED STRESS STRAIN CURVE FOR SAND
(after Grigoryan (2.3, 2.4))

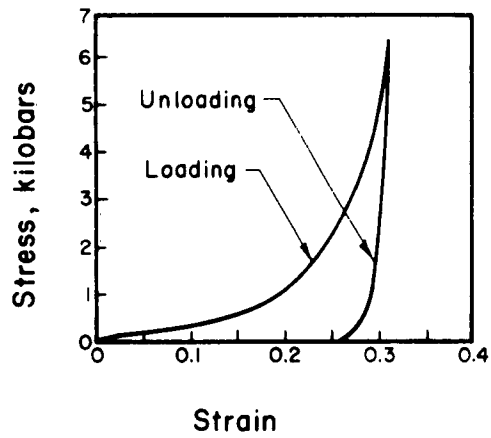


Fig. 2.2 ACTUAL STRESS STRAIN CURVE FOR SAND
(after Allen, et al (2.23))

CHAPTER 3

THEORETICAL APPROACH FOR PREDICTING THE STRESS-STRAIN BEHAVIOR OF DENSE SANDS PRIOR TO PARTICLE CRUSHING

The stress-strain behavior of most materials in the stress levels of interest may be assumed to approximately follow Hooke's law. If the material is isotropic, the stress-strain relations can be completely described by two independent elastic constants.

The discussion in the introduction to this report pointed out the fact that constants could not be used to describe the stress-strain properties of a granular medium. It was shown that it is possible to obtain almost any stress-strain curve one desires by varying the stress level, the state of stress, and displacement conditions at the boundaries. Thus, there is no unique stress-strain relation for a granular medium. This does not mean, however, that the stress-strain relations of certain prescribed granular media under a given set of boundary conditions cannot be found. The above merely indicates that, even for a greatly idealized medium such as a uniform array of equi-radii spheres, the problem of defining a stress-strain relation for a granular medium is a boundary valued problem in particulate mechanics and any analytical study of behavior under changes in stress must adequately take into account the boundary conditions.

A mechanics approach for formulating the behavior of this type of media must consider:

1. The equilibrium of each particle and the medium as a whole.
2. Certain geometrically admissible conditions on the deformations of the particles (i.e., a set of compatibility equations).
3. The relationships between the normal forces and normal displacements and shearing forces and tangential displacements at each contact point on a particle.

4. The boundary conditions on the medium.

The non-linear partial differential equations which result from even the simplest model of equi-radii spheres are extremely complex and closed form solutions can be obtained for only a few cases. Since some of the solvable problems, however, turn out to be basic ones, such an approach has a great deal of merit in adding to the understanding of the behavior of granular materials.

This chapter reviews the formulation of the theory of Granular Media according to the ideas of Mindlin and Duffy and then presents a modification of the theory which is appropriate for one dimensional compression.

3.1 The Mindlin-Duffy Theory of Granular Media

3.1.1 Basic Theory

The theory developed here follows that first formulated by Duffy, Mindlin [3.1, 3.2, 3.3] and their co-workers. The granular medium is restricted to a face centered array of equi-radii spheres (Fig. 3.1). The face centered array was chosen primarily because this array is one which provides for the densest possible packing. Hence, there is no way in which compressible deformations of the medium can take place as a result of rearrangement of the particles.

Consider the behavior of two spheres pressed together by a normal force. According to the Hertz theory, if two elastic spheres, each having radius R , shear modulus μ , and Poissons ratio ν , are mutually compressed by a normal force N , the resulting surface of contact is a plane bounded by a circle of radius

$$a = \left[\frac{3(1-\nu)RN}{8\mu} \right]^{1/3} \quad (3.1)$$

and the rate of change of the relative approach of the sphere centers, α , with respect to the normal force N , is

$$C = \frac{d\alpha}{dN} = \frac{1 - \nu}{2\mu a} \quad (3.2)$$

where C is defined as the normal compliance. Two spheres in normal contact are shown in Fig. 3.2 while Fig. 3.3 shows the distribution of the normal stress across the area of contact. A complete derivation of the Hertz compliance and the assumptions and limitations of the Hertz theory in regard to this study appear in Appendix A.

Suppose now that the system of like spheres, initially compressed by a constant normal force N is subjected to a tangential force T which acts in the plane of contact and whose magnitude increase monotonically from zero to a given value. Because of symmetry, the distribution of normal pressure remains unchanged. If it is assumed that there is no slip* on the contact, then, because of symmetry, the displacement of the contact surface in its plane is that of a rigid body. The solution of the appropriate boundary-value problem, due to Cattaneo [3.4] and Mindlin [3.5], yields the tangential component of traction τ on the contact surface and the tangential displacement, δ , of points in one sphere remote from the contact with respect to similarly situated points in the other sphere. The tangential traction is parallel to the applied force T , axially symmetric in magnitude, and increases without limit on the bounding curve of the contact area, Fig. 3.3. It is reasonable to suppose that slip is initiated at the edge of the contact since it is there the singularity in traction takes place in the absence of slip. Since without slip this traction is symmetric, the slip is assumed to

* By slip we mean relative displacement of contiguous points on a portion of the contact surface. We distinguish between "slip" and the term "sliding," which we reserve to denote relative displacement over the entire contact.

progress radially inward, covering an annular area. On this annulus it is assumed, as a first approximation, that the tangential component of traction is in the direction of the applied force and is related to the normal (Hertz) component of stress σ , already present, in accordance with Coulomb's Law of sliding friction. Hence:

$$\tau = f\sigma \quad (3.3)$$

where f is the coefficient of static friction and σ is given by

$$\sigma = \frac{3N}{2\pi a^3} (a^2 - \rho^2)^{1/2} \quad (3.3a)$$

Here ρ is the distance from the center of the contact circle. The distribution of τ with slip is also shown in Fig. 3.3. Cattaneo and Mindlin also predict the relation between the radius of the adhered portion and the applied tangential force as

$$b = a(1 - \frac{T}{fN})^{1/3} \quad (3.4)$$

where b is as shown in Fig. 3.3 and where the tangential compliance at the contact is given by

$$S = \frac{d\delta}{dT} = \frac{2 - \nu}{4\mu a} (1 - \frac{T}{fN})^{-1/3} \quad (3.5)$$

Equation (3.5) holds only for the case of an increasing T with a constant N at the contact. In the problems we will consider in this paper, T and N are both increasing so the tangential compliances appropriate for this problem are given in reference [3.6] as

$$S = \frac{2 - \nu}{4\mu_a} \left[r \frac{dN}{dT} + (1 - r \frac{dN}{dT}) (1 - \frac{T}{fN})^{-1/3} \right], \quad 0 \leq \frac{dN}{dT} \leq 1/r \quad (3.6)$$

or

$$S = \frac{2 - \nu}{4\mu_a}, \quad \frac{dN}{dT} \geq 1/r \quad (3.7)$$

Let us now consider a face centered cubic array of uniform spheres as shown in Fig. 3.1, where each sphere is in contact with 12 other spheres. A typical element of this packing is shown in Fig. 3.4. If the coordinate system shown in Fig. 3.4 is translated to the center of any sphere, Fig. 3.5, the 12 contact points would have the following coordinates in terms of the radius of the sphere.

	<u>X</u>	<u>Y</u>	<u>Z</u>		<u>X</u>	<u>Y</u>	<u>Z</u>
<u>1.</u>	0	+ R/√2	+ R/√2	<u>7.</u>	+ R/√2	- R/√2	0
<u>2.</u>	0	- R/√2	+ R/√2	<u>8.</u>	- R/√2	+ R/√2	0
<u>3.</u>	0	- R/√2	- R/√2	<u>9.</u>	+ R/√2	0	+ R/√2
<u>4.</u>	0	+ R/√2	- R/√2	<u>10.</u>	- R/√2	0	- R/√2
<u>5.</u>	+ R/√2	+ R/√2	0	<u>11.</u>	- R/√2	0	+ R/√2
<u>6.</u>	- R/√2	- R/√2	0	<u>12.</u>	+ R/√2	0	- R/√2

There are two shearing forces and one normal force at each contact point as shown on Fig. 3.5. In index notation it is convenient to identify the various components of normal forces by the symbol, N_{ij} , where the subscripts correspond to the planes in which the components lie. The two tangential force components at each contact are chosen to lie in and normal to the co-ordinate planes, and are identified by T_{ij} , and T_{kk} respectively. At all contacts where the normal has direction cosines of unlike sign the force components are further distinguished by primes. Thus the components at the contact points 1 through 12 are:

1.	N_{yz}	T_{yz}	T_{xx}	7.	N'_{xy}	T'_{xy}	T'_{zz}
2.	N'_{yz}	T'_{yz}	T'_{xx}	8.	N'_{xy}	T'_{xy}	T'_{zz}
3.	N_{yz}	T_{yz}	T_{xx}	9.	N_{xz}	T_{xz}	T_{yy}
4.	N'_{yz}	T_{yz}	T'_{xx}	10.	N_{xz}	T_{xz}	T_{yy}
5.	N_{xy}	T_{xy}	T_{zz}	11.	N'_{xz}	T'_{xz}	T'_{yy}
6.	N_{xy}	T_{xy}	T_{zz}	12.	N'_{xz}	T'_{xz}	T'_{yy}

Let us now consider the equilibrium equations of a representative cube (Fig. 3.4) due to an arbitrary initial state of stress imposed on the medium. If an increment in stress is added to the initial stress, the forces on the faces of the cube will be increased by corresponding increments dP_{ij} . Let us determine the unknown increments of force at the contacts between the spheres within the cube which result from the force increments dP_{ij} . If the stress increment in the medium is homogeneous, then the contact forces will be equal at contacts having corresponding positions on the surfaces of the spheres. The contact forces diametrically opposed on each sphere are equal, thus only 18 of 36 contact forces on each sphere are independent. Not only must the cube as a whole remain in equilibrium under the action of the increments in applied force, dP_{ij} , but each sphere and each portion of a sphere within the cube must also remain in equilibrium. Since the portions of spheres in the cube are acted on both by applied forces and by contact forces, the equations of equilibrium relate the increments in applied forces to the increments in contact forces. By writing equilibrium equations for various octants of spheres in the cube as shown in Fig. 3.6 it may be shown that there are nine independent equations of equilibrium. These equations are the following:

$$\begin{aligned}
 1. \quad & 4dT_{xx} + 2\sqrt{2} (dN_{zx} + dN_{xy} - dT_{zx} + dT_{xy}) = dP_{xx} + dP_{xy} + dP_{zx} \\
 2. \quad & 4dT_{yy} + 2\sqrt{2} (dN_{xy} + dN_{yz} - dT_{xy} + dT_{yz}) = dP_{yy} + dP_{yz} + dP_{xy} \\
 3. \quad & 4dT_{zz} + 2\sqrt{2} (dN_{yz} + dN_{zx} - dT_{yz} + dT_{zx}) = dP_{zz} + dP_{zx} + dP_{yz} \\
 4. \quad & 4dT'_{xx} + 2\sqrt{2} (dN'_{zx} + dN'_{xy} - dT'_{zx} + dT'_{xy}) = dP_{xx} + dP_{xy} + dP_{zx} \\
 5. \quad & 4dT'_{yy} + 2\sqrt{2} (dN'_{xy} + dN'_{yz} - dT'_{xy} + dT'_{yz}) = dP_{yy} + dP_{yz} - dP_{xy} \quad (3.8) \\
 6. \quad & 4dT'_{zz} + 2\sqrt{2} (dN'_{yz} + dN'_{zx} - dT'_{yz} + dT'_{zx}) = dP_{zz} + dP_{zx} - dP_{yz} \\
 7. \quad & 4dT_{xx} - 2\sqrt{2} (dN'_{zx} + dN'_{xy} - dT'_{zx} + dT'_{xy}) = -dP_{xx} + dP_{xy} + dP_{zx} \\
 8. \quad & 4dT_{yy} - 2\sqrt{2} (dN'_{xy} + dN'_{yz} - dT'_{xy} + dT'_{yz}) = -dP_{yy} + dP_{yz} + dP_{xy} \\
 9. \quad & 4dT_{zz} - 2\sqrt{2} (dN'_{yz} + dN'_{zx} - dT'_{yz} + dT'_{zx}) = -dP_{zz} + dP_{zx} + dP_{yz}
 \end{aligned}$$

The nine equilibrium equations given above are not sufficient to uniquely describe the behavior of the medium since the problem is statically indeterminate. A set of compatibility conditions are formulated by giving consideration to the admissible displacements of the medium which result from the incremental stresses. Let the components of relative displacements of the centers of spheres be designated by $d\alpha_{ij}$, $d\delta_{ij}$, $d\delta_{kk}$, to correspond, respectively, to the forces dN_{ij} , dT_{ij} , dT_{kk} (Fig. 3.7). We will require that the displacements of the center of the spheres be single valued, i.e., the vector distance around the closed path through the center of the spheres must vanish both before and after the medium is strained. Hence the sum of the relative displacements of the center of these spheres around the closed path must vanish. Expressions for this condition for all possible paths connecting the center of a sphere in the medium yields 9 independent equations of compatibility as follows:

$$\begin{aligned}
 1. \quad & \sqrt{2}d\delta_{zz} = -d\alpha'_{yz} + d\alpha_{zx} + d\delta'_{yz} + d\delta_{zx} \\
 2. \quad & \sqrt{2}d\delta_{zz} = d\alpha_{yz} - d\alpha'_{zx} - d\delta_{yz} - d\delta'_{zx} \\
 3. \quad & \sqrt{2}d\delta'_{zz} = -d\alpha_{yz} + d\alpha_{zx} + d\delta_{yz} + d\delta_{zx}
 \end{aligned}$$

$$\begin{aligned}
 4. \quad \sqrt{2}d\delta_{xx} &= -d\alpha'_{zx} + d\alpha_{xy} + d\delta'_{zx} + d\delta_{xy} \\
 5. \quad \sqrt{2}d\delta_{xx} &= d\alpha_{zx} - d\alpha'_{xy} - d\delta_{zx} - d\delta'_{xy} \\
 6. \quad \sqrt{2}d\delta'_{xx} &= d\alpha_{zx} - d\alpha_{xy} + d\delta_{zx} + d\delta_{xy} \\
 7. \quad \sqrt{2}d\delta_{yy} &= d\alpha'_{xy} + d\alpha_{yz} + d\delta'_{xy} + d\delta_{yz} \\
 8. \quad \sqrt{2}d\delta_{yy} &= d\alpha_{xy} - d\alpha'_{yz} - d\delta_{xy} - d\delta'_{yz} \\
 9. \quad \sqrt{2}d\delta'_{yy} &= -d\alpha_{xy} + d\alpha_{yz} + d\delta_{xy} + d\delta_{yz}
 \end{aligned} \tag{3.9}$$

The compatibility equations can be written in terms of force increments by using the compliances

$$\begin{aligned}
 d\alpha_{ij} &= C_{ij} dN_{ij} & d\alpha'_{ij} &= C'_{ij} dN'_{ij} \\
 d\delta_{ij} &= S_{ij} dT_{ij} & d\delta'_{ij} &= S'_{ij} dT'_{ij} \\
 d\delta_{kk} &= S_{kk} dT_{kk} & d\delta'_{kk} &= S'_{kk} dT'_{kk}
 \end{aligned} \tag{3.10}$$

Where the subscripts identify the contact. Thus Eq. (3.9) together with Eq. (3.8) yield 18 independent equations containing the applied forces dP_{ij} , and 18 independent components of the unknown contact forces, dN_{ij} , dT_{ij} , and dT_{kk} . Unfortunately, however, these 18 equations are non-linear since the equations include the compliances and the compliances are themselves functions of the contact forces. Consequently, a solution to these equations is a very difficult problem and can be obtained only for certain simple cases.

The incremental extensional and shearing strains in the array, expressed in terms of the compliances, are

$$\begin{aligned}
 d\epsilon_{11} &= \frac{1}{4R} (d\alpha_{1j} + d\delta_{1j} + d\alpha'_{1j} + d\delta'_{1j}) \\
 d\gamma_{1j} &= \frac{1}{2R} (d\alpha_{1j} - d\alpha'_{1j})
 \end{aligned} \tag{3.11}$$

Likewise the applied force increments P_{ij} in Fig. 3.4 are related to the stress increments for a face centered array by

$$dP_{ij} = 8R^2 d\sigma_{ij} \quad (3.12)$$

3.1.2 Application to a Hydrostatic State of Stress

One problem of interest which can be solved is that of a face centered array subjected to a hydrostatic state of stress. Under this state of stress we can obtain from symmetry the conditions that all normal forces at the contacts are equal and all shearing forces are equal. If we let

P_o = total force on the face of a differential element

N_o = normal contact force

T_o = tangential contact force

R = radii of spheres

the equilibrium Eqs. (3.8) reduce to

$$4dT_o + \sqrt{2}dN_o = dP_o \quad (3.13)$$

$$4dT_o - \sqrt{2}dN_o = dP_o$$

Adding Eqs. (3.13) and considering the initial condition of zero stress yields the expected condition for the tangential force

$$T_o = dT_o = 0$$

Hence, the equilibrium equation becomes

$$dN_o = \frac{1}{\sqrt{2}} dP_o \quad (3.14)$$

If ϵ_o is the hydrostatic strain in any direction, Eq. (3.11) yields

$$d\epsilon_o = \frac{1}{2R} d\alpha_o \quad (3.15)$$

where $d\alpha_o$ is the normal deformation due to dN_o and is related to dN_o by the normal compliance C_o .

$$d\alpha_o = C_o dN_o \quad (3.16)$$

From the Hertz theory

$$C_o = \frac{1 - \nu}{2\mu a_o} \quad (3.17)$$

where a_o is the radius of contact defined by

$$a_o = \left[\frac{3(1 - \nu) N_o R}{8\mu} \right]^{1/3} \quad (3.18)$$

By combining Eqs. (3.15), (3.16), (3.17) and (3.18), the incremental strain may be expressed as

$$d\epsilon_o = 1/2 \left[\frac{(1-\nu)\sqrt{2}}{\mu} \right]^{2/3} [3\sigma_o]^{-1/3} d\sigma_o \quad (3.19)$$

Integrating Eq. (3.19) and considering zero initial conditions results in

$$\epsilon_o = \left[\frac{3(1-\nu)\sqrt{2}}{8\mu} \right]^{2/3} \sigma_o^{2/3} \quad (3.20)$$

It should be noted that Eq. (3.20) is also the equivalent of the first stress invariant I, being proportional to the three halves power of the first strain invariant J.

It is of interest to compare the results of this theory with some limited experimental results available in the literature. Kjellman [3.7] carried out some tests on dry sand subjected to hydrostatic pressure and measured the strains associated with the pressure. Table 3.1

gives the variation of the first stress and strain invariants taken from his experimental results. A plot of this is shown in Fig. 3.8. Also shown is a plot of the exponential relationship indicated by the theory discussed, which is fitted to the experimental curve at the 6 kg/cm^2 stress level. The behavior of the sand is not as stiff as the dense packing theory indicates in the lower pressure regions while it becomes stiffer than the theory predicts in the higher pressure regions.

The former seems reasonable in that in the lower pressure region the number of contacts is not as large as the 12 assumed for a dense state. Hence the real sand is not as stiff as the spheres. In the higher pressure regions, it seems reasonable to associate the stiffening effect with the random size distribution of particles which differs from the equi-radii spheres assumed in the theory. If the sand grains are of different sizes, more than 12 contacts can be realized after the sand has been compressed sufficiently to allow these contacts to be made. This would tend to make the sand stiffer than the spheres. Furthermore, while every attempt was made by Kjellman to minimize the effect, any frictional resistance due to the testing apparatus would effectively stiffen the measured stress-strain relations.

From the above discussion and development, it can be concluded that the theory associated with the face centered array of spheres shows at least some qualitative correlation with the behavior of dense sand subjected to a hydrostatic state of stress.

3.2 One Dimensional Theory of Granular Media

3.2.1 Monotonically Increasing Load

Let us now extend the theory of Duffy and Mindlin developed in Section 3.1.1 to the solution of the stress-strain behavior of an array

of spheres subjected to one dimensional compression. One dimensional compression is defined as that state of stress resulting from the application of a load in the vertical or z direction when the lateral strains in the x and y directions are zero.

The radial symmetry of the one dimensional problem greatly simplifies Eqs. (3.8) and (3.9). The representative cube now becomes Fig. 3.9, and the forces on a sphere reduce to those shown on Fig. 3.10. From symmetry the following simplifications can be made for the forces and displacements:

$$\begin{aligned}
 N_{xy} &= N'_{xy} = N_1 \\
 N_{zy} &= N'_{yz} = N_{zx} = N'_{zx} = N_2 \\
 -T_{yz} &= -T'_{yz} = T_{zx} = T'_{zx} = T_2 \\
 T_{xx} &= T'_{xx} = T_{yy} = T'_{yy} = T_{zz} + T'_{zz} = 0 \\
 T_{xy} &= T'_{xy} = 0 \\
 P_{xy} &= P_{xz} = P_{zx} = P_{yx} = P_{yz} = P_{zy} = 0 \\
 P_{xx} &= P_{yy} = P_H
 \end{aligned} \tag{3.21}$$

$$\begin{aligned}
 \alpha_{xy} &= \alpha'_{xy} = \alpha_1 \\
 \alpha_{yz} &= \alpha'_{yz} = \alpha_{zx} = \alpha'_{zx} = \alpha_2 \\
 -\delta_{yz} &= -\delta'_{yz} = \delta_{zx} = \delta'_{zx} = \delta_2 \\
 \delta_{xx} &= \delta'_{xx} = \delta_{yy} = \delta'_{yy} = \delta_{zz} = \delta'_{zz} = 0 \\
 \delta_{xy} &= \delta'_{xy} = 0
 \end{aligned} \tag{3.22}$$

Furthermore, the associated compliances now become

$$\begin{aligned}
 C_{xy} &= C'_{xy} = C_1 \\
 C_{yz} &= C'_{yz} = C_{zx} = C'_{zx} = C_2 \\
 S_{yz} &= S'_{yz} = S_{zx} = S'_{zx} = S_2
 \end{aligned} \tag{3.23}$$

Using the above simplifications and considering symmetry the equilibrium Eq. (3.8) reduce to

$$dN_2 + dT_2 = \frac{\sqrt{2}}{8} dP_{zz} \quad (3.24)$$

$$dN_1 + dN_2 - dT_2 = \frac{\sqrt{2}}{4} dP_H$$

In a similar fashion the compatibility Eq. (3.9) reduces to

$$d\alpha_1 - d\alpha_2 + d\delta_2 = 0 \quad (3.25)$$

where the compliance Eqs. (3.10) now become

$$d\alpha_1 = C_1 dN_1$$

$$d\alpha_2 = C_2 dN_2 \quad (3.26)$$

$$d\delta_2 = S_2 dT_2$$

Substituting Eqs. (3.26) into Eq. (3.25) yields

$$C_1 dN_1 - C_2 dN_2 + S_2 dT_2 = 0 \quad (3.27)$$

Equations (3.24) and (3.27) are sufficient to describe the behavior of a granular medium subjected to given vertical and lateral forces P_{zz} and P_H . If, however, only the vertical force is known and the lateral force must also be determined, a further condition is necessary. This condition naturally comes from the lateral strain relationship.

Due to symmetry the lateral strain ϵ_H determined from Eqs. (3.11) reduces to

$$d\epsilon_H = \frac{d\alpha_1}{2R} \quad (3.28)$$

or

$$d\epsilon_H = \frac{C_1 dN_1}{2R} \quad (3.29)$$

Thus the behavior of a face centered array of spheres subjected to a vertical force P_{zz} and restricted to symmetrical lateral deformations can be obtained from a solution to the following equations:

$$\begin{aligned} dN_2 + dT_2 &= \frac{\sqrt{2}}{8} dP_{zz} \\ dN_1 + dN_2 - dT_2 - \frac{\sqrt{2}}{4} dP_H &= 0 \end{aligned} \quad (3.30)$$

$$\frac{C_1}{C_2} dN_1 - dN_2 + \frac{S_2}{C_2} dT_2 = 0$$

$$dN_1 = \frac{2Rd\epsilon_H}{C_1}$$

For the case of interest here, namely one dimensional compression, we require ϵ_H to vanish for all loadings. For this particular stress state and zero initial conditions, we obtain $N_1 = 0$ and Eqs. (3.30) reduce to

$$dN_2 + dT_2 = \frac{\sqrt{2}}{8} dP_{zz} \quad (3.31a)$$

$$dN_2 - dT_2 - \frac{\sqrt{2}}{4} dP_H = 0 \quad (3.31b)$$

$$dN_2 - \frac{S_2}{C_2} dT_2 = 0 \quad (3.31c)$$

where the expression for $\frac{S_2}{C_2}$ is obtained from Eqs. (3.6) and (3.7) as:

$$\frac{S_2}{C_2} = k_1 \left[f \frac{dN_2}{dT_2} + (1 - f \frac{dN_2}{dT_2}) \left(1 - \frac{T_2}{fN_2} \right)^{-1/3} \right] \quad (3.32a)$$

where

$$k_1 = \frac{2-\nu}{2(1-\nu)} \quad (3.32b)$$

The compatibility Eq. (3.31c) states that

$$d\alpha_2 = d\delta_2$$

Hence for the one dimensional case Eq. (3.32) reduces to

$$d\epsilon_{zz} = \frac{d\alpha_2}{R} = \frac{C_2 dN_2}{R} \quad (3.33)$$

It should be noted that Eqs. (3.31) are coupled non-linear differential equations because of the compliances in the third equation.

The vertical strains ϵ_{zz} associated with the behavior of this medium can be obtained from Eqs. (3.11) as

$$d\epsilon_{zz} = \frac{1}{2R} (d\alpha_2 + d\delta_2) \quad (3.34)$$

For the solution of Eqs. (3.31), let us consider first the compatibility Eq. (3.31c). Substituting Eqs. (3.32) into Eq. (3.31c) yields after some rearrangement of terms

$$\frac{dT_2}{dN_2} = f + \frac{1-k_1 f}{k_1} \left(1 - \frac{T_2}{fN_2}\right)^{1/3} \quad (3.35)$$

Introduce now the new variable

$$Z^3 = f - \frac{T_2}{N_2} \quad (3.36a)$$

and

$$N_2 Z^3 = N_2 f - T_2$$

$$dN_2 Z^3 + N_2(3) Z^2 dZ = f dN_2 - dT_2$$

or

$$\frac{dT_2}{dN_2} = f - Z^3 - 3N_2 Z^2 \frac{dZ}{dN_2} \quad (3.36b)$$

Using Eqs. (3.36), Eq. (3.35) can be transformed into the following form.

$$- \frac{3Z dZ}{Z^2 + K_2} = \frac{dN_2}{N_2} \quad (3.37)$$

where

$$K_2 = \frac{1 - k_1 f}{k_1^{1/3}} \quad (3.38)$$

Integrating both sides results in

$$\ln N_2 - \ln A = -3/2 \ln (Z^2 + K_2)$$

or

$$\frac{N_2}{A} = (Z^2 + K_2)^{-3/2} \quad (3.39)$$

where A is a constant of integration.

From Eq. (3.36a), Eq. (3.39) becomes

$$\frac{N_2}{A} = \left[\left(f - \frac{T_2}{N_2} \right)^{2/3} + K_2 \right]^{-3/2} \quad (3.40)$$

Equation (3.40) is the general solution to Eq. (3.31c) and a particular solution may be obtained by evaluating the constant of integration

A. Since we are interested in the initial conditions $P_{zz} = N_2 = T_2 = 0$, one is inclined to evaluate A from these conditions. While this is a true boundary condition, a singularity point occurs at the origin. The equation is, however, well behaved at other points and the following technique will be used to evaluate A.

Imagine a small hydrostatic state of stress initially holding the spheres in contact before the one dimensional state is imposed. This hydrostatic stress produced no initial tangential force at the contacts but it does cause a normal force of $N_2 = N_0$.

From Eq. (3.40)

$$N_0 = A(f^{2/3} + K_2)^{-3/2}$$

or solving for A, the constant of integration

$$A = \frac{N_0}{(K_2 + f^{2/3})^{-3/2}} \quad (3.41)$$

Substituting A into Eq. (3.40) yields after some rearranging and taking into account Eq. (3.38).

$$T_2 = fN_2 \left[1 - \left(\frac{1}{fK_1} \left[\left(\frac{N_0}{N_2} \right)^{2/3} - 1 \right] + 1 \right)^{3/2} \right] \quad (3.42)$$

A plot of a family of curves representing Eq. (3.42) with various values of the initial hydrostatic stress N_0 is given in Fig. 3.11. The paths of loading are indicated by arrows on the curves. For convenience the coefficient of friction f was taken as 0.3 and Poisson's ratio ν as 0.2.

If an initial hydrostatic stress is imposed we can determine the value of N_2 when the sliding occurs. For this condition we see that from Eq. (3.42)

$$\frac{1}{fK_1} \left[\left(\frac{N_0}{N_2} \right)^{2/3} - 1 \right] + 1 = 0$$

Rewriting and taking account of (3.32b) yields

$$N_2 = \frac{N_0}{\left[1 - \frac{f(2-\nu)}{2(1-\nu)} \right]^{3/2}} \quad (3.43)$$

The reader will recall that we were initially interested in defining the relation between N_2 and T_2 for a granular medium in a one dimensional state of stress which was loaded from an unstressed condition. We noted that the solution contained a singularity at the zero stress and it was necessary to provide an initial hydrostatic stress N_0 to hold the spheres in contact when loading. If we now allow N_0 to approach zero we obtain the solution desired.

On investigating Fig. 3.11 or Eq. (3.42) it is clear that if one dimensional loading commences from a completely unstressed condition ($N_0 = 0$), the relation between N_2 and T_2 is that of a straight line with a slope of $1/f$. Thus, the relationship between N_2 and T_2 for a face centered array subjected to one dimensional compression is

$$T_2 = fN_2$$

This means that sliding (differentiated from slip in Section 3.1.1) at the contacts occurs immediately on initiation of loading. This

is extremely important in that the theory developed to date along the lines of Mindlin, et al, does not allow sliding at the contacts. The authors, however, will show in the following that the stress-strain relationships in the one dimensional granular medium can be described mathematically even though sliding occurs throughout the application of a monotonically increasing load.

From compatibility, even in the case of sliding, the geometrical relationship still holds for the displacements at the contacts, i.e.

$$d\alpha_2 - d\delta_2 = 0 \quad (3.44)$$

It should be clear, however, that the tangential displacement δ_2 is no longer related to the tangential contact force T_2 by the tangential compliance S_2 because of sliding at the contacts. The tangential displacement is now made up of two effects, a sliding effect and a contribution due to slip. On the other hand, the normal forces and displacements are still connected by the compliances.

Furthermore, since Eq. (3.44) is a geometrical relationship, it holds as well for total displacements in the problem at hand. Hence,

$$\alpha_2 = \delta_2 \quad (3.45)$$

The vertical strain Eq. (3.33) is also geometrical and can be used to obtain the strain for the medium.

$$d\epsilon_{zz} = \frac{d\alpha_2}{R} = \frac{C_2 dN_2}{R} \quad (3.46)$$

Next we note that the equilibrium Eqs. (3.31a) and (3.31b), which were originally written in terms of differential stresses, also hold for total stresses. Hence

$$N_2 + T_2 = \frac{\sqrt{2}}{8} P_{zz} \quad (3.47a)$$

$$N_2 - T_2 - \frac{\sqrt{2}}{4} P_H = 0 \quad (3.47b)$$

We have already determined that N_2 and T_2 are connected by the coefficient of friction throughout the entire loading, i.e.

$$fN_2 - T_2 = 0 \quad (3.47c)$$

The behavior of a granular medium of face centered packing subjected to one dimensional compression can now be described by Eqs. (3.44), (3.54), (3.46), and (3.47).

Equations (3.47) may be combined to eliminate T_2 resulting in

$$N_2(1+f) = \frac{\sqrt{2}}{8} P_{zz} \quad (3.48a)$$

$$N_2(1-f) = \frac{\sqrt{2}}{4} P_H \quad (3.48b)$$

In theoretical and applied soil mechanics a quantity of major interest in one dimensional compression is K_0 , the ratio between the horizontal and vertical stresses at rest. From Eqs. (3.48) this ratio is clearly

$$K_0 = \frac{P_H}{P_{zz}} = \frac{1}{2} \left(\frac{1-f}{1+f} \right) \quad (3.49)$$

Some indication of the variation of K_0 with the coefficient of friction f is shown in Table 3.2.

Let us now determine the strains resulting from one dimensional compression. The substitution of Eq. (3.2) into Eq. (3.46) yields

$$d\epsilon_{zz} = \frac{(1-\nu)}{2\mu R} \left[\frac{3(1-\nu) RN_2}{8\mu} \right]^{-1/3} dN_2 \quad (3.50)$$

Combining Eqs. (3.50) and (3.48a) and noting from Fig. 3.9 that

$$\sigma_{zz} = \frac{P_{zz}}{8R^2} \quad (3.51)$$

gives

$$d\epsilon_{zz} = \frac{1}{2} \left[\frac{(1-\nu)\sqrt{2}}{\mu(1+f)} \right]^{2/3} \left[\frac{3}{8} \sigma_{zz} \right]^{-1/3} d\sigma_{zz} \quad (3.52)$$

Integration of Eq. (3.52) yields

$$\epsilon_{zz} = \left[\frac{(1-\nu)(3)\sqrt{2}}{\mu(1+f)(8)} \right]^{2/3} \sigma_{zz}^{2/3} \quad (3.53)$$

An interesting result of Eq. (3.53) is that the stress-strain behavior is independent of the radii of the particles. A comparison of the stress-strain curves for hydrostatic and one dimensional compression shows that the curves are similar in shape, but turn up at different rates. The ratio of the one dimensional strain to the hydrostatic strain at the same level of stress, σ_{zz} , is a ratio of Eqs. (3.53) to (3.20), which reduces to

$$\frac{\epsilon_{zz}}{\epsilon_o} = \frac{2}{(1+f)^{2/3}} \quad (3.54)$$

Values of f of 0.1 and 0.2 give values for ϵ_{zz}/ϵ_o of 1.88 and 1.77, respectively. This indicates that the hydrostatic and one dimensional stress-strain curves are related as shown in Fig. 3.12.

3.2.2 Unloading Cycle

When the medium is loaded the tangential forces tend to resist the sliding motion. For unloading the tangential forces tend to resist the sliding movement which is now in the opposite direction. Hence, the tangential forces reverse their direction on unloading. These two cases are illustrated schematically in Fig. 3.13. The normal and tangential forces are still related by the coefficient of friction; only now the direction of the tangential force is changed.

The new equilibrium equations become

$$N_2 - T_2 = \frac{\sqrt{2}}{8} P_{zz} \quad (3.55)$$

$$N_2 + T_2 = \frac{\sqrt{2}}{4} P_H$$

where

$$fN_2 - T_2 = 0 \quad (3.56)$$

Consider the medium to be loaded from 0 to σ_{zz}^* , Fig. 3.14 according to Eqs. (3.53). If equilibrium Eqs. (3.55) become valid at the instant ϵ_{zz} begins to decrease from ϵ_{zz}^* , then σ_{zz} will decrease instantaneously from σ_{zz}^* to some value σ_{zz}' . At the end of loading N_2 and σ_{zz}^* are related by

$$\sigma_{zz}^* = N_2 \frac{(1+f)}{\sqrt{2}R^2} \quad (3.57)$$

whereas the stress σ_{zz}' is related to the contact forces by Eqs. (3.54) and Eq. (3.51) by

$$\dot{\sigma}_{zz} = \frac{N_2 (1-f)}{\sqrt{2}R^2} \quad (3.58)$$

the relation between σ_{zz}^* and $\dot{\sigma}_{zz}$ at the instant where ϵ_{zz} just begins to decrease when the value N_2 has essentially the same value while the shearing stress has switched directions is

$$\dot{\sigma}_{zz} = \sigma_{zz}^* \left(\frac{1-f}{1+f} \right) \quad (3.59)$$

Combining Eqs. (3.55), (3.51), (3.46) and (3.2) yields for unloading

$$d\epsilon_{zz} = 1/2 \left[\frac{(1-\nu)\sqrt{2}}{\mu(1-f)} \right]^{2/3} \left[3/8 \sigma_{zz} \right]^{-1/3} d\sigma_{zz} \quad (3.60)$$

which by integration becomes

$$\epsilon_{zz} = \left[\frac{(1-\nu)\sqrt{2}}{\mu(1-f)} \right]^{2/3} \frac{2}{3} \sigma_{zz}^{2/3} \quad (3.61)$$

The entire stress-strain history for one cycle of loading in one dimensional compression is shown in Fig. 3.14 in terms of σ_{zz}^* and $\dot{\sigma}_{zz}$. The derivations above are based upon the assumption that the tangential contact forces immediately reverse directions when unloading begins. This assumption is not quite true, however, since each sphere must exhibit a small elastic tangential displacement before the tangential forces can change direction. This effect however, is small with respect to the tangential displacement due to sliding, and was neglected in the analysis. Due to the above assumption, the stress-strain curve reflects a vertical drop in stress from A to B without any change in

strain. If the small elastic tangential displacement due to slip were accounted for, the stress-strain curve would not have a cusp in it at B, and would follow the dotted line shown in Fig. 3.14.

The stress-strain behavior shown in Fig. 3.14 exhibits an energy loss after a cycle of loading and unloading but has no residual strain. Hence, this medium can absorb energy without any permanent displacements.

3.2.3 Energy Absorption

The amount of energy absorbed by the medium on loading and subsequent unloading can now be determined.

The energy E_1 required to load up to an applied vertical stress of p_1 and the strain of ϵ_1 is

$$E_1 = \int_0^{\epsilon_1} \sigma_{zz} d\epsilon_{zz} \quad (3.62)$$

$$E_1 = \frac{4}{5} (1+f) \epsilon_1^{5/2}$$

The energy taken out of the medium E_2 during unloading back to zero from a stress of σ_2 and strain ϵ_1 is

$$E_2 = \frac{4}{5} (1-f) \epsilon_1^{5/2} \quad (3.63)$$

Thus, the energy lost is

$$\Delta E = E_1 - E_2 = \frac{8}{5} f \epsilon_1^{5/2} \quad (3.64)$$

Likewise the ratio of the energy loss to the energy input is

$$\frac{\Delta E}{E_1} = \frac{2f}{1+f} \quad (3.65)$$

Thus, a very significant property of the one dimensional stress-strain curve is that the per cent of energy absorbed due to loading and unloading is always constant for a material and depends only on the coefficient of friction at the contacts. Hence, the ratio of the area between the loading and unloading curves to the area under the loading curve is a constant given by Eq. (3.65). The per cent energy absorbed for various coefficients of friction is given in Table 3.2.

In summary it should be clear how the contact forces and energies associated with this medium are connected. The work done by the normal forces during deformation $\int N_2 d\alpha_2$ is stored in the form of recoverable strain energy. On the other hand, the work done by the tangential forces $\int T_2 d\delta_2$ is a nonrecoverable energy and is dissipated as heat into the medium. As seen from Table 3.2 this energy loss during one cycle can be quite significant. In fact, with a coefficient of friction of 0.15, the dissipated energy is 26.1% of the energy put into the system.

3.3 Equivalent Discrete Mass Model for One Dimensional Static and Dynamic Behavior

In recent years, an increasing effort has been devoted to studying the static and dynamic behavior of soils using discrete mass-spring models. These models have taken many shapes with various contributions from models such as the standard Voigt and Maxwell models. These model

studies have been particularly useful in wave propagation studies, such as the work of Smith and Newmark [3.8]. The dynamic equations of motion can be integrated numerically with a digital computer using the β -method [3.9] and it is a fairly straightforward approach to modify soil parameters or spring stiffnesses as the need arises.

As might be expected from such an approach, there are certain aspects of the soil behavior which escape the mass-spring model. Part of this inaccuracy is due to the discreteness of the system and part can be attributed to choice of the model itself.

A study of the problems associated with the choice of various models for investigating the propagation of stress waves in a one dimensional medium has been carried out by Murtha [3.10].

In spite of the inherent difficulties associated with the use of models, there are some cases where the model is the only hope and in fact can be a very valuable tool. For that reason the authors would like to suggest a one dimensional model which seems to exhibit the behavior expected of dry cohesionless sand, and is based upon the theory presented in Section 3.2.

If a pressure on the surface of the earth extends over a large enough area, it may be reasonable to consider soil completely confined. If this is valid and if the soil composition is similar to sand, the one dimensional behavior discussed herein may very well be a good approximation to the in situ soil behavior.

3.3.1 Horizontal Model

Figure 3.15 gives a model representation of the sphere system developed in Section 3.2. This model yields the same stress-strain curve

as the spheres for a static load as the load increases or decreases, and the equations of equilibrium in the limit approach those of the spheres. The model consists of non-linear spring elements and Coulomb damping elements which dissipate energy in the same way as the spheres. The reason that it depicts horizontal behavior is that there are no initial stresses in the model before the load is applied. Such an assumption might be reasonable for a vertical column if the weight of the soil can be neglected compared to the applied stresses.

3.3.2 Vertical Model

The vertical model is slightly more complex than the horizontal one in that the weight of the material produces initial stresses in the model. Since the stress-strain curve for the material is non-linear, the stiffness is a function of the stress, and consequently, a function of the height of overburden. The overburden pressure increases linearly with depth and it can therefore be incorporated in the equations of motion.

A vertical model which includes the initial stresses due to the overburden of the material is given in Fig. 3.16. It includes a change in stiffness associated with the increased initial stress and follows the stress-strain behavior consistent with the analysis of the sphere medium in Section 3.2.

REFERENCE

- 3.1 Duffy, J. and Mindlin, R. D., "Stress-Strain Relations and Vibrations of a Granular Medium," Journal of Applied Mechanics, Vol. 24, Trans. ASME, Vol. 79, 1957, pp. 585-593.
- 3.2 Thurston, C. W. and Deresiewicz, H., "Analysis of a Compression Test of a Face-Centered Cubic Array of Elastic Spheres," Journal of Applied Mechanics, Vol. 26, Trans. ASME, Vol. 81, 1959, pp. 251-258.
- 3.3 Deresiewicz, H., "Mechanics of Granular Matter," Advances in Applied Mechanics, Vol. 5, Academic Press, Inc., New York, 1958.
- 3.4 Cattaneo, C., "Sul Contatto di due corpi elastici," Accademi dei Lincei, Rendiconti, Series 6, Vol. 27, 1938, pp. 342-348, 434-436 and 474-478.
- 3.5 Mindlin, R. D., "Compliance of Elastic Bodies in Contact," Journal of Applied Mechanics, Vol. 16, Trans. ASME, Vol. 71, 1949, p. A-259.
- 3.6 Mindlin, R. D. and Deresiewicz, H., "Elastic Spheres in Contact Under Varying Oblique Forces," Journal of Applied Mechanics, Vol. 20, Trans. ASME, Vol. 75, 1953, pp. 327-344.
- 3.7 Kjellman, W., "Report on an Apparatus for Consummate Investigation of the Mechanical Properties of Soils," First International Conf. on Soil Mechanics and Foundation Engineering, Cambridge, 1936, Vol. 2, p. 16.
- 3.8 Smith, R. H. and Newmark, N. M., "Numerical Integrations for One-Dimensional Stress Waves," Civil Engineering Studies, Structural Research Series No. 162, University of Illinois, August 1958.
- 3.9 Newmark, N. M., "A Method of Computation for Structural Dynamics," Proceedings ASCE, EM3, July 1959, pp. 67-94.
- 3.10 Murtha, J. P., "Discrete Mass Mathematical Models for One Dimensional Stress Waves," Ph.D. Thesis, University of Illinois, 1961.

TABLE 3.1 VARIATION OF STRESS AND STRAIN INVARIANTS

(From Kjellman [3.7])

$I_1/\lambda = \frac{1}{3} (\sigma_1 + \sigma_2 + \sigma_3)$	$\Delta v/v = (\epsilon_1 + \epsilon_2 + \epsilon_3) = J_1$	$J_{1/3}$
kg/cm ²	10 ⁻² in/in.	10 ⁻² in/in
1	0.12	0.04
2	0.24	0.08
4	0.38	0.13
6	0.47	0.16
8	0.54	0.18
10	0.62	0.21
12	0.69	0.23

I_1 = First stress invariant

J_1 = First strain invariant

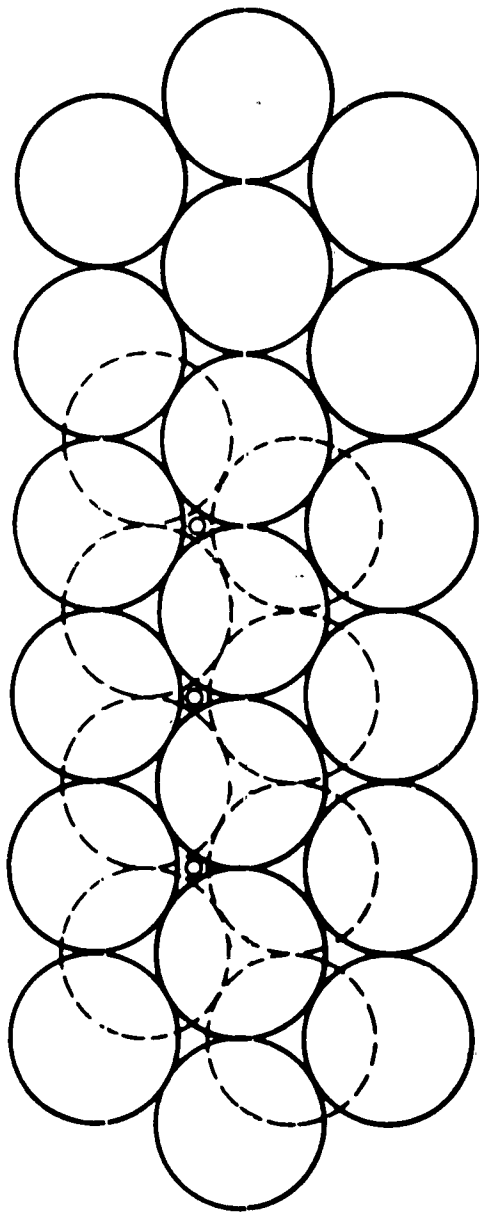
TABLE 3.2 EFFECT OF THE COEFFICIENT OF FRICTION ON
ONE DIMENSIONAL STRESS-STRAIN BEHAVIOR OF
FACE CENTERED ARRAY OF SPHERES

f	K_o	$\Delta E/E_1 \times 100\%$
		$\frac{2f}{1+f} \times 100$
0	0.5	0
0.05	0.45	9.5
0.10	0.41	18.2
0.15	0.37	26.1
0.20	0.33	33.3
0.25	0.30	40.0
0.30	0.27	46.2

f = coefficient of friction at contact points

K_o = coefficient of earth pressure at rest, p_H/p_z

$\frac{\Delta E}{E_1} \times 100\%$ = percent energy absorbed due to loading and unloading



0: Location of sphere centers in third layer
resulting in a face-centered cubic array

Fig. 3.1 CONSTRUCTION OF DENSEST PACKING OF EQUAL SPHERES
AFTER REF. 3, 3

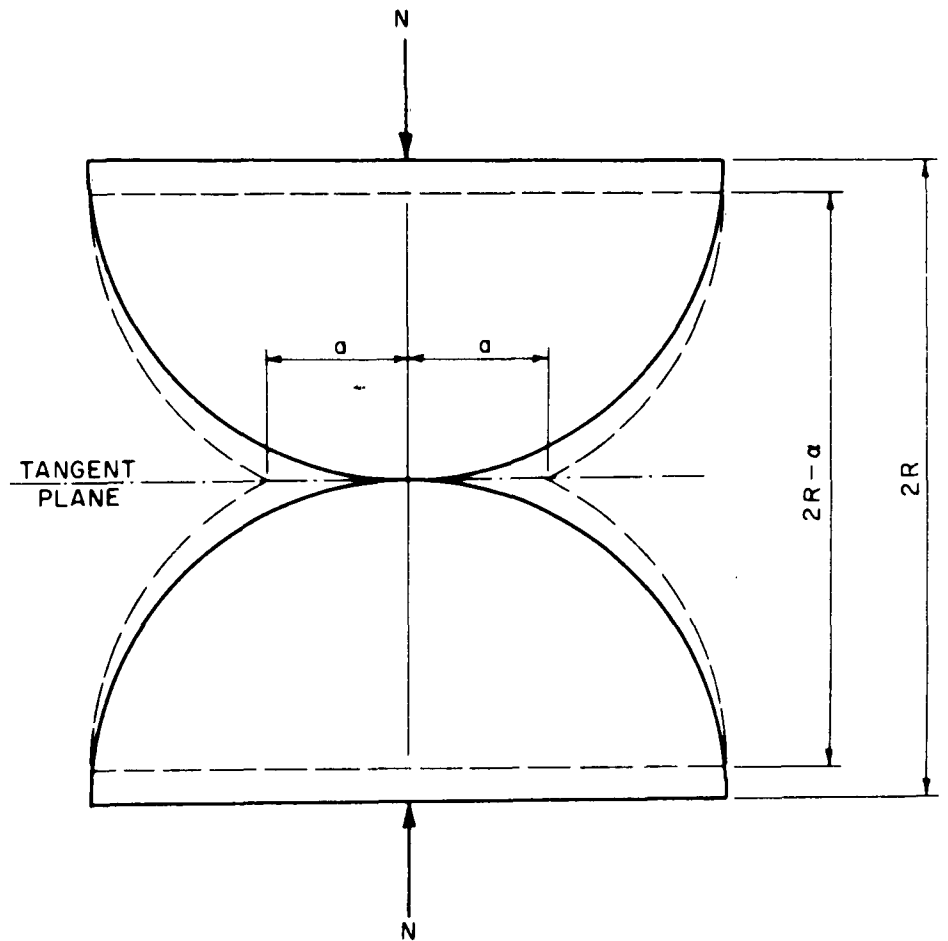


Fig. 3.2 TWO SPHERES IN NORMAL CONTACT

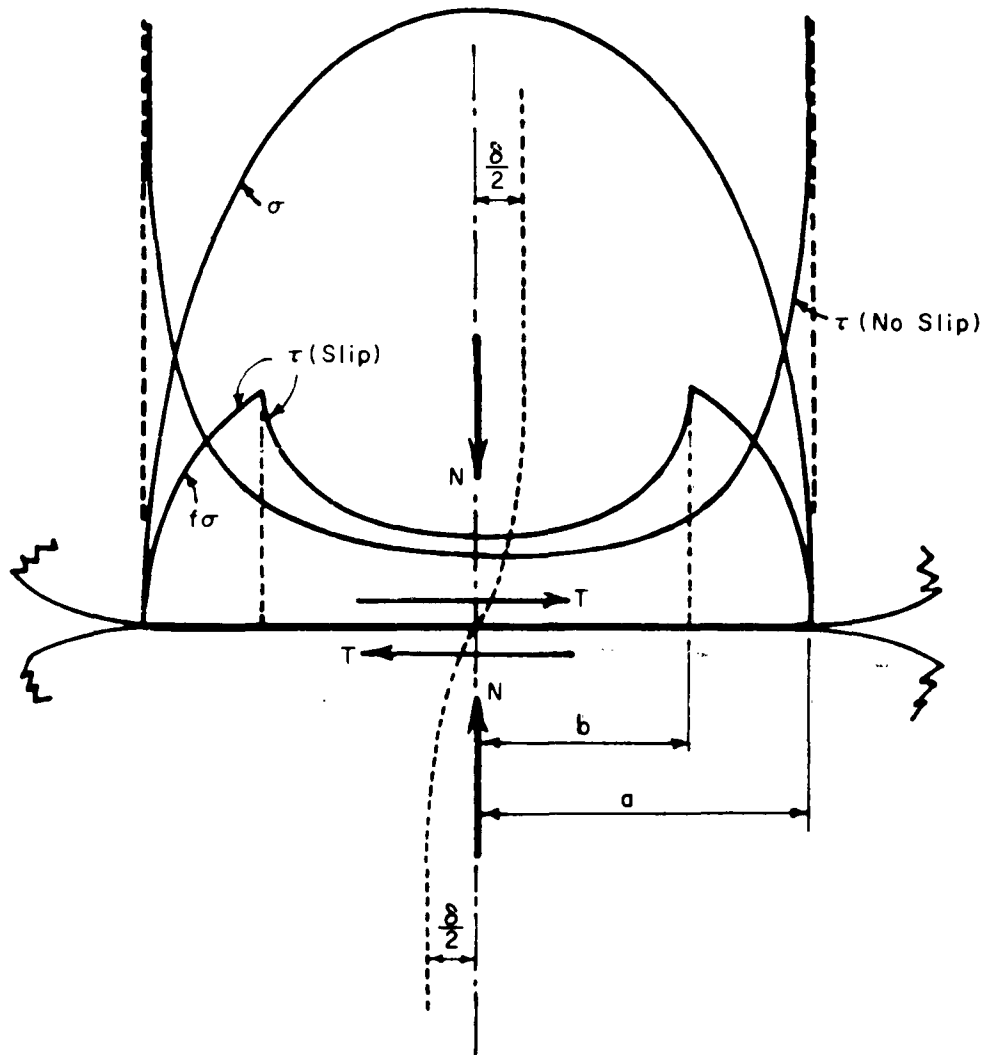


Fig. 3.3 DISTRIBUTIONS OF NORMAL (σ) AND TANGENTIAL (τ) COMPONENTS OF TRACTION ON THE CONTACT SURFACE OF TWO LIKE SPHERES SUBJECTED TO A NORMAL FORCE FOLLOWED BY A MONOTONIC TANGENTIAL FORCE (after Mindlin)

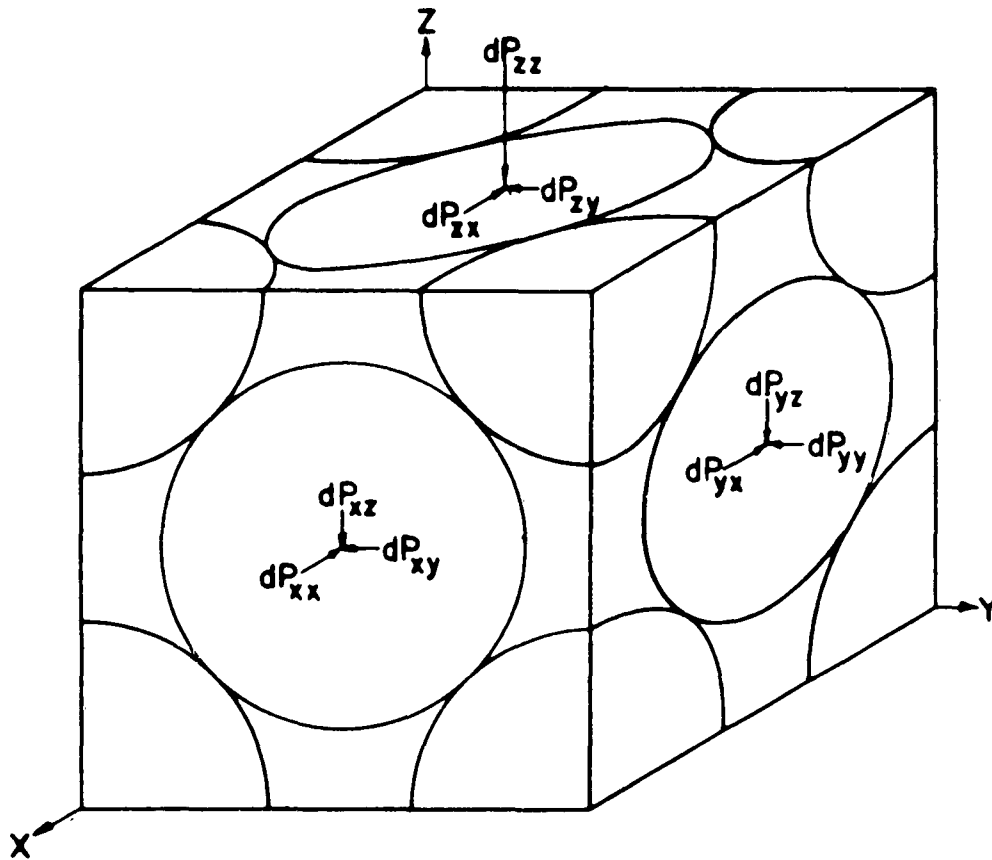


Fig. 3.4 UNIT CUBE OF A FACE CENTERED CUBIC ARRAY OF
EQUAL SPHERES SUBJECTED TO INCREMENT FORCES
AFTER REF. 3, 3

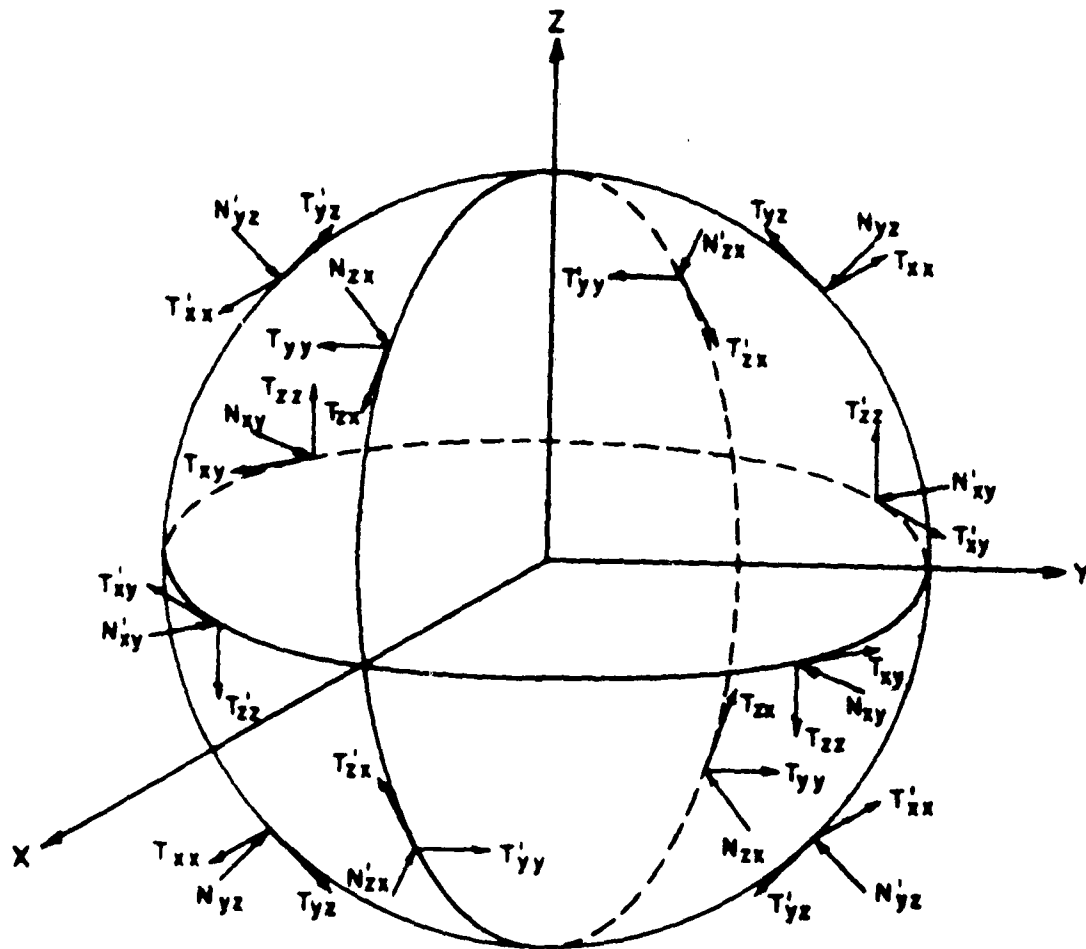


Fig. 3.5 FORCES ACTING ON A TYPICAL
SPHERE OF A FACE CENTERED ARRAY
AFTER REF. 3.2

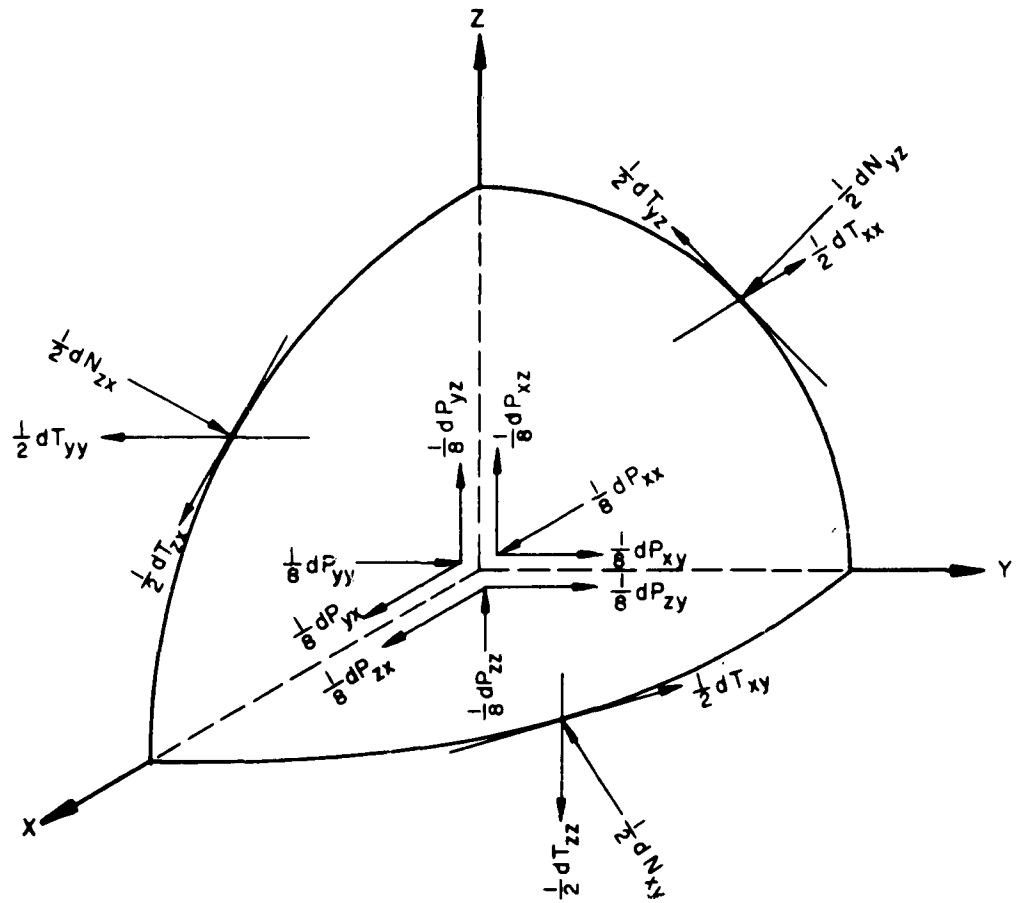


Fig. 3.6 FORCES ACTING ON AN OCTANT OF A SPHERE
(Octant Shown Here is Located at Origin
in Fig. 3.5)
AFTER REF. 3.1

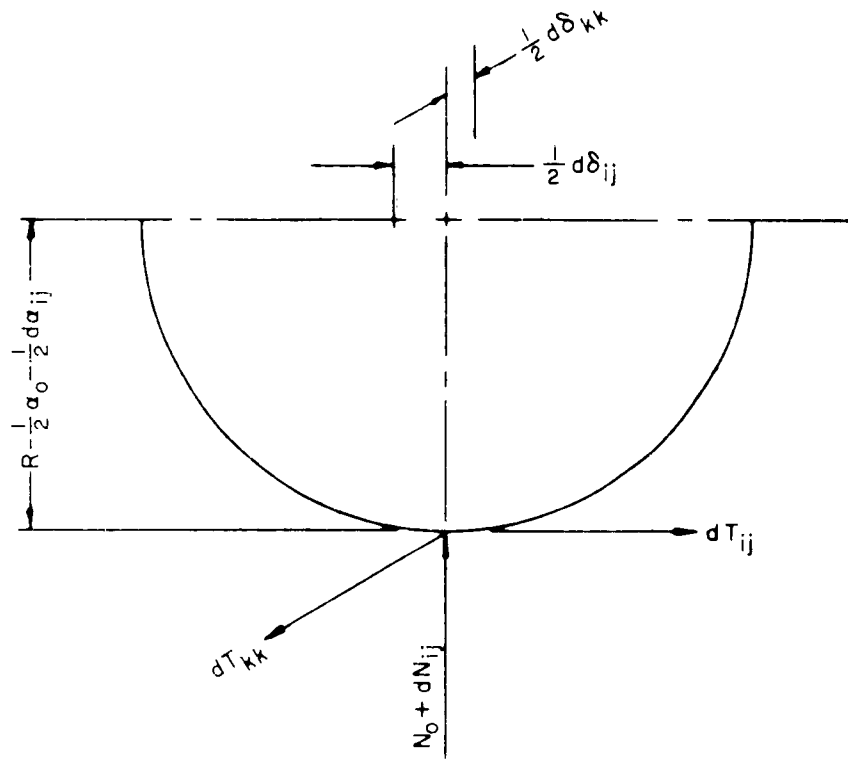


Fig. 3.7 COMPONENTS OF FORCE AT A CONTACT AND CORRESPONDING COMPONENTS OF DISPLACEMENT OF THE CENTER OF A SPHERE AFTER REF. 3.1

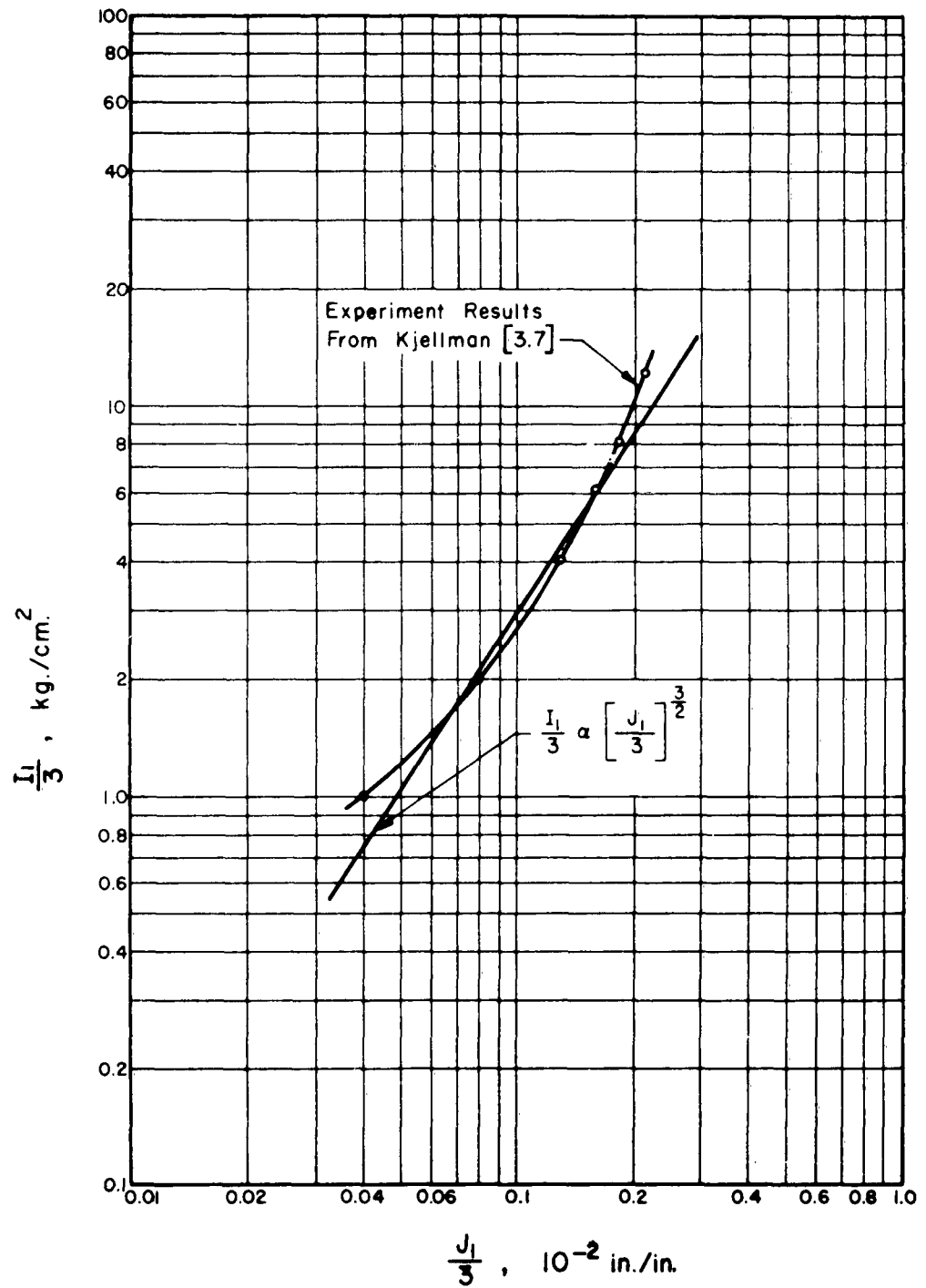


Fig. 3.8 VARIATION OF FIRST STRESS INVARIANT
WITH FIRST STRAIN INVARIANT

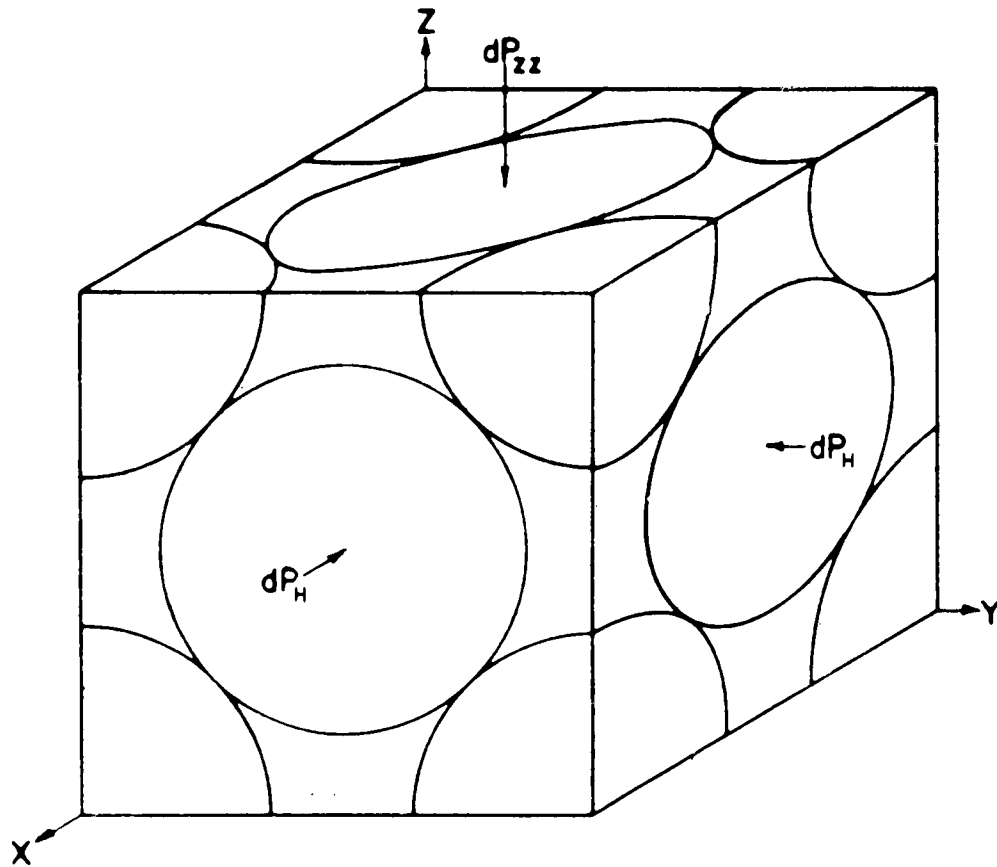
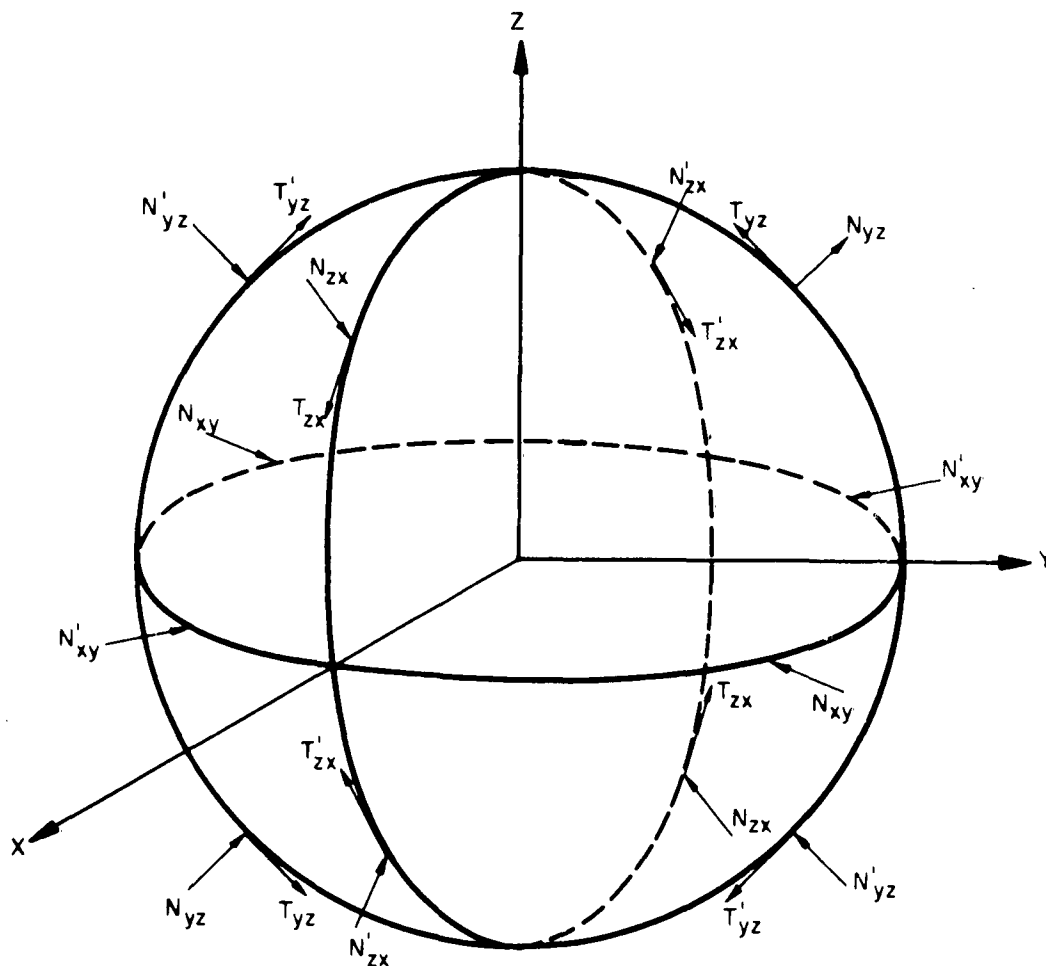


Fig. 3.9 UNIT CUBE OF A FACE CENTERED CUBIC ARRAY OF EQUAL SPHERES SUBJECTED TO INCREMENTAL FORCES IN ONE DIMENSIONAL COMPRESSION



Note That Due To Symmetry

$$T_{zx} = T'_{zx} = -T_{yz} = -T'_{yz} = T_2$$

$$N_{yz} = N'_{yz} = N_{zx} = N'_{zx} = N_2$$

$$N_{xy} = N'_{xy} = N_1$$

Fig. 3.10 FORCES ACTING ON A TYPICAL SPHERE SUBJECTED TO ONE DIMENSIONAL COMPRESSION

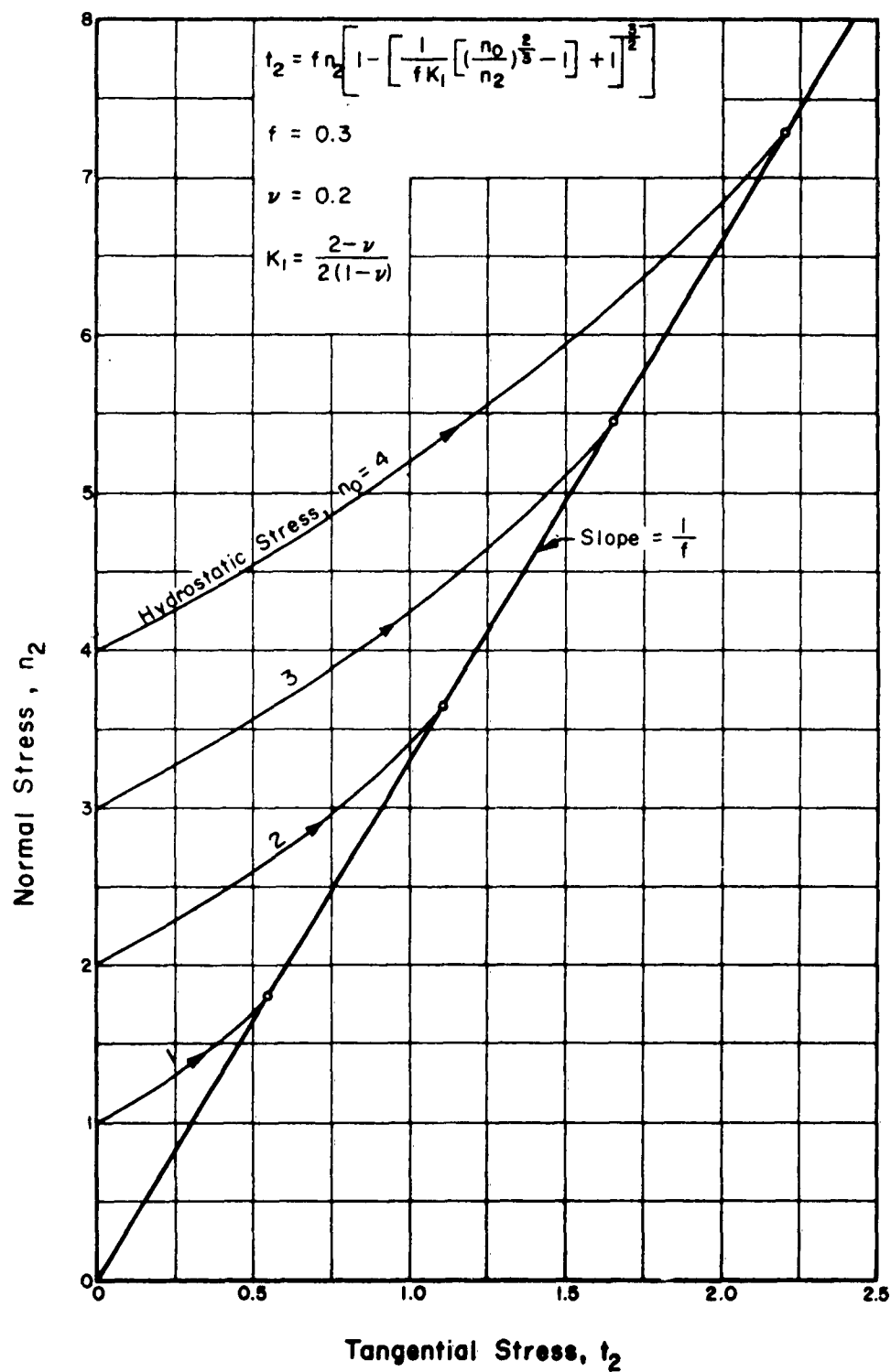


Fig. 3.11 VARIATION OF CONTACT STRESSES UNDER ONE DIMENSIONAL BEHAVIOR WITH AN INITIAL HYDROSTATIC STRESS

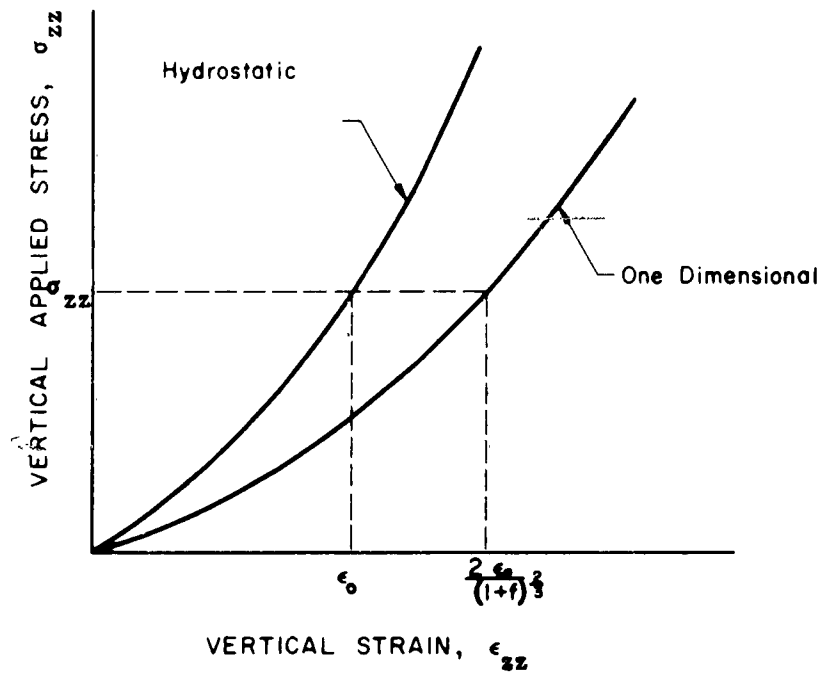
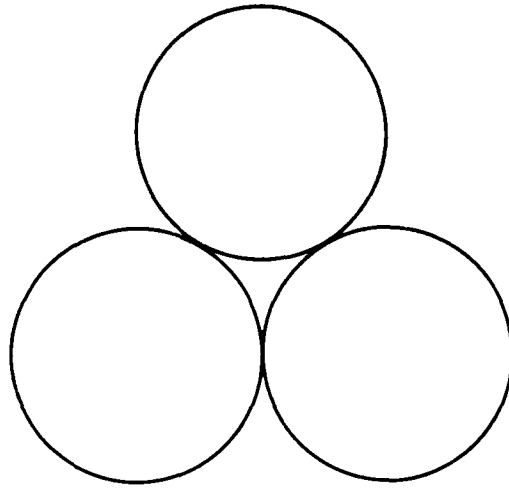
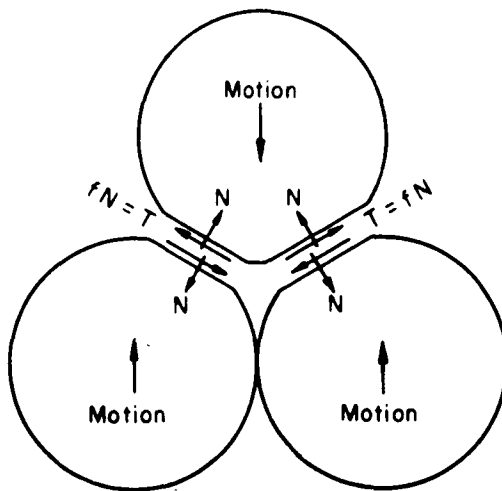


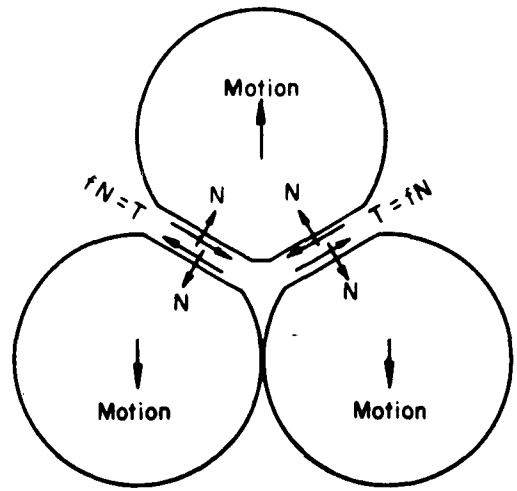
Fig 3.12 NON-DIMENSIONAL STRESS STRAIN CURVES FOR A FACE CENTERED ARRAY OF SPHERES SUBJECTED TO HYDROSTATIC AND ONE DIMENSIONAL STATES OF STRESS



(a) Unloaded State



(b) Loading Cycle



(c) Unloading Cycle

Fig. 3.13 SCHEMATIC REPRESENTATION OF THE DIRECTION OF THE CONTACT FORCES WHEN LOADING AND UNLOADING UNDER ONE DIMENSIONAL COMPRESSION

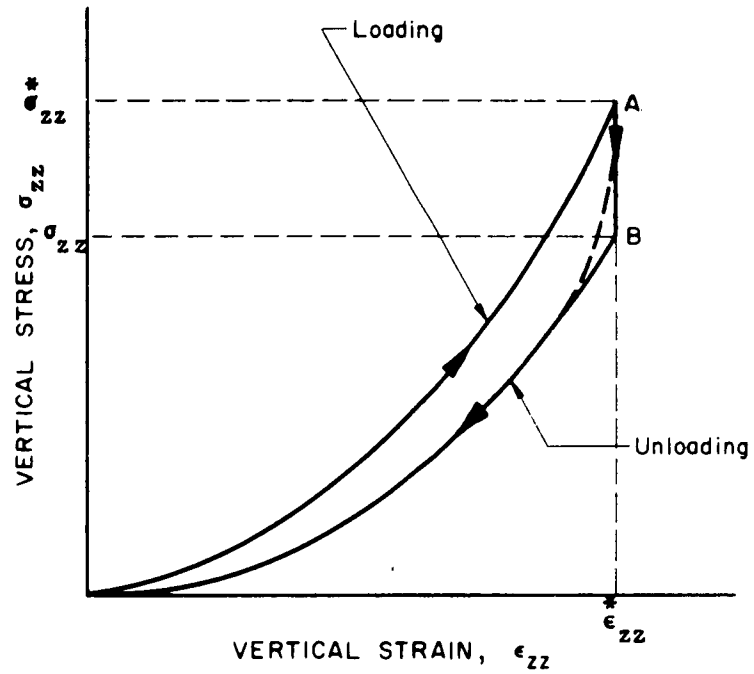
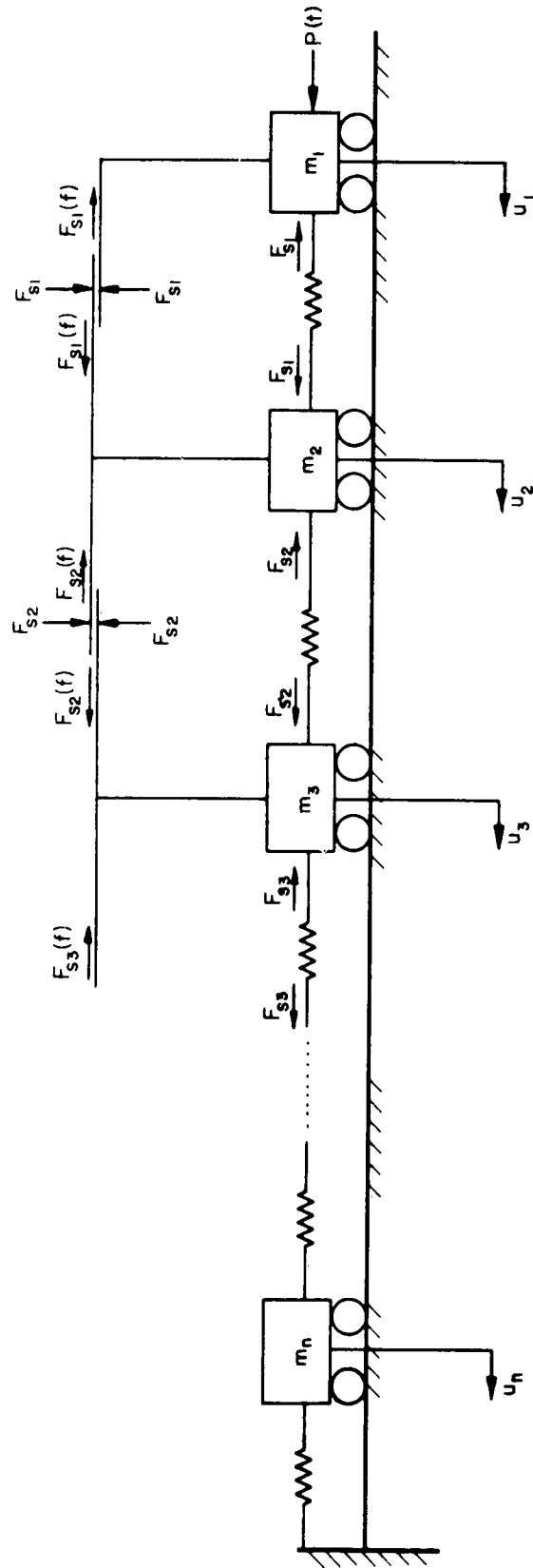


Fig. 3.14 LOADING AND UNLOADING ONE DIMENSIONAL STRESS STRAIN CURVE FOR A FACE CENTERED ARRAY OF SPHERES



$$F_{s1} = k(u_1 - u_2)^{\frac{3}{2}}$$

$$F_{s2} = k(u_2 - u_3)^{\frac{3}{2}}$$

$$F_{s3} = k(u_3 - u_4)^{\frac{3}{2}}$$

In General, $F_{sn} = k(u_n - u_{n+1})^{\frac{3}{2}}$

Fig. 3.15 ONE DIMENSIONAL HORIZONTAL SAND MODEL

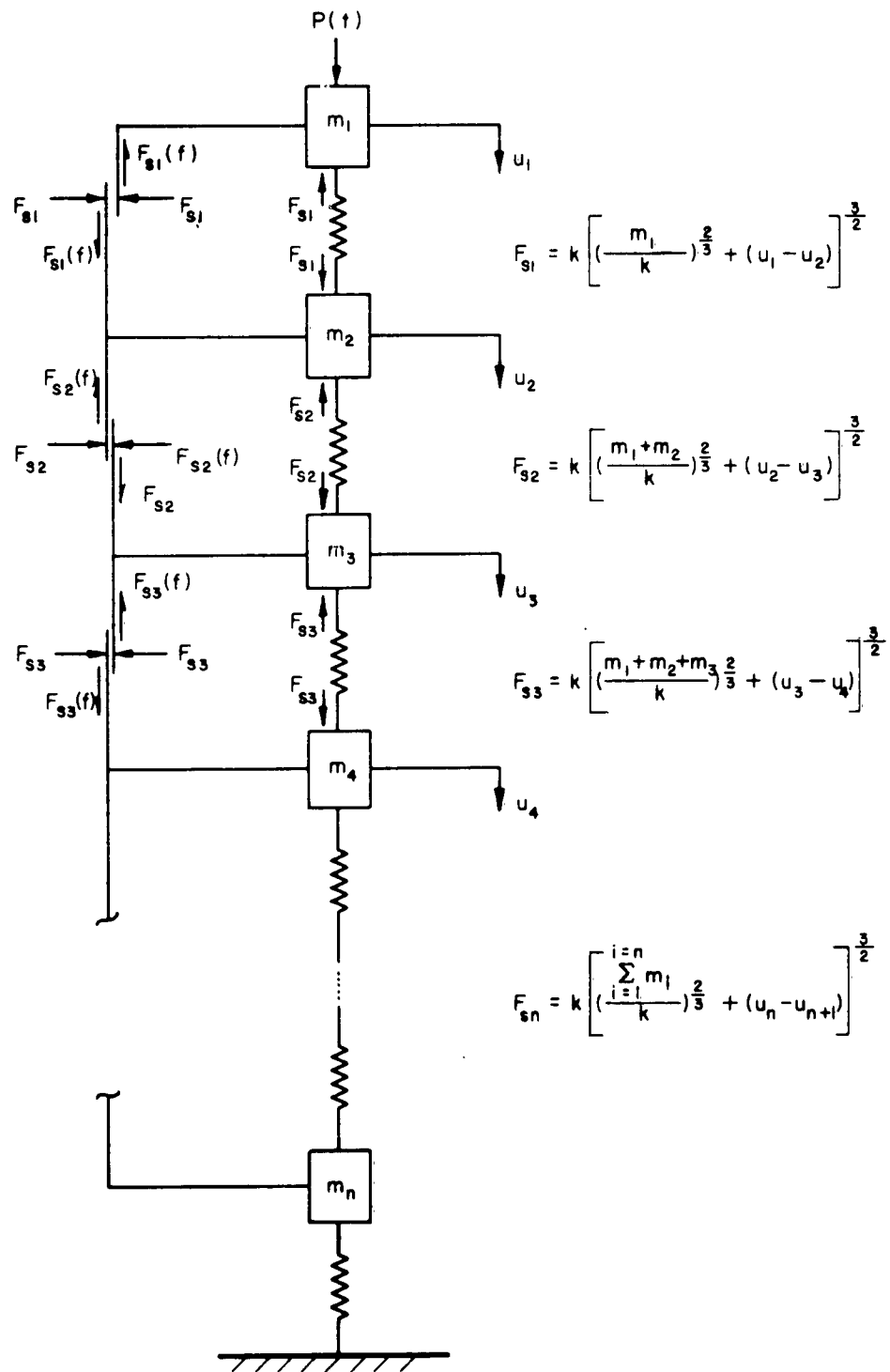


Fig 3.16 ONE DIMENSIONAL VERTICAL SAND MODEL

CHAPTER 4

EFFECT OF GRAIN CRUSHING ON THE BEHAVIOR OF SANDS

4.1 Introduction

Typical stress-strain curves for a granular material such as sand subjected to static loads in one dimensional compression are shown in Figs. 4.10 - 4.14. The general shape of these curves has been qualitatively discussed in Chapter 1. The purpose of this chapter is to make some evaluation of the energy absorbed by the sand in the pressure ranges where crushing of the grains takes place. One should note that this is only one of the mechanisms by which the sand absorbs energy; however, energy absorption in this region can be very significant.

The energy absorbed by crushing will be evaluated by determining the new surface area created as a result of crushing. The increase in new surface area will be determined from a statistical evaluation of the change in the grain size distribution curve for each pressure range. Since new surface area can be related to energy absorbed in the crushing phenomena, then energy absorption due to the creation of new surfaces can be related to the changes in the grain size distribution curve. The results of this analysis led to additional studies of stress-strain curves for sands in the crushing region, which showed that the total energy absorbed due to particle crushing is linearly related to the stress.

4.2 Energy Absorbed Due to Crushing

4.2.1 Statistical Evaluation of Grain Size Distribution Curve

Since the change in the grain size distribution curve for a sand is a measure of the change in the particle sizes, and consequently, the change in the surface area of the particles, it is also a measure

of the energy absorbed by the sand due to crushing. Since each group of particles is in some sense a random accumulation of these particles and, furthermore, since the crushing of the particles will tend to occur in a somewhat random fashion, it would appear that an investigation of the statistical distribution of the particles and certain geometric parameters is required.

To follow this thesis, the concepts presented by Orr and Dalla-
valle [4.1, 4.2] will be followed. It will be shown how certain statistical measurements of a group of particles may be used to obtain useful parameters which characterize the distribution of these particles.

If the particles are all spheres (or very nearly so) the average surface area S may be computed from the mean linear dimension d_s .

Hence

$$S = \pi \left(\frac{\sum f d}{n} \right)^2 = \pi d_s^2 \quad (4.1)$$

where

f = frequency with which a particle diameter d occurs

n = total number of particles ($n = \sum f$)

Likewise, the mean volume V is

$$V = \frac{\pi}{6} \left(\frac{\sum f d^3}{n} \right) = \frac{\pi}{6} d_v^3 \quad (4.2)$$

If due allowance is made for weighting of size and frequency, then better statistical averages would be

$$S' = \pi \left(\frac{\sum f d^2}{n} \right) = \pi d_s'^2 \quad (4.3)$$

$$V' = \frac{\pi}{6} \left(\frac{\sum f d}{n} \right)^3 = \frac{\pi}{6} d_v'^3 \quad (4.4)$$

where d_s' and d_v' are denoted the mean surface and mean volume diameters, respectively. If the particles are not spheres, then suitable correction factors called shape factors must be used; i.e.:

$$S'' = \alpha_s \left(\frac{\sum f d}{n} \right)^2 = \alpha_s d_s'^2 \quad (4.5)$$

$$V'' = \alpha_v \left(\frac{\sum f d}{n} \right)^3 = \alpha_v d_v'^3 \quad (4.6)$$

Here α_s and α_v are the surface-area and volume shape factors, respectively. Equations (4.5) and (4.6) are the correct equations to use if the particles are irregularly shaped.

Some typical values of α_s and α_v taken from [4.2], p. 27 are:

	α_s	α_v
Cube	6	1
Sphere	π	$\pi/6$
White Sand (smooth)	2.1-2.6	
Filter Sand (smooth)	2.7-2.9	
Crushed Quartz	2.1-2.5	0.14-0.28

In general, it should be noted that while there is a somewhat large variation in α_s and α_v , studies have shown that the ratio α_s/α_v is usually in the range of 6 to 7 and closer to 6.

It is sometimes of interest to determine the specific surface area S_v defined as the surface area per unit volume of the material, or sometimes the surface area per unit weight S_w . If the particles are all spheres, these turn out to be

$$S_v = \frac{6}{d_s} \quad (4.7)$$

$$S_w = \frac{6}{\rho d_s} \quad (4.8)$$

where ρ is the density and d_s is a diameter characteristic of specific surface areas as shown in Eq. (4.1).

By investigating Eqs. (4.3) and (4.6) it is seen that these equations weigh heavily in favor of larger particles. This is good for volume or mass averages, but for surface areas the finest particles become more significant. Hence the surface area computed by these equations is too low. To overcome these effects and to obtain a better statistical representation, the following procedure is useful.

Let y represent the volume or weight fraction of all particles measured having a particular diameter d . Then

$$y = \frac{fd^3}{\sum fd^3} \quad (4.9)$$

and

$$d_v = \sum yd = \frac{\sum fd^4}{\sum fd^3} \quad (4.10)$$

where d_v is a mean weight or volume diameter of the distribution. It should be noted that this diameter is larger than that calculated from Eq. (4.4), since the contribution of the larger particles is emphasized by it.

Now let the weight specific surface be denoted by S'_w and the specific surface be denoted by S_v . Then

$$S_v = \Sigma S'_v = \frac{\Sigma f d^3 S'_v}{\Sigma f d^3} \quad (4.11)$$

From Eq. (4.8) we have

$$d_{sv} = \frac{6}{S_v} = \frac{6 \Sigma f d^3}{\rho \Sigma f d^3 S'_v} \quad (4.12)$$

Since $S'_v = 6/\rho d$ there results

$$d_{sv} = \frac{\Sigma f d^3}{\Sigma f d^2} \quad (4.13)$$

The usefulness of Eq. (4.13) is that it eliminates the use of shape factors. Equation (4.13) could have also been obtained by dividing Eq. (4.6) by Eq. (4.5). Hence d_{sv} is the diameter to use to obtain the surface area per unit volume and this quantity is merely $6/d_{sv}$.

Let us now consider the frequency of an occurrence. Thus far we have been dealing with measures of a central tendency of an event happening; however, in most cases, the particle size distribution will be skewed in the direction of increasing size. (Or at least this is what is to be expected from a random sampling of particles). These distributions can be normalized, however, if the size is plotted logarithmically. Thus the frequency f with which a particle of diameter d occurs is:

$$f = \frac{\Sigma n}{\sqrt{2\pi \ln \sigma_g}} \exp \left[-\frac{\ln d - \ln M}{2 \ln^2 \sigma_g} \right] \quad (4.14)$$

where

M = geometric mean diameter

σ_g = geometric standard deviation

These are defined by

$$\ln M = \Sigma \left(\frac{\ln d}{n} \right) \quad (4.15)$$

$$\ln \sigma_g = \sqrt{\frac{(\ln d - \ln M)^2}{n}} \quad (4.16)$$

As will be seen later, these quantities can be obtained easily by graphical means from the grain size distribution curve. Furthermore, these quantities can be related to the other statistical dimensions as follows where the logarithms are to the base ten:

$$\log d_g'^2 = \log M^2 + 4.605 \log^2 \sigma_g \quad (4.17)$$

$$\log d_v'^3 = \log M^3 + 10.362 \log^2 \sigma_g \quad (4.18)$$

$$\log d_{sv} = \log M + 5.757 \log^2 \sigma_g \quad (4.19)$$

Also if

d_m = mean diameter of distribution

d_v = mean weight or volume distribution = $\frac{\Sigma fd^4}{\Sigma fd^3}$

there results

$$d_m = \log M + 1.151 \log^2 \sigma_g \quad (4.20)$$

$$d_v = \log M + 8.059 \log^2 \sigma_g \quad (4.21)$$

The above equations beginning with Eq. (4.17) are called the Hatch-Choate equations, and can be very easily applied to a specific distribution to obtain any of the various statistical parameters [4.3].

4.2.2 Graphical Determination of the Geometric Mean Diameter and Standard Deviation

If the distribution curve for a group of particles follows fairly well the distribution given by Eq. (4.14), the plot on a log probability grid of particle size versus cumulative percentages (or fractions) less than (or greater than) a specific size results in a straight line.

On this plot the size corresponding to 50% is the geometric mean diameter M . Likewise the value of the geometric standard deviation σ_g can be related to the sizes at 84.13%, 50%, and 15.87% as follows:

$$\sigma_g = \frac{84.13\% \text{ size}}{50\% \text{ size}} = \frac{50\% \text{ size}}{15.87\% \text{ size}} \quad (4.22)$$

4.2.3 Particle Size Measurements Using Sieves

The above indicated procedure would be quite simple to apply if it were known what the number of particles are in each size category. Unfortunately, this is not the case with sand when the segregation method is carried out by means of sieving. When sieving is used the results are given in terms of percent passing (or retained) by weight and not number.

If weight percentages are used and the plot is made on the log probability curve the result will still plot as a straight line if the distribution follows Eq. (4.14).

On this weight plot we define the median and standard deviation as

$$M' = 50\% \text{ size}$$

$$\sigma'_g = \frac{84.13\%}{50\%} = \frac{50\% \text{ size}}{15.87\% \text{ size}} \quad (4.23)$$

It can be shown [4.1] that these values are related to M and σ_g by

$$\begin{aligned} \sigma'_g &= \sigma_g \\ \log M &= \log M' - 6.908 \log^2 \sigma_g \end{aligned} \quad (4.24)$$

Hence the statistical diameters of interest can be obtained as

$$\log d_n = \log M' - 5.757 \log^2 \sigma_g \quad (4.25)$$

$$\log d'_v = \log M' - 3.454 \log^2 \sigma_g \quad (4.26)$$

$$\log d'_s = \log M' - 4.605 \log^2 \sigma_g \quad (4.27)$$

$$\log d_{sv} = \log M' - 1.151 \log^2 \sigma_g \quad (4.28)$$

In summary it should be noted that the items of interest in determining only the surface area for a quantity of particles do not include all of the statistical diameters given in the above discussion. Since d_{sv} is a measure of the surface area per unit weight it is the only diameter of interest for this study. The other quantities are included only for completeness.

The procedure for determining the surface area per unit volume of a material is to make a weight plot on a log probability graph and from it determine the median and standard deviation according to Eqs. (4.23). From this information d_{sv} can be obtained using Eq. (4.28). The surface area per unit volume S_v and the surface area per unit weight S_w are then

$$S_v = \frac{6}{d_{sv}} \quad (4.29)$$

$$S_w = \frac{6}{\rho d_{sv}} \quad (4.30)$$

Since Eq. (4.29) relates to the volume of the actual solids, it can be related to the volume of the loose material by proper use of the void ratio e of the material.

4.2.4 Energy - New Surface Area Relationship

In recent years rather extensive studies [4.4 - 4.12] have been carried out to determine the energy required to create new surface area when certain solids are crushed. These studies have been carried out on such materials as quartz, glass, fluorite, halite, and labradorite. The materials were subjected to both static loads and also dynamic effects created by dropping weights on the material. Very closely controlled measurements were carried out to determine how much of the energy input was actually used in the crushing of the solids.

Considerations were given to temperature changes, deformations of the loading apparatus and any other significant energy absorbing mechanisms. In general, it was assumed that the materials did not undergo plastic deformation before crushing, but only exhibited elastic effects up to the point of fracture. It was felt that this assumption was justified for the materials noted above, since under normal temperature conditions they have little ductility.

In order to determine the surface area of the materials, studies were first carried out using methods of permeametry as discussed in [4.1].

This is done by investigating the resistance offered to a flowing fluid by packed particles in accordance with the flow laws of D'Arcy. In some cases the fluid used was water; however, for smaller particles the use of air in place of a fluid is advantageous. The permeability method for measuring surface area has the advantage of being a relatively simple procedure to carry out; however, it has the disadvantage that it measures only the outside surface of a solid. Such things as cracks, fissures, and pores of microscopic and submicroscopic sizes are not detected by this method.

In view of the above, further studies in this series used gas adsorption measurements to determine the surface area of the solids. This technique is also discussed in [4.1] and is based on the idea that the surface molecules of a solid are bound on one side to inner molecules but are incompletely attached on the outside. In order to satisfy the resulting unbalance of atomic and molecular forces, the surface molecules attract gas, vapor, or liquid molecules. If the molecules attracted are those of a gas, the phenomenon is known as gas adsorption. It is generally felt that gas adsorption measurements provide the best means currently available for determining total surface area of a solid.

In simple terminology, gas adsorption techniques involve a determination of the quantity of a gas necessary to form a molecular layer on the surface to be measured. The number of molecules required to form this layer may be evaluated, and since the area occupied by each molecule is known (or may be estimated), the surface area of the material may be calculated.

These basic techniques have been applied to the crushing of single particles as well as arrays of particles for some of the materials

noted above [4.4 - 4.12]. Some variations were made in the loading techniques with dynamic as well as static applications. Two graphs summarizing some of the significant data related to the behavior of quartz were taken from [4.12] and are given as Figs. 4.1 and 4.2.

From these results it can be seen that the new area per work input was measured as about $15.1 \text{ cm}^2/\text{kg cm}$ in single particle crushing compared with about $13.8 \text{ cm}^2/\text{kg cm}$ for multiple particle crushing. The higher energy required to crush a bed of particles has been attributed to the friction energy losses which occur when a group of particles is compressed.

For the purpose of this study a value of $13.8 \text{ cm}^2/\text{kg cm}$ or $2.46 \text{ in}^2/\text{lb:in.}$ has been used and is considered fairly representative of the behavior of sand as well as quartz. Unfortunately, there are no data available on sand.

4.2.5 Analysis of A Grain Size Distribution Curve For Sand

The concepts discussed in the previous sections have been applied to determine the energy absorbed through the crushing of sand when subjected to large pressures. Unfortunately, there are little data available in the literature which can be utilized for correlation purposes and to date, the most reliable results are those shown in Fig. 4.3 which were taken from [4.13]. A similar set of data is also reported in [4.14].

Fig. 4.3 gives the changes in the grain size distribution curves for well-rounded 20-40 Ottawa sand when subjected to various ranges of pressure in a condition of one dimensional compression. The results of an analysis of these data are given in Table 4.1 and are plotted in Fig. 4.4.

The results in Table 4.1 were computed by the following procedure. In general, an evaluation was made only of that percent of material which deviated from the original grain size distribution curve. For example, at the 1000 psi range only about 3 percent of the material was affected, while at 40,000 psi about 88 percent was affected. Even in these percentages not all particles were crushed, but certain statistical average diameters were changed in this group. An investigation was made of the distribution curve of these altered percentages as shown in Figs. 4.5 - 4.8 and the specific diameter was determined for this group both before and after crushing from Eq. (4.28). From these diameters a determination of the increase in surface area per volume was determined from Eq. (4.29). This increase was converted to energy from the constant $2.46 \text{ in}^2/\#$ as discussed in Section 4.2.4. These calculations yield the energy per volume of solid material considered in the percentages altered. These values were converted back to energy per total volume of loose material assuming the void ratio to be 0.60.

It is shown on Fig. 4.4 that after the pressure reaches some 2,000-3,000 psi, the energy absorbed due to crushing seems to be linearly related to the pressure.

This is particularly interesting since crushing begins to have a pronounced effect on the sand behavior at about this pressure even though some particles begin to fail in the region of 500 to 1000 psi. From these meager data it appears that the rate of change of energy to pressure is constant and is approximately

$$\frac{1}{97} \frac{\# \text{in}/\text{in}^3}{\#/\text{in}^2} \approx 0.01 \frac{\# \text{in}/\text{in}^3}{\#/\text{in}^2}$$

Unfortunately, no other data are available which will substantiate this work. Likewise, the grain size distribution curves in Fig. 4.3 are very likely average curves for many tests. Hence this study must be viewed with some question and considered as indicating only a qualitative trend until further experimental results can be obtained.

4.3 Stress-Strain Behavior of Sand After Crushing Commences

4.3.1 Experimental Results

The statistical study carried out in Section 4.2 indicates that in the pressure region after grain crushing begins, the energy absorbed by sand due to crushing is linearly related to the stress. It was pointed out that this energy is only that due to particle crushing and does not include the compaction effect.

Whether these two phenomena are separable effects remains to be determined; however, they are distinctly different energy absorbing mechanisms. One is associated with the breakage of the molecular bonds as smaller particles are formed from larger ones. The other effect is the energy associated with the settlement and compaction due to a change in the size distribution of the particles which results in an increased density.

In Section 4.2 it was shown that the breakage of the particles seems to follow a random pattern. If it is assumed that the newly created fine particles are transported to voids in the medium in a similar random pattern, it would seem plausible that the total energy absorbed due to crushing might also be linearly related to the stress.

In order to investigate this hypothesis, let us study some experimental stress-strain curves for sand in one dimensional compression. Figure 4.9 shows a qualitative stress-strain curve for sand. If the grains

of sand do not crush the stress-strain curve will not be concave downward at B, but will continue to be concave upward. Since crushing does occur, the curve changes in its shape. If the loading curve is translated laterally by a strain of ϵ_1 until it cuts the crushed stress-strain curve at a stress σ_1 , the area A_1 between the original and the translated curve is the energy absorbed by the sand due to crushing. In the same way the energy absorbed due to crushing at some stress σ_2 is the cumulative area A_2 noted in Fig. 4.9.

Figures 4.10 - 4.14 give stress-strain curves from some tests on 20-40 Ottawa Sand carried out by MIT [4.13] where a steel chamber was used to restrict the lateral strains. A logarithmic plot of these same stress-strain curves in Fig. 4.15 shows that prior to crushing, the stress is related to some power of the strain usually between 1.3 and 1.8 and that a value of 1.5 is a fairly good average. The theory discussed in Chapter 3 for a face centered array of spheres predicts this power to be 1.5.

From Fig. 4.5 it is an easy matter to extrapolate the stress-strain behavior which would occur if crushing did not take place. This extrapolated non-crushing curve is then translated along the strain axis to determine where it crosses the true curve in order to determine the energy absorbed due to crushing.

Figure 4.16 shows the stress-strain curve of Fig. 4.10 with the translated curves extrapolated from the precrushing data. The energy absorbed due to crushing was then determined by planimetering the cumulative area under the stress-strain curve corresponding to a particular stress.

A plot of the energy absorbed due to crushing is given in Fig. 4.17 for the stress-strain curve in Fig. 4.16. The energy absorbed

due to crushing appears to be linearly related to the pressure for a large range in pressures. Similar studies were made for the stress-strain curves given as Figs. 4.10 - 4.14 and a plot of the crushing energy absorbed versus the stress is also given in Fig. 4.17. There is a definite trend in this behavior until the stresses become quite large. Hence it can be concluded from the meager data available that there appears to be a linear relationship between stress and the energy absorbed due to crushing. Further study needs to be carried out on this work as more data become available; however, these preliminary investigations are encouraging.

4.3.2 Theoretical Stress-Strain Curve in the Crushing Region

As was discussed in the previous section, there is experimental evidence to support the hypothesis that the energy absorbed due to crushing is linearly related to the stress. Similarly, a study of the stress-strain curves given in Figs. 4.10 - 4.14 as well as the experimental results carried out on this study and presented in Chapter 5 indicate that the stress prior to crushing is related to some exponent of the strain.

Figure 4.18a shows a qualitative stress-strain curve for sand with a discontinuity at σ_c the crushing stress. This stress σ_c is, of course, not a well-defined point for a real material; however, it can be determined within a reasonable range. Let the stress σ prior to crushing be expressed as

$$\sigma = \alpha \epsilon^\beta \quad (4.31)$$

where ϵ is the strain and α and β are experimental constants.

Likewise, let the stress after crushing begins be σ_1 , a function of the strain. Since the energy absorbed due to crushing appears to be linearly related to the stress we have from Fig. 4.18b.

$$\frac{d\sigma}{dE} = \gamma \quad (4.32)$$

where E is the energy and γ is an experimental constant. But the increment in energy dE is also the increment in area under the stress-strain curve as shown by dA on Fig. 4.18a. Also, since the sides of dA are assumed to be a parallel

$$dA = \sigma_1 d\epsilon \quad (4.33)$$

Since from (4.32)

$$\frac{d\sigma_1}{dA} = \gamma \quad (4.34)$$

there results from (4.33) and (4.34)

$$\frac{d\sigma_1}{\gamma} = \sigma_1 d\epsilon \quad (4.35)$$

or

$$\frac{d\sigma_1}{\sigma_1} = \gamma d\epsilon \quad (4.36)$$

Integrating Eq. (4.36) yields the exponential result

$$A\sigma_1 = e^{\gamma\epsilon} \quad (4.37)$$

where A is a constant of integration. This constant can be evaluated from the condition that at the crushing stress σ_c the strain is ϵ_c . Hence we obtain finally

$$\sigma_1 = \sigma_c e^{\gamma(\epsilon - \epsilon_c)} \quad (4.38)$$

Equation (4.38) satisfies the condition that the energy absorbed due to crushing is linearly related to the stress. The constant γ can be obtained from curves similar to those given in Fig. 4.18.

Hence analytical expressions for a one dimensional stress-strain curve take the following form

$$\begin{aligned} \sigma &= \alpha \epsilon^\beta && \text{prior to crushing} \\ \sigma &= \sigma_c e^{\gamma(\epsilon - \epsilon_c)} && \text{after crushing} \end{aligned} \quad (4.39)$$

Equation (4.38) is independent of the stress-strain behavior prior to crushing and is only contingent on the linear energy versus the increment of stress after crushing. Hence, Eq. (4.38) may not be limited to only one dimensional compression, but may be also applicable to other states of stress.

4.4 Determination of the Stresses at Which Grain Crushing Occurs

The average stress for crushing depends on many things including the initial void ratio of the medium, the angularity of the particles, the duration of loading, and the inherent strength of the mineral which composes the grains.

For the one dimensional stress-strain curve of a given material, the effect of particle breakage appears to be dependent to a large extent

on the initial void ratio of the medium. This statement is substantiated in Fig. 4.19 where the strains of Figs. 4.10 - 4.14 have been "normalized" using the strain at 20,000 psi as 100% strain. These data show that there is a general trend for sand with the higher initial void ratios to crush at lower levels of stress. This phenomenon is explainable because at a high initial void ratio there are very few contacts per unit volume, which means that for a given average stress the contact stresses are higher in a sand with a high void ratio than for a sand with a low void ratio. Further study needs to be carried out on the determination of the crushing stress of sand and how it is affected by particle sizes and arrangements.

REFERENCES

- 4.1 Orr, Clyde, and DallaValle, J. M., "Fine Particle Measurement, Size Surface and Pore Volume," The MacMillan Co., New York, 1959.
- 4.2 DallaValle, J. M., "Micromeritics, The Technology of Fine Particles," Pitman Pub. Corp., New York, 1943.
- 4.3 Hatch, T., "Determination of 'Average-Particle Size' From the Screen- Analysis of Non-Uniform Particulate Substances," *Journal Franklin Institute*, Vol. 34, 1933, p. 215.
- 4.4 Kwong, J. N. S., et al, "Energy-New Surface Relationship in Crushing, I Application of Permeability Methods to an Investigation of the Crushing of Some Brittle Solids," *Chemical Engineering Progress*, Vol. 45, Aug. 1949, pp. 508-516.
- 4.5 Adams, J. T., Johnson, J. F., and Piret, Edgar L., "Energy-New Surface Relationship in the Crushing of Solids, II Application of Permeability Measurements to an Investigation of the Crushing of Halite," *Chemical Engineering Progress*, Vol. 45, Nov. 1949, pp. 655-660.
- 4.6 Johnson, J. F., Axelson, J. W., and Piret, E. L., "Energy-New Surface Relationship in the Crushing of Solids, III Application of Gas Absorption Measurements to an Investigation of the Crushing of Quartz," *Chemical Engineering Progress*, Vol. 45, No. 12, Dec. 1949, pp. 708-715.
- 4.7 Axelson, J. W., "Energy-New Surface Relationship in the Crushing of Solids, IV Application of Slow Compression to an Investigation of the Crushing of Crystalline Quartz," Ph.D. Thesis, University of Minnesota, 1949.
- 4.8 Heney, L. J., "Energy-New Surface Relationship in the Crushing of Solids, V Impact Crushing of Single Particles of Crystalline Quartz," Ph.D. Thesis, University of Minnesota, 1951.
- 4.9 Kenny, W. J., "Energy-New Surface Relationship in the Crushing of Solids, VII Slow Compression Crushing of Single Particles of Glass," Ph.D. Thesis, University of Minnesota, 1954.
- 4.10 Schulz, N. F., Cooke, S. R. B., and Piret, E. L., "Energy-New Surface Relationship in the Crushing of Solids," *Chemical Engineering Progress*, May 1957, Vol. 53, pp. 254-258.
- 4.11 Zeleny, R. A., "A Study of the Dissipation of Energy in Single Particle Crushing," Ph.D. Thesis, University of Minnesota, 1957.
- 4.12 Zeleny, R. A., and Piret, E. L., "Studies of the Energy Requirements for Crushing," *Third Symposium on Rock Mechanics*, Colorado School of Mines, Quarterly Colorado School of Mines, Vol. 54, No. 3, July 1959.

- 4.13 "Research on the Study of Fine Grained Soils Consolidated Under High Pressure," Report for the Creole Petroleum Corporation, Maracaibo, Venezuela by Soils Engineering Division, Department of Civil and Sanitary Engineering, MIT, Sept. 1958.
- 4.14 Roberts, J. E., and de Souza, J. M., "The Compressibility of Sands," Proceedings American Society for Testing Materials, Vol. 58, 1958, pp. 1269-1277.

TABLE 4.1

ENERGY ABSORBED DUE TO THE CRUSHING OF SAND
(Analysis of Grain Size Distribution Curves in Fig. 4.5)

20-40 Ottawa Sand

$$d_{sv} = \log M' - 1.151 \log^2 \sigma_g$$

Pressure % Material Range Crushed	Specific Diameter d_{sv} (mm)		Specific Surface Area/Unit Volume, $S = 6 d_{sv}^2$, in^2/in^3			Energy per 100% Vol. Sand $E = S/2.46$ #in/in ³	Void Ratio	Energy per Gross Vol. Sands in/in ³			
	Before Loading	After Reference Figure	Before Loading	After Loading per % Affected per 100%	Increase Increase per 100%						
1,000	3	.425	.396	4.6a	358	387	29	.87	.354	.60	.22
5,000	26	.449	.288	4.6b	339	530	191	49.6	20.2		12.6
8,000	63	.513	.254	4.7	297	600	303	191.0	77.5		48.5
15,000	78	.519	.150	4.8	294	1017	723	564.0	229.0		143.5
40,000	88	.557	.0795	4.9	273	1918	1645	1450.0	589.0		368.0

 $\frac{d_p}{d_s}$

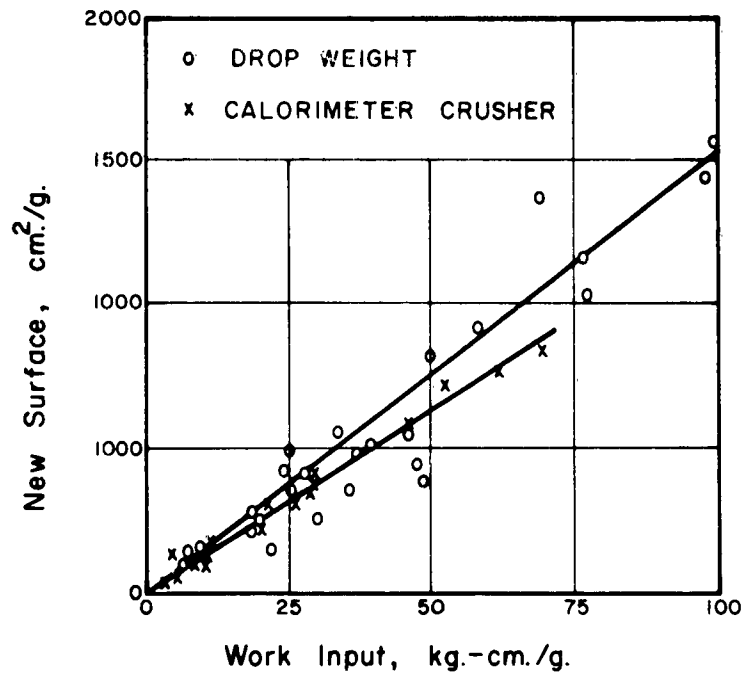


Fig. 4.1 WORK INPUT - NEW AREA RELATIONSHIP FOR SINGLE PARTICLE CRUSHING OF QUARTZ BY DROP-WEIGHT AND GLASS BY CALORIMETER CRUSHER (from Zeleny and Piret (4, 12))

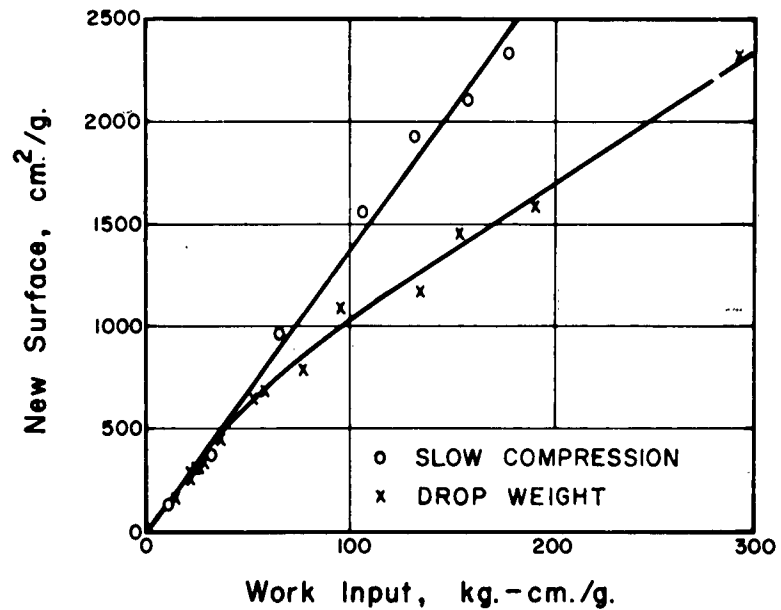


Fig. 4.2 WORK INPUT - NEW AREA RELATIONSHIP FOR MULTIPLE PARTICLE SLOW COMPRESSION AND DROP-WEIGHT CRUSHING OF QUARTZ (from Zeleny and Piret (4, 12))

GRAIN SIZE DISTRIBUTION

20-40 Ottawa Sand after Compression to Various Pressures.

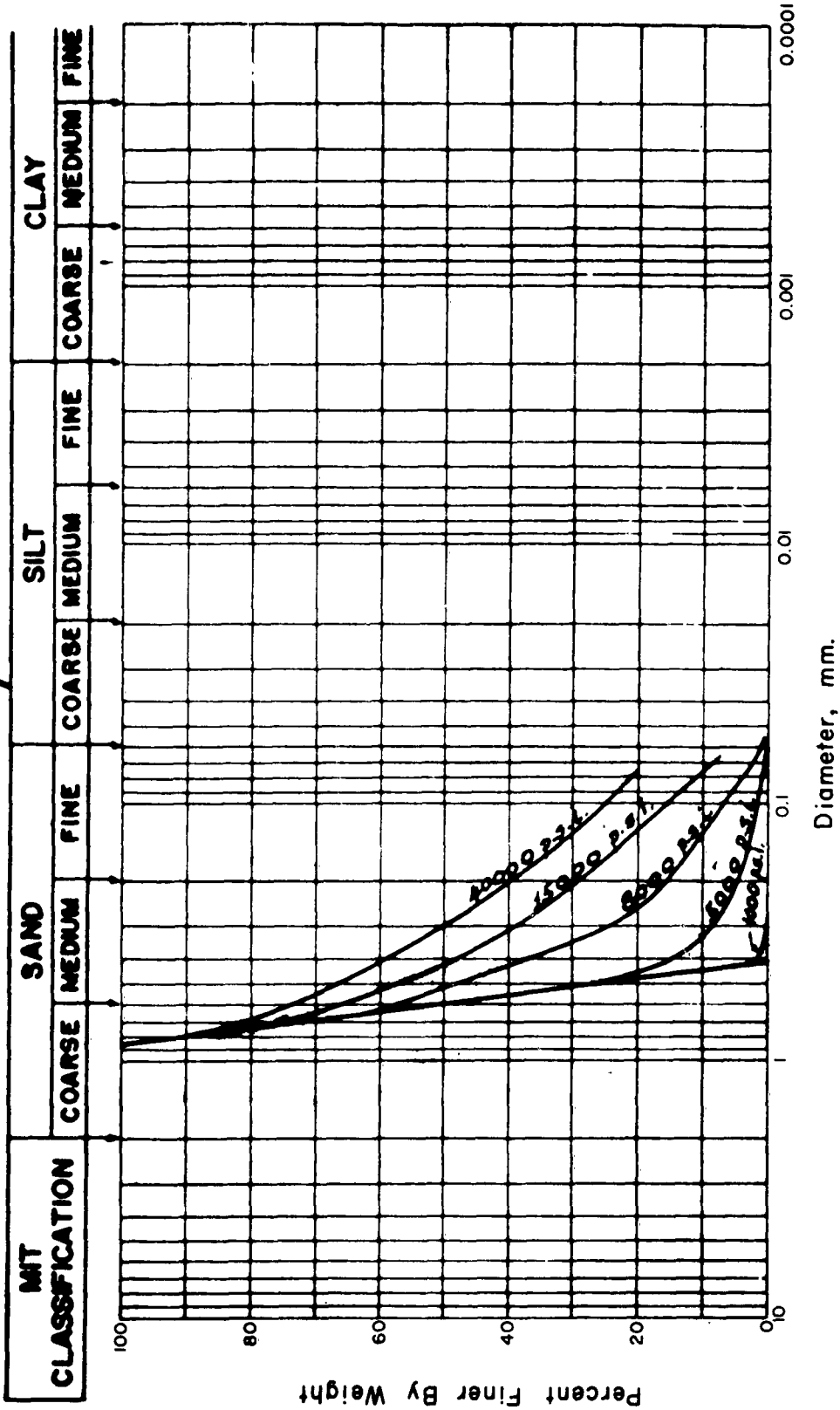


Fig. 4.3 GRAIN SIZE DISTRIBUTION CURVES FOR OTTAWA SAND
(after (4.13))

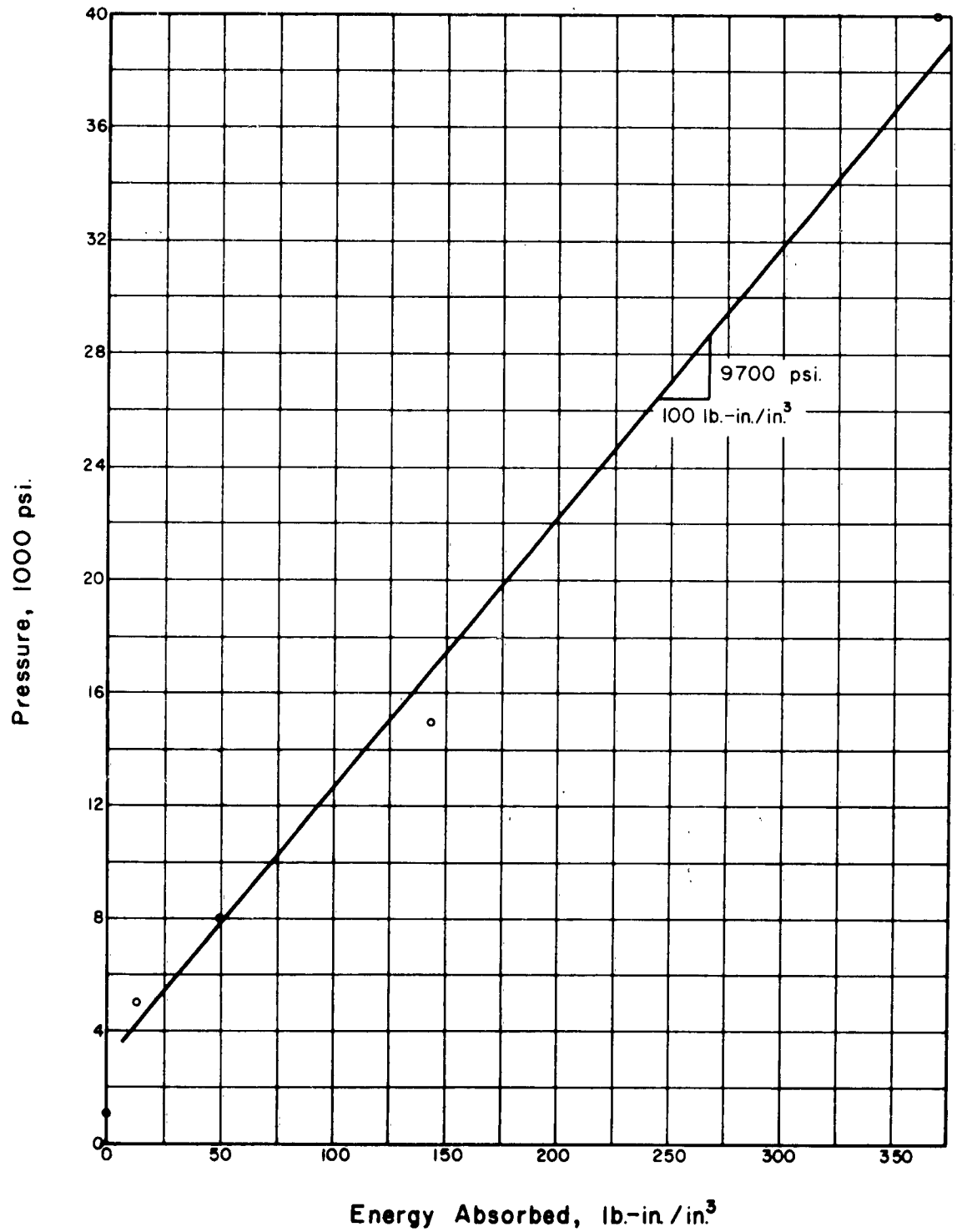
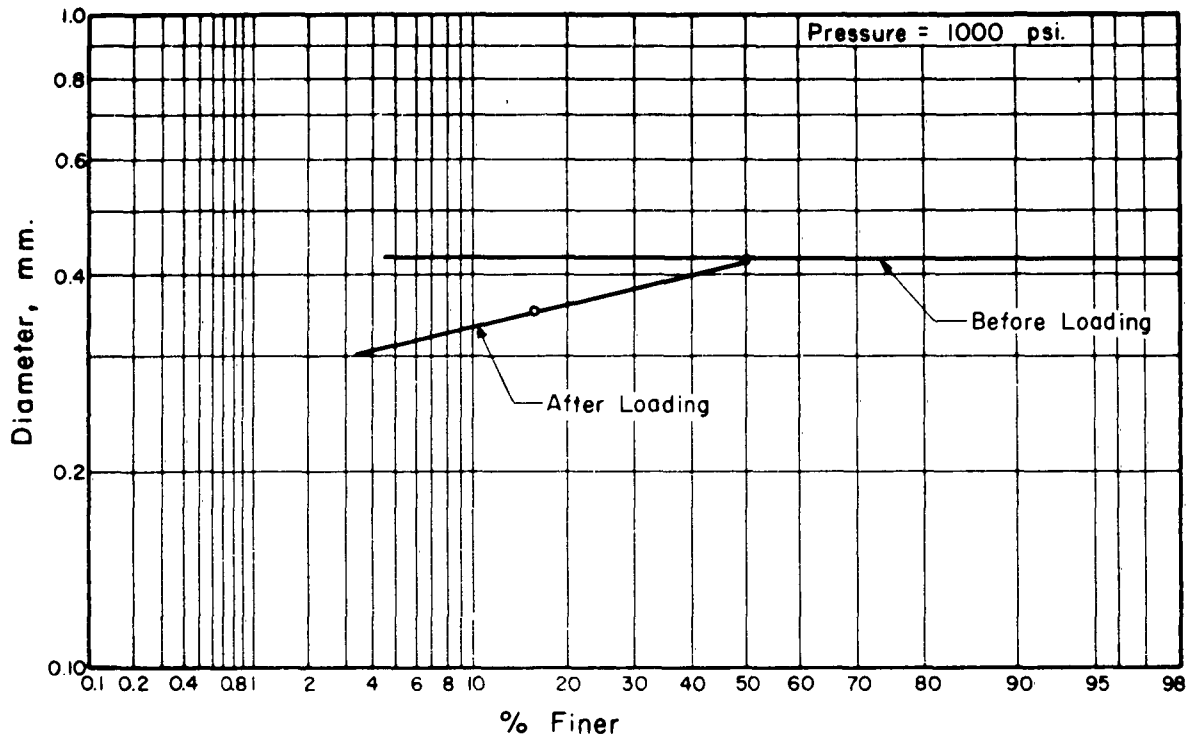
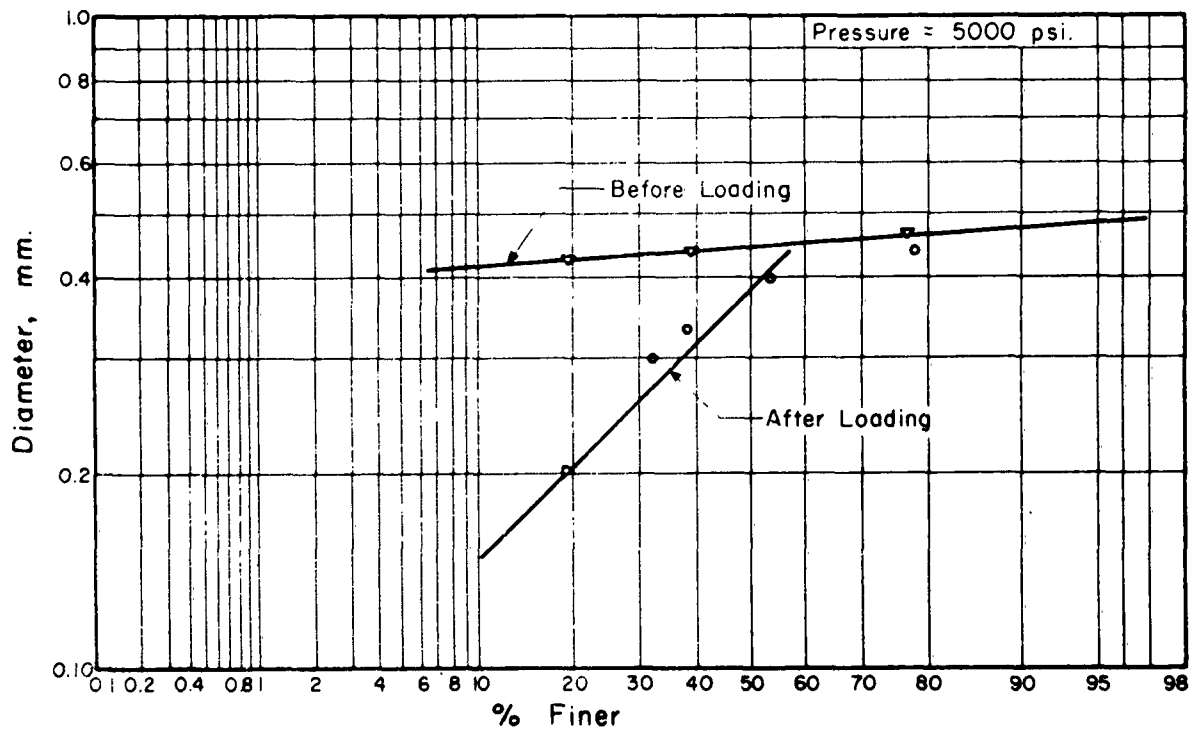


Fig. 4.4 ENERGY ABSORBED DUE TO CRUSHING OF
20-40 OTTAWA SAND



(a)



(b)

Fig. 4.5 LOG PROBABILITY PLOT OF GRAIN SIZE DISTRIBUTION CURVES

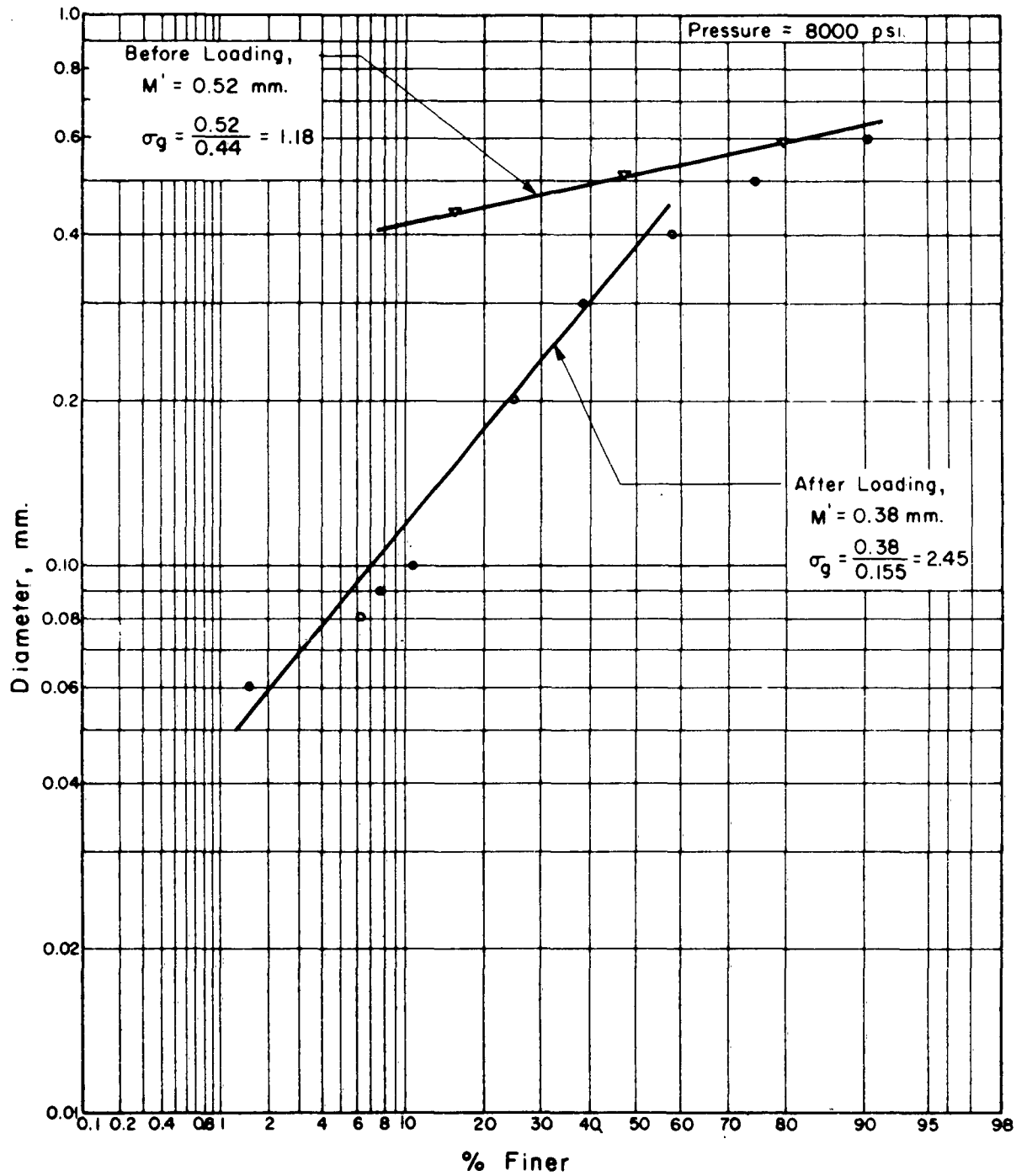


Fig. 4.6 LOG PROBABILITY PLOT OF GRAIN SIZE DISTRIBUTION CURVES

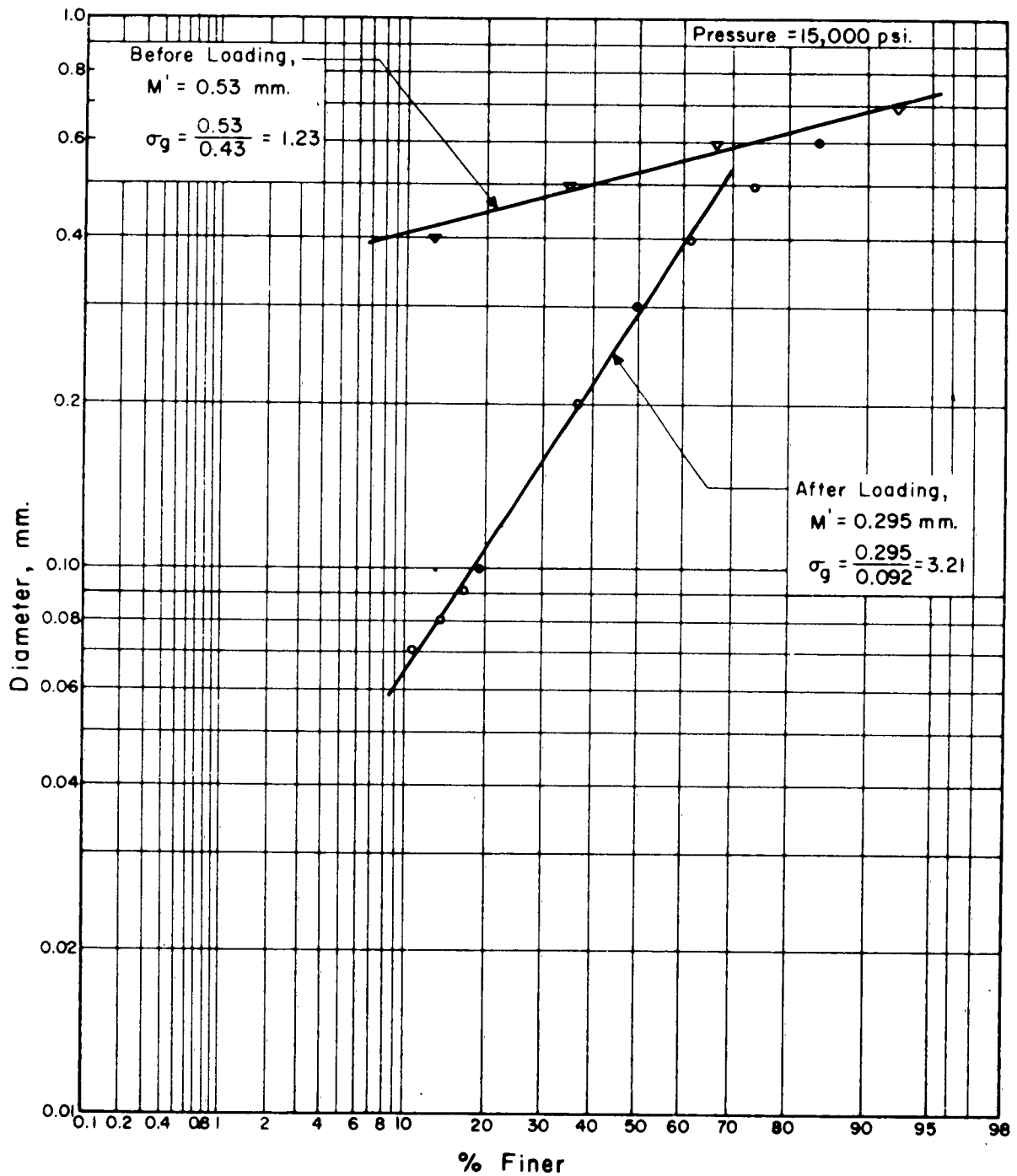


Fig. 4.7 LOG PROBABILITY PLOT OF GRAIN SIZE DISTRIBUTION CURVES

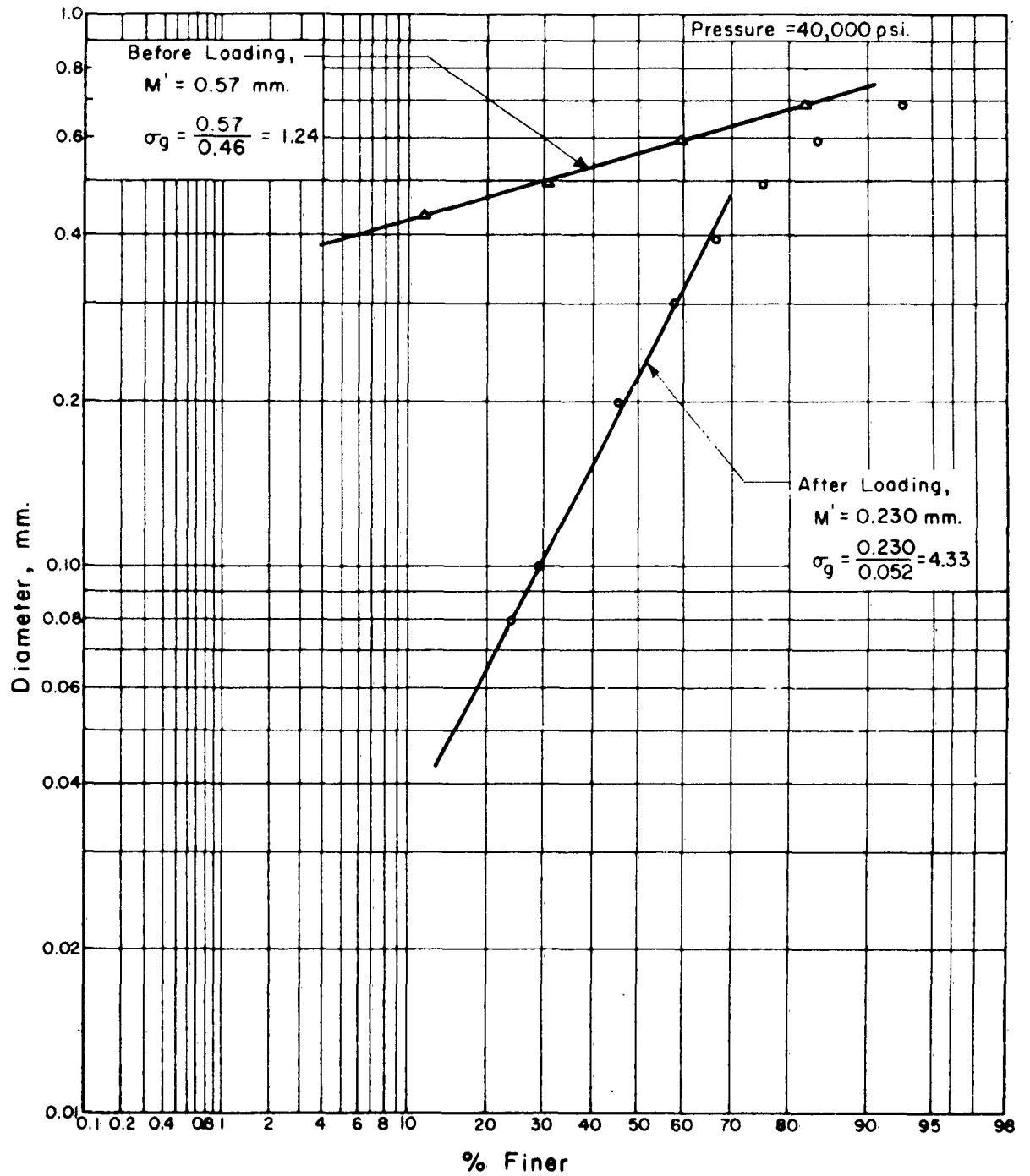


Fig. 4.8 LOG PROBABILITY PLOT OF GRAIN SIZE DISTRIBUTION CURVES

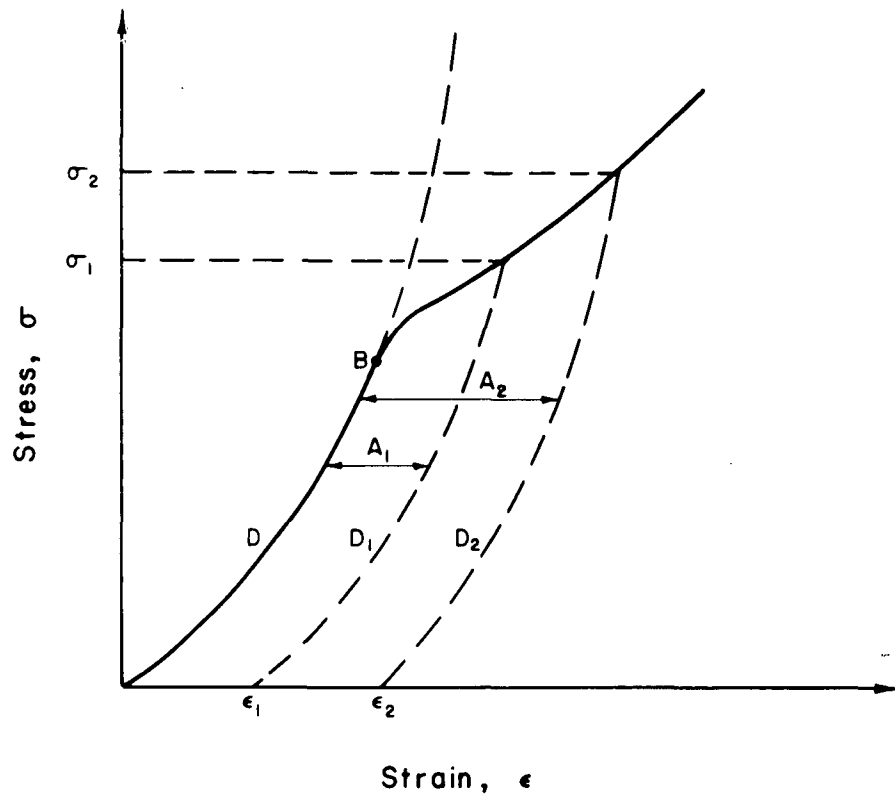


Fig. 4.9 QUALITATIVE STRESS STRAIN CURVE FOR SAND

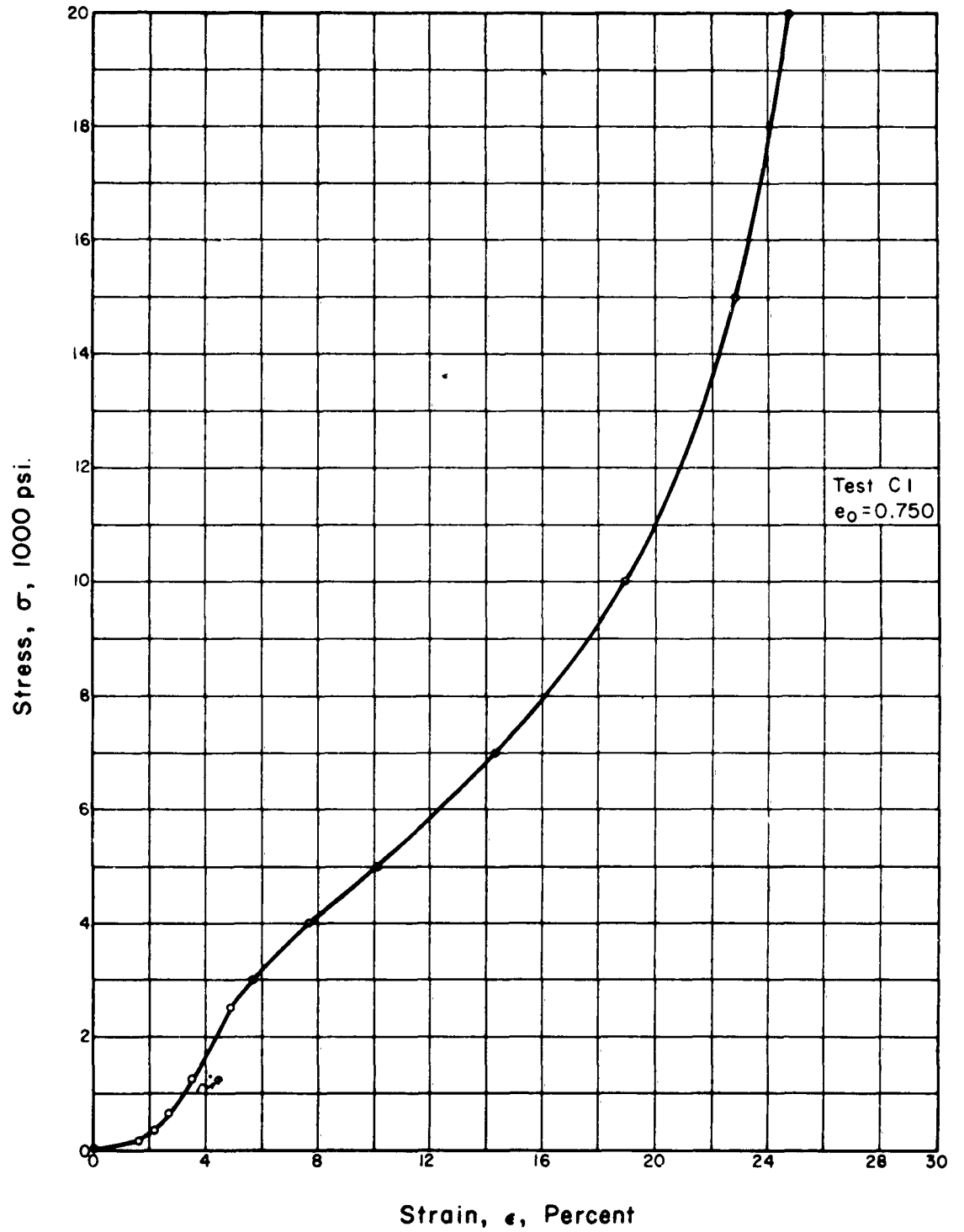


Fig. 4.10 STRESS STRAIN CURVE FOR SAND IN
ONE DIMENSIONAL COMPRESSION
(from data in (4.13))

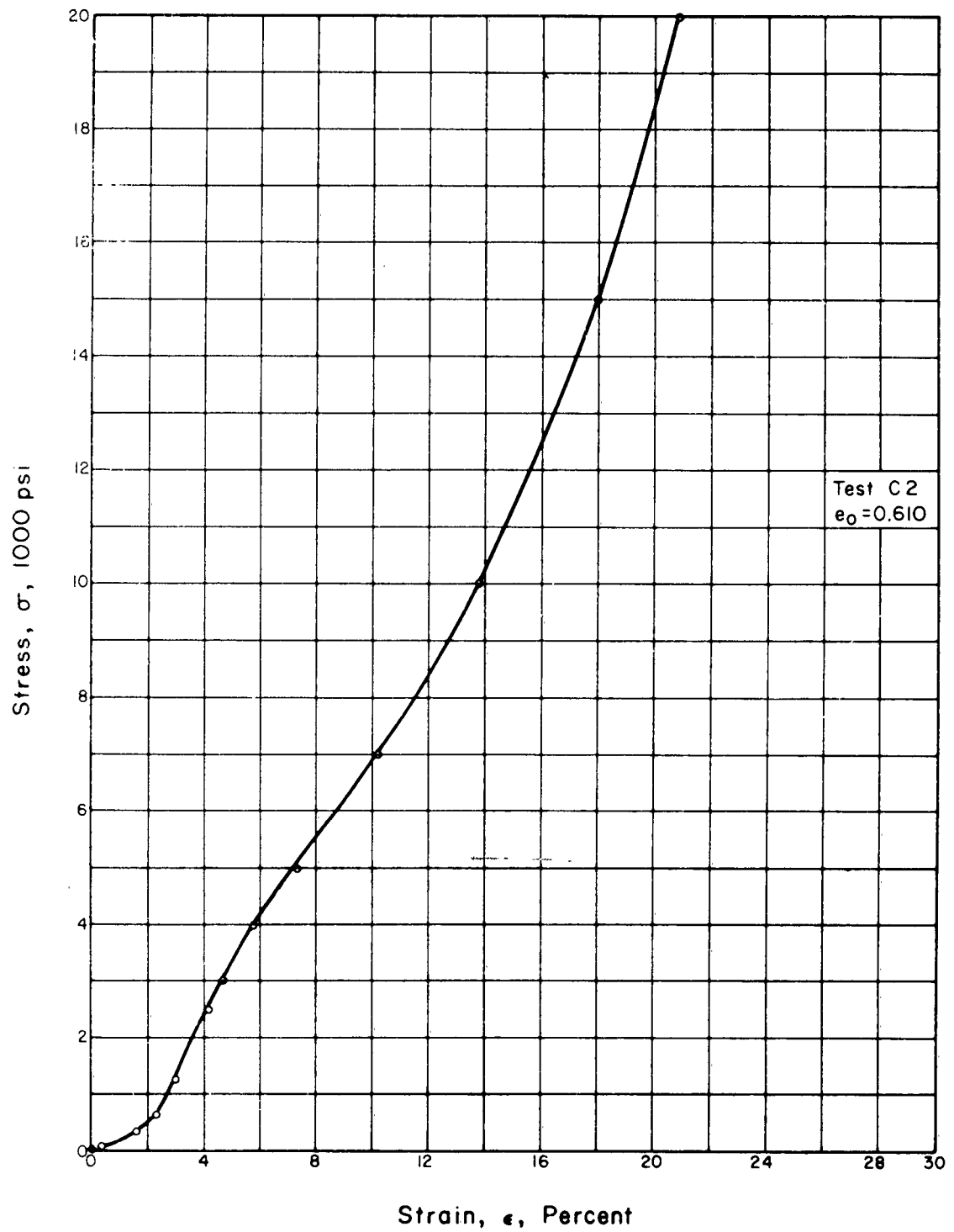


Fig. 4.11 STRESS STRAIN CURVE FOR SAND IN
ONE DIMENSIONAL COMPRESSION
(from data in (4.13))

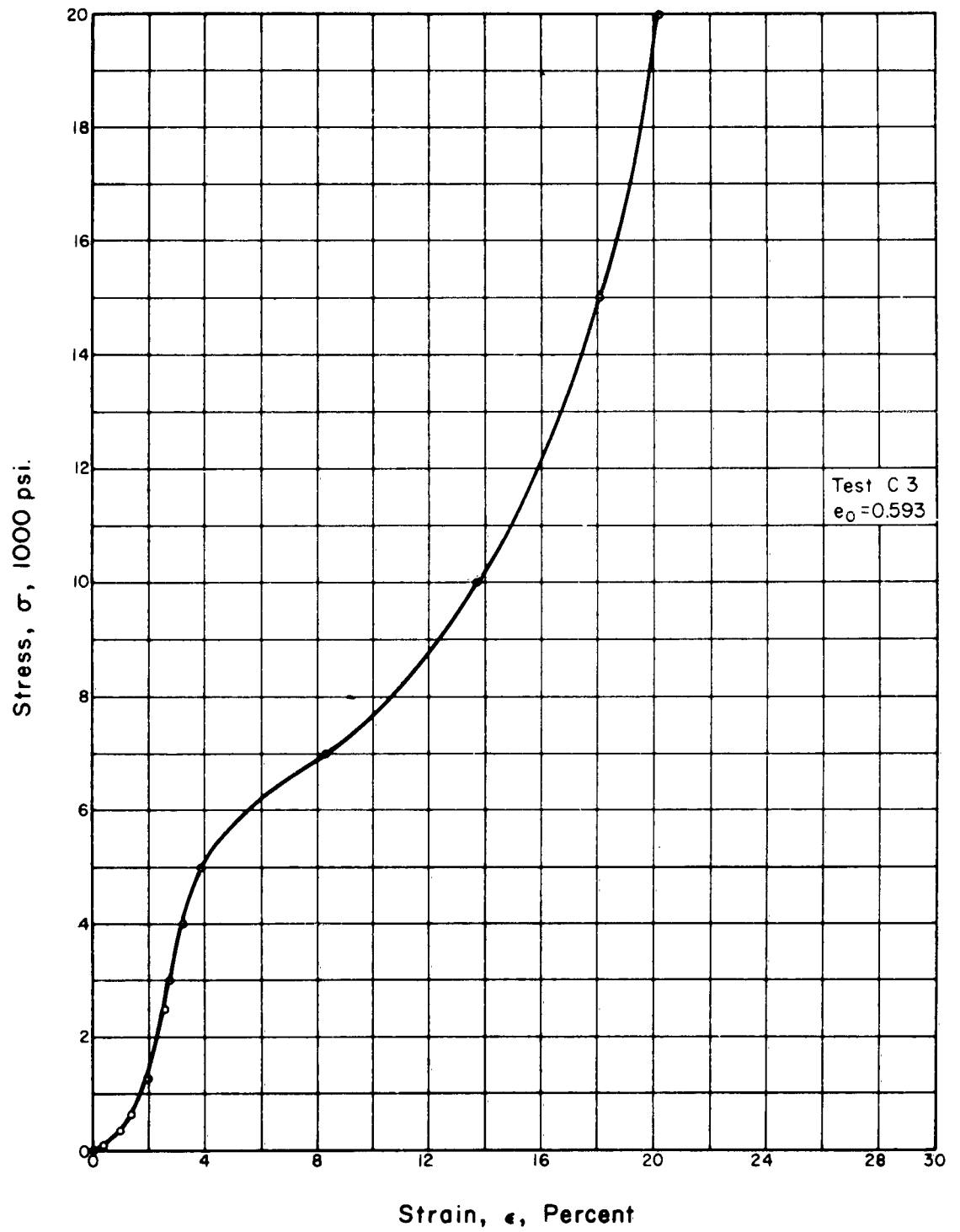


Fig. 4.12 STRESS STRAIN CURVE FOR SAND IN
ONE DIMENSIONAL COMPRESSION
(from data in (4.13))

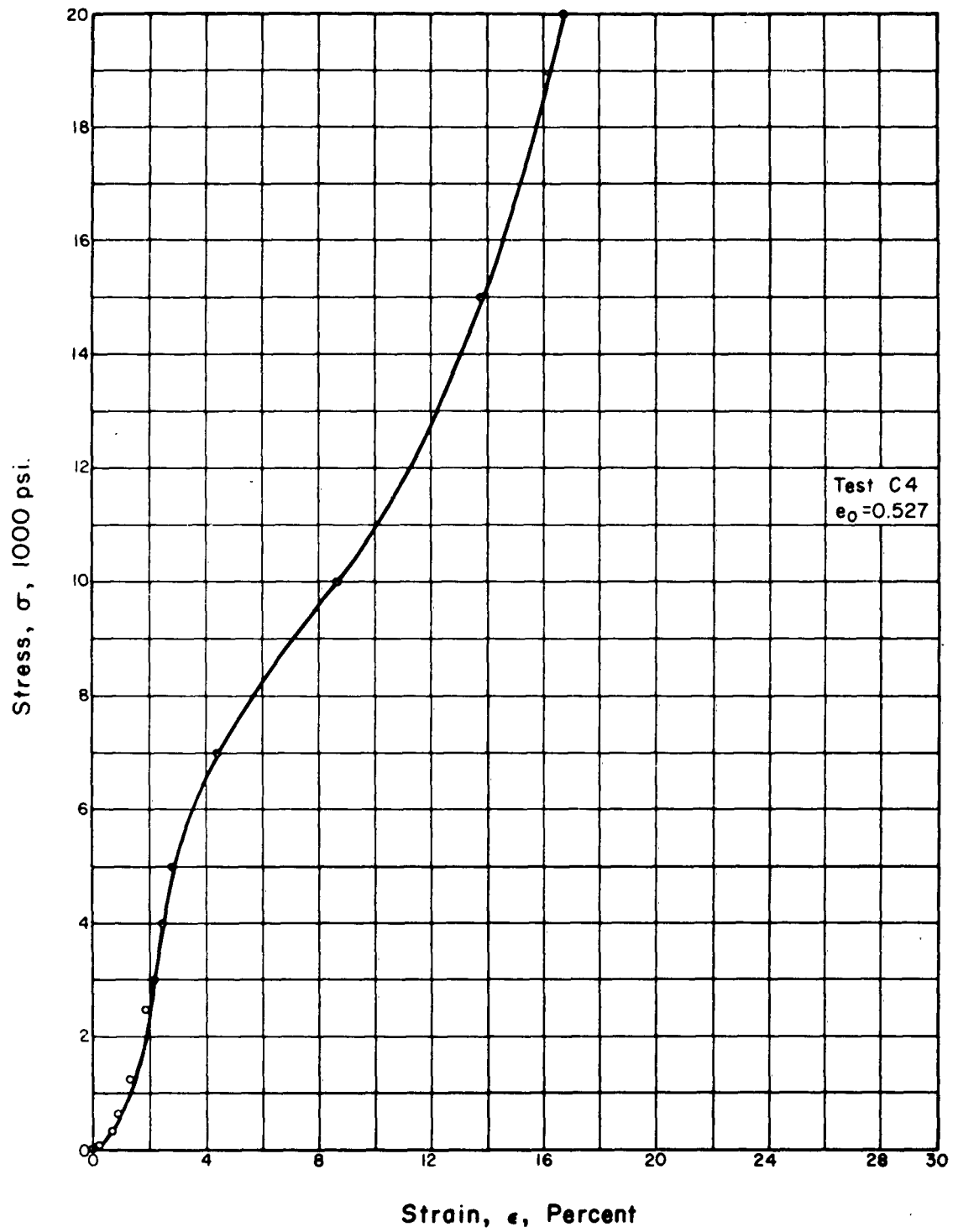


Fig. 4.13 STRESS STRAIN CURVE FOR SAND IN
ONE DIMENSIONAL COMPRESSION
(from data in (4.13))

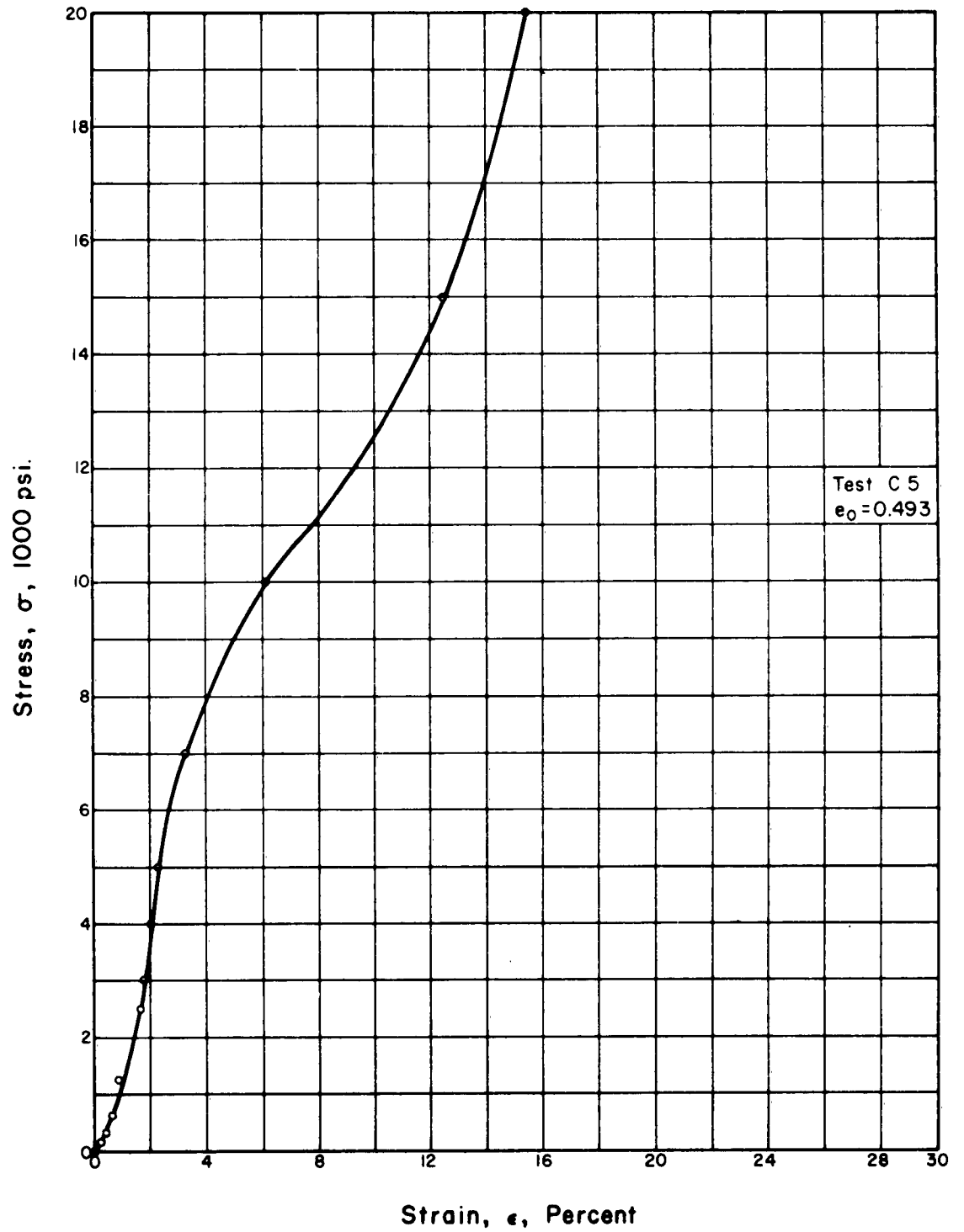


Fig 4.14 STRESS STRAIN CURVE FOR SAND IN
ONE DIMENSIONAL COMPRESSION
(from data in (4.13))

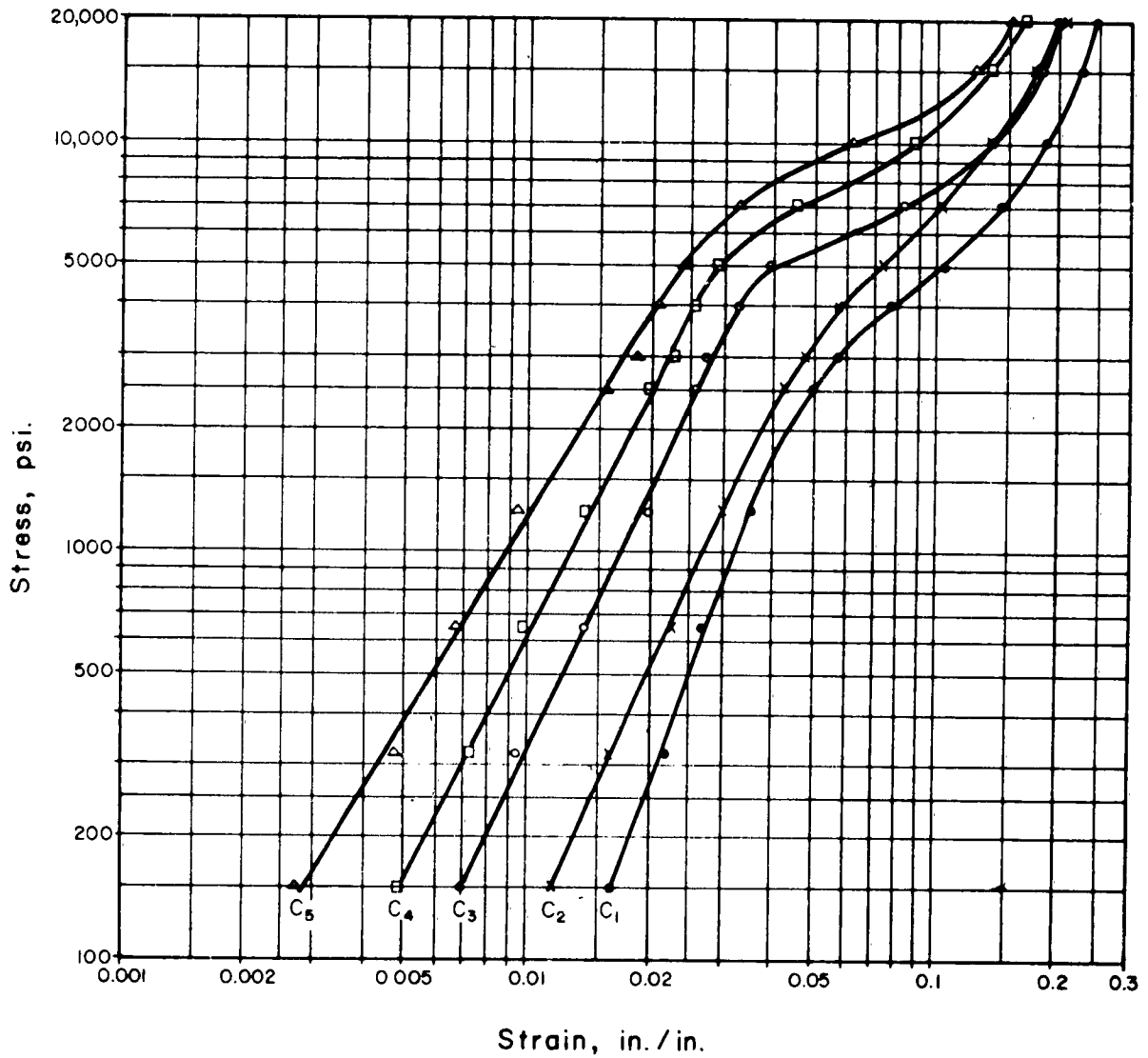


Fig. 4.15 LOGARITHMIC PLOT OF ONE DIMENSIONAL STRESS STRAIN CURVES FOR OTTAWA SAND

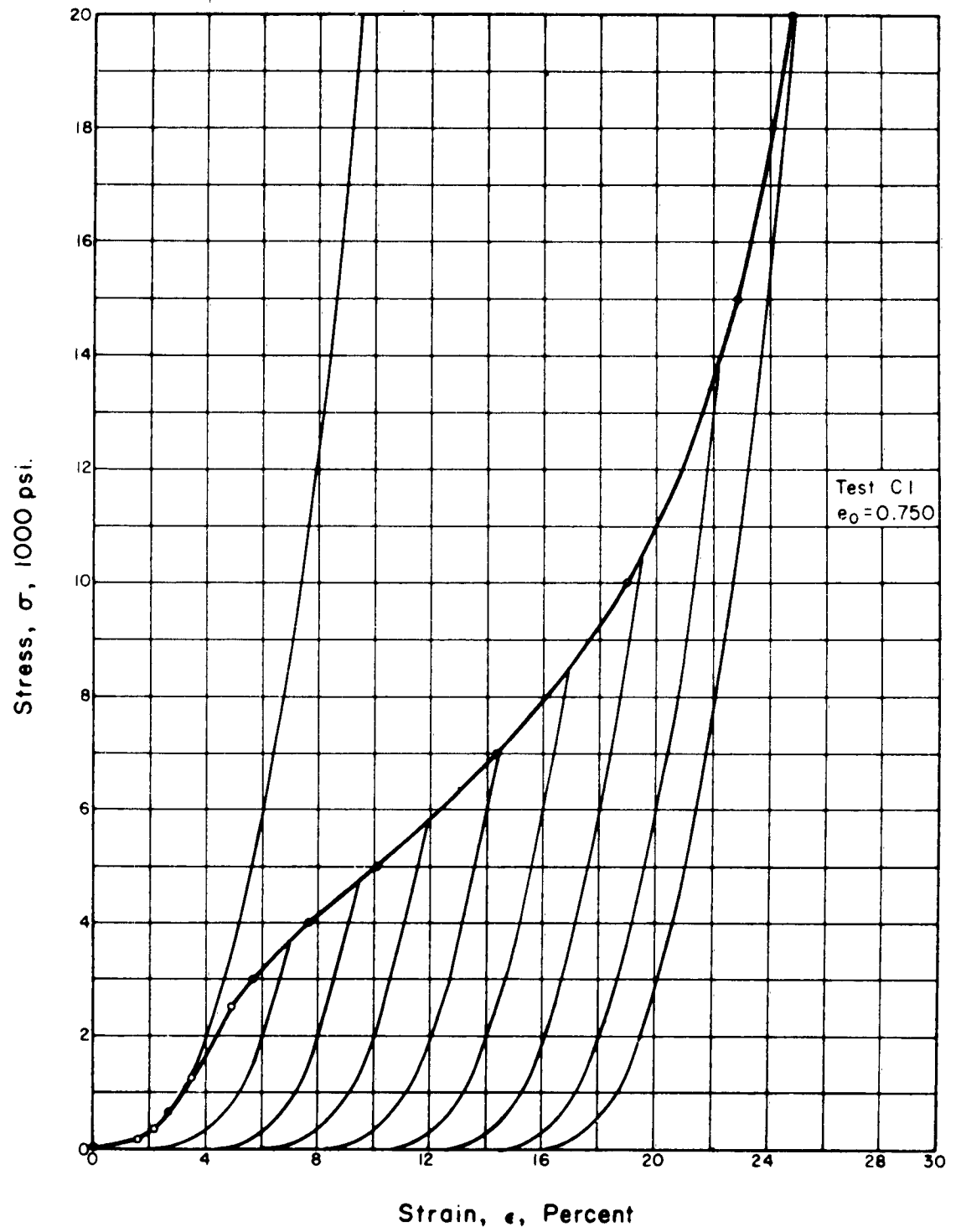


Fig. 4.16 COMPARISON OF CRUSHING AND NON-CRUSHING BEHAVIOR OF SAND

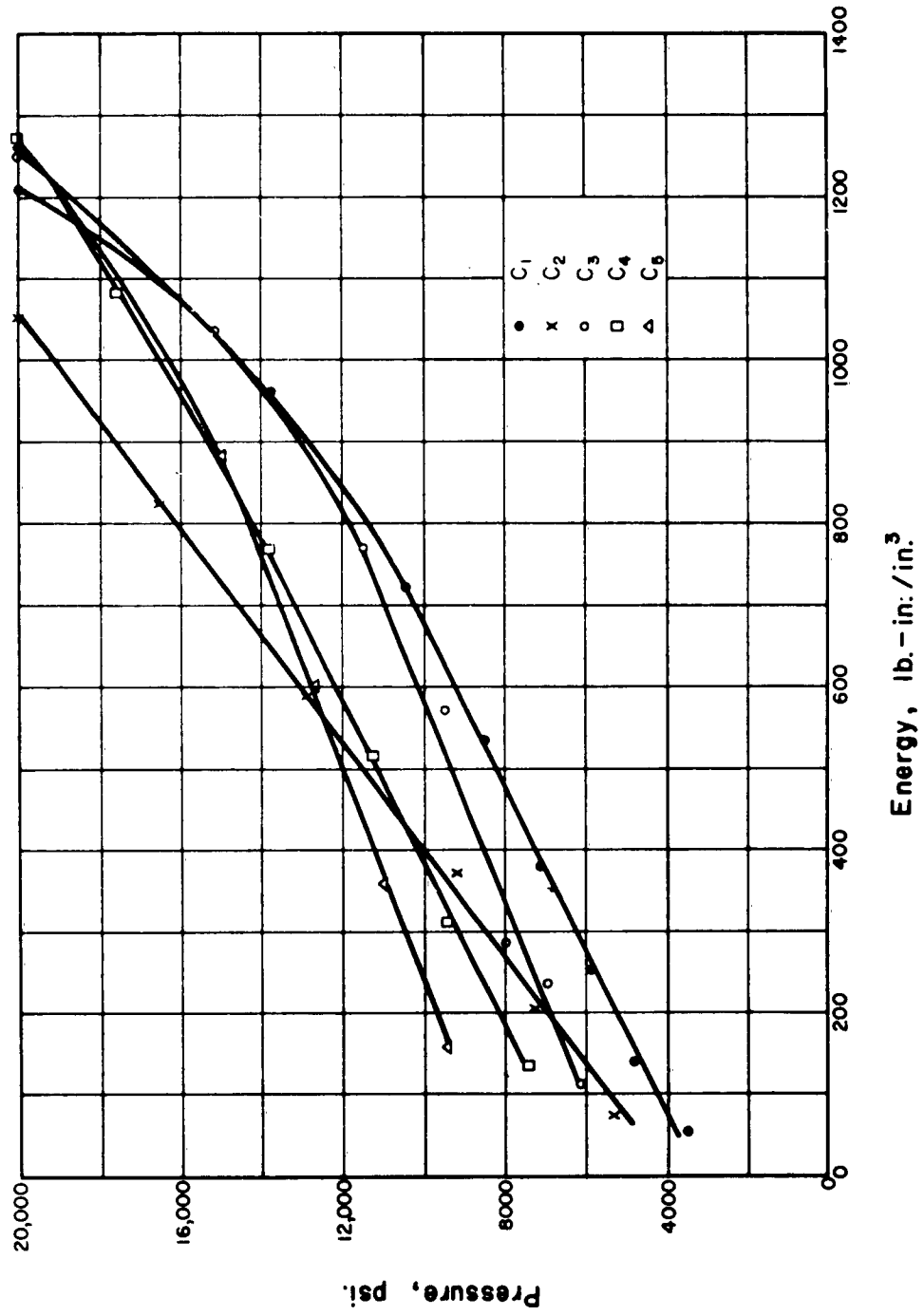
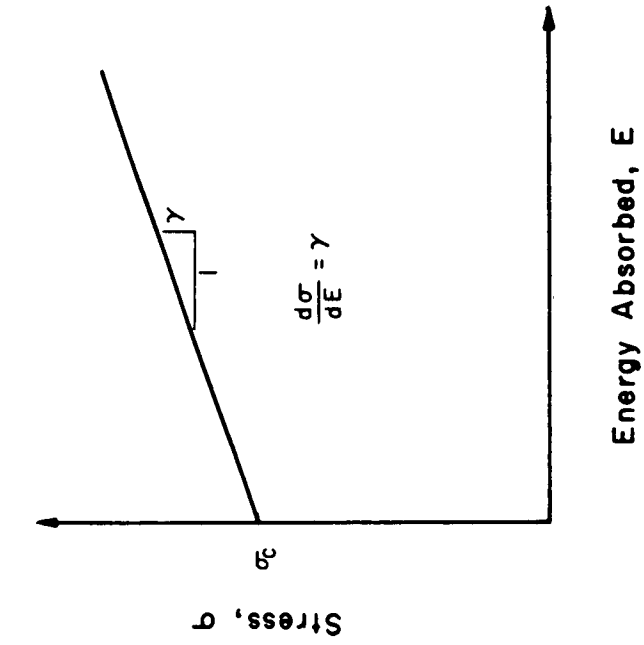
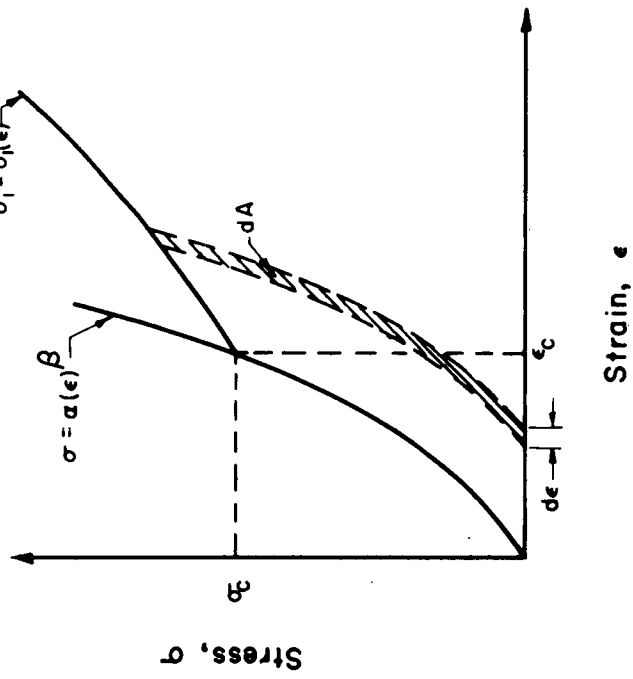


Fig. 4.17 ENERGY ABSORBED DUE TO CRUSHING



(a)



(b)

Fig. 4.18 ASSUMED STRESS STRAIN BEHAVIOR FOR SAND

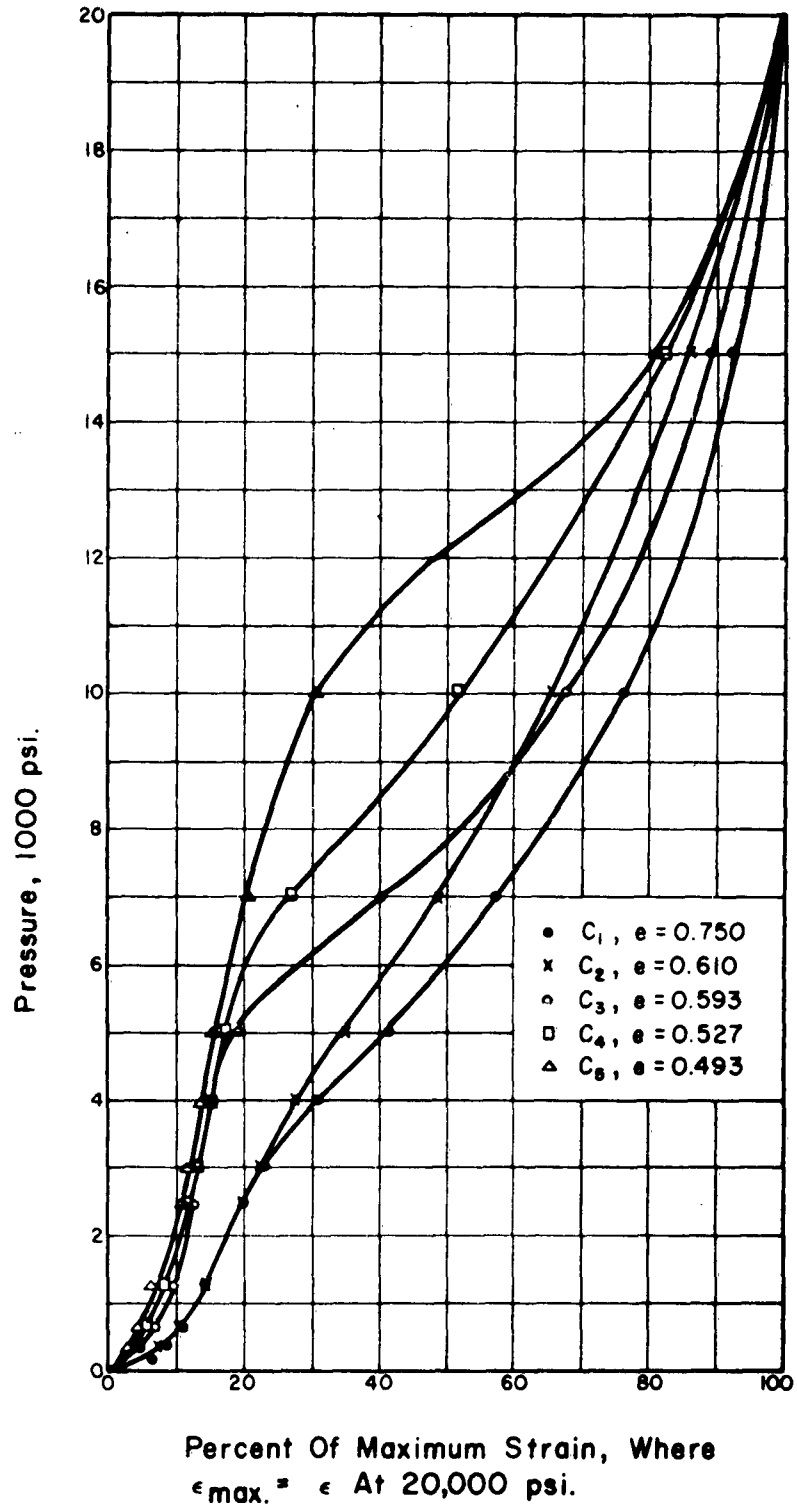


Fig. 4.19 NORMALIZED STRESS STRAIN CURVES FOR OTTAWA SAND

CHAPTER 5

EXPERIMENTAL PROGRAM

5.1 Introduction

An experimental program for the purpose of measuring the properties of real soils in one dimensional compression has been an integral part of the overall efforts of this research study. The experimental results from these tests serve several purposes:

1. The basic phenomena observed in the tests can be compared with the conclusions drawn from theoretical analyses of idealized models which are assumed to represent soil.

2. The energy absorbing capacity of soils may be measured by means of cyclic loading.

3. The various energy absorbing mechanisms may be observed for a given soil at different pressure levels in order to determine the stress ranges where each mechanism predominates.

4. The stress-strain curves obtained may be used to study one dimensional wave propagation through the particular soil media tested.

5. The lateral stress σ_H which results under conditions of zero lateral strain can be measured with the experimental apparatus.

6. The effect of lateral strain on the principal stress ratio can be measured by allowing a given strain in the horizontal direction and observing the change in σ_H/σ_V , where σ_V is the vertical stress.

7. An effective Poisson's ratio for soil in one dimensional compression can be evaluated from the experimental data on σ_H/σ_V by the relationship

$$\frac{\sigma_H}{\sigma_V} = \frac{\nu}{1-\nu} \quad (5.1)$$

A device was designed and built to investigate the one dimensional behavior of sand in the high pressure regions. The apparatus can measure the lateral stress under conditions of zero lateral strain, and provides one of the best means yet developed for attaining the condition of "zero" lateral strain. Previous investigators have generally assumed that the effects of small lateral strains are negligible, particularly when the sample is enclosed in steel rings. Research by Speer [5.1], which was recently pointed out by two of the authors [5.2], shows that lateral motion significantly affects the ratio of σ_H/σ_V . The results of Speers's research is presented in graphical form in Fig. 5.1 and shows that a lateral displacement of 4×10^{-6} inches will cause a 10% reduction in the value of σ_H/σ_V . Since Speer's work was with a sand sample $7 \frac{5}{8}$ inches in diameter, the above diameter change corresponds to a unit strain of approximately $.5 \times 10^{-6}$ in./in. It is doubtful to the writers that Speer really achieved an accuracy of $\pm 1 \times 10^{-6}$ in./in. since small temperature fluctuations would cause minor variations of at least that magnitude in the strain gage readings. However, his work does in general point out that the ratio of σ_H/σ_V is very sensitive to lateral movements. This phenomena had already been observed by Terzaghi as early as 1934 in connection with his "Large Retaining Wall Tests" at MIT [5.3]. Terzaghi concluded that an outward movement of the wall of .0007 h in the case of a well compacted dense sand was enough to fully mobilize the shear strength or, in other words, reduce the ratio of $\sigma_H/\sigma_V = K_O$ to $K_A = \frac{1-\sin\phi}{1+\sin\phi}$. This outward movement corresponds approximately to a lateral strain of about 12×10^{-4} in./in. Thus for a truly one dimensional test, whereby one also wishes to measure the magnitude of the lateral stresses which are concomitant with the vertical

load, it is extremely important to closely control the lateral displacements. In fact, preliminary calculations revealed that an extremely thick walled cylinder subjected to an internal pressure of 7,500 psi (which is an approximation to the lateral soil pressure due to a vertical load of 15,000 psi) would experience a radial strain of 3.25×10^{-4} in./in. if the specimen were 7 inches in diameter and the containing cylinder was assumed to have an infinite external radius. This strain is of the same order of magnitude as the tolerable strains listed by Speer and Terzaghi. Thus, in order to study one dimensional compression, a new experimental apparatus had to be designed which would restrict the lateral deformations. The apparatus developed on this program is discussed in the following sections.

5.2 Experimental Apparatus

5.2.1 Description of the Apparatus

An experimental apparatus was designed to determine the stress-strain relations for soil under one dimensional compression and to measure the lateral stress necessary to completely restrain the sample. This apparatus shown schematically in Fig. 5.2 consists essentially of a thin steel ring which contains a soil sample. The ring is surrounded by an annular space filled with oil which communicates freely with hydraulic jacks. The flexible ring and oil space are enclosed in a thick hollow cylinder bolted to the baseplate in order to withstand the high fluid pressures.

The principle upon which the device is based is relatively simple. As the vertical load is applied by the testing head there are lateral pressures built up in the sand which tend to increase the diameter of the thin steel ring. Any slight increase in diameter of the ring

is immediately indicated by the strain gages mounted on the flexible ring as shown in Figs. 5.2 and 5.3. In order to keep the lateral strains zero, the oil pressure is modified with changes in the vertical load in such a manner that the strain indicator remains balanced at all times during the test. When the strain indicator remains balanced there are no lateral strains and the oil pressure is equal to the lateral soil pressure acting against the side of the container.

The apparatus consists of the following four basic elements:

- (1) A thin steel ring monitored with strain gages (Fig. 5.3a).
- (2) A baseplate (Part B, Fig. 5.2).
- (3) A thick walled cylinder (Part A, Fig. 5.2).
- (4) A testing head.

The testing head and the thin steel ring contain the essential sensing devices for making the desired measurements and are discussed in the following sections.

5.2.2 Fabrication and Calibration of the Strain Gages on the Steel

Ring

Four Budd Metalfilm Strain Gages (Type C6-1161) were mounted at the mid-height of the steel ring at 90° intervals and connected in series as shown in Fig. 5.3. In this arrangement, the strains sensed by the four different gages are averaged since the change in resistance balanced by the indicator is the sum of the changes in all four gages.

The gages are "foil" gages with a gage length of one inch and a grid width of 0.09 inches. Gages of this proportion were chosen in order to have gages relatively insensitive to axial strains in the ring arising from friction between the soil and ring, but at the same time very sensitive to circumferential strains which accompany a diameter change. These gages worked very well when the axis of the one inch gage

length was aligned perpendicular to the axis of the ring. These gages were also very convenient because they are extremely thin and flat, making them rather insensitive to the all around pressure of the oil in which they are submerged during test conditions. Nevertheless, the effect of the high oil pressure on the gages could not be assumed to be negligible. The gages had to be calibrated for these effects.

The apparatus is assembled for calibration as shown in Fig. 5.4. The significant feature of this assembly is that the lower "O" ring between the bottom of the steel ring and the baseplate has been removed so that the oil in the annular space can communicate freely with the oil inside of the sample chamber. A steel plug one inch thick is also inserted into the sample chamber to confine the oil and a testing head is lowered flush with the top of the plug to supply a reaction of sufficient magnitude to keep the plug in place during calibration.

The gages were calibrated by increasing the oil pressure in increments up to 2,500 psi. Since the "O" ring at the bottom of the steel ring was omitted, the oil pressure in the annular space was equal to the pressure in the sample chamber, thus giving zero net pressure differential across the ring and no circumferential stresses or strains. Hence any change in gage reading is due to the effects of the all around oil pressure on the gages. This calibration procedure was conducted several times and the calibration curve obtained is shown in Fig. 5.5. The curve was reproducible within $\pm 4 \times 10^{-6}$ in./in. and the pressure effect amounts to 7×10^{-6} in./in. per 500 psi of oil pressure. Compensation for these pressure effects was made when the tests were conducted on sands.

After the calibration of the inner diaphragm was completed, the device was modified for testing by disassembling the apparatus and

and inserting the "O" ring between the bottom of the steel ring and the baseplate to prevent leakage of oil from the annular space into the sample chamber. The device was then reassembled as shown in Fig. 5.2 for testing.

5.2.3 Description of the Testing Head

The load was applied to the soil sample by means of a heavy, internally stiffened piston, mounted in a 120,000 lb. Baldwin hydraulic testing machine (Fig. 5.3b). The testing head is 6.800 inches in diameter and 8.125 inches high. The device consists of two rigid steel plates which are welded on two concentric steel cylinders as shown in Fig. 5.6. This figure also shows the manner in which a dynamometer is incorporated into the device to measure the pressure over the center square inch of the loaded area. This feature enables one to check the load on the center square inch against the average load over the entire area. The piston and the dynamometer were designed with approximately the same relative stiffness in order to maintain a uniform deflection of the specimen across the face of the loading device as the sample is compressed.

The vertical displacement of the sand during compression was measured by two Ames Dials mounted at 180° to each other on the loading piston as shown in Fig. 5.7. The dials measure the relative displacement between the moving piston and the thick walled cylinder designated as Part A in Fig. 5.2. This measured relative displacement is actually the sum of the vertical displacement of the soil plus the strain in the testing head from the surface of loading to the point where the dials are connected. The strains in the head were so small compared to the strains in the soil that they were neglected and the measurement was taken to represent the vertical displacement of the soil sample. The

dials are accurate to 1/10,000 of an inch and have a 1" travel. When the two dials read differently, the average reading of the two dials was taken as the vertical displacement of the soil.

5.2.4 Proportions of Test Specimen

The proportions of the test specimen, 7 inches in diameter by 2 inches high, were selected to minimize the effects of friction between the sand and the steel ring. The theoretical basis for the above statement is presented in the following analysis from [5.5].

Let us consider a confining ring of radius R and height H as shown in Fig. 5.8. At any arbitrary depth z below the surface loaded by the force P, the vertical force supported by the soil is designated as Q_z . The force Q_z may be expressed in terms of the shearing stress τ_z and the applied load P as:

$$Q_z = P - \int_0^z 2\pi R \tau_z dz \quad (5.2)$$

The shearing stress is also related to Q_z by

$$\tau_z = \frac{Q_z}{A} \cdot K_o \cdot f \quad (5.3)$$

where A is the area of the sample, K_o is the ratio of the horizontal to vertical stress and f is the coefficient of friction between the soil and the ring.

Substituting Eq. (5.3) into Eq. (5.2) yields

$$Q_z = P - \int_0^z 2\pi R \frac{Q_z}{A} \cdot K_o \cdot f dz \quad (5.4)$$

Differentiating both sides of Eq. (5.4) and rearranging results in

$$\frac{dQ_Z}{Q_Z} = \frac{-2\pi R K_o f}{A} dz \quad (5.5)$$

Integrating the above equation between the appropriate limits we obtain:

$$\int_P^{Q_H} \left[\ln Q_Z \right] = \int_0^H \left[\frac{-2\pi R K_o f z}{A} \right] = \ln \frac{Q_H}{P} = \frac{-2\pi R K_o f H}{A} \quad (5.6)$$

Rearranging Eq. (5.6) we obtain:

$$Q_H = P e^{\frac{-2\pi R K_o f H}{A}} = P e^{\frac{-2K_o f H}{R}} \quad (5.7)$$

Equation (5.7) implies that if $e^{\frac{-2K_o f H}{R}}$ approaches 1, then $Q_H = P$, and the frictional effects become negligible. This relationship shows that the R/H ratio should be as large as possible to reduce the effect of friction. In fact, increasing the R/H ratio by a factor of 2 has the same effect as reducing the coefficient of friction by 50%. The present diameter to height ratio of 3.5 used in this test is considered sufficiently large to minimize the frictional effects, but on future tests it would be desirable to vary the height of the sample in order to investigate the effect of this ratio. A practical limit is reached, however, in reducing the height of the sample since the height of the sample influences the accuracy of the vertical strain measurement. If the sample becomes too thin, the increments in the displacements can become too small for the Ames dials to sense, especially in the higher pressure regions where the constrained modulus of sand approaches 300,000 psi.

5.3 Description of Tests

5.3.1 General

A series of one dimensional compression tests with lateral earth pressure measurement was conducted on a dry sand. The sand was a well rounded, coarse, uniform, silica sand from Le Suer, Minnesota. The sand is very similar to standard Ottawa sand in all respects except that only the sizes between the No. 10 and No. 20 sieves are present in this material. Relative density tests on this material showed that the void ratios for the loosest and densest states are $e_{\max} = .675$ and $e_{\min} = .455$, respectively. The loosest state was obtained by pouring the sand in a container of known volume through a glass funnel to prevent the sand from falling. The densest state was obtained by putting the sand in the same container in 1/2" layers and tapping the sides with a mallet until it appeared as if the surface was no longer settling.

The initial void ratio, the strain rate and the pressure ranges of cyclic loading were varied in this series of tests. The variation of these parameters made possible a study of the following effects:

- (1) The influence of relative density on K_o .
- (2) The influence of strain rate on K_o .
- (3) The relationship between the overconsolidation ratio and K_o .
- (4) The effect of initial void ratio on the stress-strain curve.
- (5) The effect of initial void ratio on energy dissipation.
- (6) The effect of strain rate on the stress-strain curve.
- (7) The effect of pressure level on energy dissipation due to cyclic loading.

5.3.2 Preparation of Test Specimens

When preparing the test specimens it is extremely important to be able to reproduce the same initial void ratio for all specimens, since the relative density significantly affects the stress deformation properties of sand. Each sample of sand used in the tests consisted of 2,000 grams of oven-dry material; thus the volume of the sand solids was constant for each test. Since the void ratio e is by definition $\frac{V_v}{V_s}$, where V_v is the volume of the voids and V_s is the volume of the soil solids, it may also be written $\frac{V - V_s}{V_s}$ where V represents the total volume of the sample. Since V_s was constant for all the tests, the void ratio was determined by controlling the total volume, V . The sample was cylindrically shaped so this was easily accomplished by controlling the height of the sample.

Each test specimen was prepared by placing 2,000 grams of oven-dry sand into the sample chamber and inserting a metal plug into the chamber above the sand. This steel plug fits into the chamber as shown in Fig. 5.4. A vibrator was then set on the metal plug and the sand was vibrated until the plug settled down to a predetermined mark fixing the height of the sample. This method of sample preparation has proved to be rather simple and convenient and the test results thus far indicate that very good reproducibility has been achieved by the employment of this technique.

5.4. Test Results

5.4.1 Axial Stress-Strain Relationships

The axial stress-strain curves for each of the eleven tests are shown in Figs. 5.9 through 5.19. The curves show the entire history of loading and unloading for all tests including those tests where the samples were subjected to several cycles of load.

The stress-strain curves in general for all the tests are non-linear curves which are concave upward on both the loading and unloading portions. The non-linearity of the curves demonstrates the well known fact that the stiffness of a given sand is highly dependent upon stress level. This stiffness in the case of one dimensional compression is usually designated as the "Constrained Modulus." The variation of the constrained tangent modulus with the vertical stress for the initial loading in tests 3, 4, 9, and 13 are shown in Figs. 5.20 and 5.21. These curves also show the effect of relative density on the constrained modulus. Specimens 3 and 4 had an initial void ratio of 0.62 and had a constrained modulus of 200,000 psi at a stress of 2,500 psi; whereas specimens 9 and 13 had an initial void ratio of 0.54 and a constrained modulus of 280,000 at 2,500 psi vertical stress. Figure 5.22 shows the variation of constrained tangent modulus with the vertical stress for initial loading on all tests with an initial void ratio of 0.54.

The stress-strain curves for tests 3 and 4 are interesting because in a stress range of 2,600 - 3,000 psi the initial loading curves show a tendency for the curve to be concave downward. Crushing of the grains could be heard at this stress level and it is possible that crushing and rearrangement were responsible for this apparent decrease in rigidity. This tendency toward a decreasing modulus in the 2,800 psi range was not observed in the other tests even though the crushing could be heard, and crushed angular particles were observed after testing. The primary reason that tests 3 and 4 manifested the above phenomenon is because the sample for these tests had an initial void ratio of 0.62; whereas all the other specimens had an initial void ratio of 0.54. The sand with the higher void ratio is free to rearrange as a small amount of crushing

occurs, and the strains from this rearrangement are reflected in a decreasing modulus as in tests 3 and 4. The sands with a lower void ratio, however, are not free to rearrange to a great degree when crushing initiates and thus no significant strains due to rearrangement occur. Even the denser sands will show a decreasing modulus at some stage due to crushing, but in general, one would expect crushing to occur at a higher average stress level in a dense sand than in a loose sand. A dense sand has more contact points per unit volume than a loose sand and thus for the same average applied stress, the loose sand has higher grain to grain contact stresses than the dense sand. Therefore, the loose sand begins crushing at a lower stress than the dense sand. The phenomena discussed above is illustrated very well in Fig. 4.19 of this report.

The loading and subsequent unloading of the sample showed that on the average about 75% of the axial strain was recoverable. This strain was probably the result of elastic deformations at the points of contact. The non-recoverable portion of the strains most definitely was due to irreversible rearrangement of grains. The significant portion of the rearrangement, however, takes place on the first cycle of loading since subsequent cycles are nearly reproducible and show only a slight tendency to rearrange further. These phenomena are illustrated fairly well by test 8.

The stress-strain data from the tests are presented on graphs of \log_{10} stress versus \log_{10} strain in Figs. 5.23 through 5.33. The stress-strain data plot is a straight line on these graphs which means that the axial stress may be expressed in terms of the axial strain by

$$\epsilon_z = K\sigma_z^n \quad (5.8)$$

The above expression may also be written as:

$$\log_{10} \epsilon_z = \log_{10} K + n \log_{10} \sigma_z \quad (5.9)$$

Thus from Eq. (5.9) it is apparent that the parameter n is the reciprocal of the slope as measured from the graphs shown and K is the value of the strain at which the straight line intersects the \log_{10} strain axis. The values of n range from 0.38 to 0.53 for these tests as compared to the value of $2/3$ which was predicted for n from the theoretical analysis presented in Chapter 3. The results do show, however, that an exponential relationship does occur as predicted by theory, but the value of n from tests seems to be consistently less than $2/3$.

The theory from Chapter 3 also predicted a relationship between the constrained tangent modulus, M_c , and the vertical stress, σ_{zz} , as

$$M_c = \frac{d\sigma_{zz}}{d\epsilon_{zz}} = C_1 \sigma_{zz}^{1/3} \quad (5.10)$$

where C_1 is a constant. Figure 5.34 shows the variation of $\log M_c$ and $\log \sigma_{zz}$ for all tests on samples with an initial void ratio of 0.54. Since the relationship is a straight line the actual relationship between the constrained tangent modulus and the vertical stress is

$$M_c = C \sigma_{zz}^k \quad (5.11)$$

where k is the slope of the line. The value of k for this set of experiments is $1/2$ whereas the theory from Chapter 3 predicted that k should be $1/3$.

The small number of tests conducted thus far are not sufficient to make any definite conclusions about the effect of strain rate on the

stress-strain curves; however, there appears to be a definite trend even though the range of strain rate has been relatively small. The constrained moduli, in the 2,500 - 3,000 psi vertical stress range, for samples with an initial void ratio of 0.54 were compared for loading rates varying from 0.005 to 0.040 in./min. The results are shown below.

<u>Testing Rate</u> <u>in./min.</u>	<u>Constrained Modulus</u> <u>psi</u>
0.005	262,500
0.010	262,500
0.020	269,600
0.040	270,300
Note: Controlled stress test, i.e. test #10	245,000

The constrained modulus appears to increase slightly with increasing strain rate, but in the range of strain rates considered, this effect is not of great importance. In fact, a slight change in initial void ratio is much more effective in changing the constrained modulus than the strain rate.

5.4.2 The Coefficient of Earth Pressure at Rest

The results of the lateral earth pressure measurements for the initial loading of each specimen are shown in Figs. 5.35 through 5.45. The lateral pressure is plotted as ordinate and the vertical stress as abscissa. The experimental data plot in a straight line for all curves and K_0 , the coefficient of earth pressure at rest, is numerically equal to the slope of the straight line.

The influence of relative density on K_0 can be seen by comparing K_0 for the samples having an initial void ratio of 0.62 with the sample having an initial void ratio of 0.54. The samples with the high

void ratio had measured values of K_0 ranging from 0.390 to 0.415; whereas the denser samples tested at the same rate of loading as the above samples had K_0 values from 0.340 to 0.360. Thus K_0 appears to decrease as the relative density of the sand increases. This variation was expected since it is well known that the angle of internal friction increases as the relative density increases. Other investigators such as Jaky [5.4] have shown that the value of K_0 decreases as the angle of internal friction increases for a soil with an over-consolidation ratio of 1.

The value of K_0 for a soil of constant initial void ratio also varies slightly with strain rate. The general trend of the data shows that K_0 decreases with increasing strain rate. Tests on the dense sand ($e = 0.54$) showed that K_0 varied from 0.375 for a consolidation type test as in test 10 to as low as 0.330 for the fastest loading rate of 0.004 in./min. The values of K_0 for the intermediate loading rates of 0.01 and 0.02 in./min. were 0.350 and 0.335, respectively.

Thus far, the discussion of the coefficient of lateral earth pressure at rest has been restricted to that portion of the stress-strain curve where the ratio of the maximum previous stress to the existing stress on the sand is unity (i.e., $\frac{\text{Max. previous stress}}{\text{Present stress}} = \text{Overconsolidation ratio} = \text{OCR} = 1$). In this region the coefficient of earth pressure at rest is a constant, as predicted by the theory of Chapter 3, but if the specimen is unloaded from some maximum pressure, then the OCR becomes greater than 1 and the value of K_0 does not remain constant as unloading progresses. The variation of K_0 with OCR is illustrated in Fig. 5.46 for tests 3 and 4. This graph clearly shows that K_0 increases with increasing OCR. The maximum value of K_0 measured during unloading was 2.0 and it appeared to be still increasing. If measurements could be more accurately obtained in

the final stages of unloading where the pressures are very low, it would probably be found that the values of K_0 would ultimately approach the coefficient of passive earth pressure.

Figures 5.47 and 5.48 show the variation of lateral earth pressure with vertical stress for 1 1/2 cycles of loading in tests 12 and 13. These curves show that with cyclic loading the coefficient of lateral earth pressure can gradually be built up with each cycle of load. Observe the data for test 13 for example at points a and b. The value of K_0 at a is higher than at b even though the overconsolidation ratio is the same at these two points. Thus, the value of K_0 for a given sand is not only a function of stress history as expressed by the OCR, but it also depends on the number of preceding cycles. Further tests are expected to indicate how much K_0 can be increased at a given OCR by cyclic loading.

5.4.3 Energy Absorption

The energy absorption characteristic of the dry sand were investigated by means of cyclic loading. In general the first cycle was conducted by loading to a maximum pressure of 3,290 psi and unloading to zero. The deformations in the first cycle were only about 75% recoverable due to the fact that rearrangement of the grains caused irrecoverable strains. The sample was then loaded to some lower stress level, usually 1,100 psi, and then unloaded. It was found generally that the second cycle deformations were almost 100% recoverable, but energy was still being lost because the loading and unloading paths were different. If the second cycle was followed by a third cycle identical to the second (such as in test 3, 5, 6, 7, and 8), it was found that the third cycle traversed essentially the same loop with very little irrecoverable

strain but that a significant amount of energy was still being dissipated due to the difference between the loading and unloading paths. In fact, these loops were so nearly identical that for tests 3, 5 and 7 the second and third cycles traversed exactly the same path and the small loop shown on the stress-strain curves for these tests actually represents both the second and third cycles.

The energy lost in hysteresis loops for various tests was evaluated by computing the area enclosed in the loops traversed in the second and third cycles of loading. It was found convenient to express the energy lost as a percentage of the energy input. The results of these measurements are shown in Table 5.1. In general it was found that the ratio of energy lost to energy input is practically a constant regardless of the magnitude of vertical stress, and varies between the narrow limits of 0.275 to 0.334. For samples which had the same history of loading, it was found that the samples with the higher initial void ratios always lost more energy than those with the lower initial void ratio.

The fact that the energy lost/energy input ratio has been observed to be fairly constant regardless of the range of stress is significant, but this relationship is restricted to the maximum value of vertical stress employed in these tests. At higher stress levels crushing may be a major factor and thus other mechanisms of energy dissipation enter into the picture. Further tests into the higher pressure regions will enable a better determination of the range of pressures for which this energy ratio is applicable.

The theory of Chapter 3 predicted that the ratio of energy absorbed to input energy for a hysteresis loop from a stress of zero to any

stress below the crushing stress should be a constant related to the coefficient of friction between grains. Thus the actual measurements are in agreement with theory because this ratio was observed to be practically a constant. The laboratory measurements, however, provide another check on the theory which is quite interesting. The theory predicted that

$$K_o = 1/2 \left(\frac{1-f}{1+f} \right) \quad (5.12)$$

and

$$\frac{\Delta E}{E_1} = \frac{2f}{1+f} \quad (5.13)$$

Since K_o and $\frac{\Delta E}{E_1}$ have both been measured in the laboratory tests, the coefficient of friction or more appropriately, the pseudo coefficient of friction can be evaluated by two independent calculations for each test. If the theory is reasonably appropriate the two values of f should be in good agreement for each test. These calculations were made for each test and are presented in Table 5.2. Tests 3 and 4 do not show good agreement for the two calculated values of the coefficient of friction. Tests 5, 6, 7, 8, 9, 11, 12, and 13, however, show a very good correlation between the two independently calculated values of the coefficient of friction. The latter group of tests had an initial void ratio of 0.54 as compared to 0.62 for tests 3 and 4. Since the theory of Chapter 3 assumes a granular medium in a dense state, it is not surprising that the tests on sand in the denser state should give better correlation with the theory than tests at higher initial void ratios which allows more rearrangement of the grains.

REFERENCES

- 5.1 Speer, T. L., Personal files of R. B. Peck, Prof. Of Foundation Engrg., Univ. of Illinois, 1944.
- 5.2 Fulton, R. E. and Hendron, A. J., "Discussion to Impact Waves in Sand: Theory Compared with Experiments on Sand Columns," Proc. ASCE, Vol. 87, No. SM6, Dec. 1961, pp. 69-73.
- 5.3 Terzaghi, K. T., "Large Retaining-Wall Tests," Engineering News-Record, Feb. 1, 1934, pp. 136-140.
- 5.4 Jaky, J., "The Coefficient of Earth Pressure at Rest," Proc 2nd Int. Conf. Soil Mech., Vol. 1, pp. 103-07 (1948).
- 5.5 Taylor, D. W., "Research on Consolidation of Clays" Publication No. 82, Publications of the Department of Civil and Sanitary Engineering, Massachusetts Institute of Technology, Cambridge, Massachusetts.

TABLE 5.1

ENERGY LOSSES FOR REPEATED LOADINGS

<u>Test No.</u>	<u>Loop Range</u> <u>psi</u>	<u>Mean Stress</u> <u>psi</u>	<u>Energy Lost</u> <u>%</u>
3	0 - 1100	548	33.4
4	0 - 1100	548	33.1
5	0 - 1100	548	32.8
6	0 - 1100	548	30.2
7	0 - 1100	548	27.9
8	0 - 1100	548	27.5
8	0 - 3290	1647	27.8
9	0 - 1100	548	28.7
11	0 - 2195	1099	28.6

TABLE 5.2

CORRELATION OF f , K_o , AND $\Delta E/E_1$

Test	e_o	$f = \frac{1-2K_o}{2K_o+1}$	$f = \frac{1/2 \frac{\Delta E}{E_1}}{(1 - 1/2 \frac{\Delta E}{E_1})}$
3	.62	.12	.20
4	.62	.09	.20
5	.54	.18	.20
6	.54	.16	.18
7	.54	.20	.16
8	.54	.20	.16
9	.54	.19	.17
10	.54 (No Hysteresis loop on this test)		
11	.54	.18	.17
12	.54	.18	.14
13	.54	.18	.15

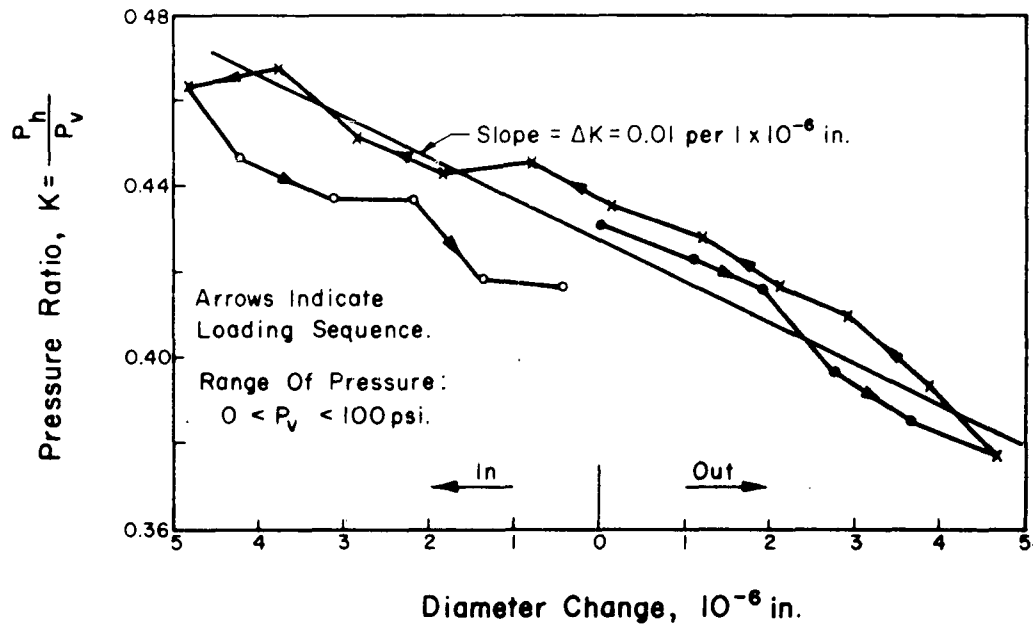
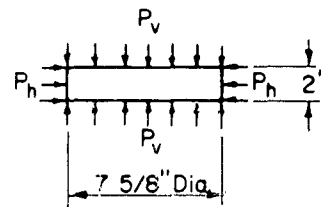


Fig. 5.1 THE EFFECT OF LATERAL MOTION ON $\frac{P_h}{P_v}$
(after Speer (5.1))

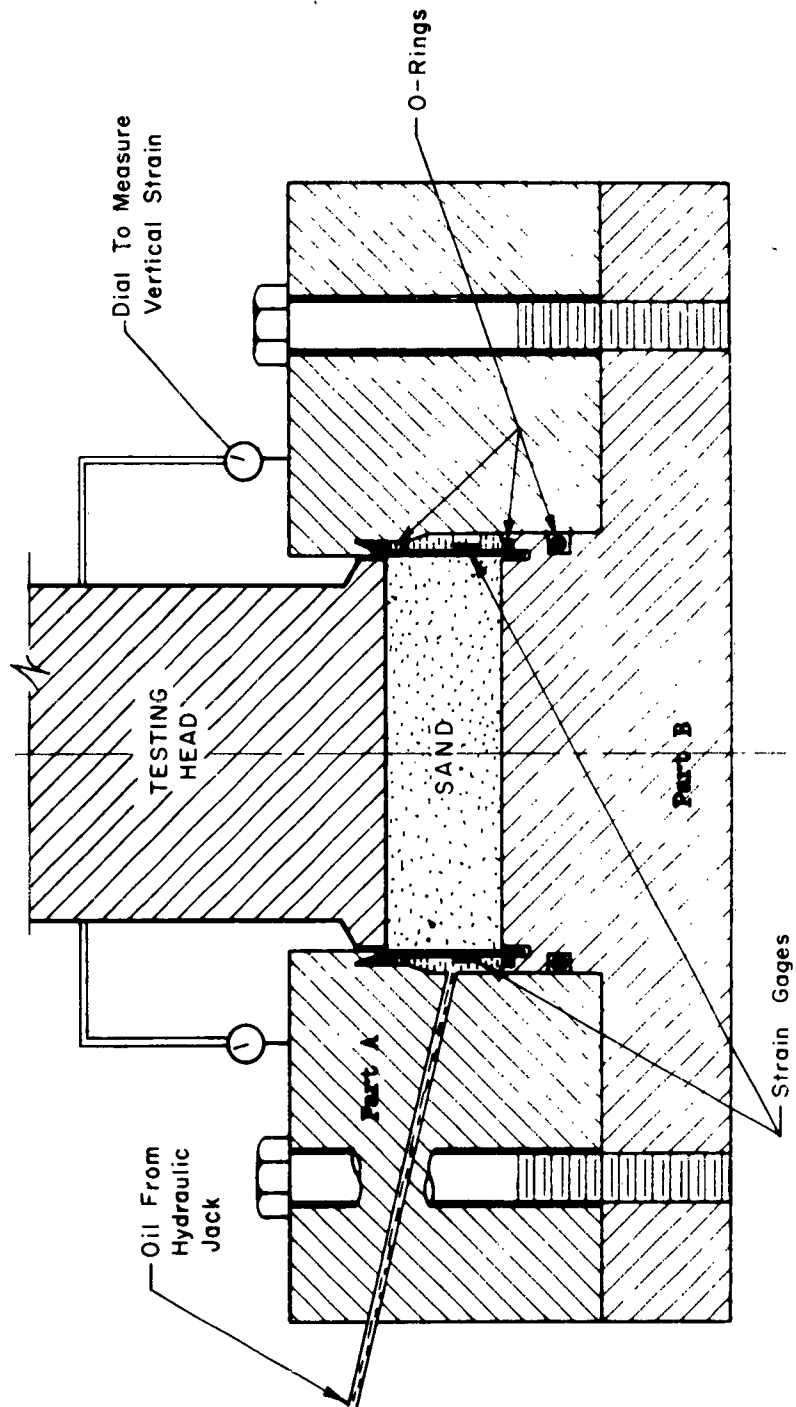
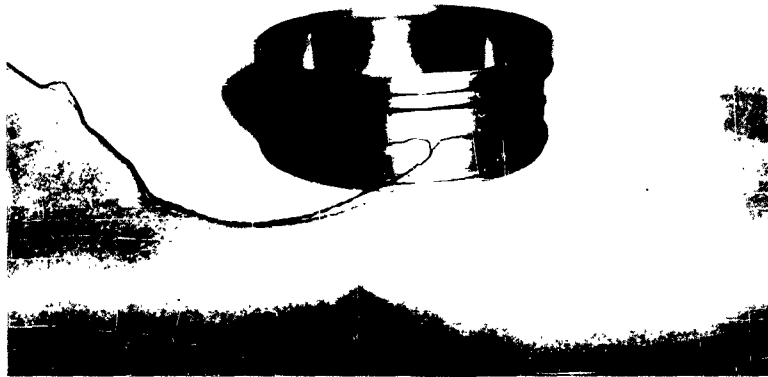
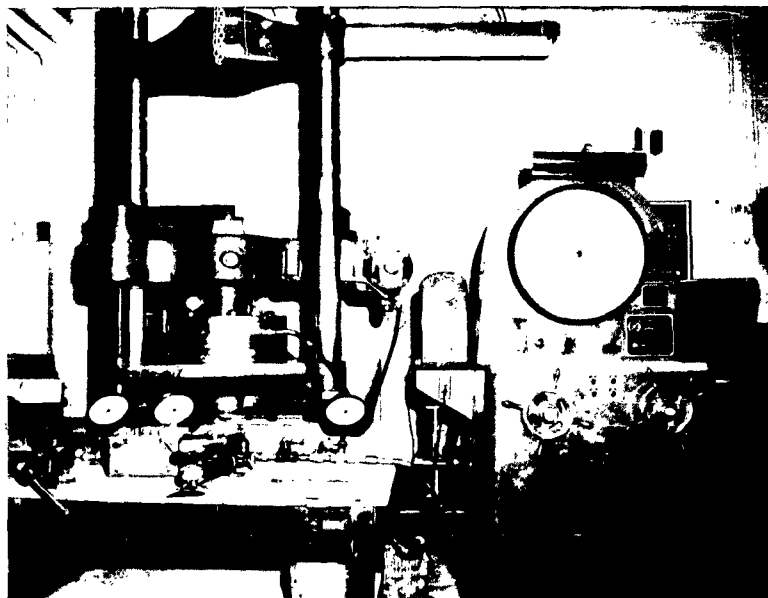


Fig. 5.2 SCHEMATIC CROSS-SECTION THROUGH TESTING APPARATUS



(a)



(b)

Fig. 5.3

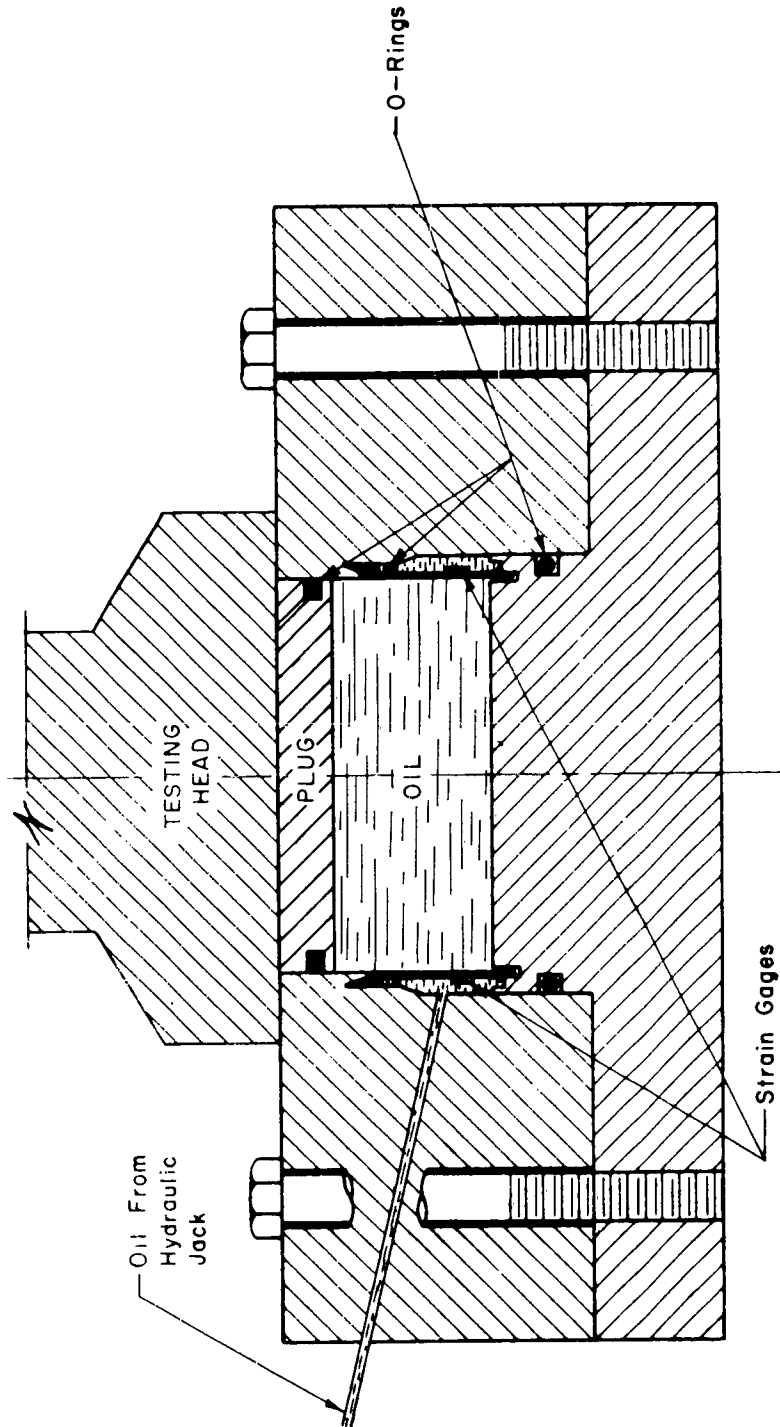


Fig. 5.4 SCHEMATIC CROSS-SECTION THROUGH TESTING APPARATUS DURING CALIBRATION

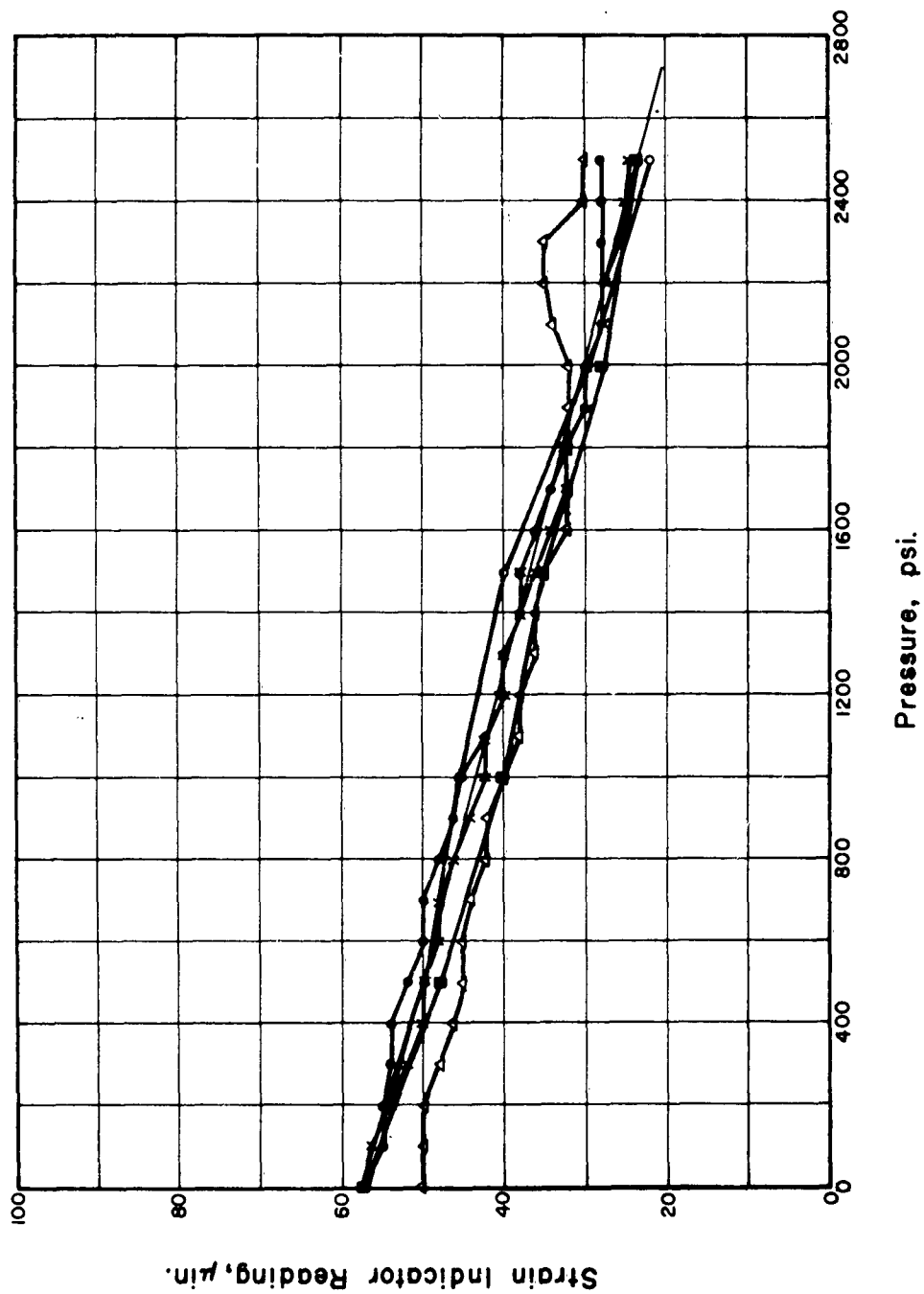


Fig. 5.5 CALIBRATION CURVE FOR THE EFFECT OF OIL PRESSURE ON THE METALFILM STRAIN GAGES

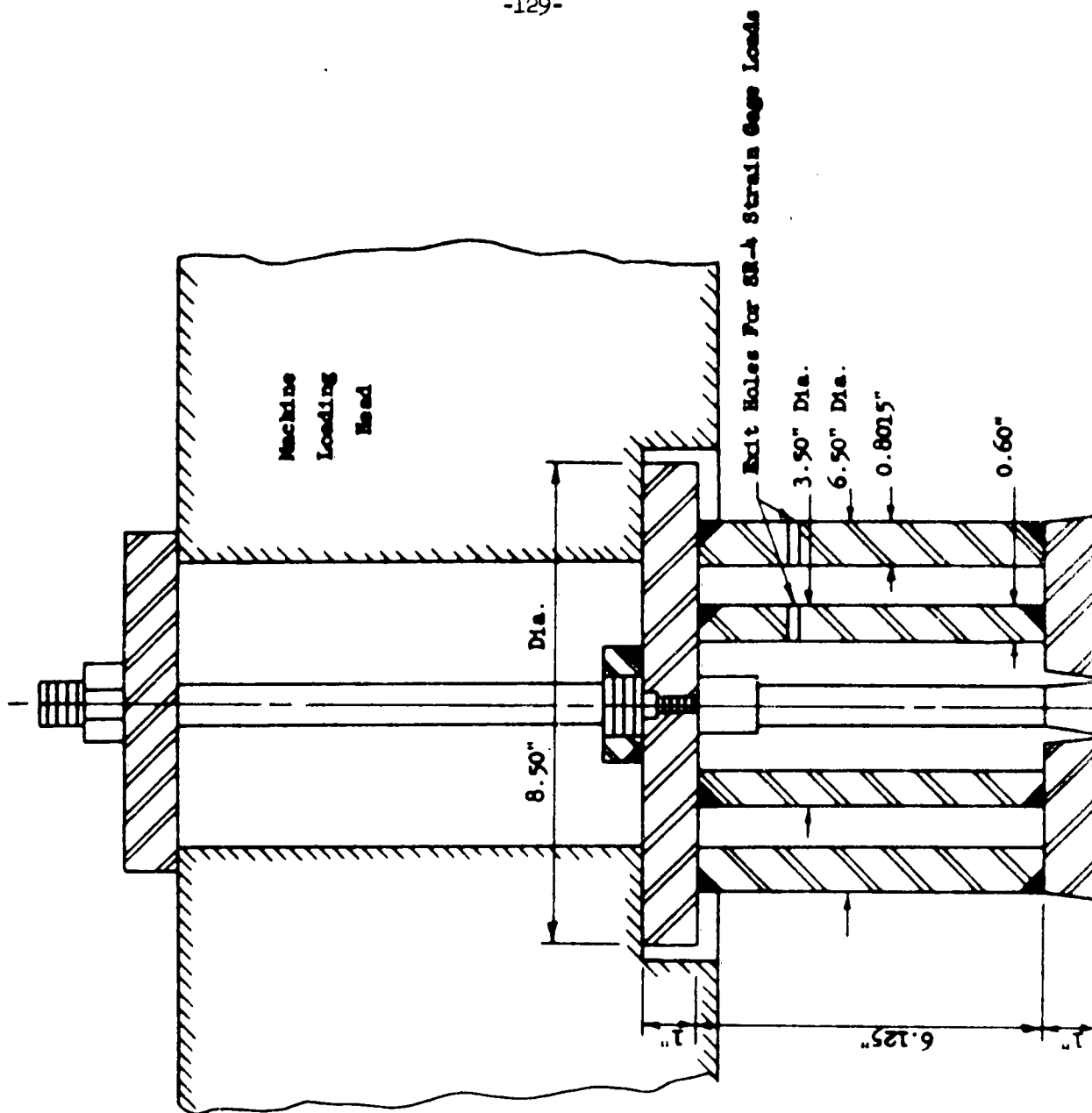
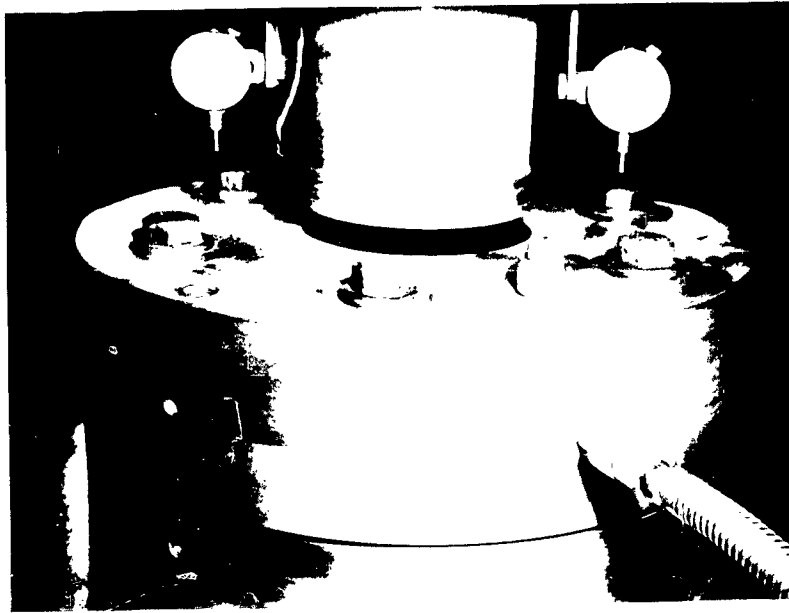
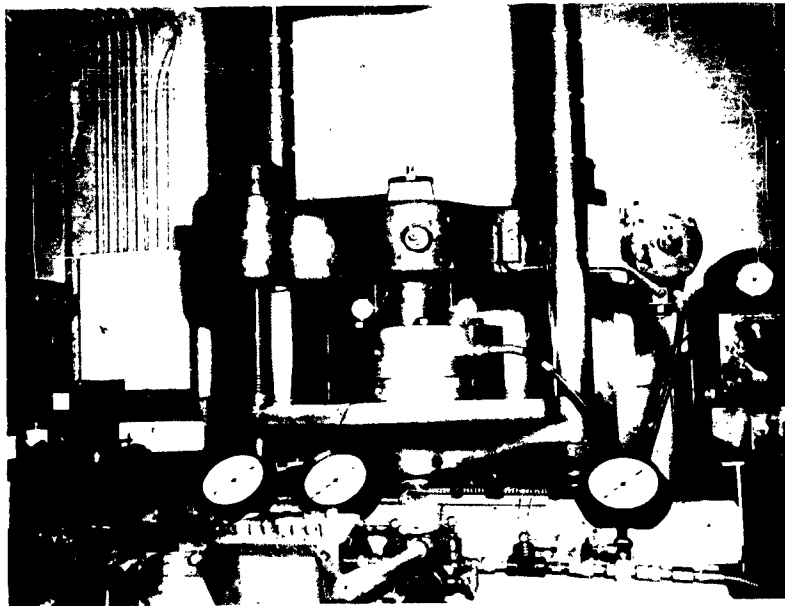


Fig. 5.6 CROSS-SECTION OF TESTING HEAD

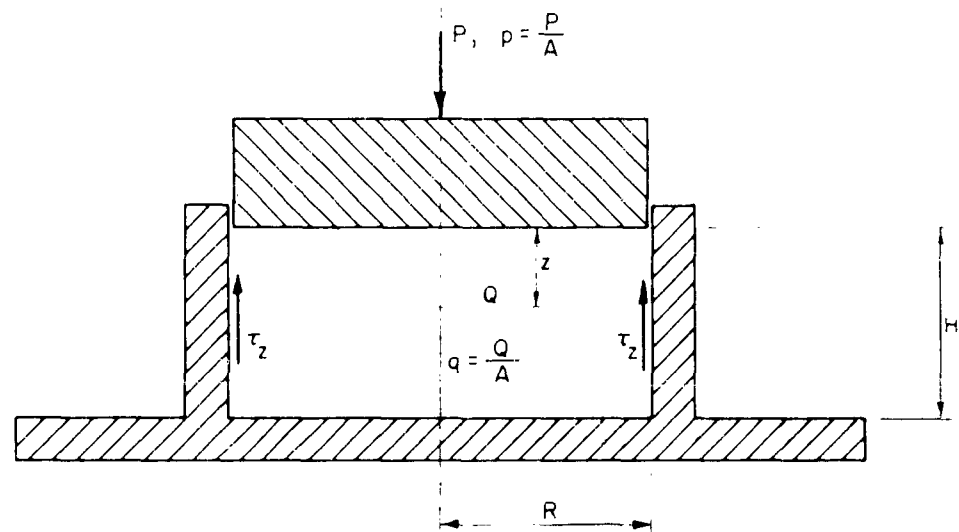


(a)



(b)

Fig. 5.7



$$K_o = \frac{\sigma_H}{\sigma_V} \quad , \quad A = \pi R^2$$

f = Coefficient Of Friction Between Soil And Ring

Fig. 5.8 SCHEMATIC DIAGRAM ILLUSTRATING THE EFFECT OF SIDE FRICTION IN ONE DIMENSIONAL COMPRESSION

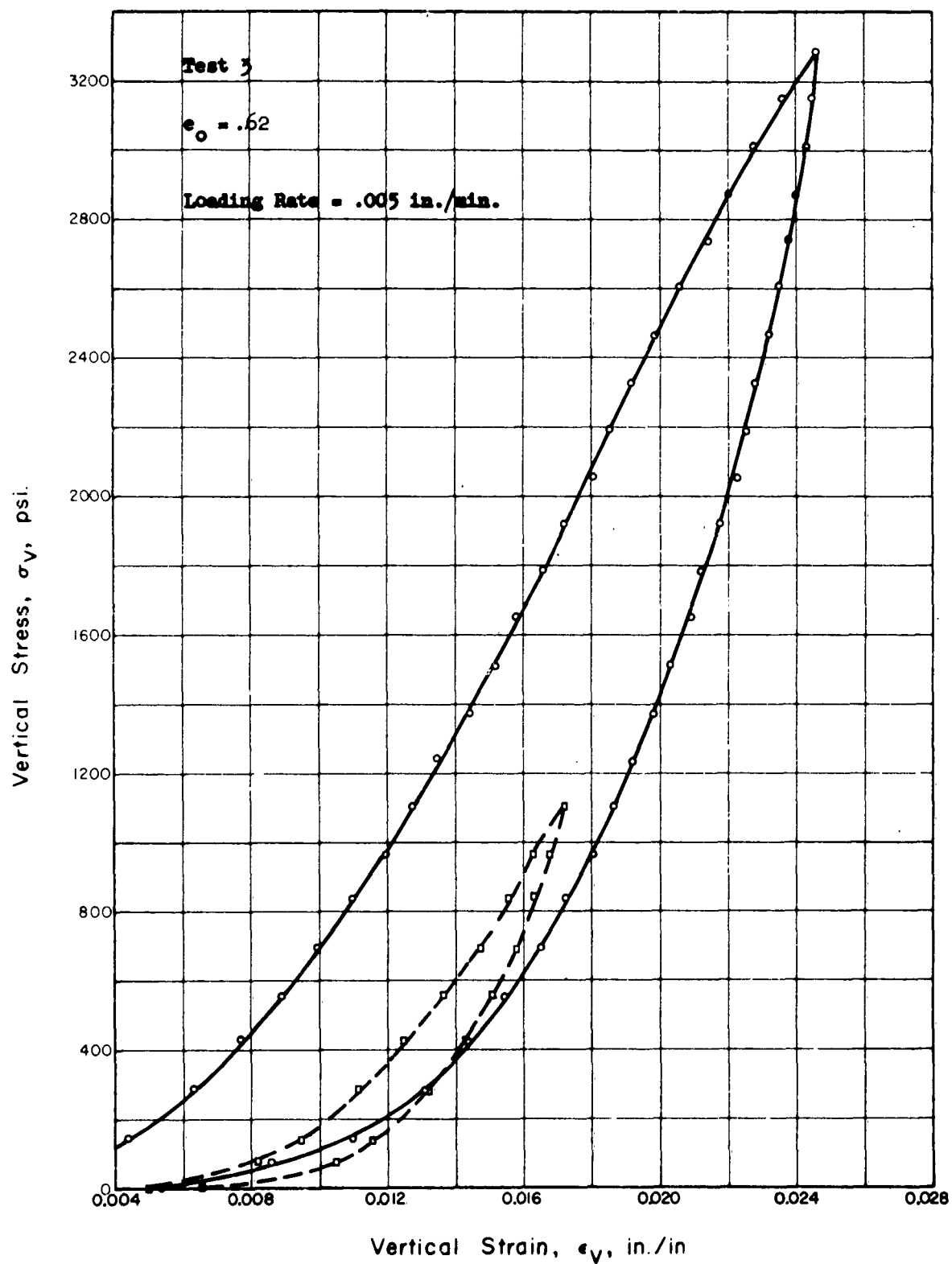


Fig. 5.9 STRESS STRAIN CURVE FOR MINNESOTA SAND
 IN ONE DIMENSIONAL COMPRESSION

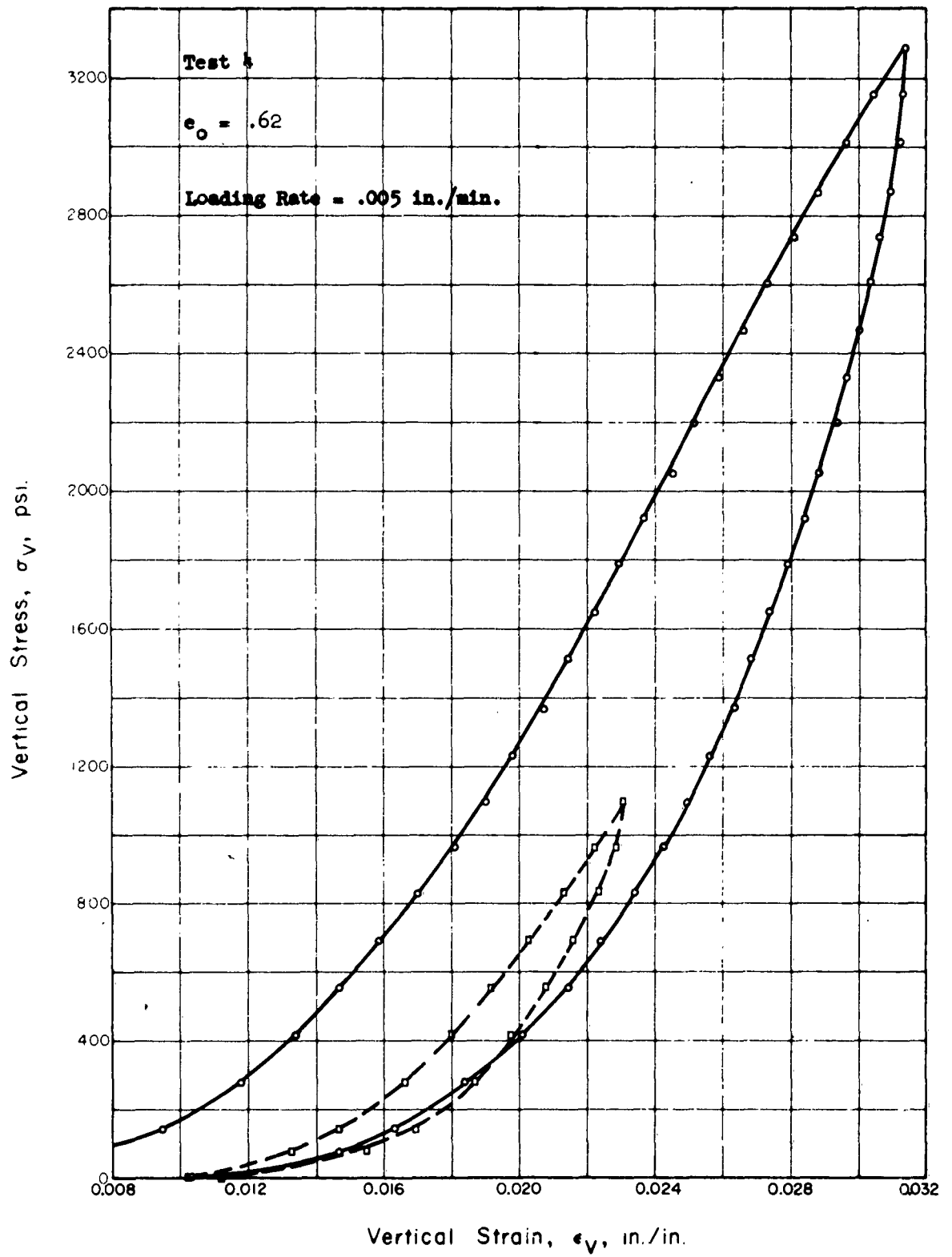


Fig. 5.10 STRESS STRAIN CURVE FOR MINNESOTA SAND
IN ONE DIMENSIONAL COMPRESSION

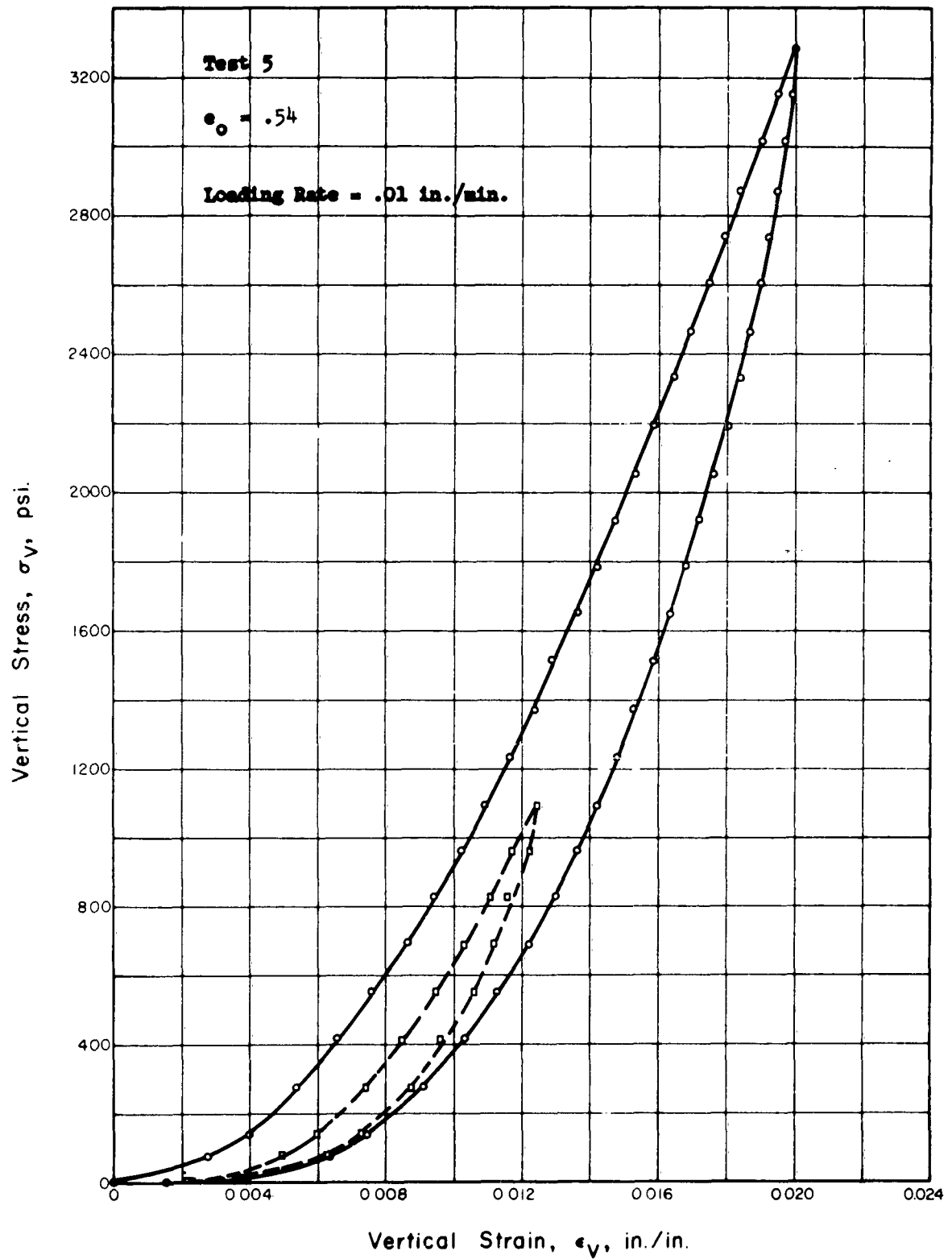


Fig. 5.11 STRESS STRAIN CURVE FOR MINNESOTA SAND
IN ONE DIMENSIONAL COMPRESSION

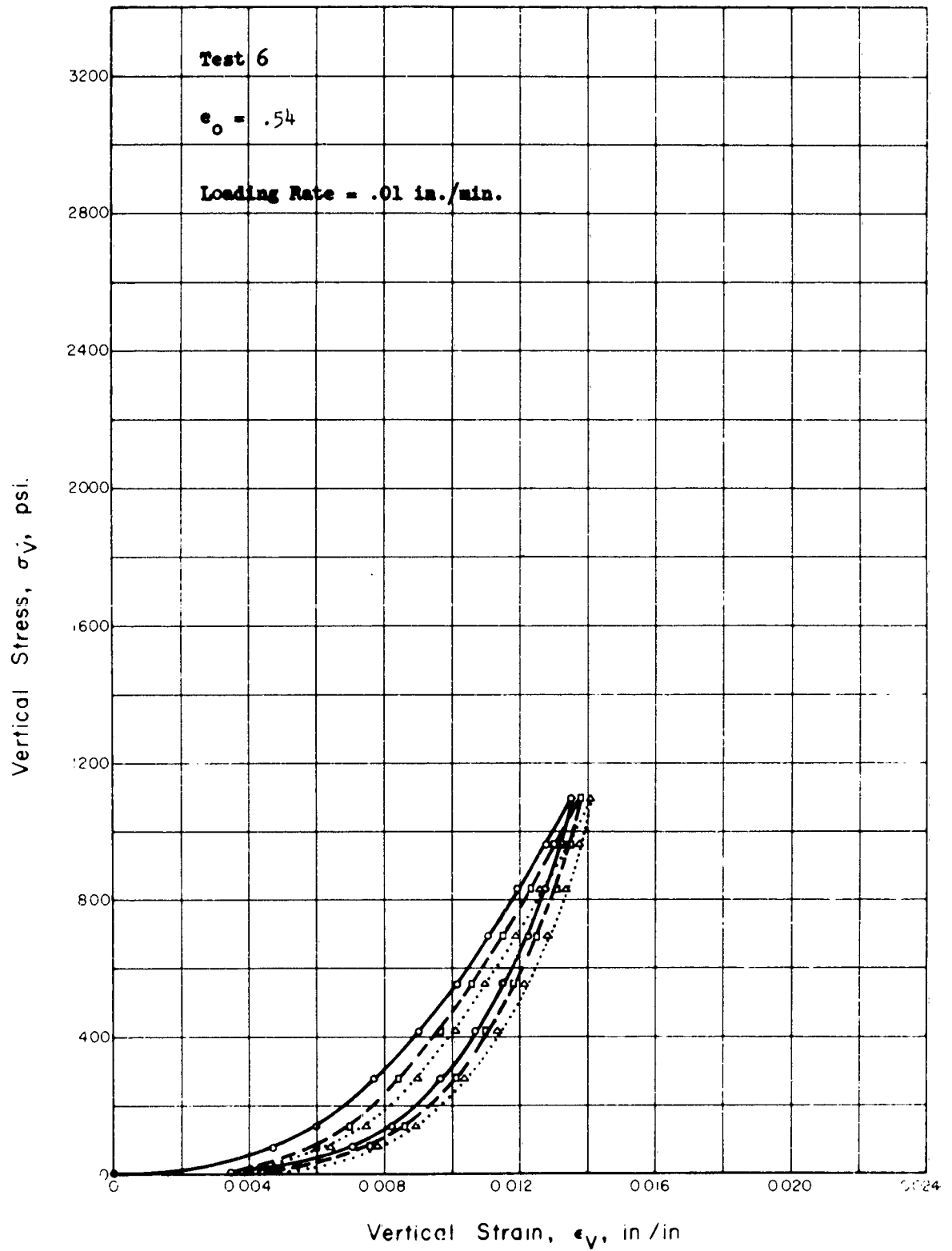


Fig. 5.12 STRESS STRAIN CURVE FOR MINNESOTA SAND
IN ONE DIMENSIONAL COMPRESSION

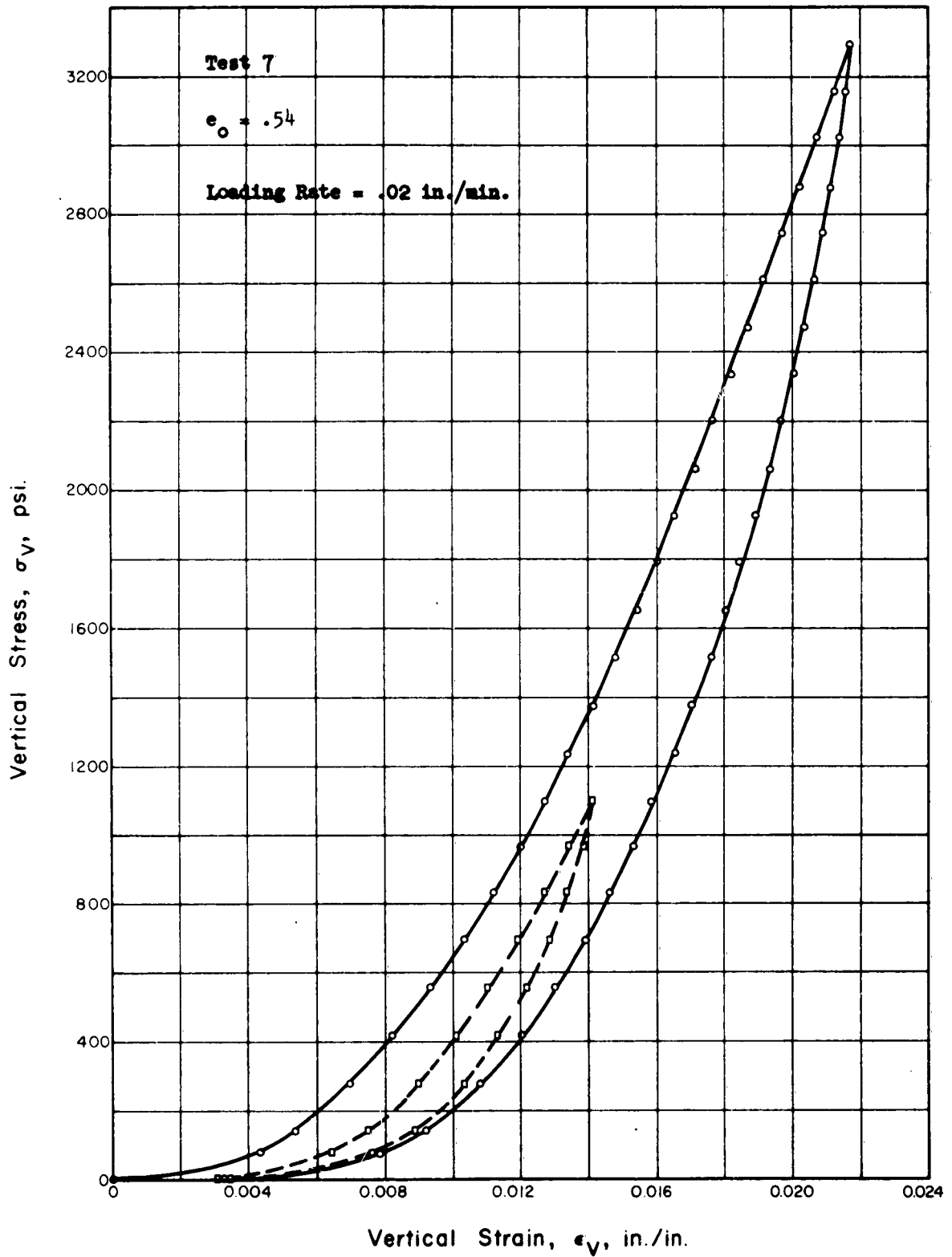


Fig. 5.13 STRESS STRAIN CURVE FOR MINNESOTA SAND
IN ONE DIMENSIONAL COMPRESSION

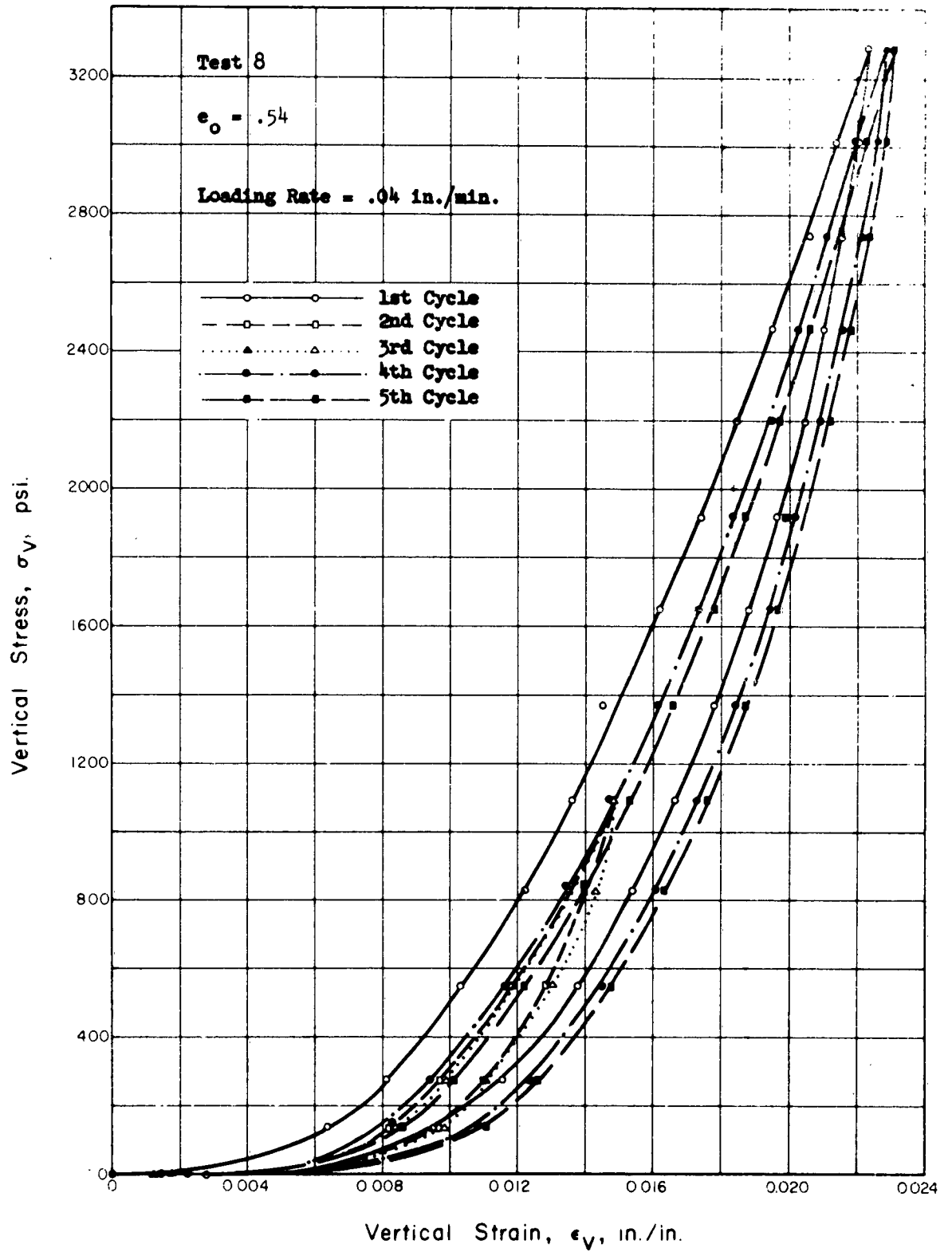


Fig. 5.14 STRESS STRAIN CURVE FOR MINNESOTA SAND
IN ONE DIMENSIONAL COMPRESSION

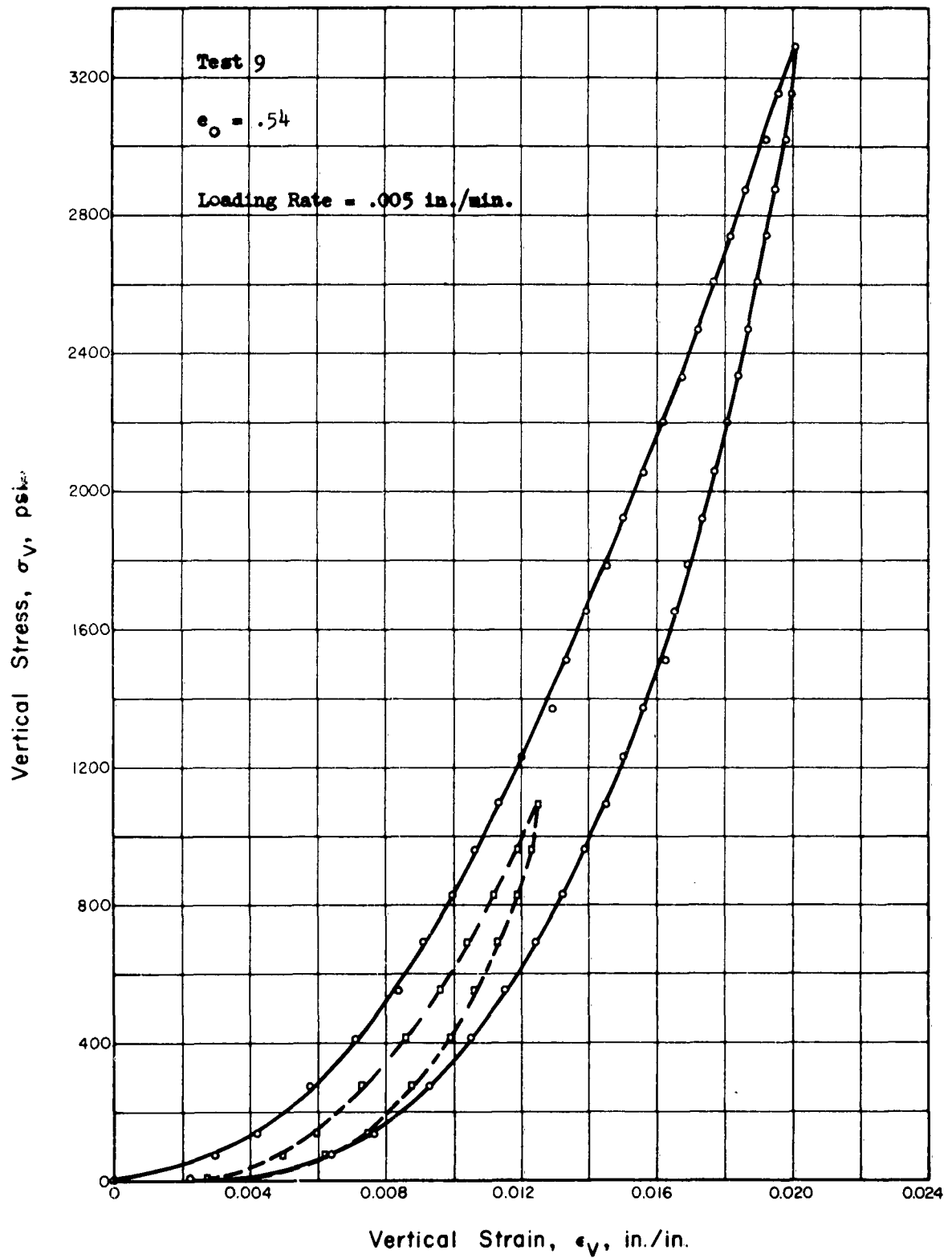


Fig. 5.15 STRESS STRAIN CURVE FOR MINNESOTA SAND
IN ONE DIMENSIONAL COMPRESSION

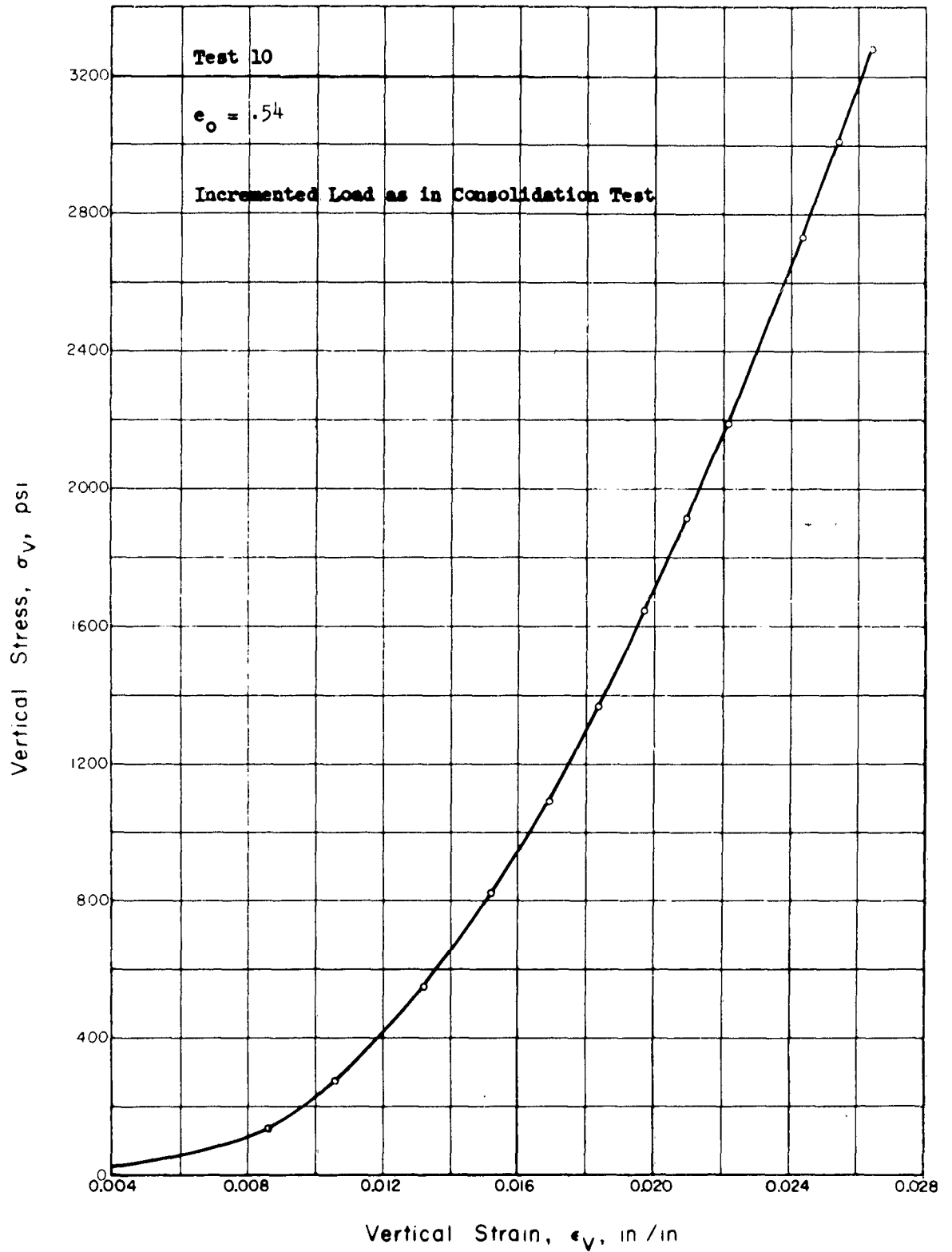


Fig. 5.16 STRESS STRAIN CURVE FOR MINNESOTA SAND
IN ONE DIMENSIONAL COMPRESSION

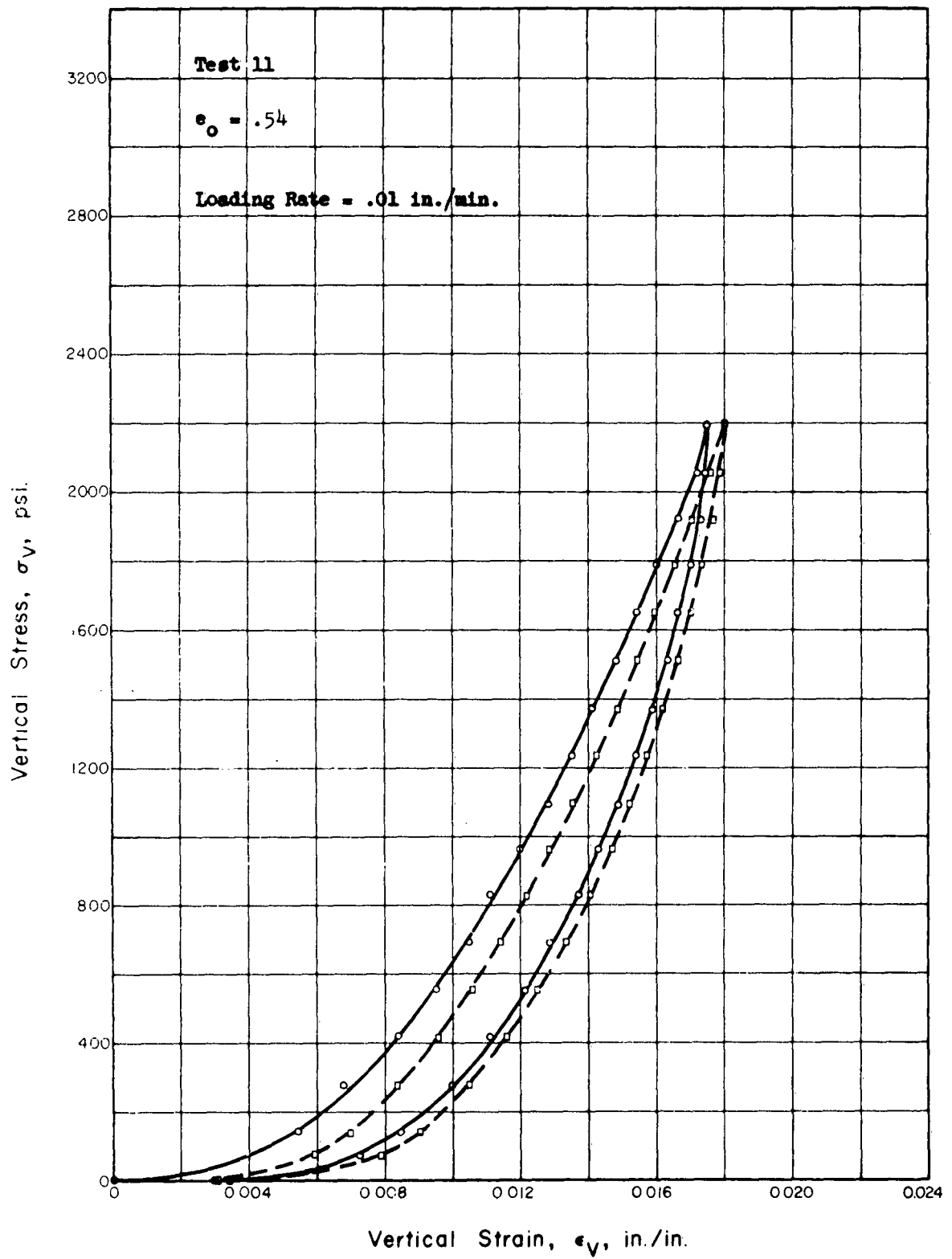


Fig. 5.17 STRESS STRAIN CURVE FOR MINNESOTA SAND
IN ONE DIMENSIONAL COMPRESSION

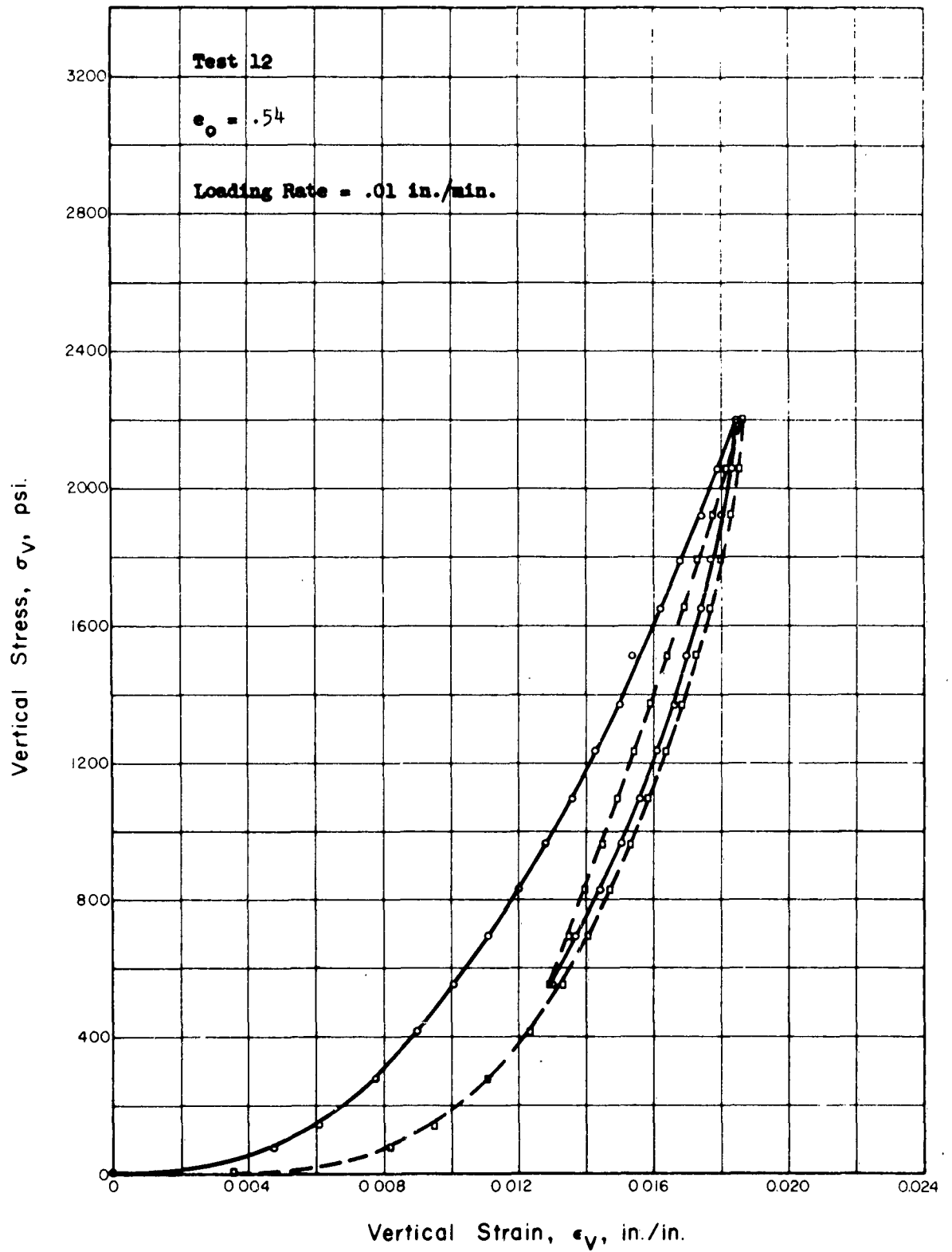


Fig. 5.18 STRESS STRAIN CURVE FOR MINNESOTA SAND
IN ONE DIMENSIONAL COMPRESSION

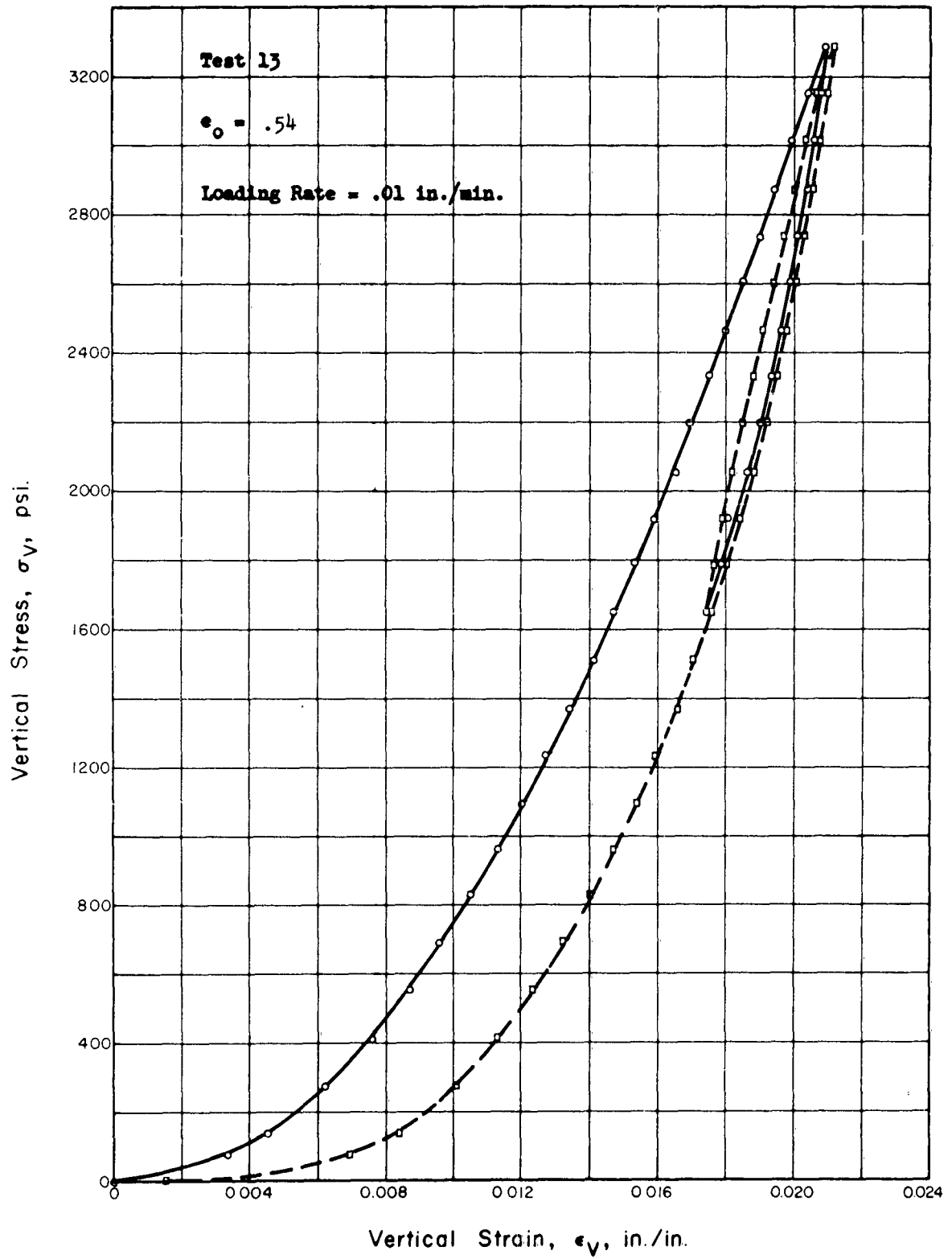


Fig. 5.19 STRESS STRAIN CURVE FOR MINNESOTA SAND
IN ONE DIMENSIONAL COMPRESSION

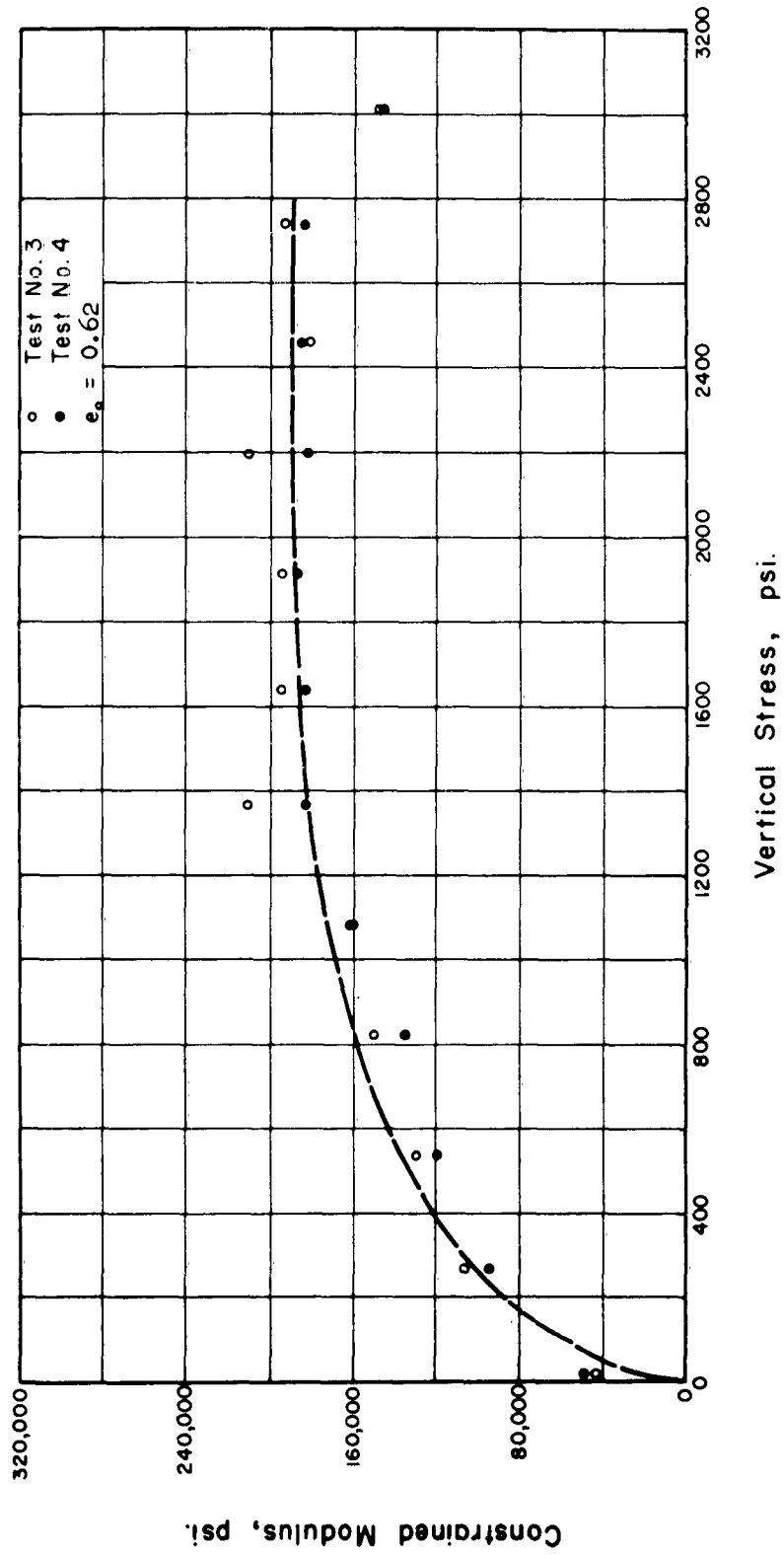


Fig. 5.20 CONSTRAINED MODULUS VS. VERTICAL STRESS

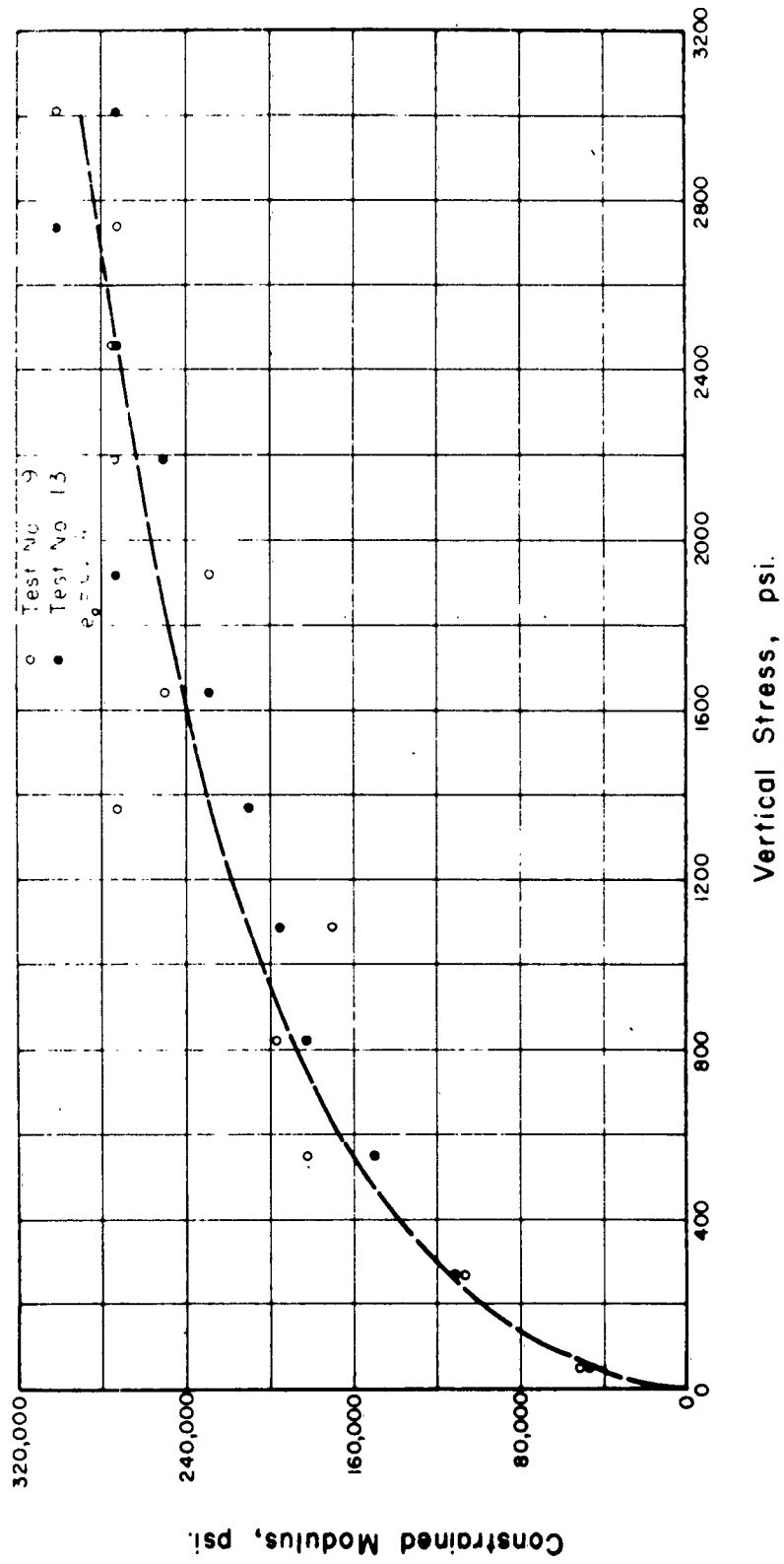


Fig. 5.21 CONSTRAINED MODULUS VS. VERTICAL STRESS

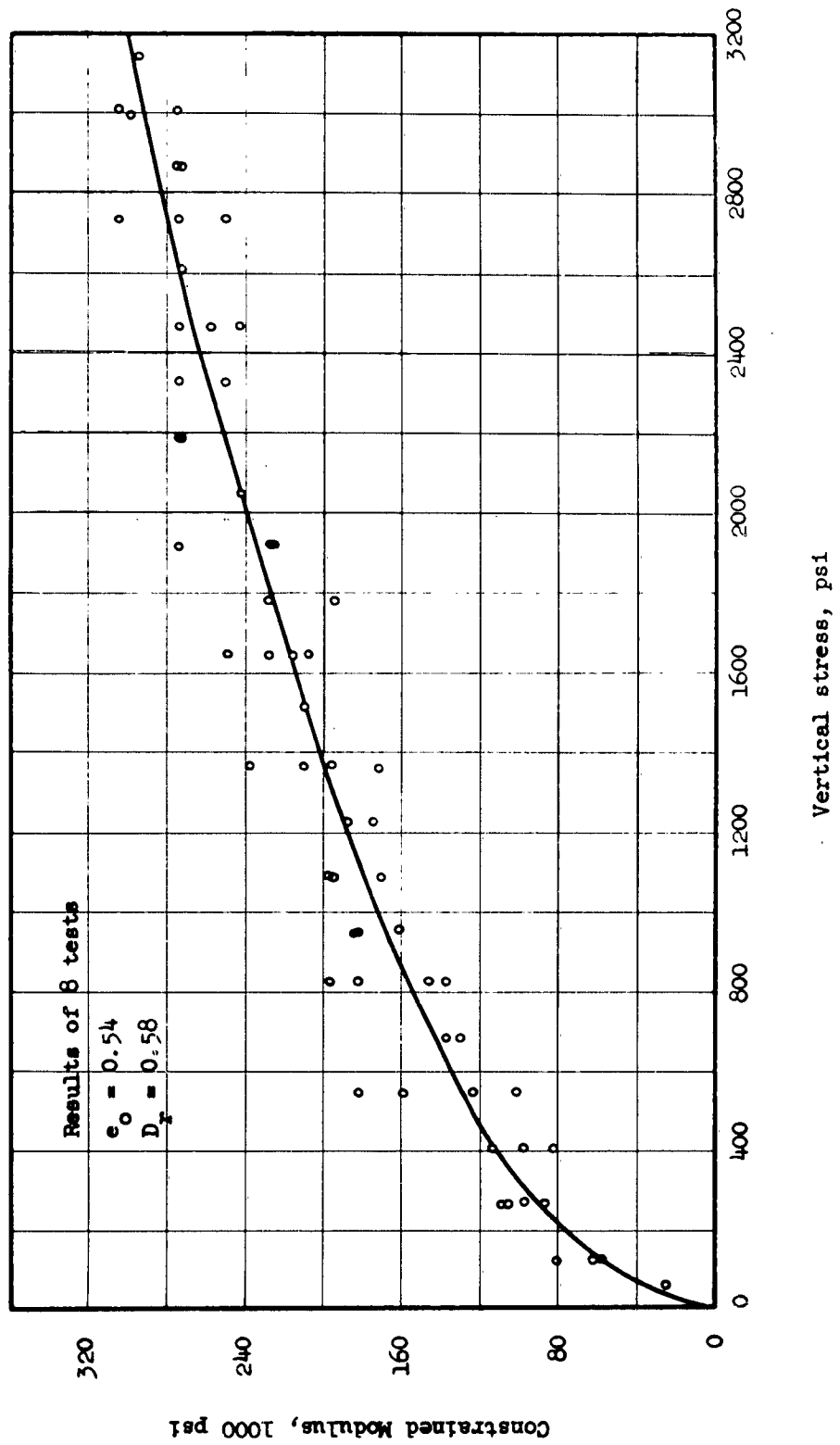


Fig. 5.22 CONSTRAINED MODULUS VS VERTICAL STRESS

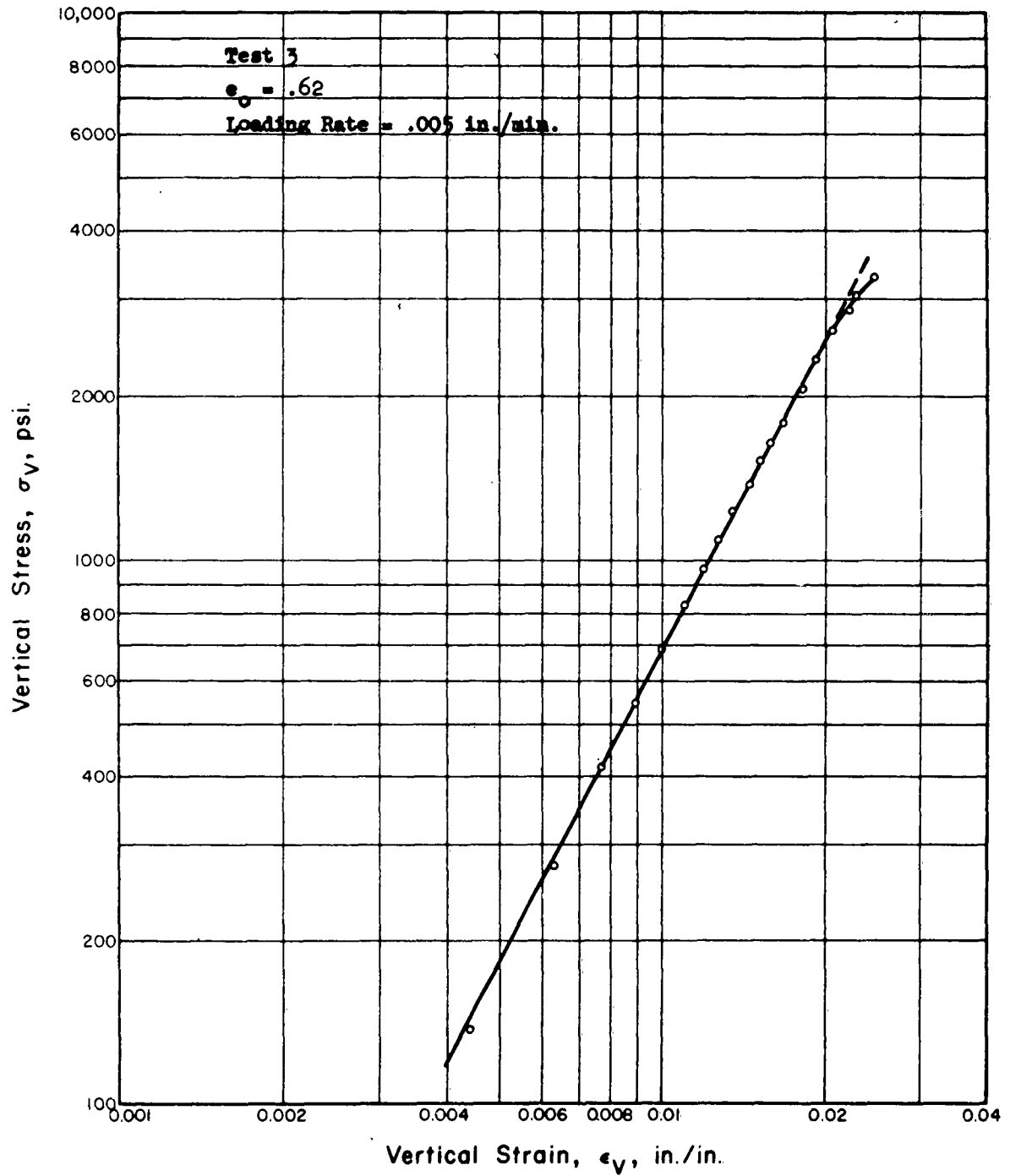


Fig. 5.23 LOGARITHMIC PLOT OF STRESS STRAIN CURVE FOR MINNESOTA SAND IN ONE DIMENSIONAL COMPRESSION

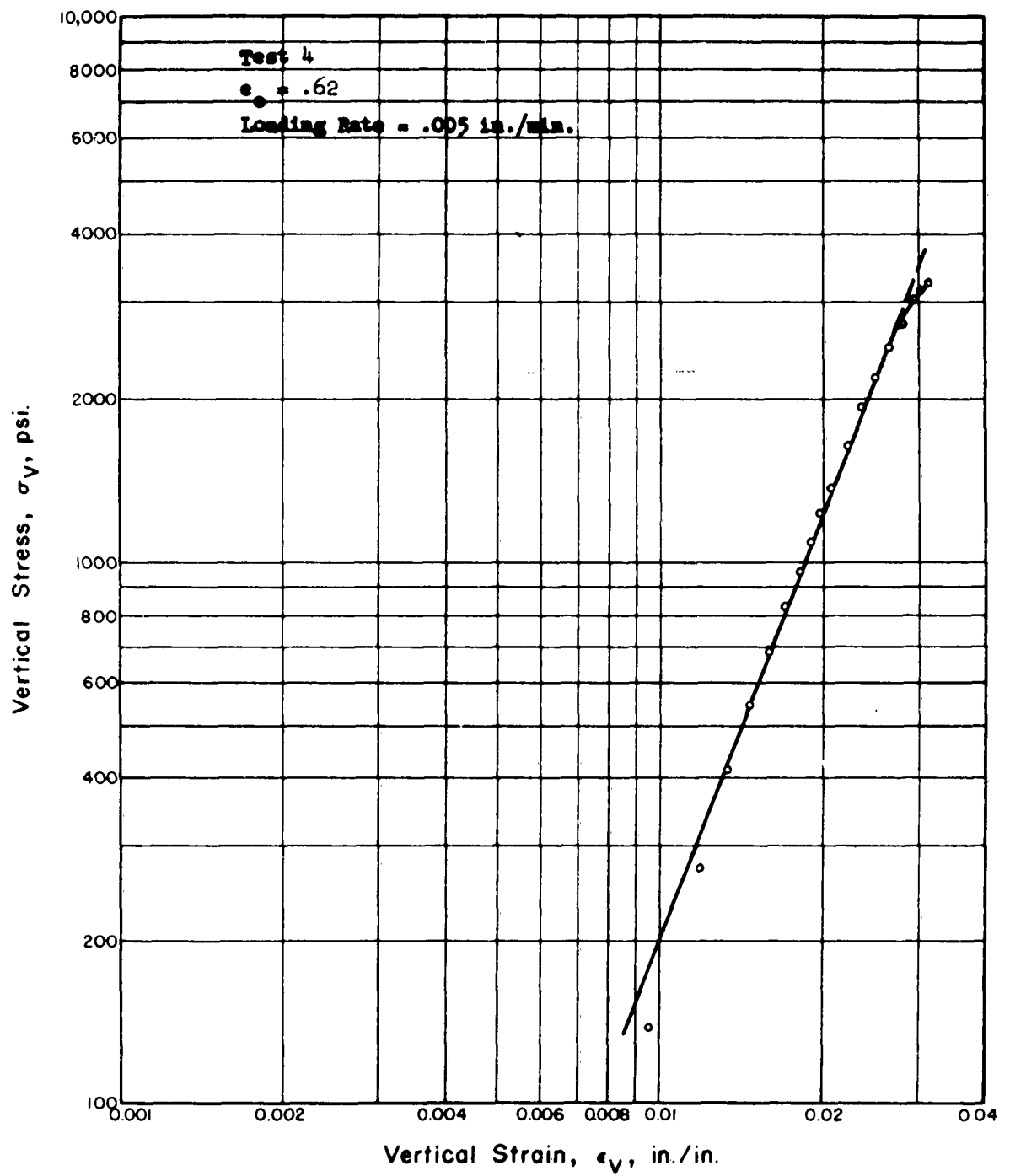


Fig. 5.24 LOGARITHMIC PLOT OF STRESS STRAIN CURVE FOR MINNESOTA SAND IN ONE DIMENSIONAL COMPRESSION

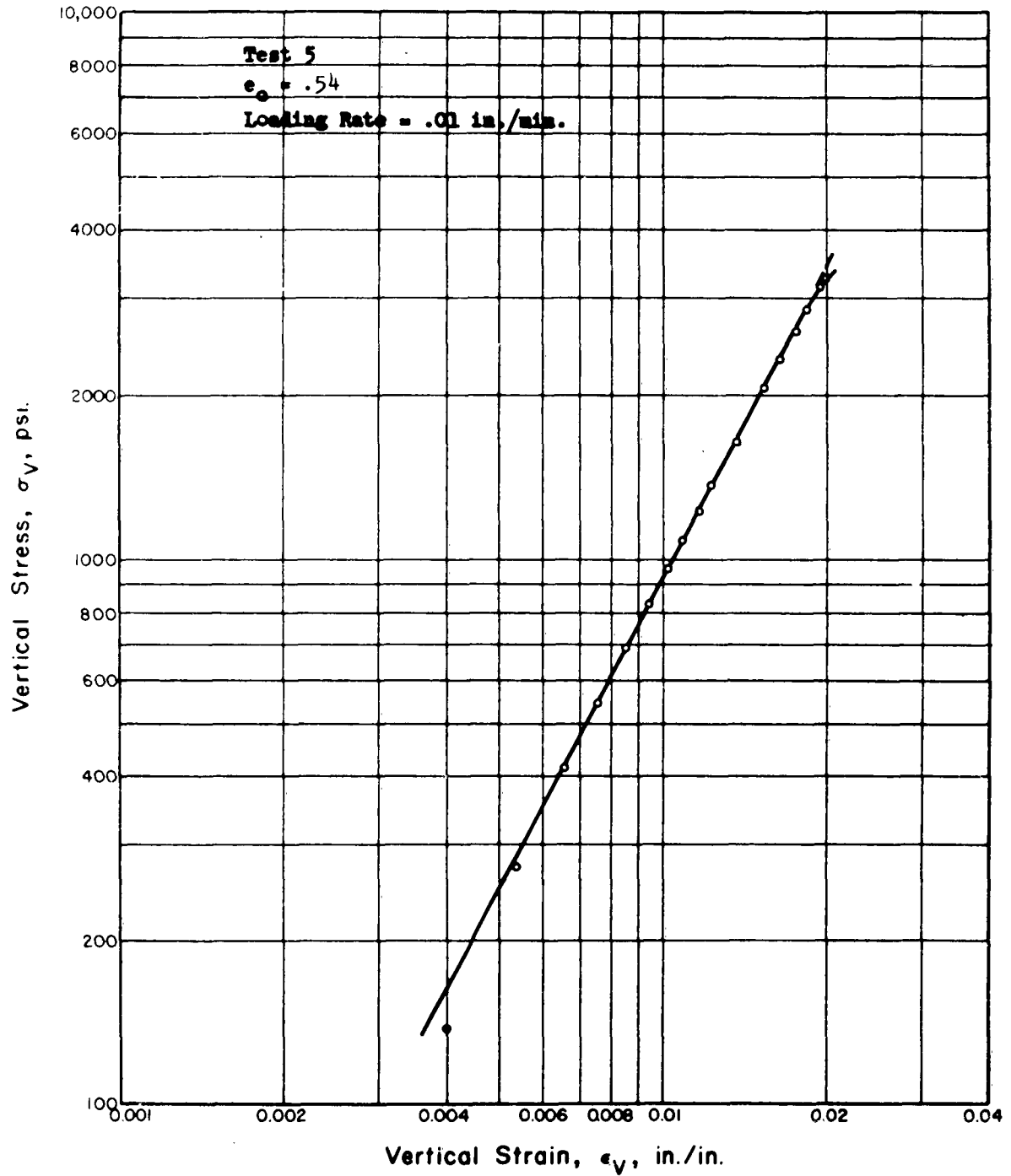


Fig. 5.25 LOGARITHMIC PLOT OF STRESS STRAIN CURVE FOR MINNESOTA SAND IN ONE DIMENSIONAL COMPRESSION

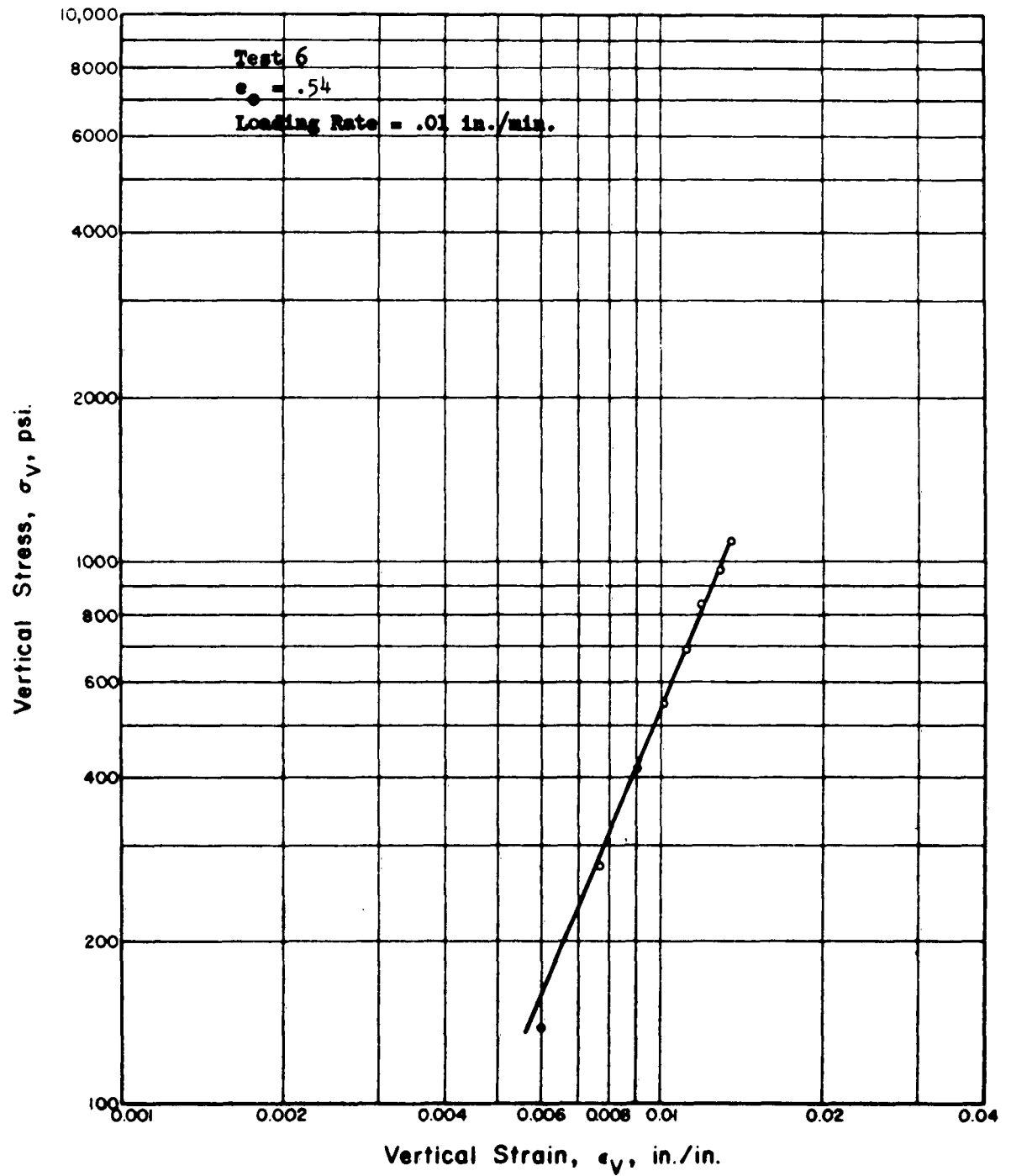


Fig. 5.26 LOGARITHMIC PLOT OF STRESS STRAIN CURVE FOR MINNESOTA SAND IN ONE DIMENSIONAL COMPRESSION

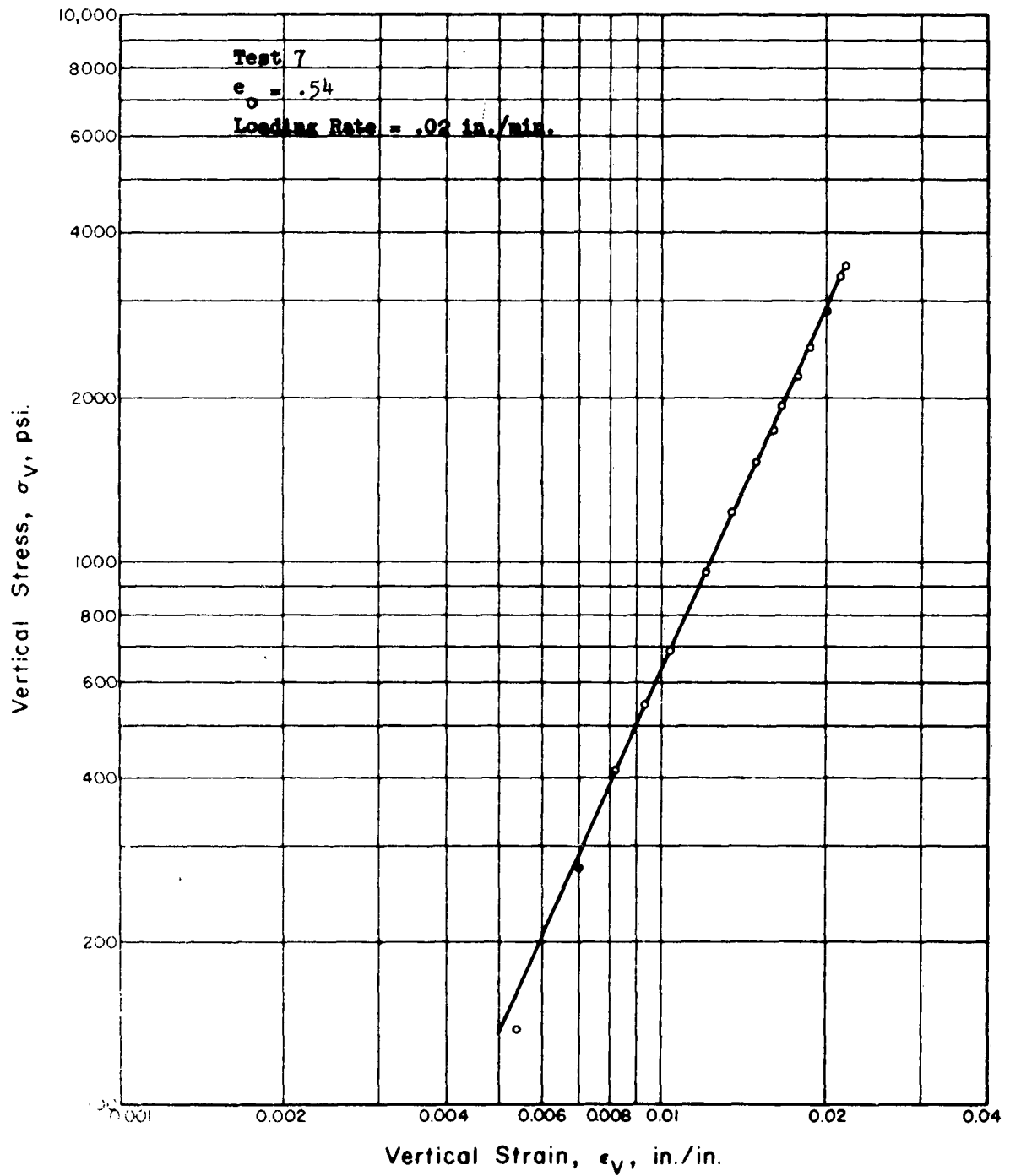


Fig. 5.27 LOGARITHMIC PLOT OF STRESS STRAIN CURVE FOR MINNESOTA SAND IN ONE DIMENSIONAL COMPRESSION

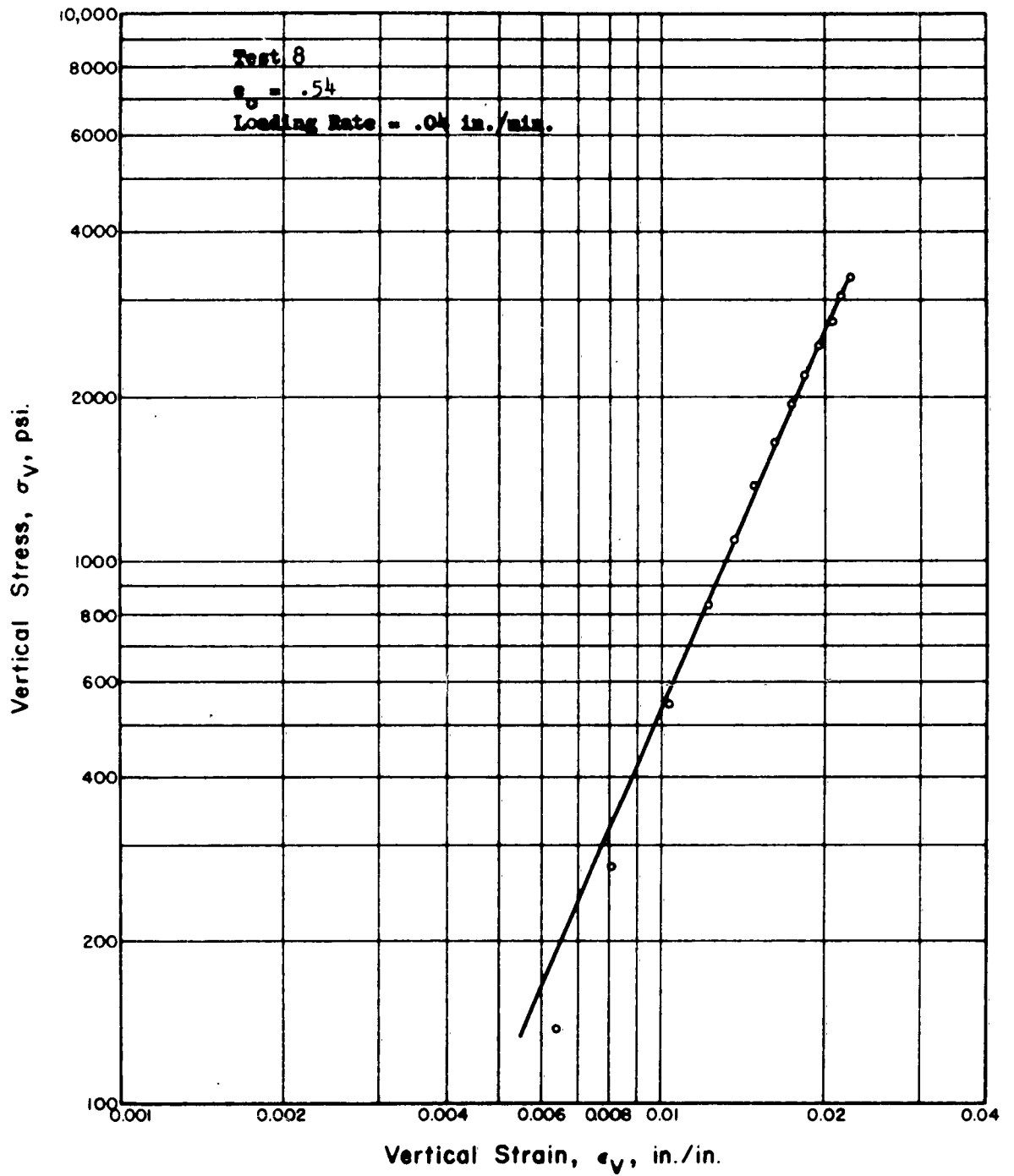


Fig. 5.28 LOGARITHMIC PLOT OF STRESS STRAIN CURVE FOR MINNESOTA SAND IN ONE DIMENSIONAL COMPRESSION

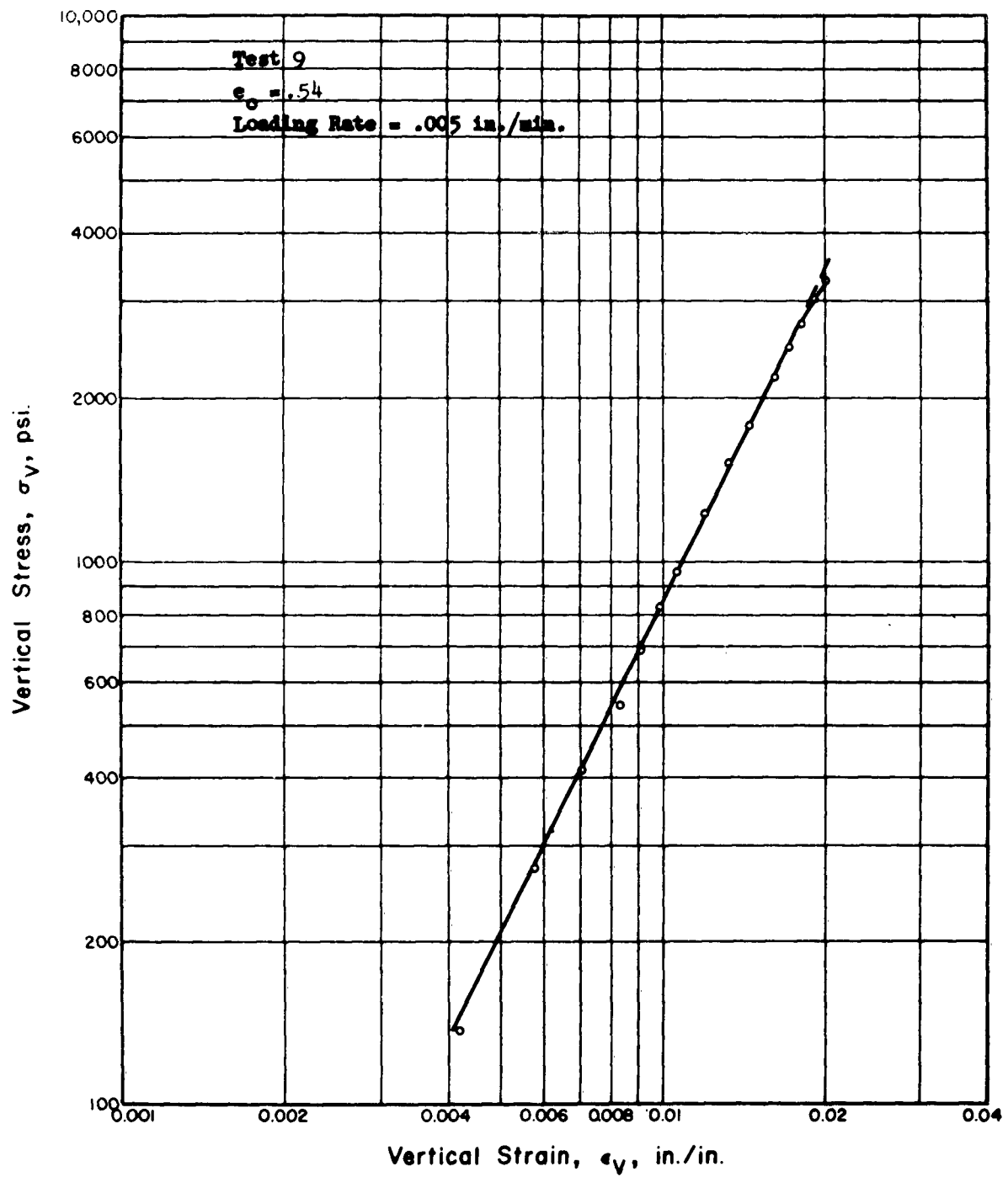


Fig. 5.29 LOGARITHMIC PLOT OF STRESS STRAIN CURVE FOR MINNESOTA SAND IN ONE DIMENSIONAL COMPRESSION

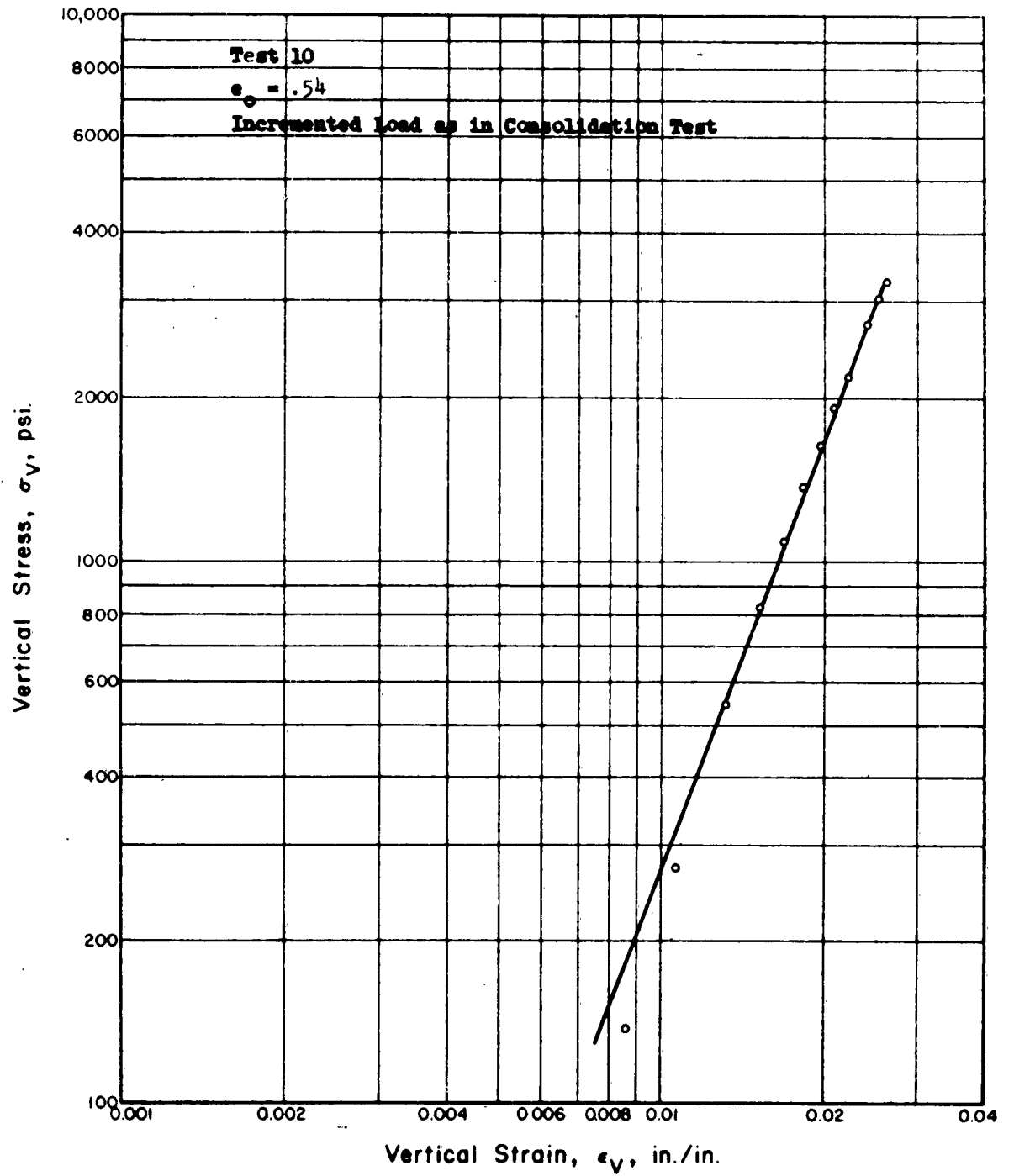


Fig. 5.30 LOGARITHMIC PLOT OF STRESS STRAIN CURVE FOR MINNESOTA SAND IN ONE DIMENSIONAL COMPRESSION

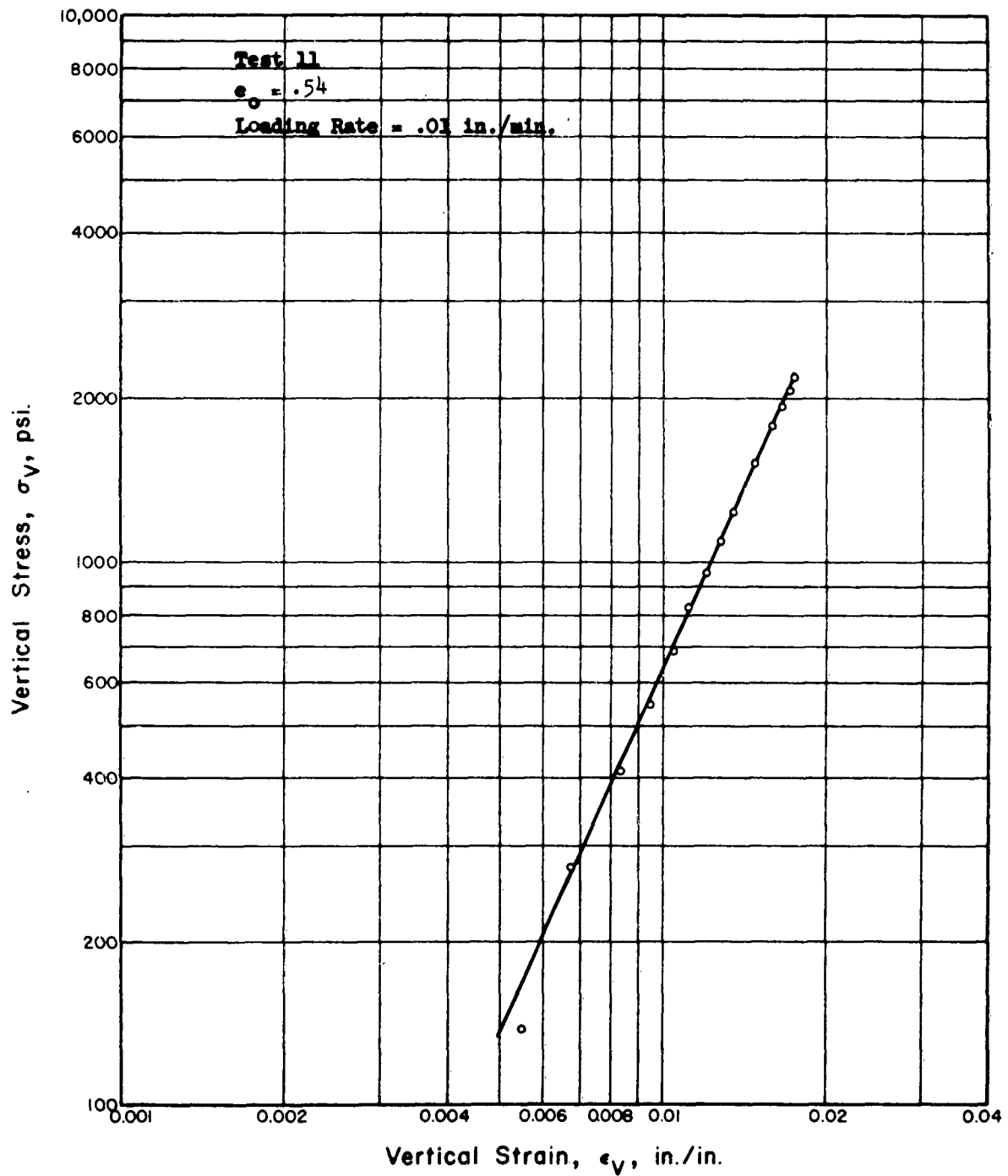


Fig. 5.31 LOGARITHMIC PLOT OF STRESS STRAIN CURVE FOR MINNESOTA SAND IN ONE DIMENSIONAL COMPRESSION

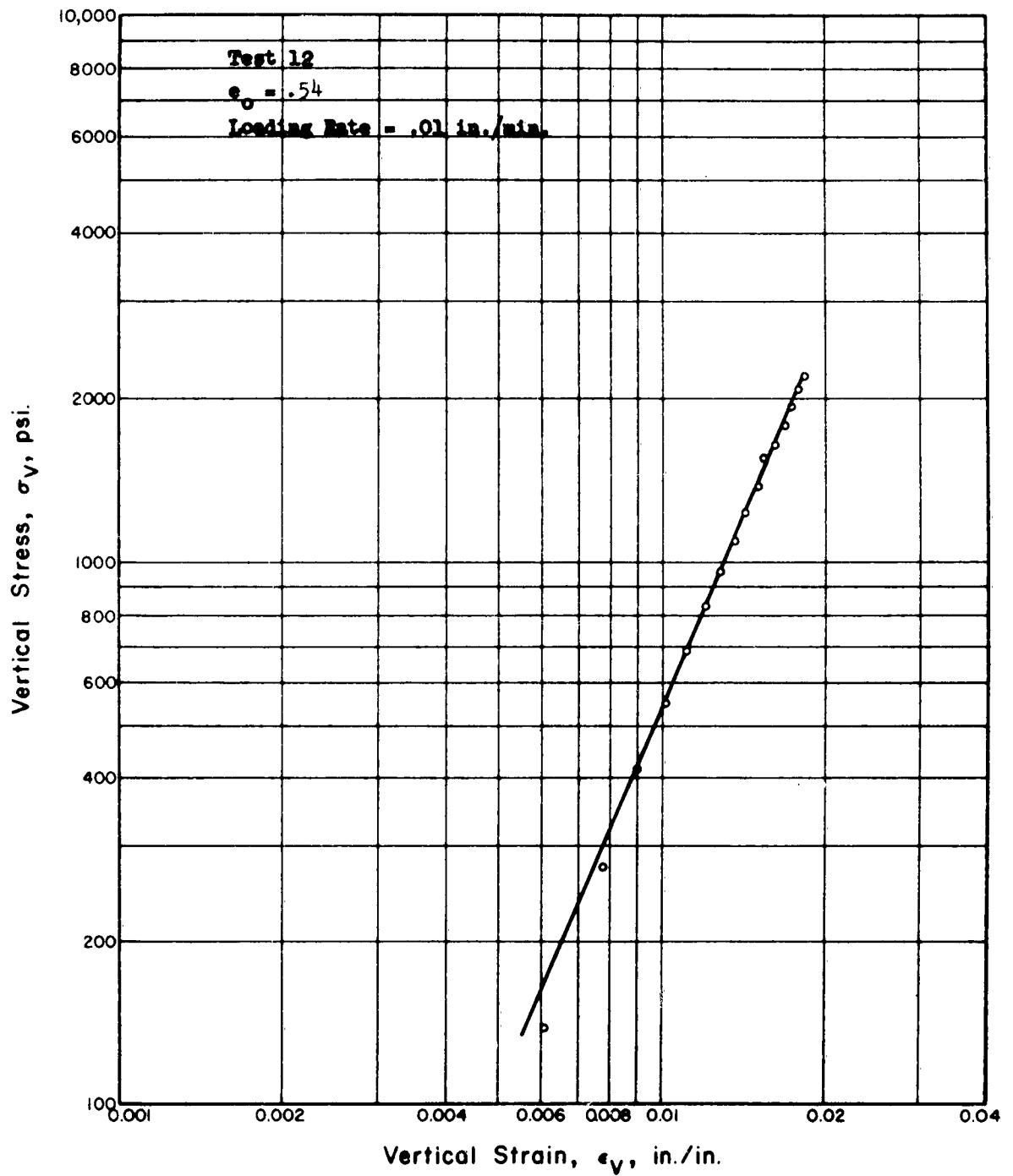


Fig. 5.32 LOGARITHMIC PLOT OF STRESS STRAIN CURVE FOR MINNESOTA SAND IN ONE DIMENSIONAL COMPRESSION

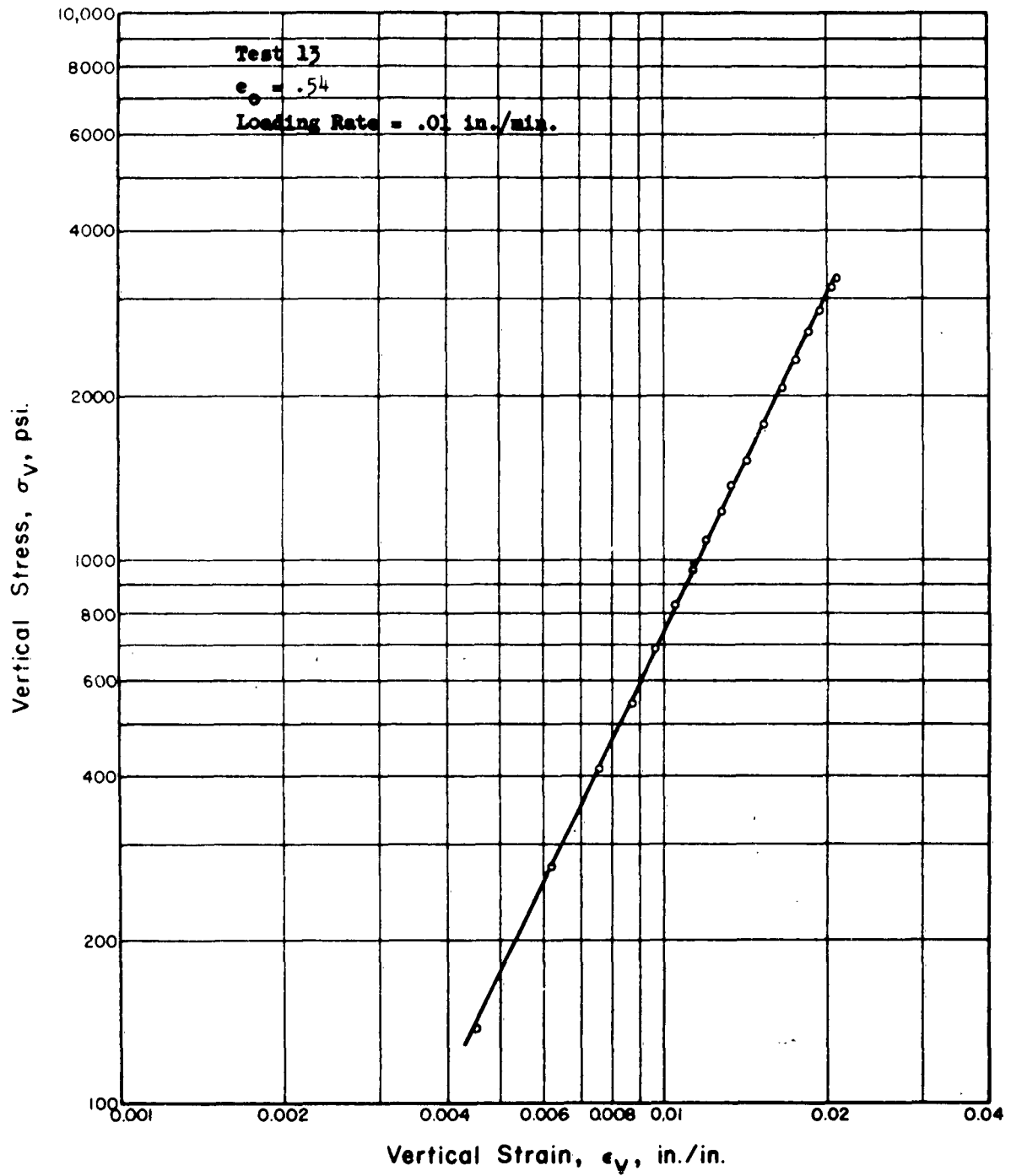


Fig. 5.33 LOGARITHMIC PLOT OF STRESS STRAIN CURVE FOR MINNESOTA SAND IN ONE DIMENSIONAL COMPRESSION

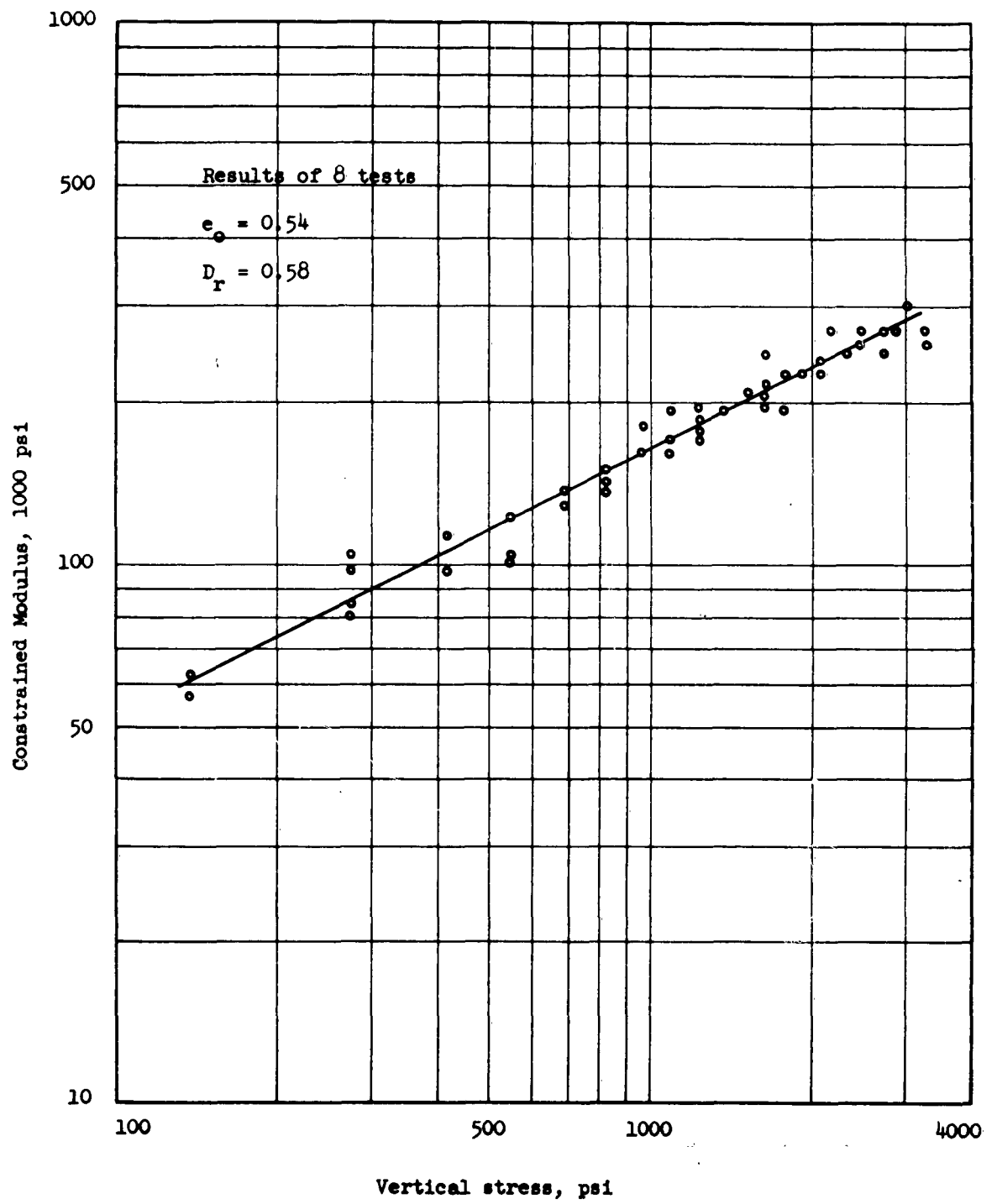


Fig. 5.34 CONSTRAINED MODULUS VS VERTICAL STRESS

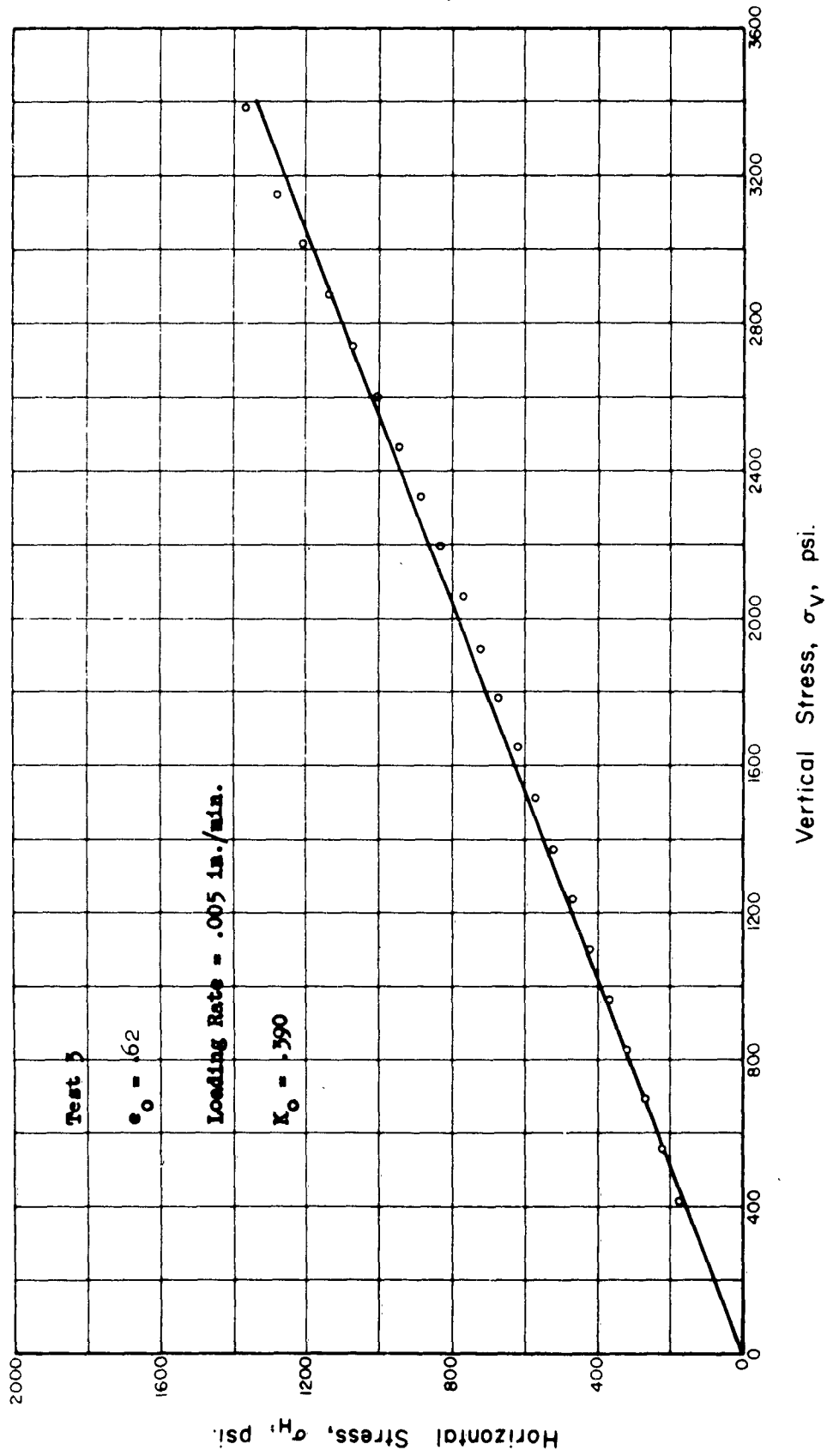


Fig. 5.35 HORIZONTAL STRESS VS. VERTICAL STRESS FOR INITIAL LOADING OF MINNESOTA SAND IN ONE DIMENSIONAL COMPRESSION

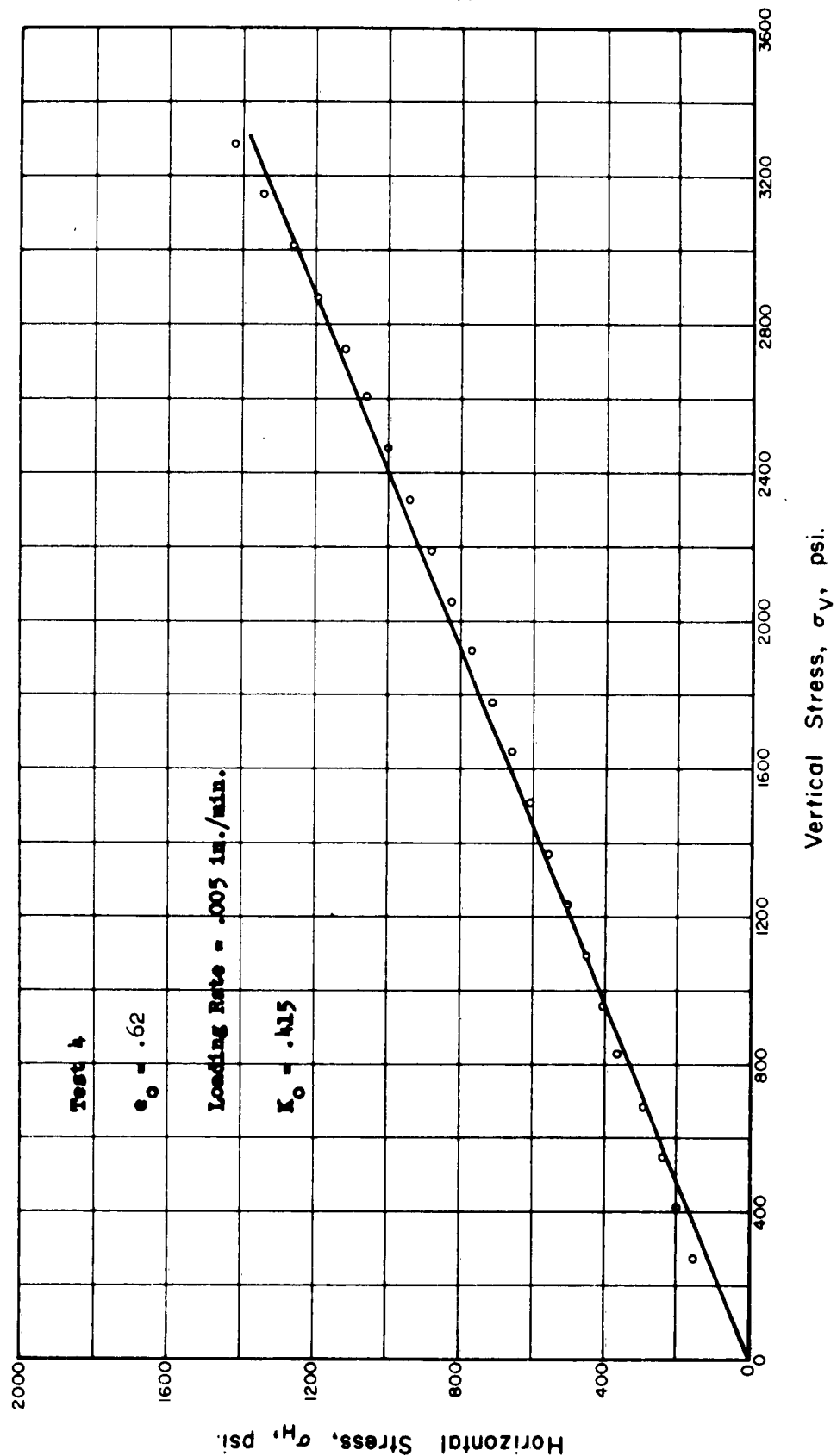


Fig. 5.36 HORIZONTAL STRESS VS. VERTICAL STRESS FOR INITIAL LOADING OF MINNESOTA SAND IN ONE DIMENSIONAL COMPRESSION

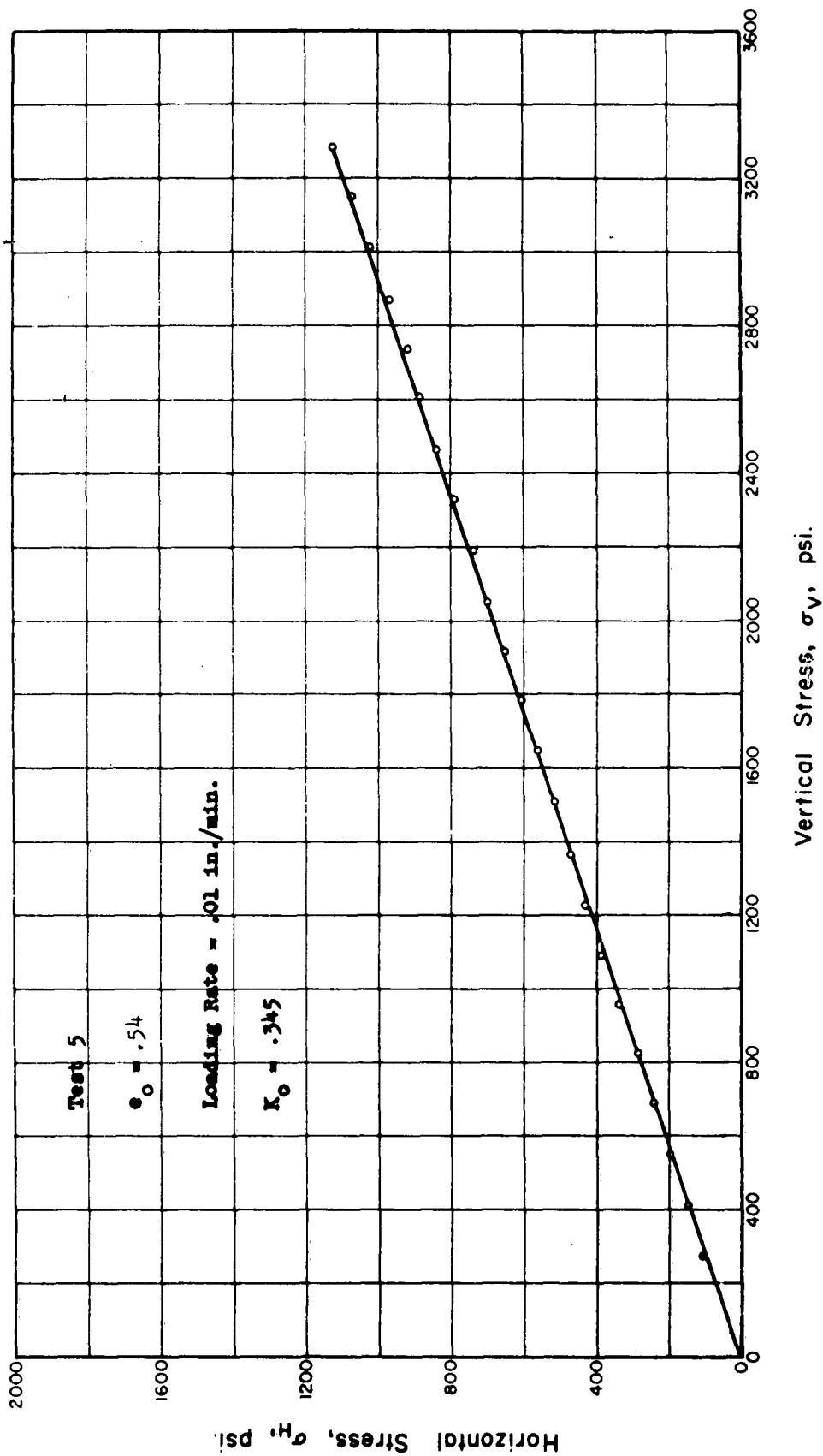


Fig. 5.37 HORIZONTAL STRESS VS. VERTICAL STRESS FOR INITIAL LOADING OF MINNESOTA SAND IN ONE DIMENSIONAL COMPRESSION

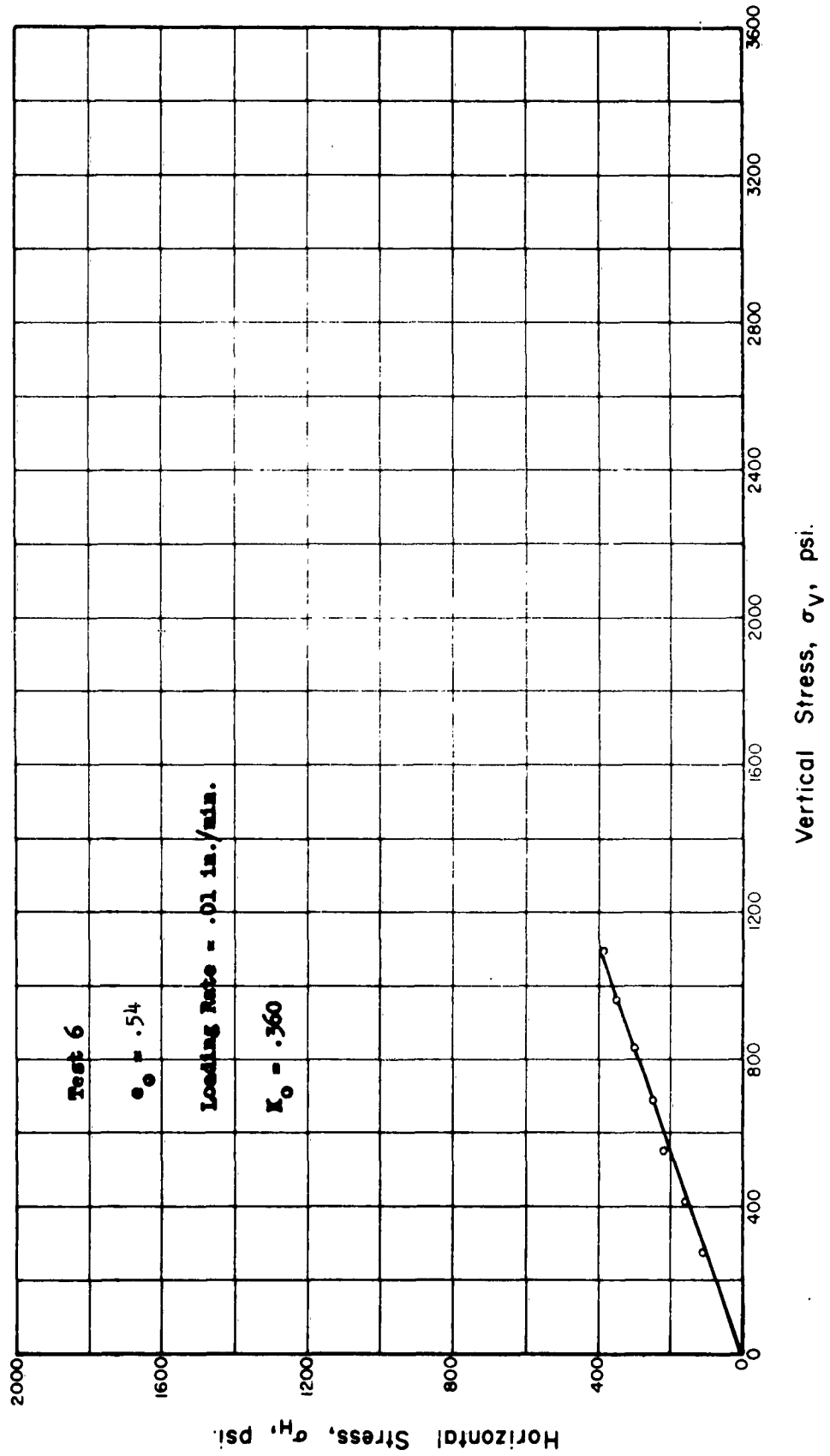


Fig. 5.38 HORIZONTAL STRESS VS. VERTICAL STRESS FOR INITIAL LOADING OF MINNESOTA SAND IN ONE DIMENSIONAL COMPRESSION

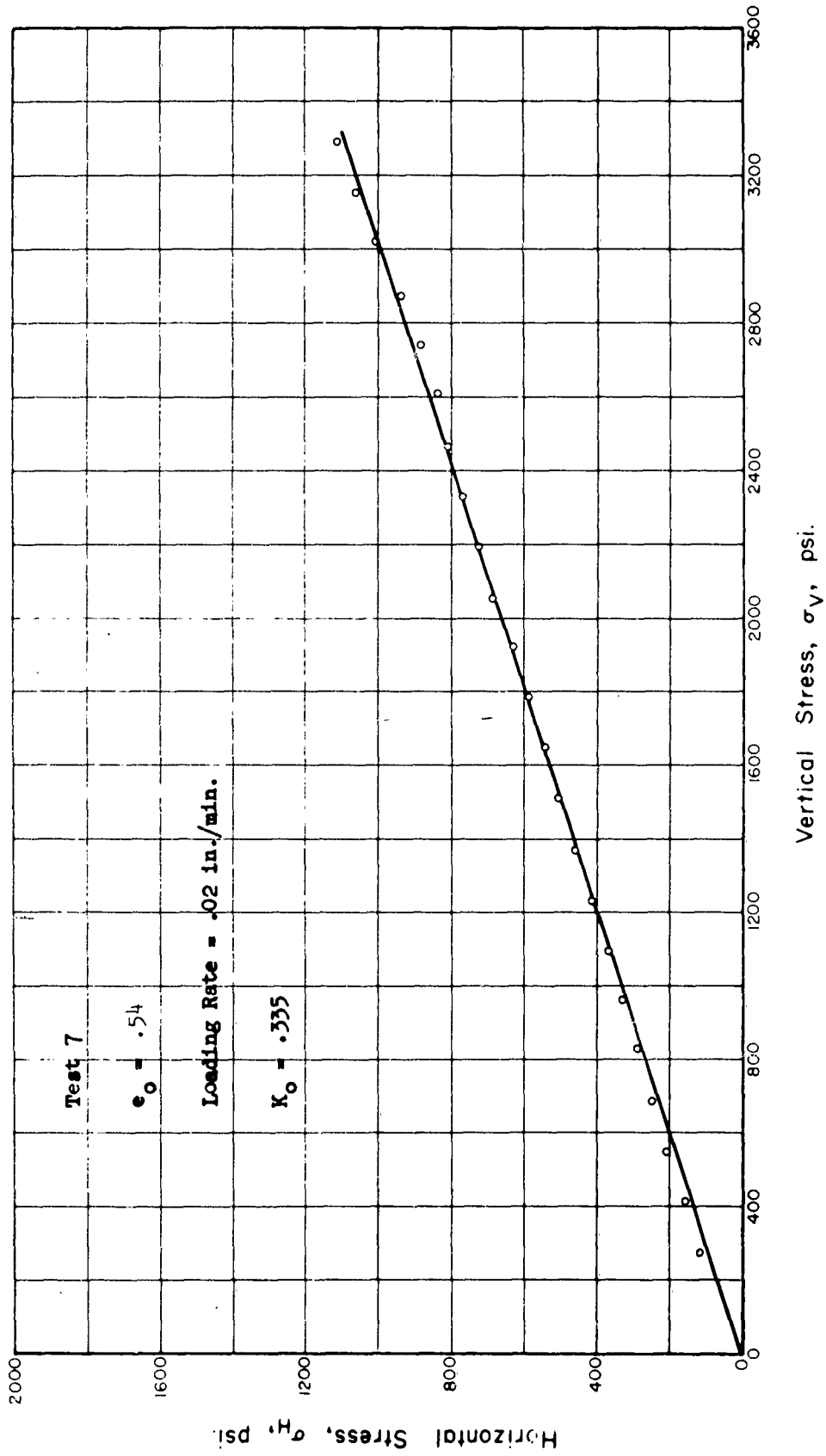


Fig. 5.39 HORIZONTAL STRESS VS. VERTICAL STRESS FOR INITIAL LOADING OF MINNESOTA SAND IN ONE DIMENSIONAL COMPRESSION

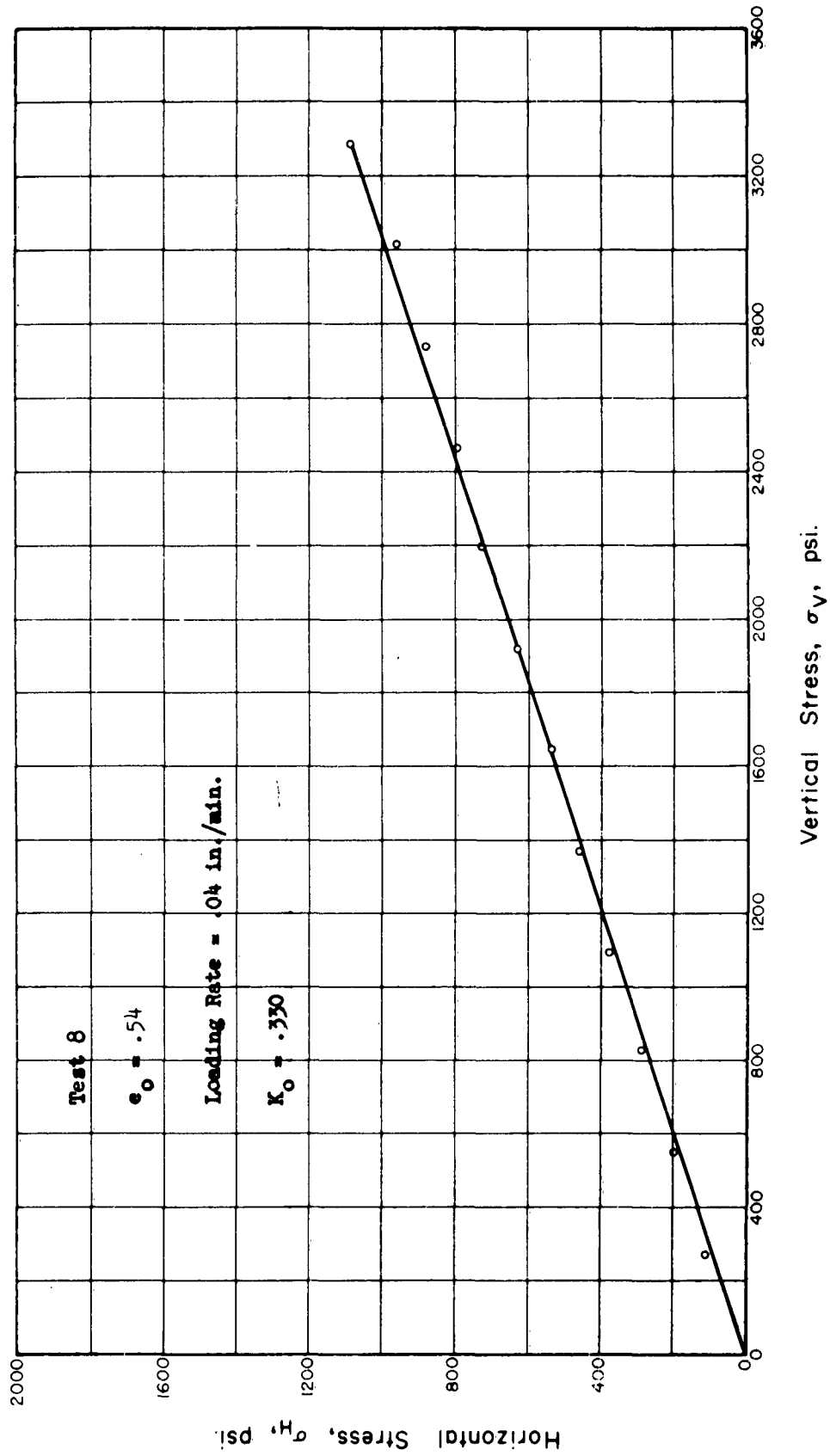


Fig. 5.40 HORIZONTAL STRESS VS. VERTICAL STRESS FOR INITIAL LOADING OF MINNESOTA SAND IN ONE DIMENSIONAL COMPRESSION

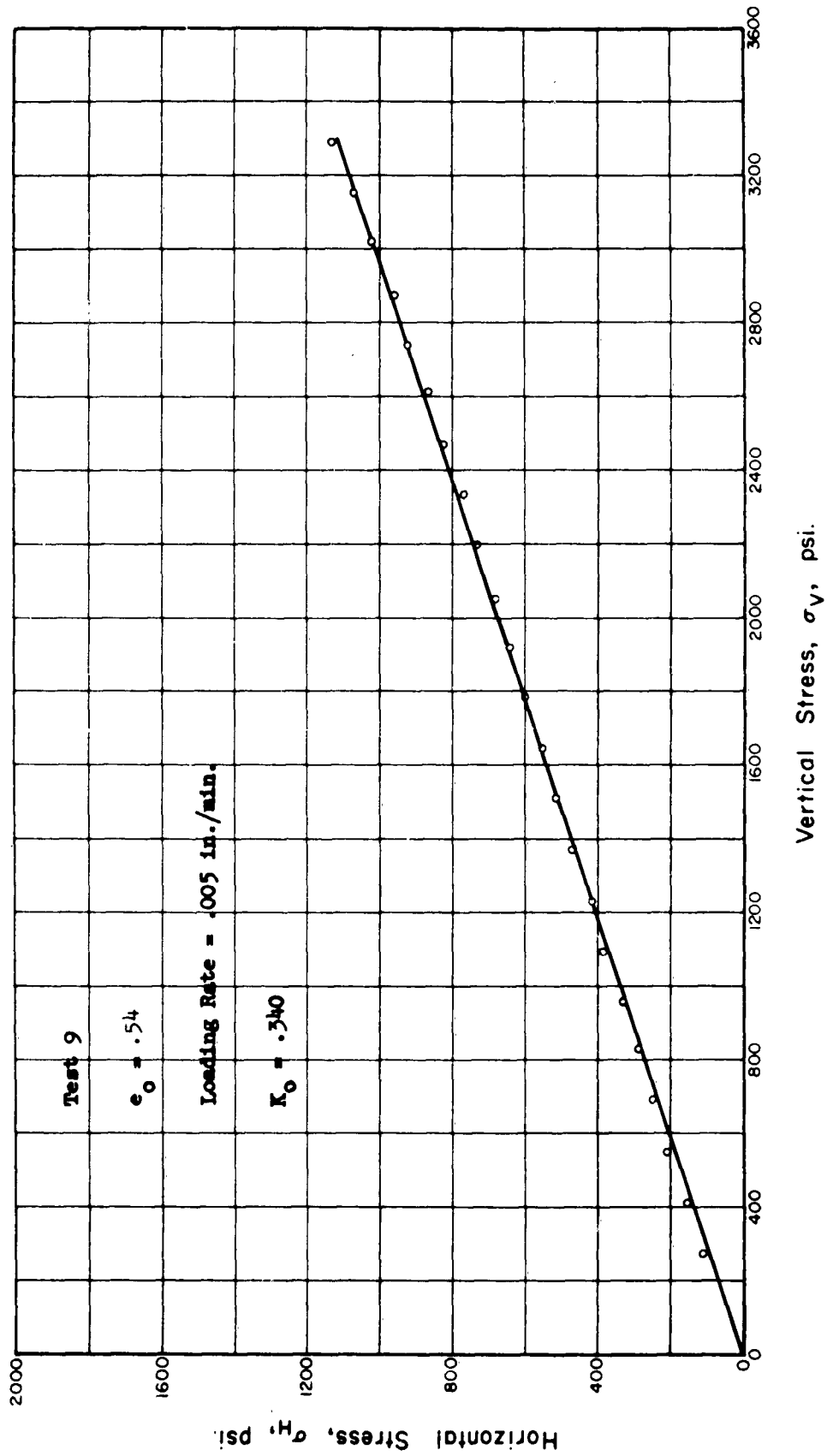


Fig. 5.41 HORIZONTAL STRESS VS. VERTICAL STRESS FOR INITIAL LOADING OF MINNESOTA SAND IN ONE DIMENSIONAL COMPRESSION

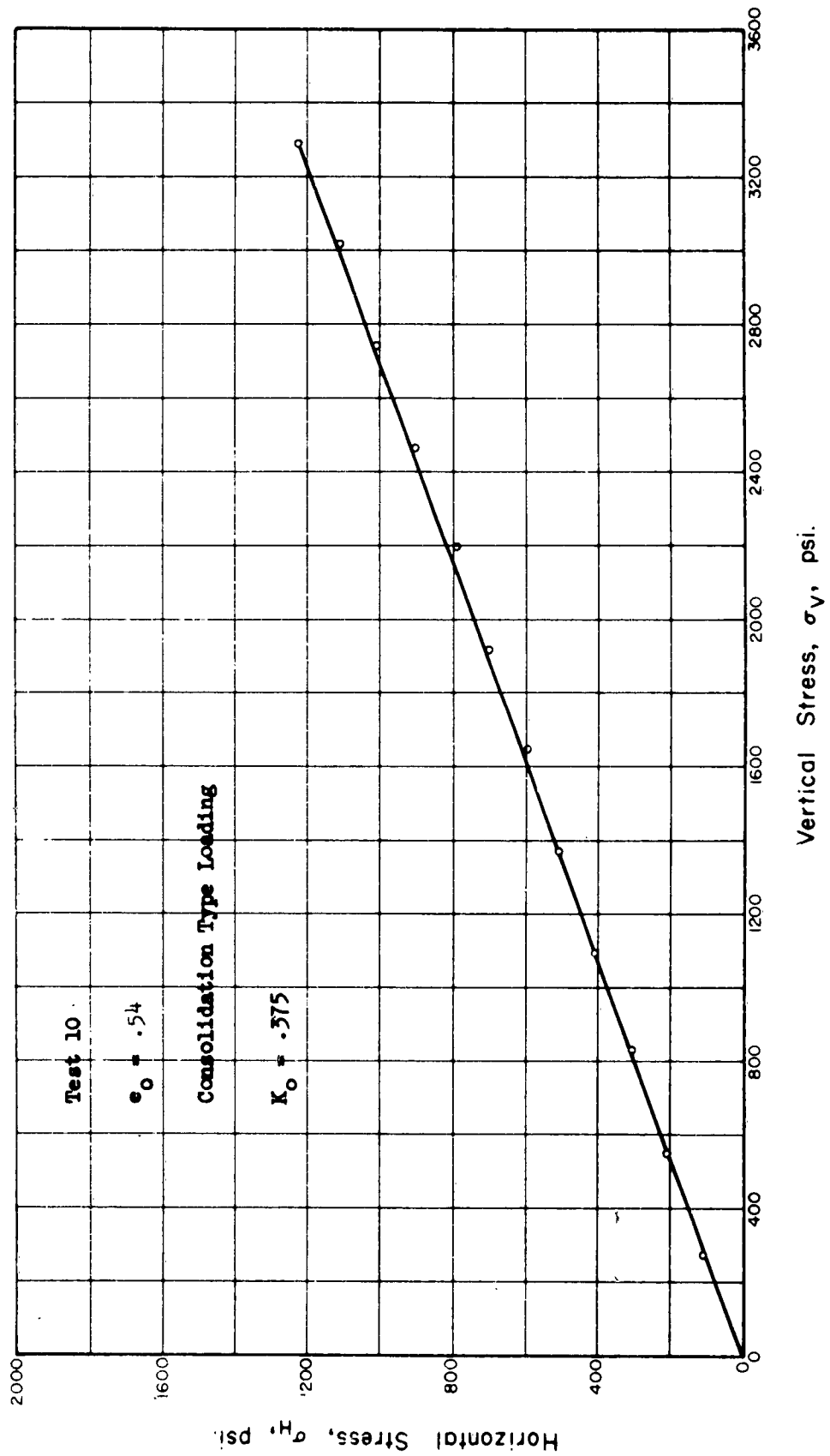


Fig. 5.42 HORIZONTAL STRESS VS. VERTICAL STRESS FOR INITIAL LOADING OF MINNESOTA SAND IN ONE DIMENSIONAL COMPRESSION

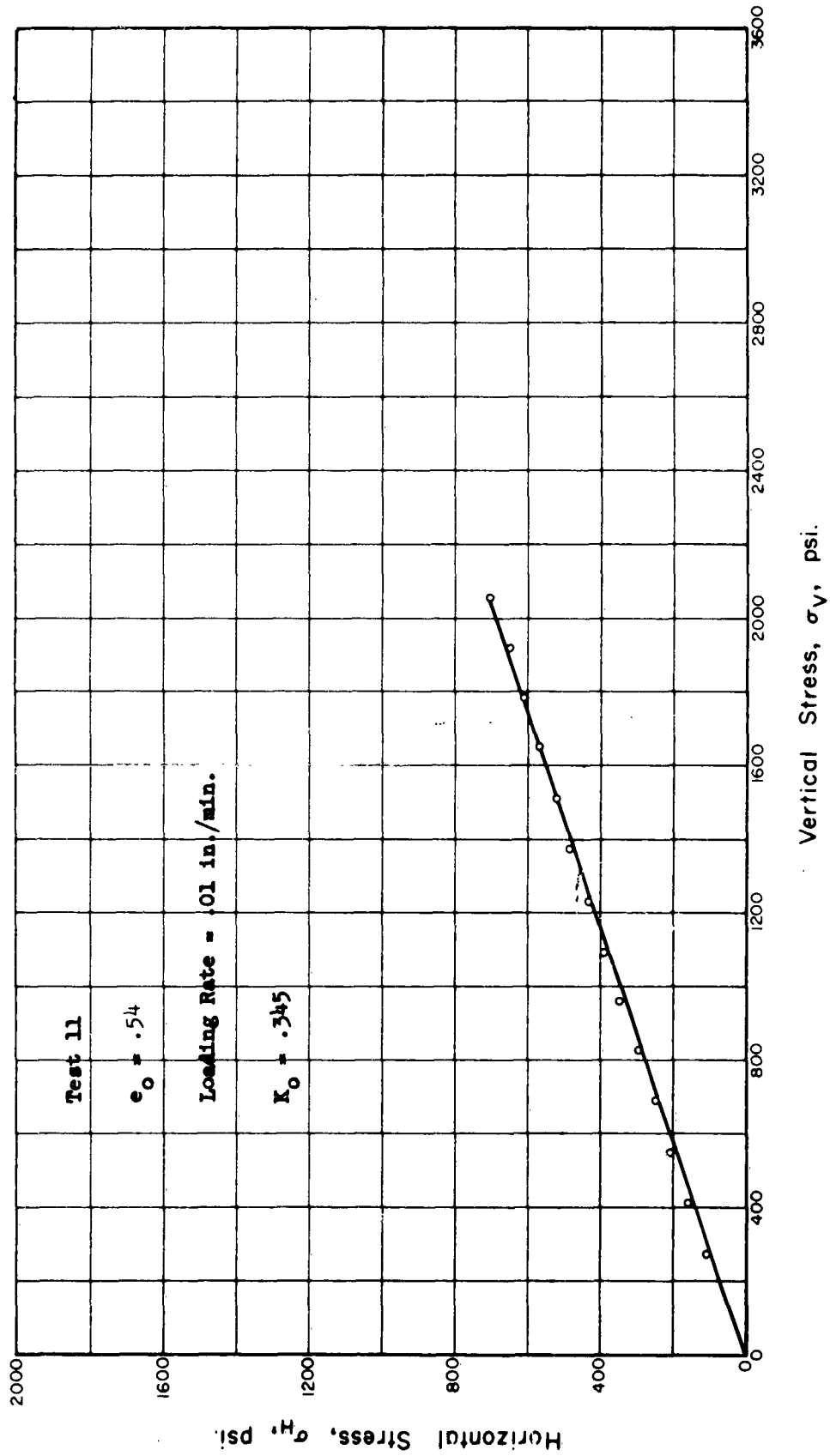


Fig. 5.43 HORIZONTAL STRESS VS. VERTICAL STRESS FOR INITIAL LOADING OF MINNESOTA SAND IN ONE DIMENSIONAL COMPRESSION.

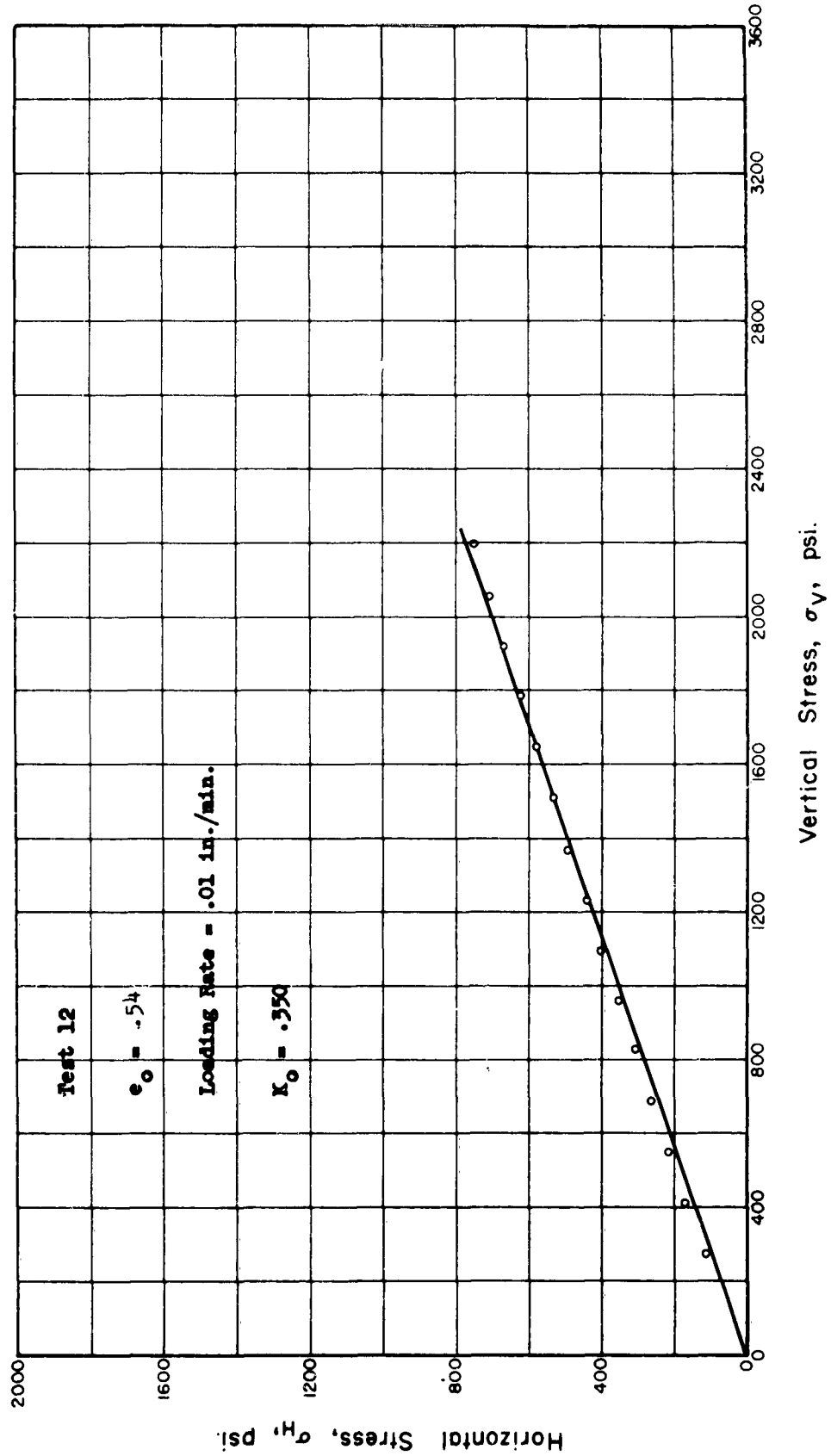


Fig. 5.44 HORIZONTAL STRESS VS. VERTICAL STRESS FOR INITIAL LOADING OF MINNESOTA SAND IN ONE DIMENSIONAL COMPRESSION

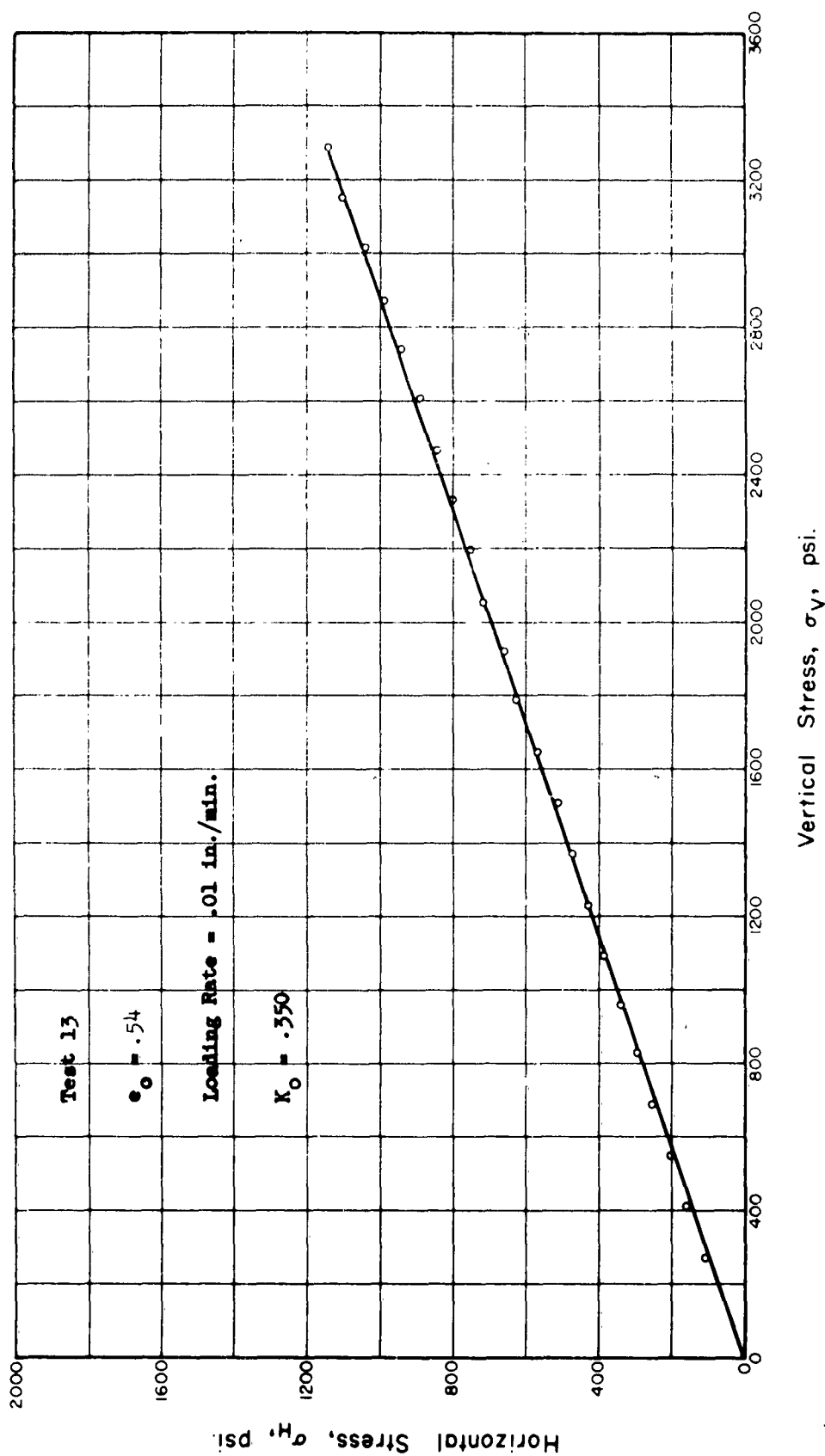


Fig. 5.45 HORIZONTAL STRESS VS. VERTICAL STRESS FOR INITIAL LOADING OF MINNESOTA SAND IN ONE DIMENSIONAL COMPRESSION

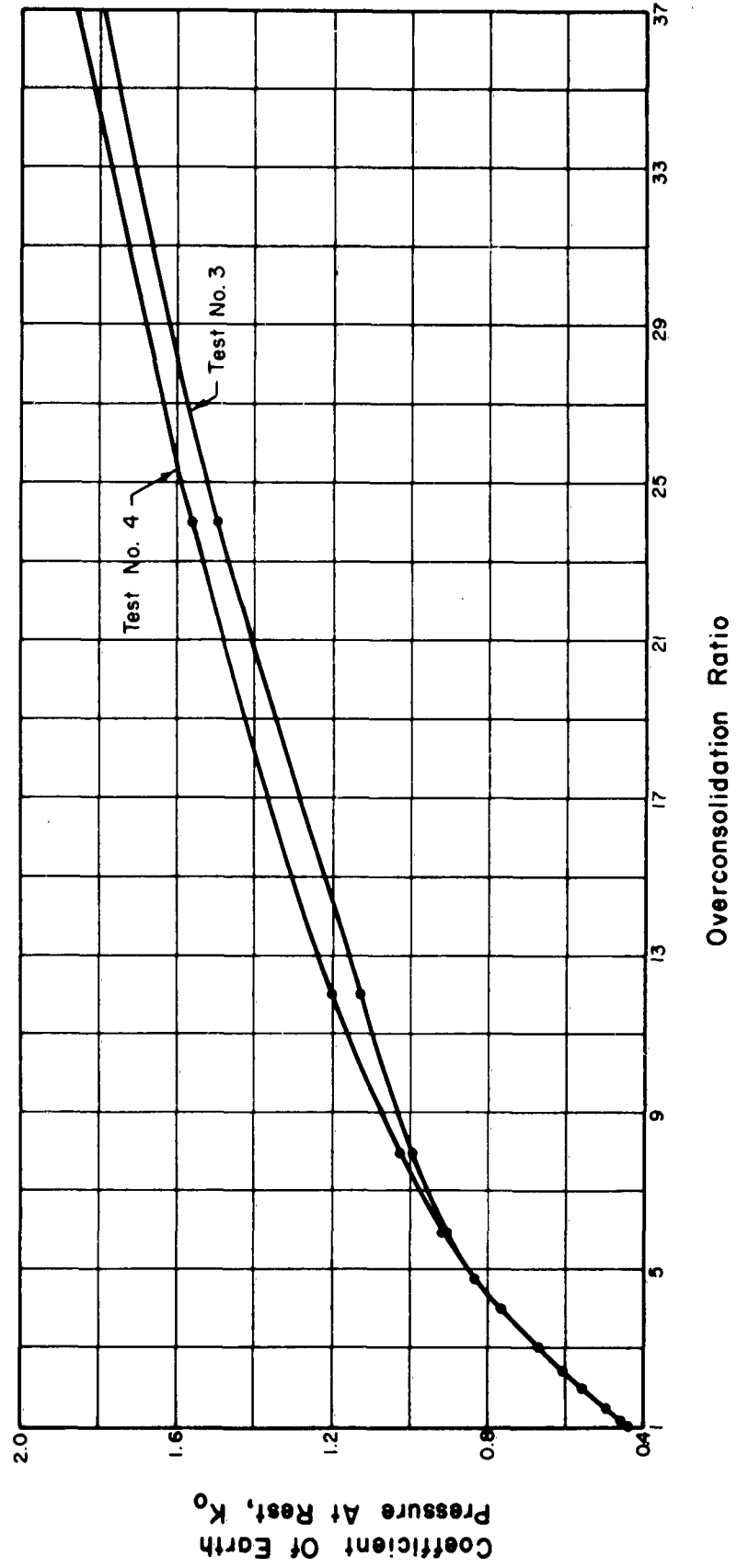


Fig. 5.46 RELATIONSHIP BETWEEN THE COEFFICIENT OF EARTH PRESSURE AT REST, K_0 , AND THE OVERCONSOLIDATION RATIO

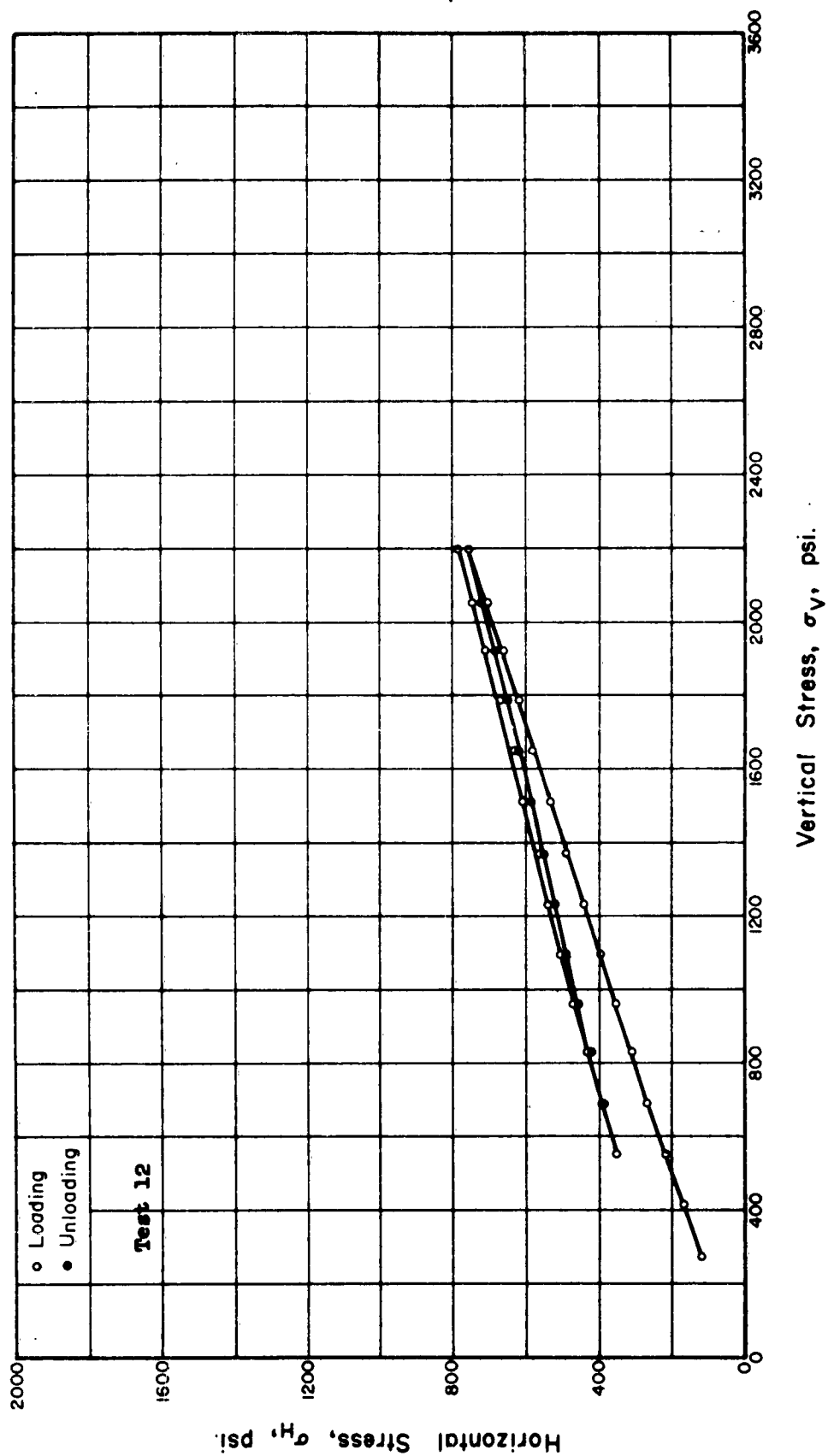


Fig. 5.47 HORIZONTAL STRESS VS. VERTICAL STRESS FOR ONE AND ONE-HALF CYCLES OF LOADING

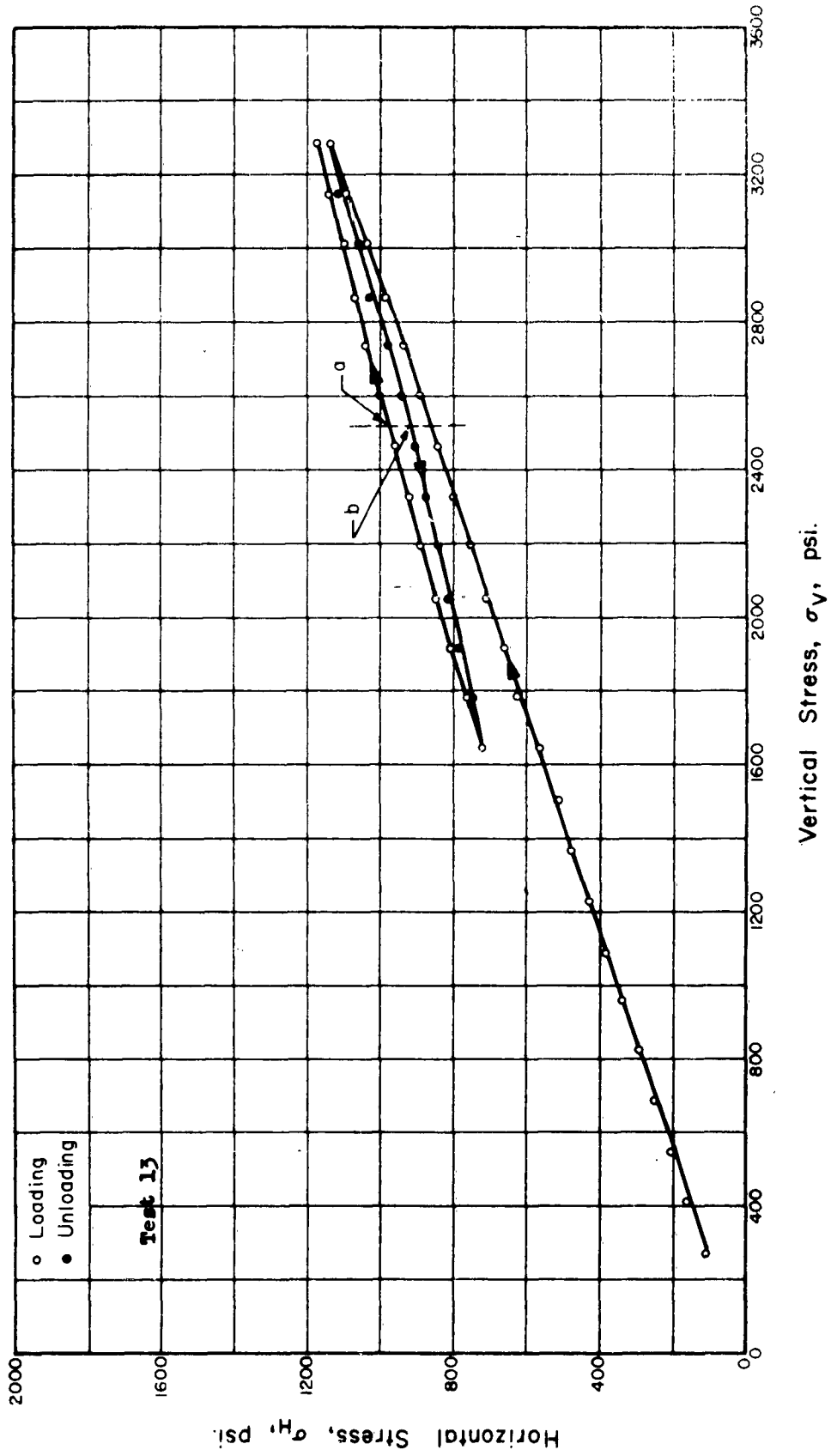


Fig. 5.48 HORIZONTAL STRESS VS. VERTICAL STRESS FOR ONE AND ONE-HALF CYCLES OF LOADING

APPENDIX A

APPLICATION OF THE HERTZ THEORY TO
THE BEHAVIOR OF A GRANULAR MEDIUM

A question of paramount importance arises in the development of a theory of granular media based on the Hertz theory [A.1]. It must first be concluded that the Hertz theory is valid in the pressure regions of interest before the theory has any usefulness. In view of this it may be worthwhile to review the development of the Hertz theory here for the convenience of the reader and note simultaneously the fundamental assumptions as they arise.

The derivation given in the following is a summary of the presentation given by Timoshenko and Goodier [A.2], and the assumptions are discussed by the writers in relation to applying the results to a granular medium composed of well rounded quartz sand.

Let us first look at the pressure between two spherical bodies held in contact by a normal force. In the solution of this problem it is assumed that at the point of contact these bodies have spherical surfaces with the radii R_1 and R_2 (Fig. A.1). If there is no pressure between the bodies we have contact at one point O. The normal distances from the tangent plane at O to points such as M and N, on a meridian section of the spheres at a very small distance r from the axis z_1 and z_2 , can be approximated in the following manner (Fig. A.2):

$$z = u \tan \beta/2 \approx 1/2 u \tan \beta$$

$$z = 1/2 u \cdot u/R = u^2/2R \quad (A.1)$$

$$z = r^2/2R \text{ where } r^2 = u^2$$

Thus in (Fig. A.1)

$$z_1 = \frac{r^2}{2R_1}, \text{ and } z_2 = \frac{r^2}{2R_2} \quad (\text{A.2})$$

The distance between points M and N is

$$z_1 + z_2 = \frac{r^2(R_1 + R_2)}{2R_1R_2} \quad (\text{A.3})$$

In the particular case of contact between two spheres of equal radius, R , we have:

$$z_1 + z_2 = \frac{r^2 2R}{2R^2} = r^2/R \quad (\text{A.4})$$

If the bodies are pressed together along the normal at O by a force P , there will be a local deformation near the point of contact producing contact over a small surface with a circular boundary, called the surface of contact. Assuming that the radii of curvature R_1 and R_2 are very large in comparison with the radius of the boundary of the surface of contact, we can apply, in discussing local deformation, the results obtained for a point load on a semi-infinite boundary. Let w_1 denote the displacement due to the local deformation in the direction z_1 of a point such as M on the surface of the lower ball (Fig. A.1), and w_2 denote the same displacement in the direction z_2 for a point such as N of the upper ball. If it is assumed that the tangent plane at O remains immovable during local compression, then, due to this compression, any two points of the bodies on the axes z_1 and z_2 at large distances* from O will approach each other

*Such distances that deformations due to the compression at these points can be neglected.

by a certain amount α , and the distance between two points such as M and N will diminish by $\alpha - (w_1 + w_2)$. If the two spheres are of equal radius, the distance between such points as M and N will diminish by $\alpha - 2w$. If finally, due to local compression, the points M and N come inside the surface of contact, we have

$$\alpha - (w_1 + w_2) = z_1 + z_2 = \frac{r^2 (R_1 + R_2)}{2R_1 R_2} \quad (\text{A.5})$$

If the spheres have a radius $R = R_1 = R_2$ then we have

$$\alpha - 2w = 2z = r^2/R$$

Thus

$$v = \frac{\alpha - r^2/R}{2} \quad (\text{A.6})$$

at any point r on the surface of contact.

Let us now consider local deformations. From the condition of symmetry it can be concluded that the intensity of pressure q between the bodies in contact and the corresponding deformation are symmetrical with respect to the center O of the surface of contact. Taking Fig. A.4 to represent the surface of contact, and M as a point on the surface of contact of the lower ball, the displacement of this point may be found in the following manner. For a point load on the surface of an infinite medium such as shown in Fig. A.3, the vertical deflection at a distance r from the load P is given as

$$v = \frac{P(1 - \nu^2)}{4Er} \quad (\text{A.7})$$

where E is Young's modulus and ν is Poisson's ratio for the medium.

Now let us consider Fig. A.4 where we have a distributed load q over the circular area of radius a . We are concerned with the displacement of point M in relation to the distributed load q . Thus the vertical deflection w at any point M within the loaded boundary is

$$w = \frac{1 - \nu^2}{\pi E} \iint_S \frac{q d\bar{a}}{s} \quad (\text{A.8})$$

where

$$d\bar{a} = ds \cdot d\psi \cdot s \quad (\text{A.9})$$

Thus

$$w = \frac{(1 - \nu^2)}{\pi E} \iint q d\psi ds \quad (\text{A.10})$$

Hence if two spherical balls of equal radii R are pressed together, at some point r the local displacement w becomes

$$2w = \alpha - r^2/R = \frac{2(1 - \nu^2)}{\pi E} \iint q d\psi ds \quad (\text{A.11})$$

The distribution of q must therefore be such that Eq. (A.11) is satisfied. It will now be shown that this requirement is satisfied by using a pressure distribution of q over the contact surface represented by the ordinates of a hemisphere of radius a constructed on the surface of contact.

If q_0 is the pressure at the center O of the surface of contact, then

$$q_0 = \frac{k}{a} \quad (\text{A.12})$$

where k is a constant factor indicating the scale of our representation of the pressure distribution. Along a chord mn the pressure q varies, as indicated in Fig. A.4 by the dotted semicircle.

Performing the integration along the chord we find

$$\int q ds = \frac{q_0}{a} A \quad (A.13)$$

where A is the area of the semicircle indicated by the dotted line and is equal to

$$A = \frac{\pi}{2} (a^2 - r^2 \sin^2 \psi) \quad (A.14)$$

Substituting Eq. (A.14) into Eq. (A.11) we find

$$2v = \alpha - \frac{r^2}{R} = \frac{(1 - \nu^2)}{E} \int_0^{\pi} \frac{q_0}{a} (a^2 - r^2 \sin^2 \psi) d\psi$$

or

$$\alpha - \frac{r^2}{R} = \frac{q_0}{a} \frac{(1 - \nu^2)}{E} \int_0^{\pi} (a^2 - r^2 \sin^2 \psi) d\psi \quad (A.15)$$

Integrating Eq. (A.15) yields

$$\alpha - \frac{r^2}{R} = \frac{q_0}{a} \frac{(1 - \nu^2)}{E} \frac{\pi}{2} (2a^2 - r^2) \quad (A.16)$$

This equation will be satisfied for any value of r , and hence the assumed pressure distribution is the correct one if the following relations exist for the displacement α and the radius a of the surface of contact between two equal radii spheres:

$$\alpha = \frac{q_0 a \pi (1 - \nu^2)}{E} = \frac{q_0 a \pi (1 - \nu)}{2\mu} \quad (A.17)$$

and

$$a = \frac{q_0 R \pi (1 - \nu^2)}{2E} = \frac{q_0 R \pi (1 - \nu)}{4\mu} \quad (A.18)$$

where μ is the shear modulus of the spheres.

If the volume of the pressure diagram between two spheres is defined as the normal force N between the spheres, then

$$N = \frac{q_0}{a} \cdot \frac{2}{3} \pi a^3$$

from which we obtain

$$q_0 = \frac{3}{2} \frac{N}{\pi a^2} \quad (\text{A.19})$$

Combining Eq. (A.19) with Eq. (A.17) and (A.18) yields

$$\alpha = \frac{3}{4} \frac{N(1 - \nu)}{a\mu} \quad (\text{A.20})$$

$$a^3 = \frac{3}{8} \frac{RN(1 - \nu)}{\mu} \quad (\text{A.21})$$

The radius of contact a may be eliminated from Eq. (A.20) and (A.21) to give

$$\alpha = 2 \left[\frac{3(1 - \nu)N}{8\mu R} \right]^{-1/3} \quad (\text{A.22})$$

Equation (A.22) shows that the relative approach of the center of two spheres is a function of the two thirds power of the contact force.

The normal compliance C is

$$C = \frac{d\alpha}{dN} = \frac{4}{3} \left[\frac{3(1 - \nu)N}{8\mu R} \right]^{-1/3} \frac{3(1 - \nu)}{8\mu R}$$

which may be simplified to

$$C = \frac{(1 - \nu)}{2\mu a} \quad (\text{A.23})$$

where a is given by

$$a = \left[\frac{3(1-\nu)NR}{8\mu} \right]^{1/3} \quad (\text{A.24})$$

There are two key assumptions in the Hertz theory which should be discussed to justify its use in a theory of granular media.

The first of these is that described by Eqs. (A.1) where it was assumed that the deviation from a tangent plane is quadratic, i.e.

$$z = \frac{r^2}{2R} \quad (\text{A.25})$$

The exact expression for this is

$$z = \frac{r^2}{2R} \frac{1}{1 - \frac{z}{2R}}$$

or

$$z = \frac{r^2}{2R} \left[1 + \frac{1}{2} \frac{z}{R} + \frac{1}{4} \left(\frac{z}{R} \right)^2 + \frac{1}{8} \left(\frac{z}{R} \right)^3 + \dots \right] \quad (\text{A.26})$$

Hence if $\frac{z}{R}$ is small with respect to 1, the assumption that the higher order terms can be neglected is quite in order.

The second assumption is of a lower order than the first and requires that the radius of contact be small compared to the sphere radius R . This assumption is associated with the use of the expression for the deflection resulting from a point load on an infinite medium, i.e. Equation (A.7). Essentially what is being assumed is that the curvature of the spheres beyond the contact area does not affect the stress distributions and deflections at the contacts. Schematically this assumption implies that the surfaces in contact are two infinite media with small bumps in them rather than two sphere (Fig. A.5). Clearly if the radius of contact is small, the curvature has little effect on the behavior.

This is particularly true when the two contact surfaces are spherical and the stresses away from the contact area damp out very fast. The two problems illustrated by (Fig. A.5) could conceivably be solved and a quantitative comparison be made; however, the effort would be a major one and the value to the study at hand is questionable as is seen in the following discussion.

The problem of concern has to do with the use of the Hertz theory to describe the behavior of a granular medium, namely sand, subjected to an average applied stress, σ_z , over the surface. Therefore, it is of interest to determine what limits are to be placed on this stress due to other reasons such as crushing. In fact it is known that crushing begins in sand compressed one dimensionally at average stresses on the order of 1000 psi. By the time the stress reaches 5,000 psi the crushing effect is a major part of the deformation behavior.

In Section 3.1.1 it was determined that the normal contact force N_2 was related to the radius of contact by Eq. (3.1)

$$a = \left[\frac{3(1-\nu)RN_2}{8\mu} \right]^{\frac{1}{3}} \quad (\text{A.27})$$

The normal force, N_2 , was related to the applied force, P_z , by Eq. (3.48a)

$$N_2 (1 + f) = \frac{\sqrt{2}}{8} P_z \quad (\text{A.28})$$

Furthermore it was shown

that the average stress σ_z is related to P_z by

$$\sigma_z = \frac{P_z}{8R^2} \quad (\text{A.29})$$

Equations (A.27), (A.28) and (A.29) may be combined to give

$$\left(\frac{a}{R}\right)^3 = \frac{2^{1/3}(1-\nu)}{8(1+f)} \frac{\sigma_z}{\mu} \quad (\text{A.30})$$

The relationship between a/R and the stress is independent of R .

Representative values of f , ν and μ for quartz which are applicable to sand are

$$f = 0.15$$

$$\nu = 0.20$$

$$\mu = 6 \times 10^6 \text{ psi}$$

Using these values and Eq. (A.30) we obtain the following relations between a/R and σ_z :

$$\left(\frac{a}{R}\right)^3 = 0.369 \frac{\sigma_z}{\mu} \quad (\text{A.31})$$

$\frac{a}{R}$	σ_z psi
0.031	500
0.039	1,000
0.057	3,000
0.085	10,000
0.10	16,300

Thus we can see that for the stresses of interest (prior to crushing) where the theory is to be applied, the radius of contact compared to the radius of the sphere will be much less than 0.10. Not only is this fairly small but it should be remembered that there are

other assumptions involved in the application of this theory to sand which may be far worse. In fact, the assumption that sand particles, even uniformly smooth ones, are spheres is perhaps more questionable than this one. Microscopic photographs of sand particles show many types of asperities which naturally cannot be easily considered in this theory. If the effort warrants it, it may be possible in the future to extend the theory to include roughness effects by using the recent work of Goodman [A.3]. Such an extension is not warranted at the present in view of the nonuniformity of sand.

Another effect ignored is that of the tangential forces at the contacts on the geometry just outside the contact area. With large contact forces there may exist little outward bumps outside the contact surfaces which would have some effect on sliding.

From the above-mentioned, it can be concluded that within the confines of the expected use of this theory, the assumption that the Hertz theory is applicable to the behavior of granular materials is certainly warranted.

References

- A.1. Hertz, H., J. Moth, (Crelle's J.) Vol. 92, 1881. Also see "Gesammelte Werke," by H. Hertz, Vol. 1, p. 155, Leipzig, 1895.
- A.2. Timoshenko, S., and Goodier, J. N., Theory of Elasticity, 2nd Ed., McGraw-Hill, New York, 1951.
- A.3. Goodman, L. E., "Contact Stress Analysis of Normally Loaded Rough Spheres," Jour. Appl. Mech. Paper No. 62-WA-19, (to be published).

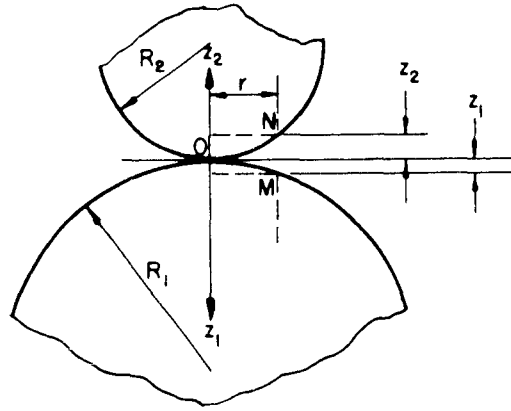


Fig. A.1 TWO UNSTRESSED SPHERES IN CONTACT

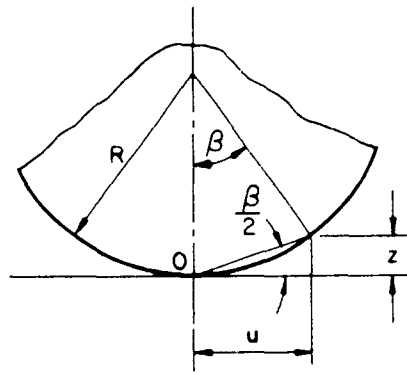
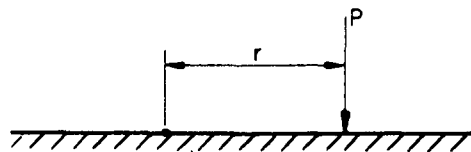
Fig. A.2 SEGMENT OF A SPHERE WITH A TANGENT AT O 

Fig. A.3 POINT LOAD ON AN INFINITE SURFACE

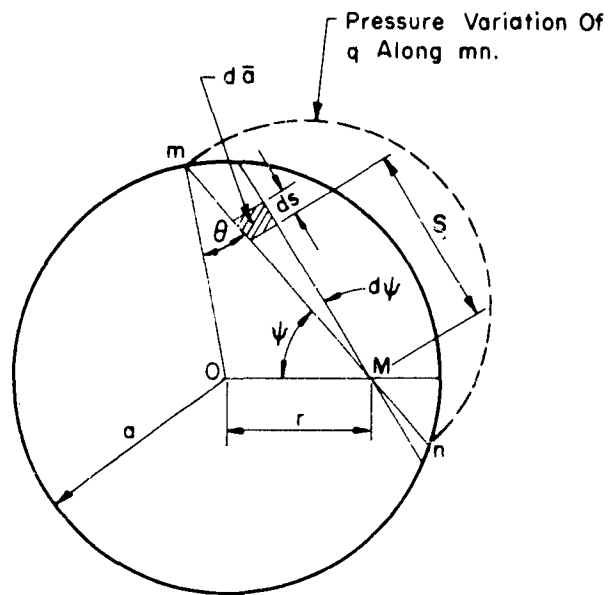


Fig. A.4 PLAN VIEW OF THE CONTACT SURFACE OF TWO SPHERES IN HERTZ CONTACT

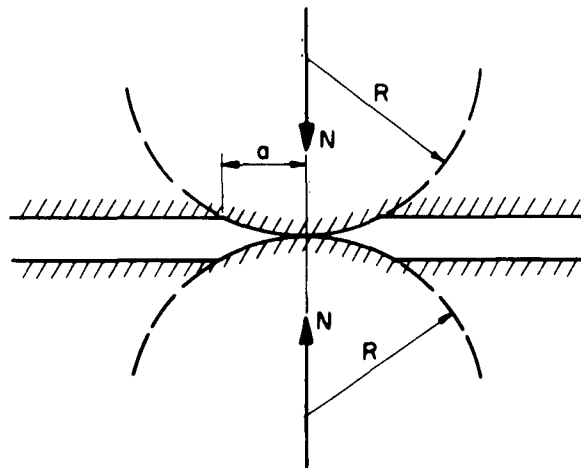


Fig. A.5 CORRELATION BETWEEN SPHERES AND INFINITE SURFACES IN HERTZ CONTACT

APPENDIX B

NUMERICAL SOLUTION TO THE EQUATIONS GOVERNING
THE BEHAVIOR OF A GRANULAR MEDIUM HAVING
RESTRICTED LATERAL STRAINS

The general equations governing the behavior of a face centered array of spheres subjected to a vertical force P_z and symmetrical lateral forces P_H have been developed in Section 3.1.1. The resulting equations including the lateral strain condition were given previously as Eqs. (3.37) and take the following form:

$$\begin{aligned}
 dN_2 + dT_2 &= \frac{\sqrt{2}}{8} dP_z \\
 dN_1 + dN_2 - dT_2 - \frac{\sqrt{2}}{4} dP_H &= 0 \\
 \frac{C_1}{C_2} dN_1 - dN_2 + \frac{S_2}{C_2} dT_2 &= 0 \\
 dN_1 &= \frac{2R}{C_1} d\epsilon_H
 \end{aligned} \tag{B.1}$$

Here the N 's and T_2 are the normal and tangential contact forces and the C 's and S_2 are the corresponding compliances. (Figs. B.1 and B.2). The radii of the spheres is R and the lateral strain is ϵ_H . Let us introduce the dimensionless variables

$$\begin{aligned}
 n_1 &= \frac{3(1-\nu)}{8} \frac{N_1}{R^2\mu}, & n_2 &= \frac{3(1-\nu)}{8} \frac{N_2}{R^2\mu}, & t_2 &= \frac{3(1-\nu)}{8} \frac{T_2}{R^2\mu} \\
 p_H &= \frac{3(1-\nu)}{8} \frac{P_H}{R^2\mu}, & p_z &= \frac{3(1-\nu)}{8} \frac{P_z}{R^2\mu}
 \end{aligned} \tag{B.2}$$

where μ and ν are the shear modulus and Poisson's ratio for the spheres.

Substituting Equations (B.2) into Equation (B.1) yields

$$dn_2 + dt_2 = \frac{\sqrt{2}}{8} dp_z \quad (B.3a)$$

$$dn_1 + dn_2 - dt_2 - \frac{\sqrt{2}}{4} dp_H = 0 \quad (B.3b)$$

$$\frac{n_2}{n_1} dn_1 - dn_2 + \frac{2-v}{2(1-v)} K dt_2 = 0 \quad (B.3c)$$

$$dn_1 = \frac{3}{2} n_1^{1/3} d\epsilon_H \quad (B.3d)$$

where K depends on t_2 and $\frac{dn_2}{dt_2}$ as follows:

a. For t_2 increasing

$$\frac{dn_2}{dt_2} > \frac{1}{f}, \quad K = 1 \quad (B.4)$$

$$0 \leq \frac{dn_2}{dt_2} \leq \frac{1}{f}, \quad K = f \frac{dn_2}{dt_2} + (1-f \frac{dn_2}{dt_2}) (1 - \frac{t_2}{fn_2})^{-1/3}$$

b. For t_2 decreasing

$$\frac{dn_2}{dt_2} \leq -\frac{1}{f}, \quad K = 1 \quad (B.5)$$

$$\frac{dn_2}{dt_2} \geq -\frac{1}{f}, \quad K = -f \frac{dn_2}{dt_2} + (1-f \frac{dn_2}{dt_2}) (1 - \frac{t^* - t_2}{2fn_2})^{-1/3}$$

where t^* is the highest value obtained by t_2 and is the value from which it is decreasing.

The strain in the vertical or z direction is given by

$$d\epsilon_z = \frac{2}{3n_2^{1/3}} \left[dn_2 + \frac{2-v}{2(1-v)} K dt_2 \right] \quad (B.6)$$

and the stresses in the vertical and horizontal directions are given, respectively, by

$$\begin{aligned} \sigma_z &= \frac{\mu p_z}{3(1-v)} \\ \sigma_H &= \frac{\mu p_H}{3(1-v)} \end{aligned} \quad (B.7)$$

The problem is now to determine a solution to the Equations(B.3).

These equations are differential equations in terms of the infinitesimal increments of the forces. One method of solution is to integrate these equations exactly where such an integration can be done. Such an integration is carried out in Section 3.2 for the case where the lateral strain ϵ_H is zero. Unfortunately it does not appear that an exact solution can be obtained for other cases, particularly for the unloading cycle. Hence, in order to study the behavior of the medium some other method of solution must be carried out.

Equations (B.5) are ideally suited for numerical solution on a digital computer. If we consider the equation not as differential increments d but as finite increments Δ the equations become

$$\begin{aligned} \Delta n_2 + \Delta t_2 &= \frac{\sqrt{2}}{8} \Delta p_z \\ \Delta n_1 + \Delta n_2 - \Delta t_2 - \frac{\sqrt{2}}{4} \Delta p_z &= 0 \\ \frac{n_2}{n_1} \Delta n_1 - \Delta n_2 + \frac{2-v}{2(1-v)} K \Delta t_2 &= 0 \\ \Delta n_1 &= \frac{3}{2} n_1^{1/3} \Delta \epsilon_H \end{aligned} \quad (B.8)$$

where K is given by Equations (B.4) or (B.5) with differences replacing the differentials.

If the initial conditions are known, Equations (B.8) can be used to trace the behavior of the spheres through a cycle of loading. The vertical load, p_z , the lateral strain ϵ_H or the lateral load p_H may be incremented and a solution to Equations (B.8) gives the increments which occur to the other forces as a result of these changes. Likewise from these results the increment to the vertical strain ϵ_z may be determined from Equation (B.6).

It should be noted that Equations (B.8) are non-linear difference equations because K is a function of n_2 and t_2 . Hence, the equations must be solved by iteration for each load increment cycle.

It was also noted in Section 3.2 that these equations have a singularity at zero. Therefore it is not possible to obtain any rational behavior by starting with the normal forces at the contacts equal to zero. To offset this problem we introduce an initial hydrostatic stress p_0 which in turn creates an initial normal force at the contacts of n_0 . As was shown in Section 3.1.2 this gives stress-strain and contact force relationships as follows:

$$\epsilon_0 = n_0^{\frac{2}{3}} \quad (B.9)$$

$$n_0 = \frac{1}{4} \sqrt{2} p_0 \quad (B.10)$$

$$\sigma_0 = \frac{\mu}{3(1-\nu)} p_0 \quad (B.11)$$

where

$$p_0 = \frac{3(1-\nu) p_0}{8R^2\mu} \quad (B.12)$$

$$n_0 = \frac{3(1-\nu) N_0}{8R^2\mu}$$

The addition of this initial stress condition does not alter the governing Equations (B.8) provided that the total normal contact forces

used in the compliance terms and strain equations include the hydrostatic effect. Hence all variables except the tangential forces include the hydrostatic contribution. The behavior in addition to the initial hydrostatic effect or the total effect can then be obtained.

In the computation procedure we remember that the theory is restricted to that behavior where sliding does not occur at the contacts. This is reflected in the condition that K must be greater than zero. When K becomes negative (or zero) sliding occurs and the solution is no longer valid.

Furthermore, to speed convergence of the iteration process and to take care of any divergence during the computation for one increment, a convergence subroutine was included in the program.

A step by step solution is as follows:

- (a) Increment loads and/or strains
- (b) Calculate all constants
- (c) Calculate dn_1 from Equation (B.3d)
- (d) Assume values for K and n_1/n_2 on the basis of the previous cycle
- (e) Compute dt_2 from a combination of Equation (B.3a) and (B.3c)
- (f) Determine dn_2 from Equation (B.3a)
- (g) Check $\frac{dn_2}{dt_2}$ for greater than or less than $1/f$
- (h) Compute K from Equations (B.4) or (B.5) depending on the results of (g). If K is negative then stop since the equations are invalid.
- (i) Compute $\frac{n_1}{n_2}$
- (j) If K_1 , n_1/n_2 agree with that assumed in (d), add increments to total variables and go on to next cycle
- (k) If K_1 , n_1/n_2 do not agree with assumed, repeat steps (f) through (i) using results of this cycle.

A flow diagram of the computation sequence is given as Fig. B.3.

In order to study the accuracy of the computer solution and to compare its results with a closed form solution, a solution was obtained to the one dimensional problem ($\epsilon_H = 0$). This corresponds to that developed in Section 3.2.1 for which an exact solution has been obtained, namely, Equation (3.51).

Figure B.4 shows a comparison of the results obtained from the computer program with those resulting from Equation (3.51). The accuracy was excellent and no difference is discernible on a graphical plot. The closeness of the two results is illustrated by the sample values noted on the figure. Further work is anticipated on this phase of the program and will be carried out as the need arises. It is expected that it will be useful in studying the unloading phases and those cases where some lateral strain is allowed.

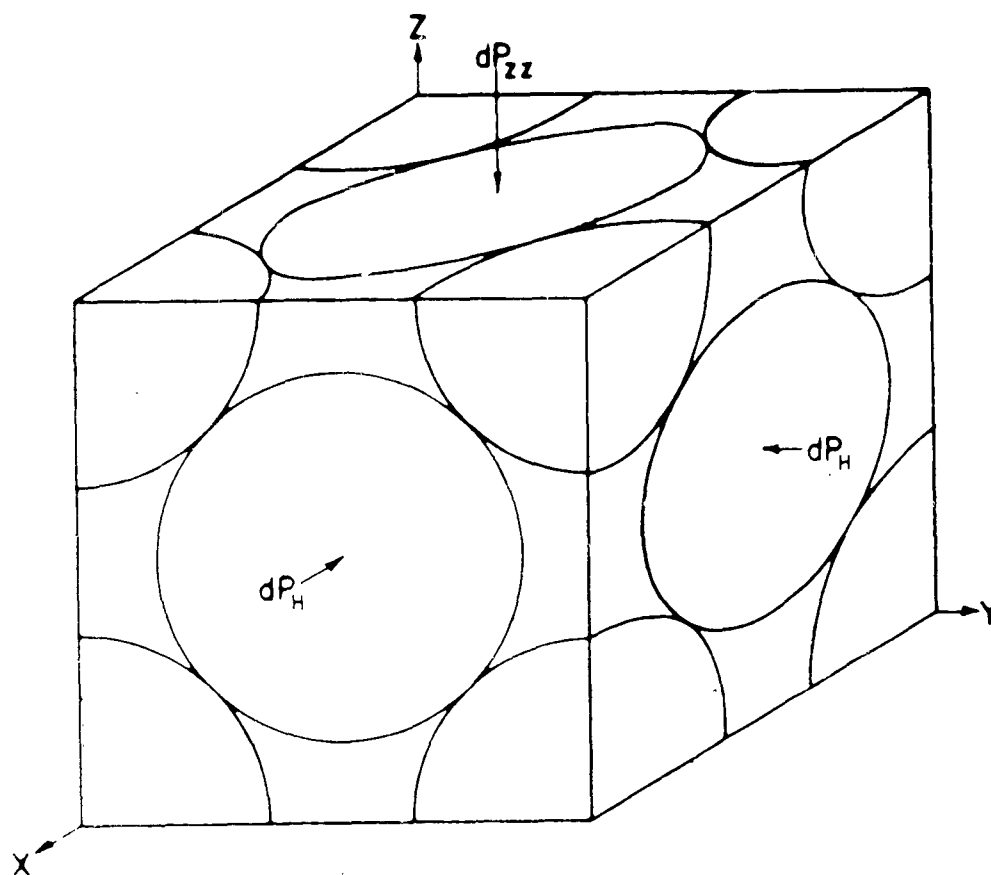
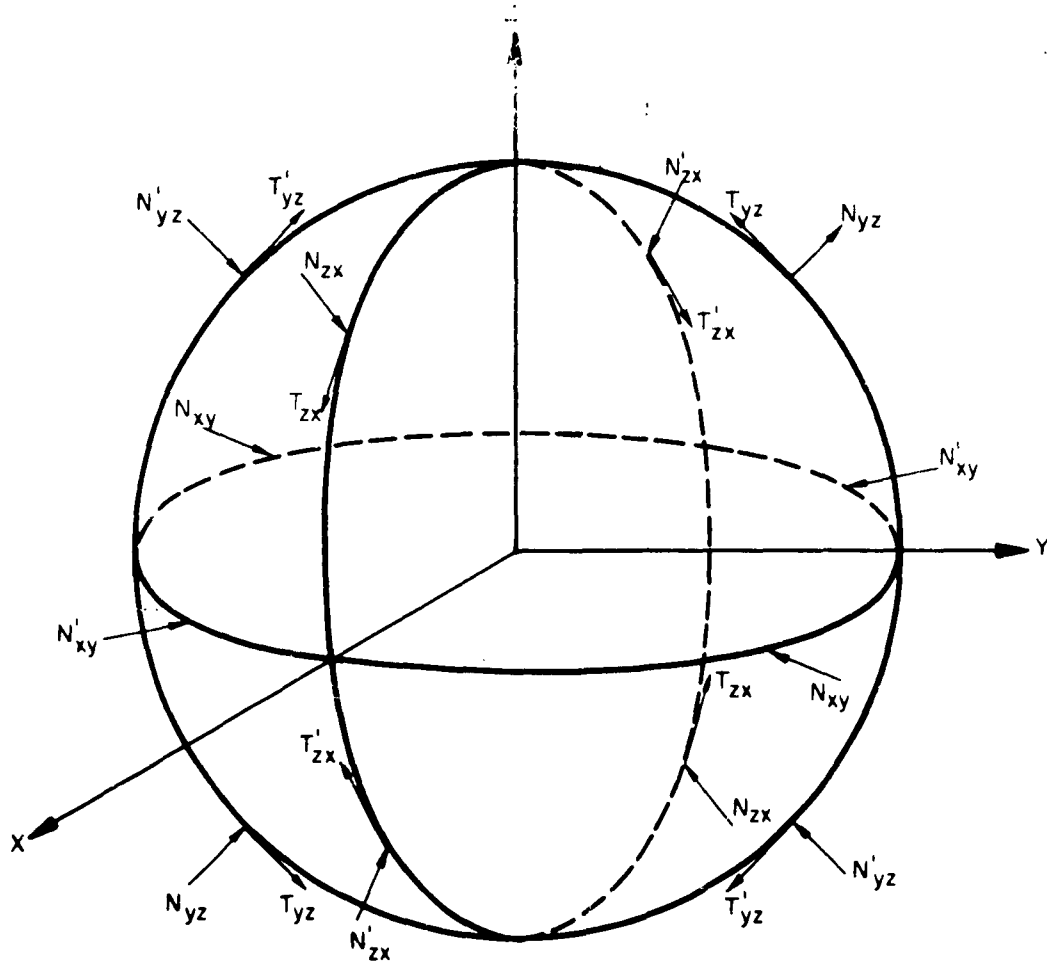


Fig. B.1 UNIT CUBE OF A FACE CENTERED CUBIC ARRAY OF EQUAL SPHERES SUBJECTED TO INCREMENTAL FORCES IN ONE DIMENSIONAL COMPRESSION



Note That Due To Symmetry

$$T_{zx} = T'_{zx} = -T_{yz} = -T'_{yz} = T_2$$

$$N_{yz} = N'_{yz} = N_{zx} = N'_{zx} = N_2$$

$$N_{xy} = N'_{xy} = N_1$$

Fig. B.2 FORCES ACTING ON A TYPICAL SPHERE SUBJECTED TO ONE DIMENSIONAL COMPRESSION

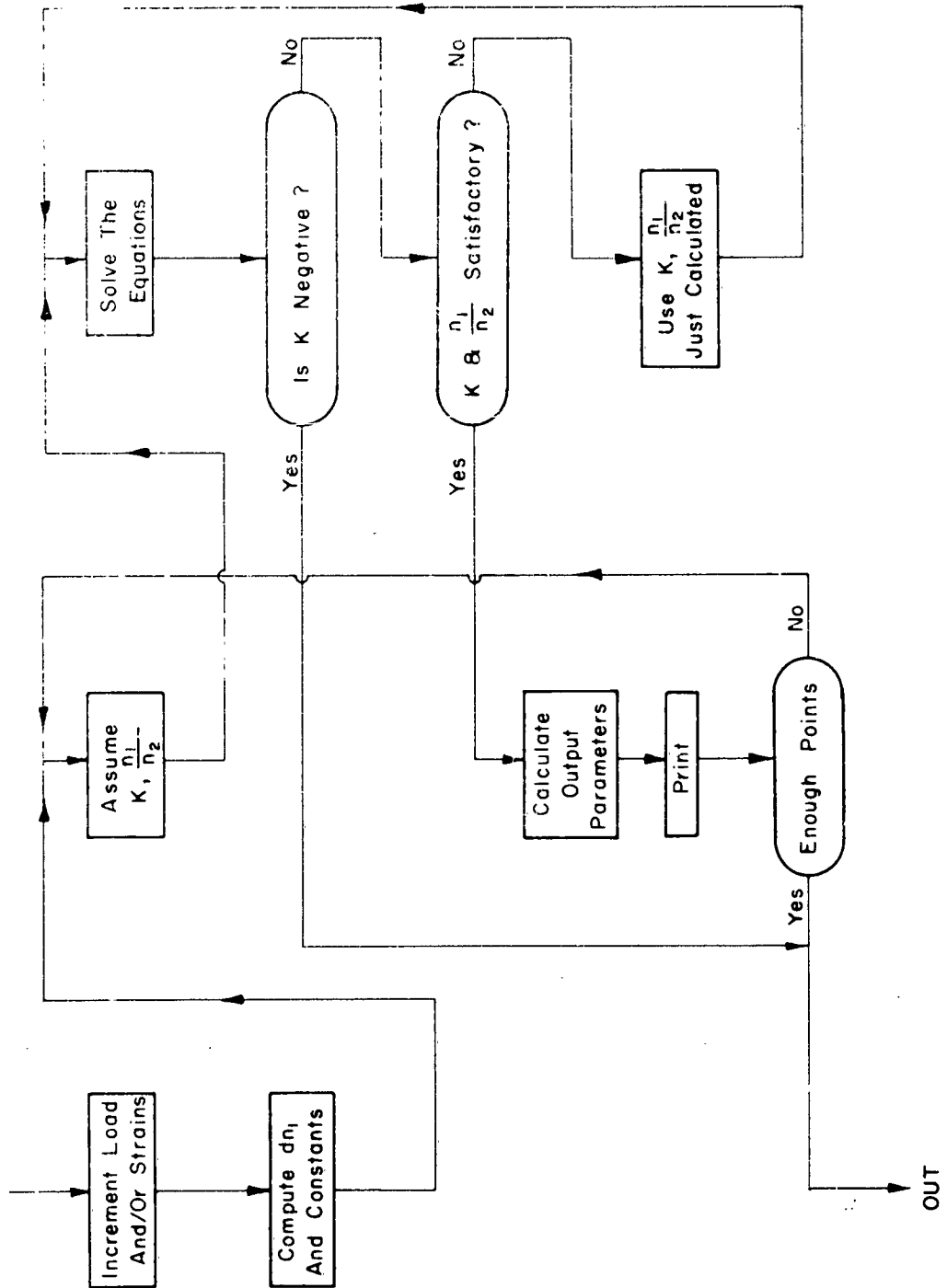


Fig. B.3 FLOW DIAGRAM OF THE COMPUTER PROGRAM

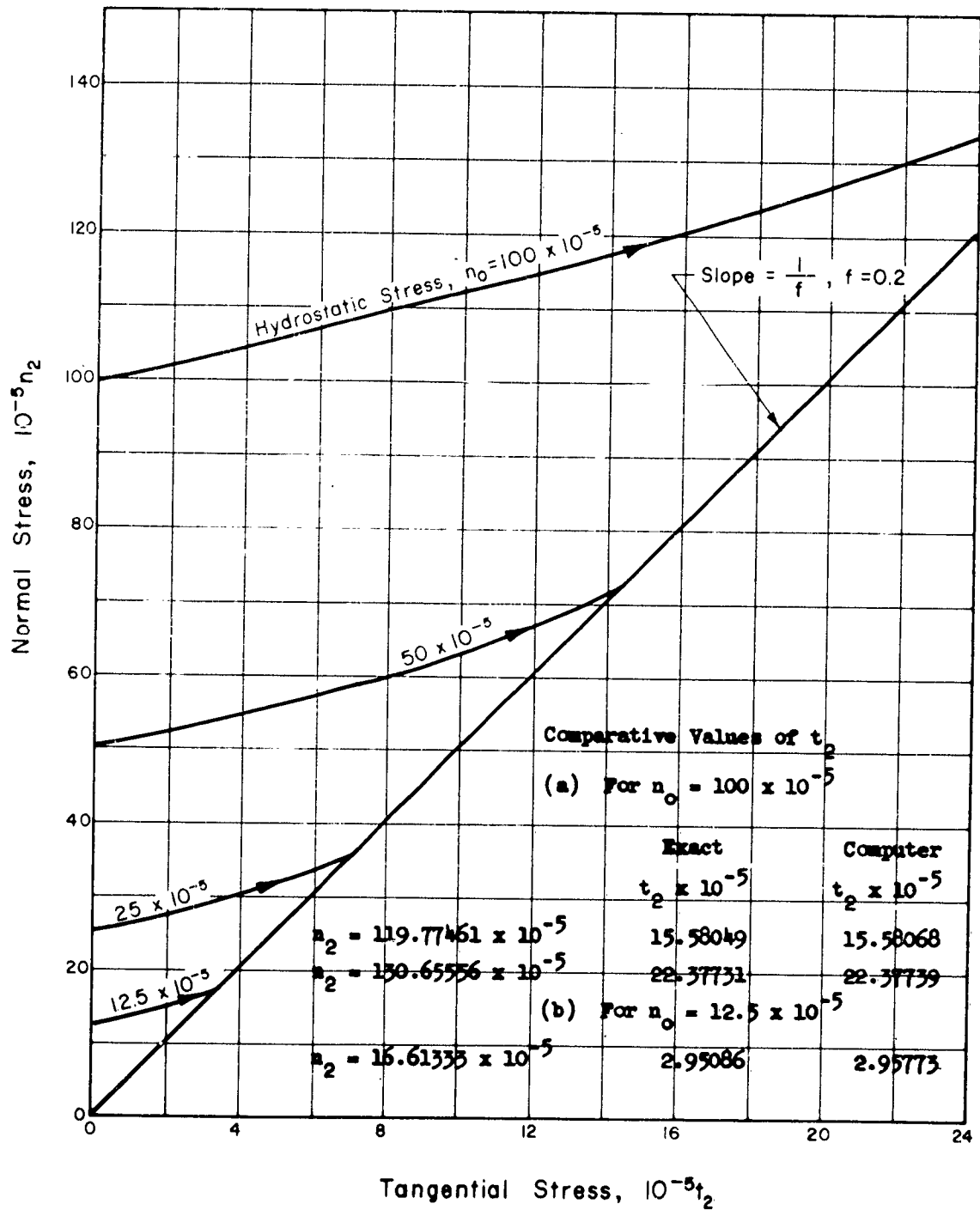


Fig. B.4 VARIATION OF CONTACT STRESSES UNDER ONE DIMENSIONAL BEHAVIOR WITH AN INITIAL HYDROSTATIC STRESS

DISTRIBUTION

No. cys

HEADQUARTERS USAF

1	Hq USAF (AFOCE), Wash 25, DC
1	Hq USAF (AFCEI-ES), Wash 25, DC
1	Hq USAF (AFRDR), Wash 25, DC
1	Hq USAF (AFRDR-NU-1), Wash 25, DC
1	Hq USAF (AFCIN), Wash 25, DC
1	USAF Dep IG for Insp (AFCDI-B-3), Norton AFB, Calif
1	USAF Dep IG for Safety (AFINS), Kirtland AFB, N Mex
1	AFOAR, Bldg T-D, Wash 25, DC
1	AFCRL, Hanscom Fld, Bedford, Mass
1	AFOSR, Bldg T-D, Wash 25, DC

MAJOR AIR COMMANDS

1	AFSC (SCT), Andrews AFB, Wash 25, DC
1	SAC (OAWS), Offutt AFB, Nebr
1	AFLC, Wright-Patterson AFB, Ohio
1	AUL, Maxwell AFB, Ala
2	USAFIT (USAF Institute of Technology), Wright-Patterson AFB, Ohio

AFSC ORGANIZATIONS

	ASD, Wright-Patterson AFB, Ohio
1	ASAPRL, Technical Doc Library
1	Director of Systems Management (ASAPTS)
1	BSD, Norton AFB, Calif
2	SSD (SSSC-TDC), AF Unit Post Office, Los Angeles 45, Calif
	ESD, Hanscom Fld, Bedford, Mass
1	ESAT
1	CRRA
1	CRZG

DISTRIBUTION (cont'd)

No. cys

KIRTLAND AFB ORGANIZATIONS

AFSWC, Kirtland AFB, N Mex

1	SWEH
50	SWOI
5	SWRS
1	US Naval Weapons Evaluation Facility (NWEF) (Code 404), Kirtland AFB, N Mex

OTHER AIR FORCE AGENCIES

2	Director, USAF Project RAND, via: Air Force Liaison Office, ATTN: RAND Library for Dr. H. L. Brode, The RAND Corporation, 1700 Main Street, Santa Monica, Calif
---	---

ARMY ACTIVITIES

1	Chief of Research and Development, Department of the Army (Special Weapons and Air Defense Division), Wash 25, DC
1	Director, Ballistic Research Laboratories, ATTN: B. Perkins, Aberdeen Proving Ground, Md
1	Chief of Engineers, Department of the Army (ENGEB), Wash 25, DC
1	Office of the Chief, Corps of Engineers, US Army (Protective Construction Branch), Wash 25, DC
1	Director, Army Research Office, Arlington Hall Sta, Arlington, Va
5	Director, US Army Waterways Experiment Sta (WESRL), P.O. Box 60, Vicksburg, Miss
1	Commanding Officer, US Army Engineers, Research & Development Laboratories, Ft Belvoir, Va

NAVY ACTIVITIES

1	Chief, Bureau of Yards and Docks, Department of the Navy, Wash 25, DC
5	Commanding Officer and Director, Naval Civil Engineering Laboratory, Port Hueneme, Calif
1	Commander, Naval Ordnance Test Station, Inyokern (Code 12) China Lake, Calif

DISTRIBUTION (cont'd)

No. cys

1 Officer-in-Charge, Civil Engineering Corps Officers, US
Naval School, Naval Construction Battalion Center, Port
Hueneme, Calif

OTHER DOD ACTIVITIES

1 Chief, Defense Atomic Support Agency (Document Library),
Wash 25, DC

3 Blast and Shock Division, ATTN: Mr. J. Lewis

1 Commander, Field Command, Defense Atomic Support Agency
(FCAG3, Special Weapons Publication Distribution), Sandia
Base, N Mex

10 ASTIA (TIPDR), Arlington Hall Sta, Arlington 12, Va

AEC ACTIVITIES

1 Sandia Corporation, ATTN: Mr. William Perret, Organiza-
tion 5112, Sandia Base, N Mex

1 University of California Lawrence Radiation Laboratory,
ATTN: Milo Nordyke, Berkeley, Calif

OTHER

1 OTS, Department of Commerce, Wash 25, DC

1 Armour Research Foundation, Illinois Institute of Technology,
ATTN: Dr. Gene Sevin, 3422 South Dearborn Street, Chicago
15, Ill

1 MRD Division, General American Transportation Corporation,
ATTN: Dr. Glen Neidhardt, 7501 North Natchez Avenue,
Niles 48, Ill

1 National Engineering Science Company, ATTN: Dr. Al
Soldate, 711 South Fair Oaks Avenue, Pasadena, Calif

1 Shannon & Wilson, Inc., Soil Mechanics and Foundation
Engineers, ATTN: Mr. Stan Wilson, 1105 North 38th Street,
Seattle 3, Wash

1 United Research Services, ATTN: Mr. Harold Mason, 1811
Trousdale Drive, Burlingame, Calif

40 University of Illinois, ATTN: Mr. A. Hendron, 207 Talbot
Laboratory, Urbana, Ill

3 University of New Mexico, ATTN: Dr. Eugene Zwoyer,
University Hill, Albuquerque, N Mex

1 University of Notre Dame, Department of Civil Engineering,
ATTN: Dr. Harry Saxe, Notre Dame, Ind

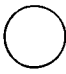


1 Stanford Research Institute, ATTN: Mr. Fred Sauer, Menlo
Park, Calif

DISTRIBUTION (cont'd)

No. cys

1	University of Washington, ATTN: Dr. I. M. Fyfe, Seattle 5, Wash
1	Purdue University, Civil Engineering Department, ATTN: Prof. G. A. Leonards, Lafayette, Ind
1	Massachusetts Institute of Technology, Department of Civil and Sanitary Engineering, ATTN: Dr. Robert Whitman, 77 Massachusetts Avenue, Cambridge 39, Mass
1	Paul Weidlinger and Associates, ATTN: Dr. M. L. Baron, 770 Lexington Avenue, New York 21, NY
1	University of Michigan, Department of Civil Engineering, ATTN: Prof. F. E. Richart, Jr., Ann Arbor, Mich
1	University of California, Department of Civil Engineering, ATTN: Prof. H. Bolton Seed, Los Angeles, Calif
1	Recan Incorporated, ATTN: Dr. Grover L. Rogers, Box 3622 MSS, Tallahassee, Fla
1	University of California, College of Engineering, ATTN: Prof. C. Martin Duke, Assistant Dean, Los Angeles, Calif
1	North Carolina State College, ATTN: Dr. Ralph Fadum, Head, Dept of Civil Engineering, Raleigh, North Carolina
1	The Mitre Corporation, ATTN: Warren McCabe, P. O. Box 208, Bedford, Mass
1	St. Louis University, Institute of Technology, ATTN: Dr. Carl Kisslinger, 3621 Olive Street, St. Louis 8, Mo
1	United Electrodynamics, Inc., ATTN: Mr. R. Obenchain, 200 Allendale Rd, Pasadena, Calif
1	Space Technology Laboratories, Inc., ATTN: Dr. M. V. Barton, P. O. Box 95001, Los Angeles 45, Calif
1	Iowa State University, ATTN: Dr. D. F. Young, Dept of Nuclear Engineering, Ames, Iowa
1	Official Record Copy (SWRS, Capt Auld)

<p>Air Force Special Weapons Center, Kirtland AF Base, New Mexico Rpt. No. AFSC-TDR-62-91. THE ENERGY ABSORPTION CAPACITY OF GRANULAR MATERIALS IN ONE-DIMENSIONAL COMPRESSION. 202 p. incl illus, tables, 64 refs. January 1963</p> <p>Unclassified Report</p> <p>Energy absorbing mechanisms in sand subjected to one-dimensional compression are reported. For pressures below crushing of the grains, a granular medium of equal radii elastic spheres in a face-centered cubic array is analyzed. Expressions are obtained for the axial stress-strain curve, constrained modulus, coefficient of earth pressure at rest, and relationship between absorbed energy and input energy for one cycle of loading. The energy absorbed as a result of</p> <p>○</p>	<ol style="list-style-type: none"> 1. Absorption 2. Plastic deformation 3. Sands -- effects of blast 4. Soil mechanics 5. Stress and strain I. AFSC Project 1080, Task 108001 II. Contract AF 29(601)-4302 III. Illinois, Univ., Urbana Dept. of Civil Engineering IV. Alfred J. Hendron, Jr., Robert E. Fulton and Bijan Mohraz V. DASA WEB No. 13.146 VI. In ASTIA collection 	<p>Air Force Special Weapons Center, Kirtland AF Base, New Mexico Rpt. No. AFSC-TDR-62-91. THE ENERGY ABSORPTION CAPACITY OF GRANULAR MATERIALS IN ONE-DIMENSIONAL COMPRESSION. 202 p. incl illus, tables, 64 refs. January 1963</p> <p>Unclassified Report</p> <p>Energy absorbing mechanisms in sand subjected to one-dimensional compression are reported. For pressures below crushing of the grains, a granular medium of equal radii elastic spheres in a face-centered cubic array is analyzed. Expressions are obtained for the axial stress-strain curve, constrained modulus, coefficient of earth pressure at rest, and relationship between absorbed energy and input energy for one cycle of loading. The energy absorbed as a result of</p> <p>○</p>	<ol style="list-style-type: none"> 1. Absorption 2. Plastic deformation 3. Sands -- effects of blast 4. Soil mechanics 5. Stress and strain I. AFSC Project 1080, Task 108001 II. Contract AF 29(601)-4302 III. Illinois, Univ., Urbana Dept. of Civil Engineering IV. Alfred J. Hendron, Jr., Robert E. Fulton and Bijan Mohraz V. DASA WEB No. 13.146 VI. In ASTIA collection
<p>Air Force Special Weapons Center, Kirtland AF Base, New Mexico Rpt. No. AFSC-TDR-62-91. THE ENERGY ABSORPTION CAPACITY OF GRANULAR MATERIALS IN ONE-DIMENSIONAL COMPRESSION. 202 p. incl illus, tables, 64 refs. January 1963</p> <p>Unclassified Report</p> <p>Energy absorbing mechanisms in sand subjected to one-dimensional compression are reported. For pressures below crushing of the grains, a granular medium of equal radii elastic spheres in a face-centered cubic array is analyzed. Expressions are obtained for the axial stress-strain curve, constrained modulus, coefficient of earth pressure at rest, and relationship between absorbed energy and input energy for one cycle of loading. The energy absorbed as a result of</p> <p>○</p>	<ol style="list-style-type: none"> 1. Absorption 2. Plastic deformation 3. Sands -- effects of blast 4. Soil mechanics 5. Stress and strain I. AFSC Project 1080, Task 108001 II. Contract AF 29(601)-4302 III. Illinois, Univ., Urbana Dept. of Civil Engineering IV. Alfred J. Hendron, Jr., Robert E. Fulton and Bijan Mohraz V. DASA WEB No. 13.146 VI. In ASTIA collection 	<p>Air Force Special Weapons Center, Kirtland AF Base, New Mexico Rpt. No. AFSC-TDR-62-91. THE ENERGY ABSORPTION CAPACITY OF GRANULAR MATERIALS IN ONE-DIMENSIONAL COMPRESSION. 202 p. incl illus, tables, 64 refs. January 1963</p> <p>Unclassified Report</p> <p>Energy absorbing mechanisms in sand subjected to one-dimensional compression are reported. For pressures below crushing of the grains, a granular medium of equal radii elastic spheres in a face-centered cubic array is analyzed. Expressions are obtained for the axial stress-strain curve, constrained modulus, coefficient of earth pressure at rest, and relationship between absorbed energy and input energy for one cycle of loading. The energy absorbed as a result of</p> <p>○</p>	<ol style="list-style-type: none"> 1. Absorption 2. Plastic deformation 3. Sands -- effects of blast 4. Soil mechanics 5. Stress and strain I. AFSC Project 1080, Task 108001 II. Contract AF 29(601)-4302 III. Illinois, Univ., Urbana Dept. of Civil Engineering IV. Alfred J. Hendron, Jr., Robert E. Fulton and Bijan Mohraz V. DASA WEB No. 13.146 VI. In ASTIA collection

<p>crushing is considered by analyzing statistical relationships between changes in grain size distribution curves and the new surface areas created. An apparatus is described which has the capability of maintaining conditions at zero radial strain under increasing axial stress. The lateral stresses developed under these conditions are measured. Preliminary experimental results are presented for one sand which show the variation of the coefficient of earth pressure at rest and the stress-strain relationships with initial void ratio, overconsolidation ratio, and strain rate. A correlation of theory and test results is presented.</p> 		<p>crushing is considered by analyzing statistical relationships between changes in grain size distribution curves and the new surface areas created. An apparatus is described which has the capability of maintaining conditions at zero radial strain under increasing axial stress. The lateral stresses developed under these conditions are measured. Preliminary experimental results are presented for one sand which show the variation of the coefficient of earth pressure at rest and the stress-strain relationships with initial void ratio, overconsolidation ratio, and strain rate. A correlation of theory and test results is presented.</p> 	
<p>crushing is considered by analyzing statistical relationships between changes in grain size distribution curves and the new surface areas created. An apparatus is described which has the capability of maintaining conditions at zero radial strain under increasing axial stress. The lateral stresses developed under these conditions are measured. Preliminary experimental results are presented for one sand which show the variation of the coefficient of earth pressure at rest and the stress-strain relationships with initial void ratio, overconsolidation ratio, and strain rate. A correlation of theory and test results is presented.</p> 		<p>crushing is considered by analyzing statistical relationships between changes in grain size distribution curves and the new surface areas created. An apparatus is described which has the capability of maintaining conditions at zero radial strain under increasing axial stress. The lateral stresses developed under these conditions are measured. Preliminary experimental results are presented for one sand which show the variation of the coefficient of earth pressure at rest and the stress-strain relationships with initial void ratio, overconsolidation ratio, and strain rate. A correlation of theory and test results is presented.</p> 